Effect of Shear Patterns and EPS on Fouling in Microfiltration

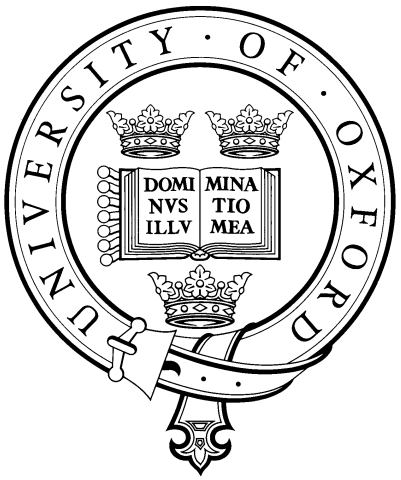

Pharima Pongpairoj
Lady Margaret Hall

A thesis submitted for the degree of Doctor of Philosophy

Department of Engineering Science, University of Oxford

Hilary term 2013

The candidate confirms that the work submitted is her own and that appropriate credit has been given where reference has been made to the work of others. This copy has been supplied on the understanding that it is copyright material and that no quotation from the thesis may be published without proper acknowledgement.

Effect of Shear Patterns and EPS on Fouling in Microfiltration

Pharima Pongpairoj
Lady Margaret Hall, University of Oxford

Thesis submitted for the Degree of Doctor of Philosophy in Engineering Science
Hilary term 2013

Abstract

Concentration polarisation and fouling reduce performance as well as increase costs. In order to mitigate these effects, understanding the cause and effects of these phenomena is crucial. It has been hypothesized, and to a certain extent shown, that amelioration of fouling can be achieved through the use of time varying shear for example use of air-sparging or sharp changes in crossflow velocity. Nevertheless the effect of shear on membrane fouling, in particular its effect on the foulant deposition and the transmission of small molecules in microfiltration, is not well understood.

The goal of this project was to achieve an understanding of various foulant behaviour. The work was divided into two parts. Firstly, the observations of fouling by freshwater algae, *Chlorella Sorokiniana*, were carried out at Nanyang Technological University, Singapore. Observations using macroscopic parameters were examined with an optical non-invasive observation technique called Direct Observation Through Membrane (DOTM). The result yielded a novel relationship between operating flux, crossflow velocity and transmission of extracellular polysaccharide. Interestingly shear was shown to have positive as well as negative effects on fouling of microfiltration membrane. The analysis of permeate has clearly shown that a maximisation of shear rate was not ideal.

The second part was concerned with observations of the effect of shear patterns on membrane fouling using newly fabricated special membrane filtration cell, Direct Shear Stress Test Cell (DSSTC), designed to fit an Anton Paar rheometer and operate at constant flux. Unlike the-constant-shear-filtration cells, one could impose a very wide variety of shear regimes including intermittent sharp changes of direction and sinusoidal oscillations in the DSSTC. The effect of shear patterns on transmission and fouling of a model polysaccharide (Dextran Blue) through microfiltration membranes was carried out at various conditions. Again, the results showed that the maximisation of shear rate was not ideal. The effect of shear patterns and EPS on fouling by yeast suspension was also studied using the DSSTC. The benefit of oscillatory shear is foulant dependent. For example, square wave oscillatory shear led to lower relative fouling for yeast EPS, but it resulted in higher relative fouling for unwashed yeast.

Acknowledgements

Firstly, I would like to thank my supervisors, Professors Robert Field and Zhanfeng Cui. I have worked closely with Prof. Robert Field, and I cannot thank him enough for his input to the project, his patient guidance, and his valuable advice. He has assisted me greatly, and his open-mindedness has allowed me to explore researches in a different dimension which made my DPhil an interesting and enjoyable experience. I am also very grateful for Prof. Zhanfeng Cui's advices and suggestions. He has provided valuable guidance and insight.

Secondly, I would like to thank Professors Anthony Fane, Robert Field, and Wang Rong for providing me the opportunity to carry out part of my research at SMTC, NTU, Singapore. During my visits, my special thanks go to Dr. Filicia Wikicaksana who introduced me to DOTM equipment. I would also like to thank all my friends and colleages at SMTC especially Thiengi Aung for cultivating the algae.

Thirdly, I would like to thank all my departmental colleages, especially Dr. Alex Lubansky for his advice and friendship, as well as Dr. Cathy Ye, and Dr. Julian George. The DSSTC module would not exist without several Oxford technicians. To my knowledge these include Graham, Steve and Garry who are all thanked. I very much appreciate Xiafu Shi and Aimee Guha Roy for their help and supports. To Xiafu Shi in particular, I am very grateful for his assistance when things went wrong.

Lastly, I owe a lot of gratitute to my family, who have been very supportive. Many friends who have made my DPhil a very enjoyable time. I am extremely grateful to Dr. Songpol Chuenkhum for his invaluable advices throughout my time at Oxford. I really appreciate Flight Lieutenant Eddleston, Lisa Cheowtirakul, and Dr. Graciana for their supports and advices. I would like to take the opportunity to thank my other friends and colleagues including Sylvestre Burgos, Jin lee, Julian David Hunt, and Miroslawa Alunowska Figueroa for motivation, support and friendship.

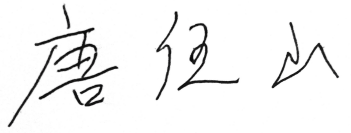

& Mush

Contents

List of Figures

List of Tables

Nomenclature

Abbreviations

a^*, b^*, f	Geometric constants
A_0	Initial clean membrane area (m^2)
A_0	Initial clean membrane area
A_c	Cake area
C_p	Permeate concentration
c_B	Bulk concentration
C_{La}	Constant for laminar flow
c_s	Solid volume concentration (kg/m^3)
C_{Tu}	Constant for turbulent flow
d	diameter of rod shape particles
d_h	Hydraulic diameter
D_{aq}	Molecular diffusion coefficient in liquid (m/s)
D_f	Molecular diffusion coefficient in biofilm (m/s)
d_p	Spherical particles diameter

e	Annular gap
F	Oscillation frequency (Hz)
J_{ci}	Critical flux for irreversibility
J_{cs}	Strong form of critical flux
J_{cw}	Weak form of critical flux
J_c	Critical flux
k_1	Parameter
K_c	Cake blocking co-efficient
K_s	Standard blocking co-efficient
$k_d(r)$	Local mass transfer coefficient at a fixed surface (m/s)
k_{vc}	Velocity coefficient
M_w	Molecular weight (Da)
n_n	Empirical parameter (n_2, n_3 = compressibility parameters)
P_f	Pressure on filtrate side
P_{ip}	Module inlet pressure
P_{op}	Module outlet pressure
P_o	Overall transmembrane pressure
Q_j	Average flow rate through membrane (m^3/s)
Q_{CFV}	Crossflow velocity (in volume flow rate)
r	Radial position (m)

r_g	Radius of gyration
r_p	Membrane pore radius (m^2)
R_{ad}	Adsorption resistance
R_{cl}	Cake layer resistance
R_{cp}	Concentration polarisation resistance
R_{cr}	Critical radius (m)
R_{cy}	Inner cylinder radius (m)
R_c	Radius at centre of channel (m)
R_F	Radius of the stationary plate (m)
R_f	Fouling resistance (m^{-1})
R_{irrev}	Membrane irreversible resistance (m^{-1})
R_i	Inner radius of the channel
R_m	Clean membrane resistance (m^{-1})
R_{Om}	Outer radius of the membrane
R_o	Outer radius of the channel
R_{pb}	Pore blocking resistance
R_{rev}	Membrane reversible resistance (m^{-1})
R_{To}	Total membrane resistance (m^{-1})
R_T	Radius of rheometer plate (m)
T_c	Time dependent consolidation effect

Ta	Taylor number
a1, a2, a3, a4	Constants
C	Concentration
c	Volume of particles deposited by unit volume of filtrate
G	Shear rate (at below critical shear) (s^{-1})
H	Channel height (m)
J	Flux or flowrate through membrane (LMH)
k	Mass transfer co-efficient (m/s)
L	Channel length (m)
N	Number of pores
P	Pressure
Q	Flow rate (m^3/s)
R	Membrane resistance (m^{-1})
rpm	Revolutions per minute
S	Mass fraction of particles in the feed
u	Fluid velocity through membrane pore (m)
V	Cumulative volume filtered
v	Fluid velocity
W	Channel width (m)
z	Distance from the membrane

Greek Symbols

α^*	Specific cake resistance(mass basis) (m/kg)
β	Compressibility parameter
δ	Boundary layer thickness
$\dot{\gamma}_a$	Apparent shear rate (s$^-$1)
$\dot{\gamma}_w$	Wall shear rate (s$^-$1)
$\dot{\gamma}_{La}$	Shear rate under laminar flow
$\dot{\gamma}_{Tu}$	Shear rate under turbulent flow
$\dot{\gamma}_{wl}$	Local shear rate in laminar flow (s^{-1})
$\dot{\gamma}_{wp}$	Membrane pore wall shear rate
$\dot{\gamma}_{wt}$	Local shear rate in turbulent flow (s^{-1})
$\dot{\gamma}_{WRec}$	Wall shear rate using rectangular die approximation
$\dot{\gamma}_{WSlit}$	Wall shear rate using slit die approximation
γ_0	Concentration of particles in the feed
γ_s	Feed suspension density
λ	Ratio of the radius of gyration to the radius of pore
μ	Dynamic viscosity
μ_p	Permeate viscosity
ν	Fluid kinematic viscosity (m^2/s)
ω	Disk angular velocity

ϕ	A function of the variables
ψ	Shape factor
ρ	Fluid density
σ	Clogging co-efficient (for spherical=$1.5\frac{\gamma_s S}{\gamma_0 d_p \psi}$, for rod-like =$4\frac{\gamma_s S}{\pi\gamma_0 d\psi}$)
τ_w	Shear stress at membrane wall (Pa)
θ	Half angle of the cone
ε	Membrane porosity (%)

Acronyms

AFM	Atomic Force Microscopy
AFR	The product of displacement amplitude, oscillation frequency, and radial position.
CLSM	Confocal Laser Scanning Microscopy
CPTC	Cone-Plate Test Cell
DNA	Deoxyribonucleic acid
DO	Direct Observation on Hollow Fibre Membrane
DOTM	Direct Observation Through Membrane
DSSTC	Direct Shear Stress Test Cell
EPS	Extracellular Polysaccharides
ESEM	Environmental Scanning Electron Microscopy
FESEM	Field Emission Scanning Electron Microscopy
FRR	Fouling Resistance Ratio

IC	Inorganic Carbon
IFRR	Irreversible Fouling Resistance Ratio
Javg	Average flux (LMH)
LB-EPS	Loosely bound extracellular polysaccharides
LSFCM	Laser scanning fluorescene confocal microscopy
MBR	Membrane bioreactor
MF	Microfiltration
MFCP	Microfiltration Cone and Plate Test Cell
MFS	Membrane Fouling Simulator
NdTMP/dt	Normalised rate of increase of transmembrane pressure
NF	Nanofiltration
NIL	Nanoimprint lithography
NTr	Normalised observed transmission
PAA	Poly acrylic acid
PAC	Powdered activated carbon
PEO	Polyethylene Oxide
PES	Polyethersulfone Membrane
PET	Polyethylene Terephthalate
PIV	Particle Image Velocimetry
PT	Projector Technique

PVDF	Polyvinylidene difluoride
Re	Reynolds number
RO	Reverse Osmosis
Sc	Schmidt number
SEM	Scanning Electron Microscopy
Sh	Sherwood number
SIN	Sinusoidal wave
SQ	Square wave
TB-EPS	Tightly bound extracellular polysaccharides
TEM	Transmission Electron Microscopy
TMPavg	Average transmembrane pressure (kPa)
TOC	Total Organic Carbon
USTC	Uniform Shear Test Cell
UTDR	Ultrasonic Time Domain Reflectometry
VSEP	Vibratory Shear Enhanced Processing

1 Introduction

1.1 Background

Membrane filtration has been used widely for water purification, pharmaceutical downstream processing, as well as in the food and other industries. Microfiltration and Ultrafiltration are particularly important for removal of chlorine-resistant pathogens in water treatment industries. Microfiltration and Reverse Osmosis are also used for purification for pure water production in the electronic, chemical, and pharmaceutical industries. Other important applications of Microfiltration include separation of "low-volume high-value" heat-sensitive feed, an example of this is yeast cell removal from cider and wine[1].

Fouling of membranes is still an ongoing problem and is one of the main obstacles for the future expansion of membrane filtration. Also the fouling of membranes is costly due to increased operating costs arisen from pumping, operations under higher pressure, and cleaning as well as the need to change the membranes. There are several methods for fouling mitigation, this is summarised in Figure 1.1.

		Shear	Unsteady shear
Hydrodynamics			
	Crossflow	Yes	No
	Air-bubbling	Yes	Yes
	Vibration / Dynamic	Yes	Yes
Cleaning			
	Backwash	No	No
	Chemical enhanced backwash	No	No

Figure 1.1: Fouling mitigation methods

Membrane cleaning can contribute between 5 and 20% of the operating cost[2]. Cleaning of membrane can be done via physical cleaning, chemical cleaning or other methods[3]. Physical cleaning includes backwashing of membrane to remove foulants. The use of harsh chemicals can be employed to help dislodge foulants from the membrane surface, however it usually causes deterioration of membranes especially for polymeric ones[3]. Chemical cleaning cannot always restore the original membrane resistance, and in some cases, it can worsen the membrane performance[2]. Moreover, in food or phamaceutical industries, special care must be taken to remove trace elements of these chemicals.

Prevention of fouling using hydrodynamics is therefore seen as a more promising approach, much research has been carried out in this area using various methods. Application of shear is one of the most popular and widely used methods for reducing concentration polarization and fouling. Generally, a higher mass transfer co-efficient hence lower concentration polarisation leads to higher flux, or lower rate of TMP increases. The use of hydrodynamic conditions to enhance mass transfer co-efficient (k) in the system has been found effective. These methods include the use of crossflow filtration module, the use of air bubbling, and vibration of the membrane module. For these systems it is generally difficult to quantify the shear

and the imposition of various shear patterns may not be possible. For thorough studies on the effect of shear the inclusion of the effect of shear intermittency, i.e., periodically alterations between the low and high shear, is desirable.

The fouling mechanism varies with foulants and the membrane used. Generally, foulants whose size is greater than the membrane pore size lead to cake formation on top of the membrane surface, this creates further resistance to the fluid flow. The foulants whose size is smaller than the membrane pore tends to deposit in the wall of the membrane pore leading to pore narrowing. For mixed suspension where both larger-than-pore and smaller-than-pore size particles are presented together, the situation becomes more complicated. This is because the smaller foulants can either pass through the membrane pore or be retained within the cake of larger foulants[4]. Fouling by mixed foulants is therefore complex especially for the live feed suspension. The current understanding of the effect of shear on fouling and transmission is limited, particularly for the filtration which involves foulants with various size and type.

1.2 Objectives

The objectives of this thesis are to gain better understanding of the fouling phenomena of mixed suspension as well as to observe the influence of shear patterns on transmission and fouling of small molecules through microfiltration membranes. This involves the use of a readily available tool as well as design and development of a novel tool in house for investigation of fouling phenomena under the influence of various well defined shear conditions. The Direct Observation Through Membrane or DOTM module (Singapore Membrane Technology Centre, Nanyang Technological University, Singapore) serves as an optical tool for in-situ visual observation of the deposition of particles onto the membrane surface as well as their removal. And the Direct Shear Stress Test Cell or DSSTC provides an integrated module capable

of generating different shear patterns necessary for thorough studies.

1.3 Structure of the thesis

Chapter 1 and Chapter 2 consist of Introduction and relevant previous literatures to the case studies respectively. Chapter 3 is based on DOTM studies on microfiltration of microalgae under various conditions. This chapter focuses on critical/threshold fluxes obtained using visual observation and transmembrane pressure data. Chapter 4 is concerned with the transmission and fouling of the extracellular polysaccharide (EPS) in algal microfiltration. The highlights of this chapter include the significance of the level of shear and its effect on fouling and transmission of the EPS. Moreover, the use of visual observation enables better understanding of the deposition and removal mechanisms of a complex feed such as the algae.

DSSTC was employed in both Chapters 5 and 6. Chapter 5 concerns the effect of various shear patterns on fouling and transmission of a model polysaccharide, Dextran Blue. The shear patterns used include steady shear, smooth or sharp change in oscillatory shear, as well as intermittency of shear. These enabled a better understanding of the benefit of shear of various patterns and levels on fouling mitigation. Chapter 6 involves comparisons between different shear patterns on fouling by unwashed yeast suspensions, washed yeast suspensions, and yeast EPS. Finally, Chapter 7 consists of conclusions and suggestions for future work.

2 Literature Review

2.1 Membrane separation processes

The phrase "membrane separation process" refers to separation of two or more components through "a semi-permeable barrier (the membrane)"[5]. The movement of one or more species through the membrane is faster than another resulting in separation of these species[5]. The retained part of the feed is known as a retentate while a permeate refers to the portion of feed that is transmitted through the membrane[5]. Pressure driven membrane processes can be divided into three categories based on size, these are ultrafitration (UF), and microfiltration (MF), nanofiltration (NF), and reverse osmosis (RO)[6]. The comparison between UF, MF, NF and RO is summarised in table 2.1.

	Microfiltration	**Ultrafiltration**	**Nanofiltration**	**Reverse Osmosis**
Pore size (μm)	0.1-10	0.001-0.1	0.001-0.01	0.0001-0.001
Pressure drop (kPa)	10-100	100-800	500-2000	800-8000

Table 2.1: Comparison between Microfiltration, Ultrafiltration, Nanofiltration and Reverse Osmosis ([5]Modified)[7, 8]

2.2 Membrane modules

Membrane modules can be roughly divided into two categories based on the type of membranes. These are flat sheet and hollow fibre or tubular membrane. The flat

sheet membranes can be incorporated into several modules, these include the three basic modes of operation which are dead-end cell, stirred cell, and crossflow cell. The more advance membrane modules which employ the use of shear for fouling mitigation include dynamic membrane systems such as Vibratory Shear Enhanced Process (VSEP)[9] and Cone-Plate Test Cell (CPTC)[10]. The main advantages and disadvantanges of these modules are summarised in Table 2.2. Direct Shear Stress Test Cell (DSSTC) which is newly developed as a part of this project is also included here for comparisons.

Module type	Constant flux	Constant pressure	Shear	Advantages	Disadvantages
Hollow fibre/Tubular membrane	Y	Y	Y	Large membrane surface area. Possible to introduce air-bubbling.	Non-uniform pressure distribution.
Flat sheet crossflow cell	Y	Y	Y	Quick and easy to set-up, equipments are widely available. Possible to introduce air-bubbling.	Non-uniform shear profile and pressure distribution. Denting of membrane due to crossflow
Dead-end cell	Y	Y	N	Quick and easy to set-up, equipments are widely available.	No shear.
Stirred cell	Y	Y	Y	Quick and easy to set-up, equipments are widely available. Capable of generating shear in the system.	Shear profile is non-uniform. Not possible to generate oscillatory shear profile.
Dynamic membrane system (eg. VSEP, CPTC)	Y (CPTC)	Y (VSEP)	Y	Capable of generating steady shear or oscillatory shear. Uniform shear stress on membrane surface (CPTC).	Cannot directly compare the effect of steady shear and oscillatory shear. Alteration of feed channel height is not possible. Difficult to clean all components.
DSSTC	Y	N	Y	Capable of generating both steady shear and oscillatory shear. Both steady and oscillatory shear are precisely adjustable. Easy to alter channel height . Possible to change channel height during the run. Easy to dissemble and clean.	Operation in constant pressure mode is not possible at present. Difficult to model feed concentration profile.

Table 2.2: Advantages and disadvantages of different type of filtration module

2.3 Operation of membrane processes

2.3.1 Driving force in membrane separation process

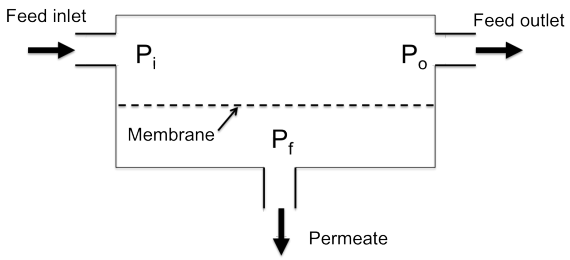

Figure 2.1: Transmembrane pressure in crossflow (modified after [6])

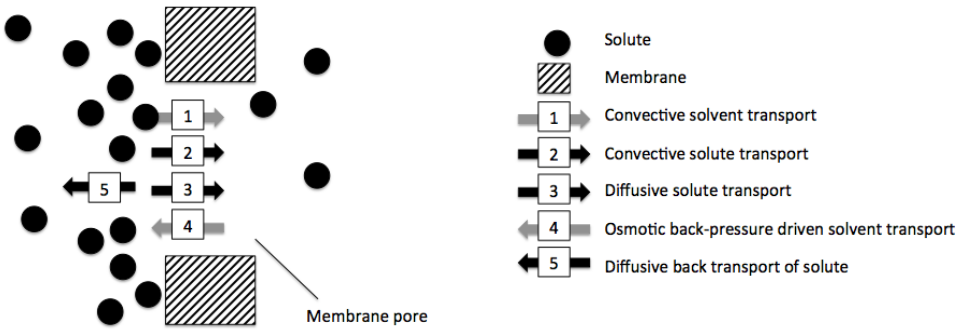

Figure 2.2: Solute and solvent transport (modified after [11])

The primarily driving forces in membrane separation include transmembrane pressure (TMP), concentration or electrochemical gradient, osmotic pressure, electrostatic field. Schematic diagram is shown in Figure 2.2. Transmembrane pressure is the main applied driving force. When TMP is applied, the solvent and solute molecules are transported towards the membrane, mainly by bulk convection. It can be generally illustrated by Figure 2.1.

$$\triangle P = \frac{P_{ip} + P_{op}}{2} - P_f \tag{2.1}$$

where $\triangle$P is transmembrane pressure, P_{ip} is module inlet pressure, P_{op} is module outlet pressure, and P_f is pressure on the filtrate side.

'The solute molecules may be fully transmitted, partially transmitted or totally retained (rejected) by the membrane'[11]. The level of rejection is determined by steric, hydrodynamic, thermodynamic, and electrostatic effects. Some components in the feed are rejected by the membrane (e.g. salts in RO, proteins in UF, and cells in MF). The rejected components will be of greater concentration adjacent to the membrane surface. This layer of highly concentrated materials is known as mass transfer boundary layer. This phenomena is known as concentration polarisation, it contributes to a resistance to driving force.

In addition, back-diffusion of accumulated solutes near the membrane surface to the bulk occurs. This is determined by the transport properties of the solutes together with the hydrodynamics on the feed side of the membrane. Electric field can occasionally be applied externally in order to achieve a higher rate of the back-transport of solute molecules. In some cases, electric field is also used to enhance selectivity by promoting transmission of specific molecules through the membrane[11].

2.3.2 Modelling of flux

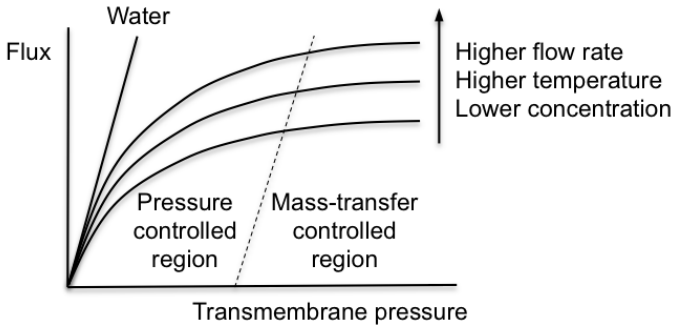

Figure 2.3: Generalized correlation between operating parameters and flux, indicating the areas of pressure control and mass transfer control (modified after [6])

Flux in a membrane process is dependent on the cross-flow rate, temperature, feed concentration, and transmembrane pressure, membrane pore size, and operating time. When the system operates at low pressures, low feed concentrations, and high feed velocities, the resulting effects of concentration polarisation are considered minimal. At this condition, flux depends largely on transmembrane pressure, this is known as pressure control region[6]. On the other hand, when the system operates at high pressures, high feed concentrations, and low feed velocities, the resulting flux is in the mass transfer controlled region, i.e., where flux can no longer be enhanced, or very slightly enhanced by an increase in transmembrane pressure[6].

2.3.2.1 Pressure controlled region

Hagen-Poiseuille law for streamline flow through channel is considered the best description of fluid flow through micropores but is only exact when the microporous membrane consists of uniform cylindrical pores. The flow rate, J, expressed by the Poiseuille model is shown below [6, 12] :

$$J = \frac{\varepsilon r_p^2 \triangle P}{8 \mu_p L} \tag{2.2}$$

where J is the flow rate through the membrane, r_p is the pore radius, P is the applied transmembrane pressure, μ_p is the viscosity of the fluid permeating the membrane and L is the length of the channel, ε is the surface porosity of the membrane. Often J is quoted in $\mu m s^{-1}$ or $l m^{-2} h^{-1}$ (LMH). Assumptions[6] of the above equation are (i) laminar flow through pore, Re<1800 (ii) incompressible liquid (density remains constant) (iii) steady state conditions (flow does not change with time) (iv) Newtonian fluid (viscosity only changes with solid concentration (feed concentration) and temperature, not with velocity, and (v) end effects negligible[6].

Equation is straight forward to use if the membrane filter is both symmetric and microporous. However the model can be adjusted to suit asymmetric membranes those cannot be visualised as having cylinder pores[6]. One can assume 2 layers, a

skinlayer and a support layer. Nevertheless, this method can be used in principle, but in practice it is hard to estimate the skin thickness and porosity accurately.

2.3.2.2 Concentration Polarisation

In membrane processes, components on the feed side are convected to the membrane surface under transmembrane pressure. A fraction of them may be rejected due to size exlusion or some other effects. Therefore, the rejected components will accumulate in the area adjacent to the membrane surface, which forms a mass transfer boundary layer between the bulk solution and the membrane as shown in Figure 2.4. The concentration gradually increases across this layer to the membrane surface[6]. This phenomenon is called concentration polarisation and is a natural consequence of the perm-selectivity of a membrane. It is inevitible in filtration processes and the resultant high concentrations at locations are relevant to fouling[13].

As a result of this concentration gradient, the rejected components will diffuse back to the bulk solution. Assuming that there is no chemical reaction in the system, the density is constant, the concentration difference parallel to the membrane is negligible, and Fickian diffusion takes place[14], the steady-state mass balance between convection and back-diffusion can be expressed as

$$JC - JC_p = -D\frac{dC}{dz} \tag{2.3}$$

where J is the volumetric flux, C is the concentration, C_p is the permeate concentration, D is diffusivity, and z is the distance from the membrane.

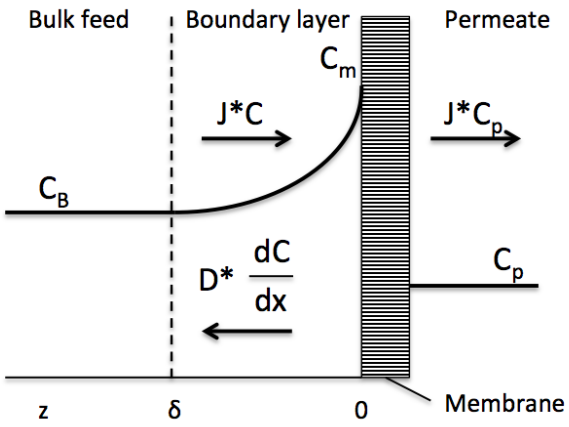

Figure 2.4: Concentration polarisation; concentration polarisation profile under steady-state conditions (modified after [14])

Integrating the above equation with boundary conditions, $C = C_m$ at $z = 0$, and $C = C_B$ at $z = \delta$, yields

$$J = \frac{D}{\delta} ln \frac{(C_m - C_p)}{(C_B - C_p)} \tag{2.4}$$

where C_m, C_B are the concentration at membrane surface and in the bulk respectively, δ is the boundary layer thickness, and $\frac{D}{\delta}$ is known as the mass transfer coefficient, k.

When total rejection (100%) is assumed, and both concentration profile and permeate flux effects on the mass transfer coefficient, k, is neglected[15]. The concentration of solutes at the surface can be written as[15]

$$C_m = C_B exp(\frac{J}{k}) \tag{2.5}$$

The mass transfer coefficient is significantly affected by hydrodynamic of the sys-

tem, it is related to Sherwood number (Sh). Sherwood number is the ratio of convective to diffusive mass transport, it can be correlated with Reynolds number and Schmidt number as

$$Sh = \frac{k * d_h}{D} = a1 * Re^{a2} * Sc^{a3} * \left(\frac{d_h}{L}\right)^{a4} \tag{2.6}$$

where Re is Reynolds number, Sc is Schmidt number, d_h is the hydraulic diameter, L is the channel length, and a1, a2, a3, and a4 are constants[14]. Reynolds number is a dimentionless number which relates inertial forces to viscous forces in the fluid system[16]. It can be used to characterise flow regimes e.g. laminar flow and turbulent flow. Reynolds number is defined as

$$Re = \frac{\rho v L}{\mu} \tag{2.7}$$

where ρ is the fluid density, v is the fluid velocity, and μ is the dynamic viscosity. Schmidt number relates diffusivity of momentum to that of mass, it can be written as

$$Sc = \frac{\nu}{D} \tag{2.8}$$

where ν is the fluid kinematic viscosity. The correlations for mass transfer in a binary rotating-fixed disc system in a closed cylinder at the enclosed fixed disc and at the enclosed rotating disc for under steady shear operation will be presented in Section 5.2.3.

2.4 Membrane fouling

One of the biggest challenge for membrane operation is the fouling of membrane. Membrane fouling leads to reduced permeate flux in constant pressure operation and increases in transmembrane pressure in constant flux operation. This reduces

productivity as well as increasing cost relating to the system downtime, membrane cleaning, and changing of membrane.

In operation, the actual flux through the membrane can only be a fraction of pure water flux as the performance is diminished by polarisation phenomena. After the steady state condition occurred, there should be no further decrease in flux, and these phenomena are reversible. But in practice, a continuous decline in flux is usually observed. This results from a decrease in hydraulic permeability which is caused by membrane fouling[11]. Fouling includes adsorption, pore blocking, precipitation, and cake formation. The type of membrane used, the feed condition, and operating condition determine the extent of fouling. In certain types of membranes, flux decline could also result from membrane compaction[11]. Moreover, fouling also alters behaviour of solute transmission [11]. Figure 2.5 shows the impact of fouling on flux as compared to concentration polarization.

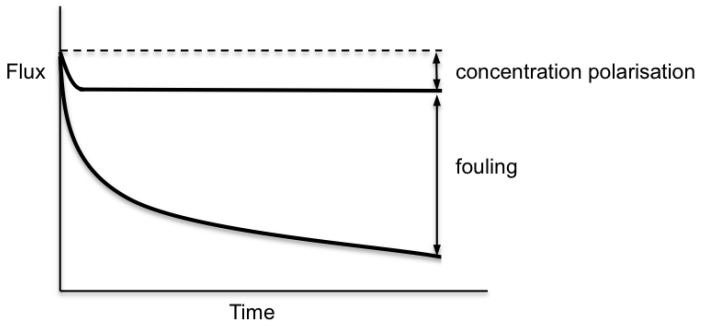

Figure 2.5: Effect of fouling and concentration polarization on flux (modified after [6])

Fouling of membranes can be roughly characterized to internal pore fouling and external pore fouling. Internal pore fouling is due to smaller-than-pore-size substances within the feed. External fouling refers to blockage of membrane pores by larger-than pore-size substances. Internal fouling has been found to cause severe fouling that is difficult to remove[17]. In several cases, the presence of large cells

within feed is beneficial as they act as filter-aid and could prevent EPS from coming to contact with the membrane[18].

External membrane fouling can involve the adsorption/deposition on the external surface of filtration membrane, resulting in elevated membrane resistance, as well as alteration of transmission characteristic of solute through the membrane[11]. This is because some pore entrances are blocked and/or constricted, and the effective membrane thickness is increased. This process is the consequence of two main mechanisms, diffusional transport to membrane and bulk convection and sieving[11]. In the former, the molecules from the bulk fluid diffuse through the fluid boundary layer to the membrane, and in the latter, the molecules 'are carried by solvent molecules to the pore entrance, where they are retained by a sieving mechanism'[11]. This is also known as surface filtration. In internal fouling, some pores are internally blocked or constricted, and pore tortuosity is altered. This results from three mechanisms, direct interception, inertial impaction, and diffusional transport to pore walls[11].

The fluid with particles larger than pore size passes through the membrane; the particles are removed by direct interception. Whereas if the particles are smaller than the pore size, they will be removed by 'bridging effect and partial occlusion of pores by the collected particles'. For inertial impaction, particles in the stream posses a certain momentum. The fluid stream consisting of the fluid and the particles passes into the membrane via 'the path of least resistance to flow, and will be diverted around the pore wall'[11]. 'Because of their inertia, the particles will tend to continue in the previous established flow direction and impact upon filter medium[11]. Diffusion interception mechanism is more relevant to gas filtration[11].

Fouling is highly influenced by feed velocity or shear stress at the membrane surface. Deposited material could be sheared off by generating high shear rates at the membrane. This leads to a reduction in the hydraulic resistance of the fouling layer. Increasing fluid velocity or the recirculation rate and/ or decreasing flow channel dimensions are the most common method of minimising the thickness of

fouling layer[11].

2.4.1 Factors affecting membrane fouling

Fouling of membrane is extremely complex, it is a result of deposition of colloids, macromolecules, salt or particles within the membrane pore or on the membrane surface. Type of fouling is dependent on the membrane process and nature of foulants[19]. Physicochemical factors affecting fouling can be divided into three categories[20]

1. Membrane properties or morphology: membrane materials, porosity, morphology, membrane hydrophobicity, charge, membrane molecular weight cut-off and membrane pore size.

2. Feed contents: feed species, feed concentration, feed characteristic, ionic strength and pH.

3. Hydrodynamic conditions: flux, crossflow velocities, temperature, module design, and operating conditions.

2.4.2 Foulants

Fouling is largely affected by the type of foulants contained within the feed. Foulants can be categoried based on its size into macromolecules and particulates. Macromolecules can be subdivided into humic acid substances, polysaccharides, and proteins. Mixtures of these substances often occur in natural feed. For examples ground water generally contains Natural Organic Matters (NOM), which consists of humic substances, amino acids, polysaccharides, lipids, lignins, waxes and organic acids. The presence of bacteria or algae and their secretion is common in surface water. The fouling behaviour of such mixed suspensions can be drastically different from that of single feed. And to date, the understanding of complex fouling mechanism is not well understood[21].

It is well known that fouling by the particulates depends on its concentration and size. The higher the concentration and the smaller the particle size usually lead to higher membrane resistance. This is due to larger number of particles near the membrane surface and thickening of the cake layer. Fouling by particulates is also controlled by hydrodynamic conditions. While the increase in crossflow velocity led to removal of particles especially larger ones, the more compact layer of cake due to smaller particles can lead to greater cake resistance. The colloidal cake formation is influenced by the physicochemical properties of the membrane, characteristics of colloids, the feed solution, and the hydrodynamics. Moreover the surface charge of both the membrane and the colloids governs the interactions by electric double layer[21].

The particle deformability has significant factor on membrane performance because softer particles leads to a more compact structure during filtration[22]. Cake layer formation during soft colloid microfiltration started by deposition and rearrangement of the molecules on the membrane surface which cause increases in resistance due to pore blocking[23]. After the first layer of deposition has been formed, the formation of the cake layer occurred. This causes rapid increase in resistance and decreases in porosity of the cake. Since the colloid is soft and deformable, the cake formed is compressible and cake compression will cause further increase in resistance[24] The cake formed adjacent to the membrane surface has a compact skin layer with approximate thickness of only about 10-20% of the cake thickness but its resistance is about 90% of total resistance[24]. Gradual increase in resistance occurred afterwards due to loose packing of further deposition[24]. During filtration of dextran-MnO_2, a deformable soft-swollen dextran material, the cake compression occurred throughout experiments even if pressure remained constant[25]. The rejection was 100%[25].

Fouling by macromolecules is dependent on macromolecule-macromolecule interactions and macromolecule-membrane interactions[21]. Macromolecule-membrane

interactions mainly refer to adsorption of the solutes to the membrane. This effect is more significant when for membrane and solutes with high hydrophobicity. Adsorption mechanism often consists of more than one type of interaction, these include protein-membrane, membrane bound proteins and solution interactions[26]. Abruption of the structure of the bound proteins due to protein-membrane interactions is assumed to be responsible for extensive membrane fouling[11]. The adsorbed layer also alters the conformation and chemical properties of membrane surface chemistry[27]. The resulting changes in membrane surface roughness, hydrophobicity and charge can lead to further modification of filtration characteristics[21]. Macromolecule-macromolecule interactions are capable of alteration of fouling mechanisms and specific membrane resistance. In the mixed feed suspension, the presence of much smaller solutes such as proteins in alginate suspension can result in lower alginate transmission[28]. The BSA-alginate cake resistance was slightly lower than pure alginate cake which indicates that the lower binding of mixed feed[21]. Solution chemistry such as ionic strength, pH, and metal ion concentration significantly influence fouling of membranes[21]. Decreases in electrostatic interactions between Humic acid molecules can be achieved by increasing the ionic strength or lowering the pH[21]. The presence of metal ions in the feed containing extracellular polysaccharide or natural organic matters may lead to crosslinking of the molecules or changes in molecular conformation[21].

The fouling mechanism for mixed suspension is more complicated than that of single feed. Influence of polydispersed particles on fouling is dependent upon the fouling mechanism. The presence of small macromolecules together with larger particulates may lead to the filter-aid or over clogging situation[18]. Larger particles can be beneficial while in other cases it can lead to elevated transmembrane pressure. For mixed suspensions, depositions of larger particles which occur at above the critical flux form a barrier that prevent smaller substances from depositing onto the membrane surface. This refers to the 'filter-aid' situation where the cake layer

of large particles acts as secondary membrane so as to benefit the overall filtration performance[18]. In this case, it has been reported that membranes can be easier to clean when operating at above critical flux than at sub-critical level[29]. Under sub-critical conditions, Hughes et al.[18] has observed overclogging situation during unwashed yeast filtration through 0.1μm membrane, while significant difference during washed-unwashed yeast filtration through 0.2μm membrane was not found.

The feed containing microorganism generally consists of both macromolecules and particulates. The situation here became more complex as the effect of the solution chemistry and environment on microbial behaviour should also be considered. The fouling characteristic is largely dependent on the cake layer, which is commonly compressible. Compressibility of microbial cake occurs as a result of particle rearrangement or particle deformation[30]. This alters porosity of the cake and particle-fluid interface area[30]. The ratio between crossflow velocity and permeate flux has been found to directly affect rod-shaped cell orientation during filtration, hence changes in cake porosity[30, 31]. Operating pressure alter specific cake resistance irreversibly for powder cake, however for microbial cake, reversible cake compresibility has been observed[30, 32]. Meireles et al. reviewed that specific resistance of the yeast cake from literatures was pressure dependent for pressure range 0-400kPa, and Carman-Kozeny equation for Stoke flow through granular bed with similar particle size as the yeast cells predicted much lower cake resistance than experimental values[32]. Cake compressibility was believed to be due to greater particle contact as a result of particle rerangement and deformation[32]. Cake compressibility constant differs depending on the yeast type, and it was not due to the shape or aspect ratio of the deposited cells[33, 30]. "Compact skin layer" occurred adjacent to the membrane surface, and this was assumed to be "due to the mass of particles"[32]. It is important to note that the area adjacent to the membrane surface is the location where the compressive pressure was greatest[32]. Influence of pressure on fouling by yeast EPS was not considered in their paper.

The procedure for treating the microbial cells prior to filtration may also affect filtration performance. Increases in pellet porosity with time has been found when the pellets , i.e., the cells, are left in the supernatant after centrifugution[30]. The behaviour of microbial cells are complex and changes in porosity of the pellets is likely to result in altered filtration performance, it is therefore essential that the exact procedure was used each time prior to filtration. And this may explain variation in filtration performance for washed yeast cell suspension found in literatures. Alteration of pH of the microorganism feed lead to changes in filtration performance because surface properties of the cells can change as pH and ionic strength were altered[34].

Pretreatment can alter the membrane performance by affecting the feed particle deformability. Recently the influence of particle deformability of modified yeast suspension during filtration in dead-end mode has been observed[35]. Pretreatment of yeast with glutaraldehyde resulted in changes in deformability of the yeast. It was concluded that the softer particles led to greater pore blocking hence a more severe flux decline, while the increase in particle rigidity would lead to improved membrane performance[35]. Nevertheless glutaraldehyde is known to seal ions by crosslinking the membrane proteins[36], and alteration of cell environment directly affects the amount of soluble component in the feed and hence changes in the fouling characteristic.

2.4.3 Resistance model

The basic equations for resistance model can be modified to allow the effect of concentration polarisation and fouling. A simple and commonly used method involves the use of resistance-in-series, this is known as membrane hydraulic resistance model[6]. Membrane hydraulic resistance model includes the influence of fouling by addition of fouling resistance to the original equation. This method needs constants to be obtained experimentally[6]. Total membrane resistance can be written as

$$R_{To} = R_m + R_f \tag{2.9}$$

where R_m is the intrinsic membrane resistance, R_f is the total fouling resistance, and R_{To} is the total membrane resistance. Using Darcy's law, flux becomes

$$J = \frac{\triangle P_o}{\mu \left(R_m + R_f\right)} \tag{2.10}$$

where $\triangle P_o$ is the overall transmembrane pressure, and μ is the viscosity. Fouling resistance is the sum of fouling resistance by different fouling mechanism. R_f can be written as

$$R_f = R_{cp} + R_{ad} + R_{pb} + R_{cl} \tag{2.11}$$

where R_{cp} is the resistance of concentration polarisation, R_{ad} is the adsorption resistance, R_{pb} is the resistance due to pore blocking, and R_{cl} is the cake layer resistance[3].

Where the concentration polarisation layer resistance, which consists of the resistance of gel-polarized layer and associated boundary layer, is a function of applied pressure. R_{cp} can be written as

$$R_{cp} = \phi \Delta P_T \tag{2.12}$$

where ϕ is a function of the variables affecting mass transfer properties in the system[6].

2.4.4 Classic modes of fouling

The increase in transmembrane pressure during constant flux filtration or reduction in permeate flux during constant pressure filtration is the result of deposited particles in or on the membrane surface[4]. For microfiltration of particles in col-

loid size range, the size and shape of the foulant are the major factors determining fouling mechanism[4]. Deposition of foulants within the membrane pores by smaller particles can slowly but eventually result in pore closure[4]. Blockage of pores may be caused by particles with similar size to the pore size[4]. Cake layer on the membrane surface can be formed by particles with larger dimension than the membrane pore size[4].

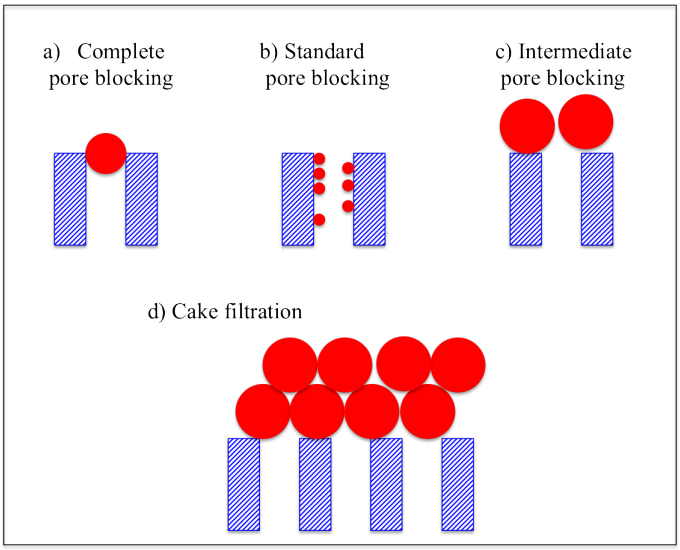

Figure 2.6: Fouling mechanisms of porous membranes [37]

Fouling can be classified into four categories based on the size of the foulant and the membrane pore size. These are demonstrated by Figure 2.6. Particles of comparable size to the membrane pore may result in complete pore blockage resulting in a lessening number of pores, while smaller solutes will result in pore narrowing. For mixed suspension where both larger-than-pore and smaller-than-pore size particles are presented together, transmission of smaller particles occurred at the beginning[4]. However, these smaller particles can be retained within the cake later on[4]. For compressible cake filtration, the cake may contain deformable particles, it has non-uniform cake structure and has a tight skin layer adjacent to the membrane which causes severe flux decline or TMP increase[35]. In general,

constant flux blocking law uses Darcy's law with the modified initial pore area to compensate for the obstruction caused by foulants[38]. These are summarised in table 2.3 and 2.4.

2.4.5 Critical flux

Fouling of membrane can be influenced by permeate flux, concentration polarisation, pH, salt concentration, feed concentration, protein aggregation, and protein denaturation. Critical flux is defined by the level of flux where fouling is minimal. 'The critical flux hypothesis is that if on start up of a membrane operation, flux is controlled there exists a critical flux below which a decline in flux over time does not occur'[41]. In microfiltration experiments, it is possible to operate at a constant flux while maintaining the transmembrane pressure. The fouling occurred was also slight or negligible[41]. As transmembrane pressure is increased, fouling layer accumulates, and flux declines. This decrease in flux is not generally reversible even if transmembrane pressure is then lowered to the previous value.

Critical flux is one of the most important and widely used concepts for fouling control since its establishment in 1995[41]. Recently, Scopus reported that it has been cited 506 times since 1996[42], with 51 citations in 2012. This shows significance of critical flux concept on fouling control of membrane filtation systems. Moreover it also indicates that fouling control is still an ongoing research topic in this area. The definition of critical, threshold, and sustainable flux will be clarified in this section.

Critical flux is defined for crossflow mode as "a flux below which a decline of flux with time does not occur; above it fouling is observed"[41] . It is later clarified as "the flux at which fouling is first observed for a given feed concentration and given crossflow velocity"[29], it is "a criterion for the transition between concentration polarisation and fouling" on the system as a whole[43]. In constant flux operation, the increase in transmembrane pressure due to fouling is negligible if the system

Type of fouling	Expression for TMP		Relation between P and V
	$\triangle P$	$\triangle P = fn(\triangle P_0)$	$\frac{d(\triangle P)^2}{d^2V} = k_1 \left(\frac{d(\triangle P)}{dV}\right)^{n_1}$
Nature of equation	$R_m * \mu_p \frac{Q}{A_0}$ (2.13)	$\triangle P_0$ (2.14)	$k_1 = 0,\ n_1 = 0$
Pore blocking[38]			
Complete pore blocking	$R_m * \mu_p \frac{Q}{A_0 - \sigma V}$ (2.15)	$\frac{\triangle P_0}{1 - (\frac{\sigma}{A_0})V}$ (2.16)	$k_1 = 2\left(\frac{\sigma}{A_0 \triangle P_0}\right)^{\frac{1}{2}},\ n_1 = \frac{3}{2}$
Standard pore blocking	$R_m * \mu_p \frac{Q}{A_0(1 - 0.5K_sV)^2}$ (2.17)	$\frac{\triangle P_0}{(1 - 0.5K_sV)^2}$ (2.18)	$k_1 = \frac{3}{2}\triangle P_0^{-\frac{1}{3}} K_s^{\frac{2}{3}},\ n_1 = \frac{4}{3}$
Intermediate pore blocking	$R_m * \mu_p \frac{Q}{A_0 * exp(\frac{-\sigma V}{A_0})}$ (2.19)		$k_1 = \frac{\sigma}{A_0},\ n_1 = 1$
Cake filtration[39];			
Incompressible cake filtration	$(R_m + \frac{\alpha^* C_b V}{A_0}) * \mu_p \frac{Q}{A_0}$ (2.21)	$\triangle P_0 + K_c V$ (2.20)	$k_1 = 0,\ n_1 = 0$
Linearly compressible cake		$\frac{\triangle P_0 + K_c V}{1 - K_c n_2 V}$ (2.22)	$k_1 = 2K_c^{\frac{1}{2}} n_2 * (1 + n_2 \triangle P_0)^{-\frac{1}{2}},\ n_1 = \frac{3}{2}$
Powerlaw compressible cake			N/A
Compressible cake with T_c [a][40]	$(R_m + \frac{\alpha^* C_s Q t}{A_c}) * \mu_p \frac{Q}{A_c}$ (2.23)		$n_4 = \gamma_1 G + \gamma_2$

[a] T_c refers to time dependent consolidation effect. When flux is maintained, creep consolidation across the whole cake is assumed, and G(shear rate) is below critical shear rate for cake disturbance.

Table 2.3: Summary of constant flux pressure equations, part 1 (modified after [39, 38, 40])

Type of fouling	**Nature of fouling**	**Comments**
Pore blocking[38]		
Complete pore blocking	Lessen numbers of pores	
Standard pore blocking	Pore narrowing	; $K_s = \frac{2c}{\pi r_0^2 LN} = \frac{2c}{L\varepsilon A_0}$
Intermediate pore blocking	Clogging at pore entrance	
Cake filtration[39]; $\frac{d^2t}{d(\triangle P)^2} = k\left(\frac{dt}{d(\triangle P)}\right)^n$	Increased R due to cake growth	$K_c = \frac{\mu_p Q c_b \alpha *}{A_0^2}$
Incompressible cake filtration	: pressure independence	α^* independent of pressure
Linearly compressible cake	: linear pressure dependence	$\alpha^* = \alpha_0^*(1 + n_2 \triangle P)$
Powerlaw compressible cake	: power law pressure dependence	$\alpha^* = \beta * \triangle P^{n_3}$
Compressible cake with T_c [a][40]	See note*	$\alpha^* = \alpha_0(1 - e^{-\frac{t}{\tau}}) * \triangle P^{n_4}$

Note: [a]T_c refers to time dependent consolidation effect. When flux is maintained, creep consolidation across the whole cake is assumed, and G (shear rate) is below critical shear rate for cake disturbance.

Table 2.4: Summary of constant flux pressure equations, part 2 (Modified after [39, 38, 40])

operates at below the critical flux.

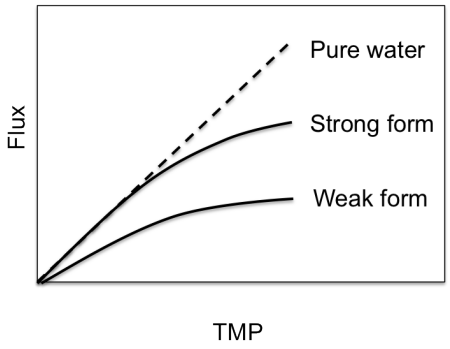

Figure 2.7: Strong and weak form of critical flux (modified after [41])

Critical flux can be divided into 3 classifications, strong form of critical flux (J_{cs}), weak form of critical flux (J_{cw}), and Critical flux for irreversibility (J_{ci})[43]. Strong form of critical flux refers the permeate flux at which the J-TMP curve starts to deviate from that of clean water. Weak form of critical flux refers to the permeate flux at which the irreversible fouling occurs. The Strong form of critical flux therefore discriminates no fouling to any kind of fouling. The weak form of critical flux occurs during filtration with rapid initial fouling due to adsorption[44]. Critical flux for irreversibility discriminates between reversible fouling and irreversible fouling. Definitions of critical flux is summarised in Figure 2.5.

Definitions	**Abbreviations**	R_{To} **below** $=$	R_{To} **above** $=$
Strong form of critical flux	J_{cs}	R_m	$R_m + (R_{rev} + R_{irrev})$
Weak form of critical flux	J_{cw}	$R_m + R_{ads}$	$R_m + R_{ads} + (R_{rev} + R_{irrev})$
Critical flux for irreversibility	J_{ci}	R_{To} where $R_{irrev} = 0$	R_{To} where $R_{irrev} > 0$

Table 2.5: Definitions of critical flux (modified after [43])

Threshold flux is the flux "at or below which a low and near constant rate of fouling occurs but above which the rate of fouling increases markedly"[29], i.e., it

is the flux that distinguishs low from high fouling rates. The term "critical flux" commonly used in literature indeed refers to this "threshold flux" as a zero rate of TMP rise can hardly be seen in practice. The concept of threshold flux is therefore more applicable especially for direct mode of operation (semi dead-end) as used in the water industry. Nevertheless the concept can be applied to both filtration in crossflow and dead end mode[29].

Another concept that has been used especially in industries where fouling occurs throughout, even at low flux operations, is the concept of sustainable flux. Sustainable flux can sometimes be regarded as economically sustainable flux or "net flux that can be maintained using mechanical and chemical enhancing means to meet an operation cost objective over the project life of the membrane"[45][29]. Above sustainable flux, a sharp increase in fouling rate occurs, below this flux exists a slow sustainable level of fouling. The optimal flux changes with energy prices and membrane costs when the system's overall productivity is considered[29]. It is therefore not surprising that sustainable flux can be chosen to be above the threshold flux providing that the fouling can be removed easily at an acceptable frequency[29].

2.4.5.1 Factors affecting critical flux

The main factors affecting critical flux include membrane pore size, particle size, and the level of shear. Although larger membrane pore size generally means a lower membrane resistance, one should note the influence of membrane pore size to solute ratio[46]. In the filtration of a model colloid[46], critical flux was found to decrease as membrane pore size increased.

It is widely accepted that higher shear within the system generally will result in lower deposition on the membrane surface hence better filtration performance. Gesan-Guiziou et al. considered that critical flux was the result of the balance between convective force on particles towards the membrane and back-transport[47]. The critical parameter was defined as $\frac{J_c}{\tau_w}$, below this value should lead to no particle

deposition and high stable filtration performance[47]. This parameter was considered more appropriate than $\frac{\triangle P_{crit}}{\tau_w}$ as $\frac{J_c}{\tau_w}$ is independent of initial membrane resistance and membrane pore size.

The effect of shear on critical flux is also dependent on the size of particles. This is because the back transport mechanism of solutes due to shear is mainly governed by particle size. For particles in the smaller size range the removal of particles relies more on Brownian diffusion than other mechanisms. As particle size increases the back transport mechanism becomes more dependent on shear-induced diffusion and inertial lift. Shear-induced diffusion starts to dominate for particle sizes between 0.3μm and 10μm. For much larger bouyant particles the back transport is controlled by inertial lift. These are summarized in table 2.6.

Particle size	**Brownian diffusion**	**Shear-induced diffusion**	**Inertial lift**
10nm-0.1μm	√		
0.1μm-1μm	√	√	
1μm-10μm		√	
Buoyant particles larger than 10μm			√

Table 2.6: Back transport mechanism for particles in different size range (modified after [48])

2.5 Monitoring of membrane fouling

The main components for fouling monitoring techniques include measurement of performance and assessment of fouling[49]. The former requires pressure drop or flux information. The latter involves online, in-situ, non-invasive, and foulant composition analysis[49].

The most basic and commonly used methods for analysis of fouling during membrane filtration are permeate flux monitoring for constant pressure mode and transmembrane pressure monitoring for constant flux mode. The accuracy of these meth-

ods is largely dependent on the sensitivity of the equipments used. Increases in the rate of increase of transmembrane pressure when operating at constant flux or decreases in flux when operating at constant TMP revealed that the fouling has already taken place. In many cases, these fouling are not fully reversible after the operating condition has changed to lower flux or lower transmembrane pressure, or after membrane cleaning. Other fouling monitoring techniques were therefore employed in conjuction with the basic technique to achieve early fouling notification. These can be roughly classified to invasive and non-invasive techniques[49].

2.5.1 Invasive and non-invasive techniques

For observations using invasive techniques it is necessary that the membranes must be removed from the module. This may disturb the foulant materials or lead to loss of the samples[49]. Examples of invasive techniques for used membrane includes use of electron microscope techniques or other 3D imaging techniques. Field Emission Scanning Electron Microscopy (FESEM), Scanning Electron Microscopy (SEM), and Transmission Emission Microscopy (TEM) require drying/coating or staining of samples but are able to obtain high resolutions of samples of 0.7, 1 and 4nm respectively[49]. Environmental Scanning Electron Microscopy (ESEM) does not require sample preparation; however, slightly lower resolutions of 10-20nm can be achieved[49]. Atomic Force Microscopy (AFM) and Confocal Laser Scanning Microscopy (CLSM) are capable of producing 3D images[49]. AFM allows visualizations of morphology and adhesion characteristics of deposition which are extremely useful for fouling studies of feed containing extracellular polysaccharides. Characterization of foulant, visual observation of different foulant distributions can be achieved by using CLSM[49].

Non-invasive techniques for observation of membrane processes reveal vital fouling information during filtration without removing the membrane from the filtration module. Non-invasive observations contribute very much to greater understanding

of the phenomena because they can provide direct in-situ information with minimal sample disturbance. Non-invasive observation can be roughly classified in to two categories: Optical and non-optical techniques[50].

2.5.2 Optical and non-optical techniques.

Optical techniques make use of high magnification apparatus such as a camera or a video camera coupled with a microscope to investigate fouling of membrane or particle deposition on the membrane surface[50]. Direct in situ visualised observation on deposition of biomass under flow was accomplished by Bustnes et al[51]. In their study, Laser scanning fluorescene confocal microscopy (LSFCM) was equipped with a crossflow cell to visualise deposition and removal of solutes from domestic wastewater effluent on PET fibre[51]. The importance of "local nature of the surface geometry" on formation of deposition was emphasised[51]. Small particles were found to deposit on the surface of the fibre.

An example of low-resolution optical observations is the Projector Technique (PT). Resolution of 1mm in PT allows visualisation of foulant thickness but individual particle interactions are not possible[49]. Greater resolution optical techniques involve the use of microscopes. Examples of these include Direct Observation Through Membrane (DOTM), Direct Observation on Hollow Fibre Membrane (DO), Particle Image Velocimetry(PIV), and Membrane Fouling Simulator (MFS). Observation of particle deposition is clear in DOTM and MFS but the cake thickness is difficult to quantify in these systems[49]. The cake thickness measurement is possible in DO, but the focus around the membrane edge is still a challenge[49]. Cake thickness can also be visualised using Laser Beam Excitation, but it is not possible to observe cake structure using this technique[49].

Non-optical approaches are especially useful when visibility and resolution of the observed area are low. Non-optical approaches employ the use of more complicated systems involving various radio frequencies, electric field, or heat transfer, therefore

these methods require a complex signal processing for the analysis. Measurement of cake thickness can be done using sound waves (Ultrasonic Time Domain Reflectometry, UTDR) or infrared light (Photo-interrupt sensor). UTDR is able to detect transparent molecules without the need of foulant labelling[49]. Species of foulants could also be identified with the use of NMR imaging, CAT (computer aided tomography), as well as radiolabelling[50]. Measurement of shear force at the membrane surface can be achieved using an electrochemical shear probe, this is especially useful during filtration with bubbling application[49].

2.6 Fouling amelioration

In order to minimise membrane fouling, an appropriate membrane and operating condition for the application must be chosen[19]. Factors affecting or ameliorating fouling can be divided into 5 categories; pretreatment, membrane properties, module process, cleaning, and compaction. Pretreatment of feed prior to filtration may also be necessary in some cases, the method is selected depending on the quality of feed, quality of permeate, and the membrane performance[52]. Alteration of membrane properties can be done via modification of membranes, the common techniques used include changes in membrane hydrophilicity and preadsorption of membrane (e.g. preadsorption of hydrophilic polymers on hydrophobic membranes[53], and preadsorption of membrane with activated carbon such as powdered activated carbon (PAC) in hybrid system)[19]. Improvement of module process involves methods for reducing concentration polarization which can generally be achieved by enhancement of mass transfer coefficient[52]. Cleaning of fouled membranes can be carried out using several methods eg. mechanical, hydraulic, chemical, and electric uses. However, it is not necessary that the original membrane performance be regained but the loss of permeability with time needs to be relatively slow[52]. Compaction refers to mechanical control of deformation of the membrane structure, this is par-

ticularly important for a polymeric membrane matrix. Introduction of pretreatment will be discussed here. This will be followed by sections on membrane modification and improvement in hydrodynamics for fouling mitigation.

Pretreatment can be subdivided to physical, chemical, biological, and electrical pretreatment[52]. Physical pretreatment uses physical forces for pre-separation of solutes; examples include the use of MF and UF applications prior to NF/RO, and the use of media filter and adsorption by activated carbon for colloidal filtration and organic matter, respectively[52]. Chemical pretreatment employs the use of chemicals to alter feed characteristics. Scaling can be prevented by addition of scaling inhibitor or by adjusting pH[52]. Moreover, adjustment of pH during operation to the isoelectric point of proteins should lead to minimised fouling, whereas others recommend pH values to be adjusted far removed from the isoelectric point[6, 14]. Addition of disinfectant to remove microorganisms can be beneficial; nevertheless it has also been reported that an adverse effect occurred due to microbial reaction[52]. Pre-coagulation/flocculation can also be used as an antifouling method. Coagulation is a process to destabilise colloids by neutralising the electrical charges on their surfaces with the addition of coagulant chemicals to reduce the repulsive forces that keep them apart. Then, usually this process is followed by flocculation, which is a process of further contact and adhesion of the destabilised colloids to form larger-size clusters, called flocs. Coagulation process is thermodynamically irreversible, while flocculation is reversible. Coagulation by chemical addition to virus and NOM feed suspension has been found to improve viral removal[54]. Moreover, the removal properties of membrane increased with time due to development of cake layer of coagulated NOM and virus[54]. Chemical pretreatment by coagulant resulted in decreases in algal cake resistance by 71-86%[55], while preozonation reduces cake compressibility during algal microfiltration which led to 54% and 70% reduction in cake resistance in chemically conditioned and untreated algae respectively[55]. Coagulation prior to membrane filtration is popular due to its relatively low cost

and easy operation. This method has been proven to improve the membrane's performance and the contaminants' removal[56]. Therefore, it can further reduce usage of cleaning chemicals and hence, the subsequent formation of disinfection by-products[57].

Application of electric field has been implemented at the laboratory scale in order to control concentration polarisation. The effect of electrophoresis, electroosmosis, and electrolysis should be considered[58]. Electrophoresis refers to electrophoretic mobility which causes charged particles to migrate away from the membrane surface when an electric field is applied[58]. This is the mechanism that prevents particle deposition. Electroosmosis is important for the deposited cake. It results in changes in ion cloud at the membrane which can cause fluid movement through the membrane. The electroosmosis effect is small for hydrodynamic controlled systems and can be neglected in microfiltration[58]. Electrolysis refers to chemical reaction at the electrodes; depending on the configuration of the modules, the effect of electrolysis may alter the product or the feed suspension[58]. Pulsed electric field is found to be more efficient than a constant one[11]. Bowen and Ahmad[11, 59] found that pulsed electrophoretic filter-cake release in dead-end module with BSA was very effective. Weigert et al. has achieved nearly 4 times the permeate flux during electrofiltration[58].

2.6.1 Membrane modification

Organic and microorganism fouling are believed to be controled by interactions between membrane material and various foulants on the membrane surface. Such interactions include adsorption, hydrophobic forces, hydrogen bonding, electrostatic interactions, and van der Waals attractions[19]. Membrane surface properties have strong effects on the fouling behaviour. Thus, prevention or minimisation of membrane fouling may be achieved via modification of its surface. For instance, increasing hydrophilicity on the membrane surface can form a water layer via hydrogen

bonds[19]. This layer prevents the foulants adsorbing on the membrane surface. It is also desirable to have similar surface charge between the foulants and the membrane surface because fouling can be detered by the electrostatic repulsion forces[19]. Change of surface roughness also influences the fouling process because the surface roughness of membrane affects particle adhesion[60]. Greater fouling often happens for membrane with high roughness, as it increases the total surface area [19]. Under static conditions, it has been found that surfaces with greater roughness led to higher adhesion of nano-size particles on the surface[60]. For crossflow systems, surface roughness provides friction force which assists particle adhesion, however enhanced membrane performance with higher surface roughness has also been observed[60].

Grafting base polymeric membranes such as Polyethersulfone Membrane (PES) or Polyvinylidene difluoride (PVDF) with hydrophilic monomers is known to reduce fouling by proteins and bacteria such as E. Coli[19]. Hydrophilicity of the surface plays an important part because adhesion properties depend on both hydrophillicity/hydrophobicity of the microorganism and the membrane[61]. Adhesion to the membrane was lower for more hydrophilic cells than for hydrophobic ones[61]. Moreover, microorganism attachment for hydrophobic membrane was greater than hydrophilic membranes[61].

In contrast to previous findings, the membranes with greater hydrophobicity can also be desirable. Biological cells have been observed to deposit by either packing or elongation of cells on the channel topography[62]. Some membranes, Sharklet AF, were therefore designed to have hydrophobic surface whose topography has feature dimensions smaller than the foulant as this would reduce overall adhesion strength due to bridging effect[62]. This is because the bridging reduces the contact area between the cell and the membrane[62]. 85% reduction in cell deposition (Ulva linza zoospores) has been achieved using this method[62]. Recently, modification of membrane surface pattern using nanoimprint lithography (NIL) was capable of increasing critical flux by 19-45% during filtration of colloidal silica particle suspensions[63].

The NIL technique involves thermal embossing of polymeric film which led to alteration of surface pattern without changes in membrane surface chemistry[63]. This demonstrates the significance of the nanoscale surface pattern of membrane on mitigation of colloidal deposition[63].

Modification of membrane to include biocide substances was particularly useful for reduction of biofouling, as it can inhibit growth of the microbial at the fouling layer[61]. Addition of TiO_2 which has photobactericidal effect to the membrane has been found to increase water flux by approximately 200%[61].

2.6.2 Enhancement of hydrodynamics

Membrane performance can be enhanced by increasing mass transfer co-efficient, k, which leads to a reduction in concentration polarisation[11]. Mass transfer co-efficient in a membrane module is controled by the hydrodynamic condition[11]. Generally, it is more dependent upon the Reynolds number in the turbulent region[11]. Increases in hydrodynamics can simply be achieved by increasing crossflow velocity or shear rate[11]. Increasing cross-flow velocity will result in an increase in mass transfer coefficient as well as a decrease in concentration polarisation within the stagnant film. Hence the permeate flux is enhanced in constant pressure operation or a lower rate of increase of transmembrane pressure is observed in constant flux operation[11].

Introduction of shear increases back diffusion and may give rise to turbulence; the cake properties are also altered[64]. Fouling characteristics under the influence of shear is different to that in dead-end mode[29], while the increase in shear leads to significant reduction in cake thickness and possibly a slight increase in cake porosity due to strong agitation[64]. The influence of polydispersity or selective packing due to particle size results in the cake with smaller particle size[64]. The cake with smaller particle size can lead to greater cake resistance[64], but the reduction in the cake thickness may overcome this increase in resistance[65].

For polydisperse feed such as microbial suspension, crossflow velocity plays important roles; crossflow operation can result in greater cake resistance that that under dead-end mode[66]. It has been found that at higher crossflow velocities, the steady state flux was lower even though there was thinner cake height[65]. The increase in specific cake resistance is assumed to be due to higher affinity for smaller particle depositions[66]. Inertial lift is greater for larger particles than for smaller particles under the same velocity. This resulted in more deposition of smaller particles and elongated particles as they are less likely to roll off[66]. These effects lead to higher specific cake resistance. It has been suggested that in crossflow filtration, crossflow velocity and membrane resistance could determine the specific cake resistance[65].

Increases in crossflow velocity usually result in lower hydraulic resistance, due to decreased amount of deposits on the membrane[67, 68], but as a certain crossflow velocity can be more effective at removal of larger particles while leaving the smaller particles behind causing increased membrane resistance due to the formation of a less porous cake[67, 68, 69], there may be an optimum velocity. Increases in crossflow velocity resulted in lower specific resistance until a minimum value was reached; further increases in shear no longer affect specific resistance[70]. However, for feed with higher concentration, increase in specific resistance was found when crossflow velocity exceeded a certain value[70]. Moreover, the influence of high crossflow velocity on the transport of small solutes through the membrane is not well understood. It is therefore essential to control shear stress to an appropriate level, as greater amount does not always lead to better membrane performance[67, 70].

Crossflow velocity (v) has significant effect on mass transfer coefficient (k)[11]. Typical relationships between k and v are as follows.

$$k \propto v^n \tag{2.24}$$

where n = $\frac{1}{3}$ or $\frac{1}{2}$ for laminar flow and n =$\frac{1}{8}$ for turbulent flow. Hence increasing

the degree of turbulence in the system would lead to improved membrane performance. However enhancing the permeate flux by increasing cross-flow velocity is not the most cost effective approach; it is limited by constraints such as capacity of the pump used and the pressure drop across the module[11]. Equipping the system with a variety of turbulence promoters, for example modified spacers required for the stability of the modules in plate-frame and spiral wound modules, can enhance turbulence without excessively increasing the pressure drop.

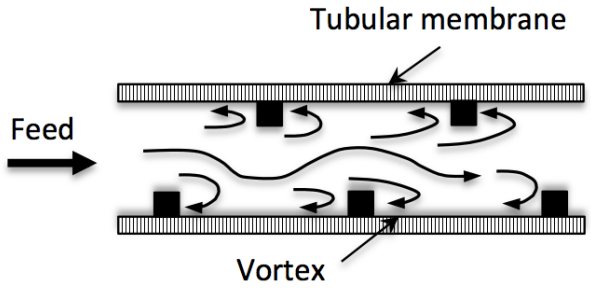

Figure 2.8: Improving membrane performance by buffles and inserts (modified after [11])

Turbulence enhancement can be done by increasing the Reynolds number in the system in order to introduce flux enhancement and increase the rate of forced convection. The optimum position of the turbulence promoters depends upon the flow condition in a particular system. With turbulence enhancers, membrane modules can produce the same flux at a reduced crossflow velocity, while operating at the same or a lesser amount of pressure drop, compared with those without. Hence, at the same operating flux, the modules with spacers consume lower energy per unit of permeate than those without. Baffles and tube inserts, a schematic picture of which is shown in Figure 2.8, are also used to create turbulence by creating good local mixing especially at the membrane surface area[11]. This increases the mass transfer coefficient which results in a reduced concentration polarisation and improved

membrane performance[11, 71, 72, 73, 74, 75, 76, 77].

Increases in mass transfer in a filtration module can also be achieved by modification of flow patterns. Enhancement of the heat and mass transfer and modification of the laminar-turbulent transition can be achieved with the use of pulsed flow or pulsatile flow[11]. With pulsatile flow, the time averaged permeate flux is higher than with continuous flow[11], this is shown in Figure 2.10b. This flux enhancement method was used by several researchers[11, 78, 79]. Moreover, it can be used in conjunction with a mechanically modified system such as the tube flat dimpled/furrowed membrane or baffled tubular membranes[71] to further reduce concentration polarisation and fouling. The pulsatile flow also increases the distance of migrated solid particles from the wall, while shifting 'the maximum velocity under laminar flow conditions towards the wall region', i.e., resulting in a disruption of concentration polarisation layer development[11]. In summary, the enhanced flux is the result of 'induced backflushing and shear-rate changes'[11]. It has been observed that there is 'an optimum range of frequencies and pulse duration' for the different systems[11].

Pulsed flow can be attained by several methods, such as changing the volumetric flow rate and introducing various mean of vibrations, for example, 'a porous plate above the membrane surface, pump vibration, or ultrasound'. Several researchers [11, 80, 72, 81, 82, 83] have observed the positive influence of the oscillatory feed flow on filtration systems. It is believed that oscillatory feed flow reduces membrane fouling and intermittently disrupts concentration polarisation[11]; as a result, filtration performance is enhanced.

Another recently developed technique involves the use of rotating or vibrating membranes. Enhancement of Reynolds number without increasing the flow rate can also be done by the use of dynamic filtration systems. These systems can be used for several filtration types including ultrafiltration and microfiltration. The dynamic filtration systems are capable of generating very high shear rate up to the order of $10^5 s^{-1}$[84]. The shear can be generated at the membrane itself, or at the surface

adjacent to the membrane surface. Dynamic filtration is known to benefit membrane performance by reducing concentration polarization and fouling[84]. The complexity of the modules, the small membrane area, and the costs and energy required are the main limitation of dynmic filtration[84, 11]. The dynamic filtration systems can be roughly divided into two types depending on the shear used, these are rotating and vibrating systems.

The two main construction types of rotating filtration systems are rotating cylindrical type and rotating disk systems, Schematic drawing of these are shown in Figure 2.9. The former consists of rotating cylindrical membranes inside a concentric cylindrical housing[84]. The Taylor vortices are created at the annular space between the membrane and the housing which result in greater shear rate. This type of membrane system has been used for blood purification[84]. The rotating disk systems consist of rotating disks with stationary membranes or stationary disks with rotating membranes. Multi-disk systems have been employed in commercial rotating disk systems with stationary membranes in order to increase capacity and membrane area. These are mostly used for treating pulp and paper effluents or pigment recovery[84].

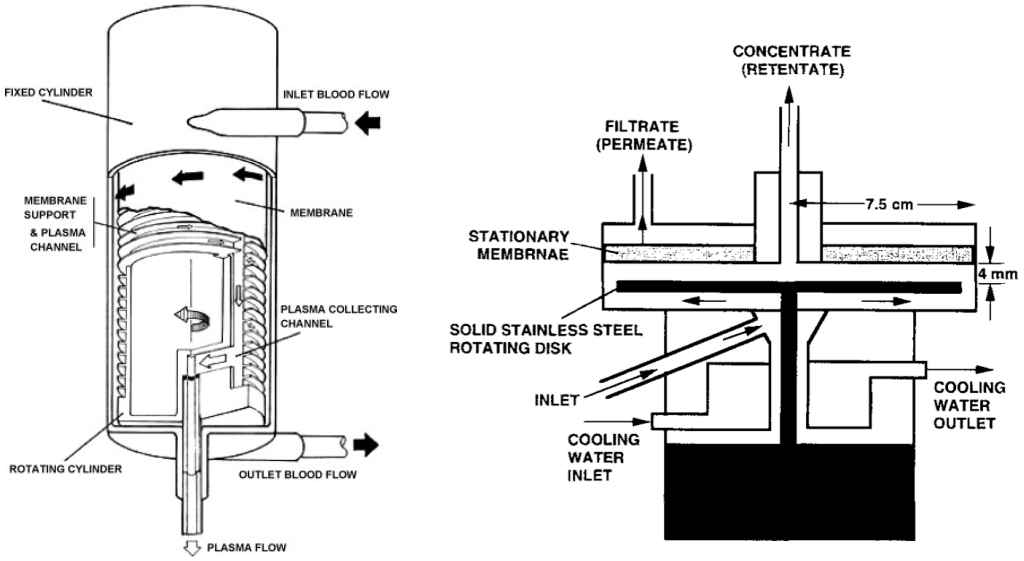

(a) Rotating cylindrical filter for plasma collection from donors (reproduced with permission [84]).

(b) Single stage rotating disk dynamic membrane filter system (reproduced with permission [85])

Figure 2.9: Schematic drawing of a rotating cylindrical system (a) and a rotating disk system (b)

The first generation vibrating membrane system uses flat sheet membranes and is known as Vibratory Shear-Enhanced Processing or VSEP[84]. VSEP consists of a stack of azimutual oscillating membranes that are separated by the gaskets and permeate collectors[84]. The frequency used for the VSEP is approximately 60Hz which is its resonant frequency[84]. The main advantages of VSEP include improved membrane performance and its ability to withstand high operating pressure (40bar). 85% enhancement in flux during microfiltration of yeast has been achieved[86]. Permeate flux during ultrafiltration of humic subtances increased by 50% when VSEP was employed[87]. Generally increases in vibration displacement of VSEP led to improved membrane performance[88]. When displacement of VSEP increased from 1.25 to 2.5cm, it resulted in 50% enhancement in permeate flux for ultrafiltration of paper plant effluent[89, 86].

Later vibrating membrane systems have involved hollow fibre membrane cart-

ridges, however these operate more in laminar regimes and lower frequency has been used[84]. The maximum of 325% improvement during yeast filtration was obtained in vibrating hollow fibre system[90]. The enhancement of solute transmission has been observed during filtration with a vibrating membrane. With vibration high BSA transmission of 85% was retained even after 5 hours of filtration, while without vibration the transmission decreased with time to approximatey 55% after 5 hours[91]. Vibration also led to enhancement of fractionation of proteins from mixed suspension[91].

Gas sparging or bubbling has been used to enhance hydrodynamics in filtration modules without increasing the feed flow rate. In the gas sparging system used in ultrafiltration processes[11], e.g. [92, 93, 94, 95, 96, 97, 98], inert gas such as air and nitrogen will be injected into the feed stream in the form of bubbles. These bubbles induce secondary flow as shown in Figure 2.10a and increase the bulk flow. As a result, hydrodynamics is improved as well as the mass transfer coefficient, which in turn enhances the permeate flux[11]. The effectiveness of this method varies with the type of modules[11]; it is most effective for tubular membrane modules, reasonably effective for flat sheet tangential flow devices, and less effective in hollow fibre membranes[11]. Among two-phase flow investigated, it was found that the most effective one is the slug flow regime[11]. For flat sheet tangential flow devices, flux performance is also affected by ratio between a bubble width and the gap between the membranes[99].

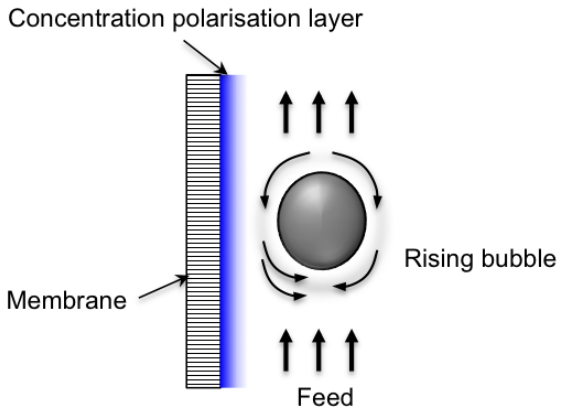

(a) Bubble induced secondary flow (modified after [11])

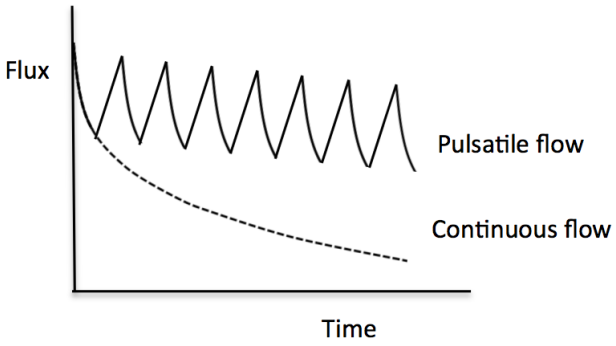

(b) Enhancement of permeate flux using pulsatile flow (modified after [11])

Figure 2.10: Bubble induced secondary flow and enhancement of permeate flux using pulsatile flow

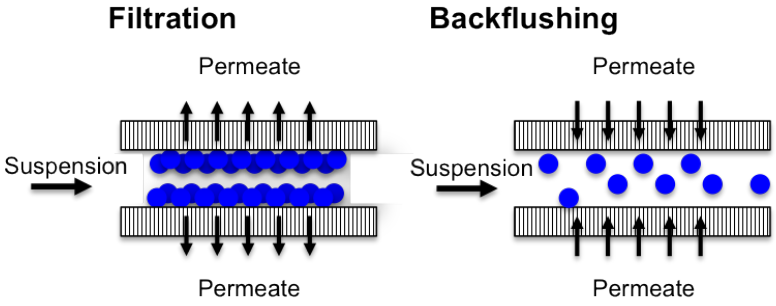

Figure 2.11: Principle of back-flushing (modified after [11])

Back flushing can be considered as a method for cleaning of membrane, but it can be employed periodically during filtration process. Back flushing or pressure pulsing method has been used[11, 100, 101, 102, 103, 104], it involves the use of 'timed pressure pulses on the permeate side in order to periodically change the direction of material flow within the pores'[11]. Its aim is the reverse of the permeate flow through the membrane in order to remove the foulants and obtain higher flux. Cake layers on the feed side will be removed or reduced, hence a reduction of the influence of fouling. It is necessary that the modules are capable of operating at high pressure if the back flushing is to be used. Moreover, it needs to be carried out periodically so as to maintain high flux. Use of backflushing in conjuction with air bubbling has been found to be more effective than increasing crossflow velocity alone. Qaisrani et al. reported 80% reduction in particle retention during microfiltration of yeast suspension when air bubbling and back flushing were used together, while increases in crossflow velocity only led to 45% reduction in particle retention[105].

In addition to the shear stress another main factor affecting separation is permeate flux. Decent filtration performance can be achieved by operating below critical flux [67]. There have been several findings relating the permeate flux and the shear stress. For example, normalised hydraulic resistance and protein transmission during crossflow microfiltration of skimed milk was found to correlate well with the ratio between permeate flux and efficient wall shear stress. Efficient wall shear stress in their study refers to the difference between wall shear stress and critical wall shear stress for erosion. There exists critical flux-efficient wall shear stress ratio values where sudden changes in normalised fouling resistance and transmission occur[67].

2.6.3 Shear quantification in various systems

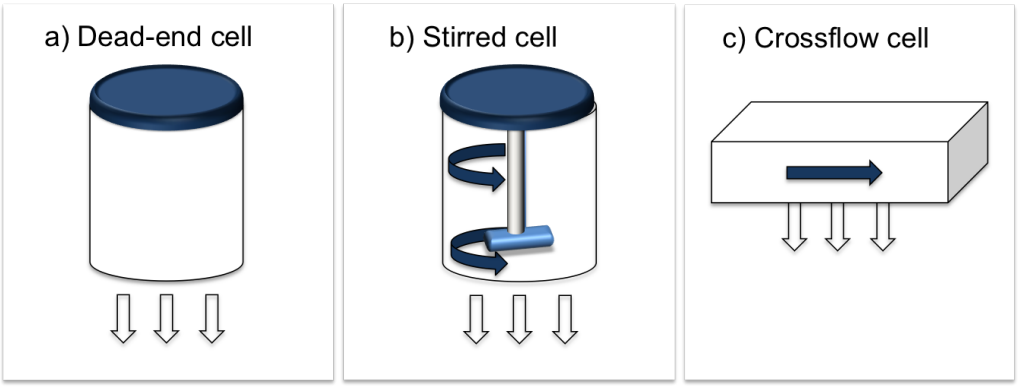

Figure 2.12: Schematic pictures of typical membrane filtration modules.

Three common types of filtration modules are illustrated by Figure 2.12(a to c), these are dead-end cell, stirred cell and crossflow cell respectively. The deadend cell is not capable of generating shear stress, and the shear stress in a stirred cell is generally non-uniform and difficult to accurately quantify. Crossflow cell allows easy to quantify shear stress level, however, the patterns and the level of shear are limited in these cells.

The shear stress in stirred cell depends upon the agitator speed, the agitator size and its position, and the viscosity of the feed[106]. Shear stress in stirred cell is therefore likely to vary from one module to another. The flow field at the base of stirred cell is divided into two regions, these are the inner region with the radial position being less than the critical radius (R_{cr}) and the outer region with the radial position greater than R_{cr}. At R_{cr} the shear stress is at its maximum. The maximum shear stress was generally found to be at 0.6-0.75 of the base radius[106].

For the inner region (r $< R_{cr}$) shear stress can be expressed as

$$\tau = \frac{0.825\mu\omega r}{\delta} \tag{2.25}$$

where δ is the momentum boundary thickness or $(\mu/\rho\omega)^{0.5}$

For the outer region (r $> R_{cr}$) shear stress can be written as

$$\tau = \frac{0.825\mu\omega R_{cr}}{\delta}\left(\frac{R_{cr}}{r}\right)^{0.6} \tag{2.26}$$

The most simple module for shear quantification is that of crossflow type. Flow in rectangular channel can be approximate to slit-die or rectangular die. For slit-die approximation, it is necessary that the channel width must be much greater than the channel height. The apparent shear rate for flow in rectangular channel using slit-die approximation is

$$\dot{\gamma} = \frac{6Q}{WH^2} \tag{2.27}$$

where Q is the flow rate, W is the channel width, H is the channel height. The apparent shear rate for flow in a rectangular channel using rectangular-die approximation yields slightly different value from that of slit-die. Son et al.[107] approximated this as the apparent shear rate times the channel aspect ratio and a function of geometric constants which is channel aspect ratio dependent

$$\dot{\gamma} = \frac{6Q}{WH^2}\left(1 + \frac{H}{W}\right) f\left(\frac{H}{W}\right) \tag{2.28}$$

where $f\left(\frac{H}{W}\right)$ is a function of geometic constants. Equation 2.28 approaches equation 2.27 when H:W ratio comes close to zero.

Dynamic membrane systems gained popularity due to their improved membrane performance by reducing cake formation and concentration polarisation[108]. The shear quantification of dynamic membrane modules is more complicated. It depends upon the module type as well as the operating condition used. The shear rate for the three types of rotating dynamic filtration systems are summarised in Table 2.7.

Other dynamic filtration systems of interest are those operating under vibrations or oscillatory shear such as the VSEP and the vibrating hollow fibre modules. The local shear rate in VSEP system[84] can be written as

Type	Shear rate	Note:
Cylindrical rotating system[84]	$\dot{\gamma}_{cr} = \frac{0.23Ta^{0.5}\omega R_{cy}}{e}$ (2.29) $\dot{\gamma}_{cr} = 0.23\omega^{1.5}R_{cy}^{1.25}e^{-0.25}\nu^{-0.5}$ (2.31)	$Ta = \frac{\omega R_{cy}^{0.5}e^{1.5}}{\nu}$ (2.30)
Rotating disk system[109, 84]	$\dot{\gamma}_{La} = C_{La}(k_{vc}\omega)^{1.5}r\nu^{-0.5}$ (2.32)	$C_{La} = 0.77$ for stationary membranes $C_{La} = 1.81$ for rotating membranes
	$\dot{\gamma}_{Tu} = C_{Tu}(k_{vc}\omega)^{1.8}r^{1.6}\nu^{-0.8}$ (2.33)	$C_{Tu} = 0.0296$ for stationary membranes $C_{Tu} = 0.057$ for rotating membranes
Cone and plate system [10, 18]	$\dot{\gamma} = \omega\,(sec\theta)$ (2.34)	

where $\dot{\gamma}_{cy}$ is the shear rate on the inner cylinder (the membrane), Ta is the Taylor number, ω is the angular velocity, R_{cy} is the inner cylinder radius, e is the annular gap, ν is fluid kinematic viscosity, $\dot{\gamma}_{La}$ is shear rate under laminar flow, $\dot{\gamma}_{Tu}$ is shear rate under turbulent flow, k_{vc} is velocity coefficient, r is the radius, C_{La} is a constant for laminar flow, C_{Tu} is the constant for turbulent flow, and θ is the half angle of the cone.

Table 2.7: Shear rate for the three types of rotating dynamic filtration systems

$$\dot{\gamma}(r,t) = (\frac{rd_A}{R_{Om}})d_A(\pi F)^{1.5}\nu^{-0.5}(cos\omega_1 t - sin\omega_2 t) \tag{2.35}$$

where d_A is the membrane displacement at radius r, R_{Om} is the outer radius of the membrane, and F is the oscillation frequency ($\omega_1/2\pi$).

2.6.4 Transport of polymeric molecules through membranes

Filtration of macromolecules, especially polymers which exist in solution as flexible coils, involves some distinct transport phenomena due to their polymeric nature such as relatively large size and flexible molecular conformation. The random motion of chain segments renders a polymer many configurations. Therefore, the measure of its dimension is usually a statistical average such as the radius of gyration, r_g.

Besides random variations in molecular shape, the flow may also induce molecular deformations in polymers[110]. These conformational changes may lead to polymers passing through pores considerably smaller than their average sizes in the bulk solution. The ratio of the size of polymer to that of the pore it approaches is often expressed as

$$\lambda = \frac{r_g}{r_p} \tag{2.36}$$

where λ is the ratio of radius of gyration to the radius of pore , r_g is the radius of gyration, and r_p is the membrane pore radius. Theoretical works on linear polymers entering a narrow channel have proposed mechanistic models in detail for several occasions.

At $\lambda < 1$, a polymer generally starts by aligning its longest axis along the channel axis without much extension along the channel. This is followed by parallel expansion of the polymer along the channel. Afterwards, the chain conformation within the channel changes to that of a random coil[111]

At $\lambda > 1$, Hermsen et al.[112] studied the random walk of a linear chain entering

a pore. Their results showed that the translation started with a small portion of the chain was stretched first into the pore while the main part was still coiled outside, at which the molecule appeared in a flower shape with the part inside the pore as a stem and that outside as the crown. When the chain reaches a certain level into the channel, an suction may occur to pull the crown fraction into the pore[113]. And once the whole chain enters the channel, it coils up again, see Figure 2.13[112]. These phenomena have also been observed under pressure gradient or flow by molecular modelling and direct UF experiments.

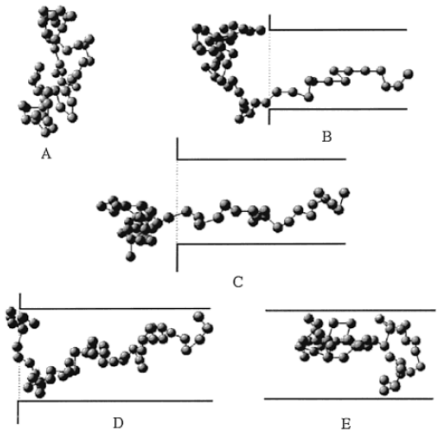

Figure 2.13: "Snapshots of various degrees of polymer penetration ϕ: (A) bulk, (B) ϕ= 28%, (C) ϕ= 42%, (D) ϕ= 89%, (E) bulk pore". (Reproduced with permission [112])

The transport of polymers through a narrow channel is significantly affected by the concentration of the polymer. At sufficiently low concentrations the polymer chains have lower probability to enter the channel. The increases in concentration lead to decreases in the polymer characteristic length. And at sufficiently high concentrations, where the polymers' characteristic length becomes smaller than the pore diameter, the polymer chains will readily enter into the channel. This is known as weak-to-strong penetration transition[111]. At high polymer concentrations, the hindrance effect of polymer mobility due to chain-chain interaction can

be present[114], making the critical deformation rate lower, and the extensional viscosity increases[115].

Extensional flow or elongational flow, referring to "a flow where the velocity changes in the direction of the flow"[116], can deform the polymeric molecules subject to the flow[117]. Such flow pattern may occur at the entrance of pores in MF or UF due to the abrupt changes in area. The abrupt contraction-expansion in the flow path can result in flow instabilities; examples include unstable streamlines along the depth of the channel during flow of 0.1-0.5%PAA (Poly acrylic acid) in water, a growth of vortices upstream, and a suppression of those downstream during flow of polyehtylene oxide (PEO) solution at low concentration[114]. Furthermore, it resulted in the deposition of PEO material on the surface near the contraction throat, this deposited material was asymmetric and led to asymmetric flow [114]. It has also been observed that the abrupt contraction-expansion channel can also lead to increases in pressure drop with Reynolds number upto the point where the polymer chains reached their finite extensibility limit[114].

The transport of polymers through channels is affected by the strength of extensional flow because polymer conformation is hydrodynamically dependent[118]. There exists a critical flow rate below which the polymer can keep its coiled shape and above which the hydrodynamic force starts to elongate a linear polymer chain in a good solvent from coil to stretch[119]. Recently, this first-order transition has been observed in a UF experiment[120]. However, when the extensional flow is at extremely high strength, polymer chains can be laterally compressed to a fold formation instead of being uncoiled. In the fold formation, the polymer has higher rigidity and further chain extension proceeds slowly[121].

This fundamental knowledge on the effect of flow on variation of chain conformation by the flow has been used to explain the observations in filtration of flexible biopolymers, such as Deoxyribonucleic acid (DNA). Greater transmission of DNA was obtained at higher transmembrane pressure due to elongation or deformation of

DNA due to shear[122, 123]. Moreover, transmission of supercoiled plasmid DNA through ultrafiltration membranes was flux-dependent according to de Genne's theory, the transmission increased from zero to nearly one as flux increases[124].

Since the conformation and transmission of polymers are highly dependent on the hydrodynamic forces[118], there is a high possibility that fouling of membranes can be minimised if suitable hydrodynamic conditions are used; these will depend on the surface porosity of the membranes as well as pore size and flux. Fouling mitigation can be crucial especially for microfiltration of live feed where fouling generally dominated by polymeric substances such as extracellular polysaccharides.

2.7 Summary

The relevant literature on the membrane fouling and the influence of shear have been reviewed. The introduction of shear into a filtration system not only alters mass transfer coefficient and hence causes changes in concentration polarisation and fouling behaviour, but also leads to alterations of the macromolecule conformation. This results in changes in fouling behaviour and transmission profile. The current understanding of influence of shear on fouling and transmission is limited, especially for the mixed feed system. The optical observation on fouling of larger particulates has been carried out, but the influence of the presence of small solutes on overall fouling behavior and transmission has not been fully understood. There exists the need to observe this mechanism thoroughly in order to understand the influence of shear of fouling and transmission during mixed feed filtration. While optical techniques for analysis of membrane fouling allows direct observation of the foulant deposition, the shear within these modules cannot be precisedly controlled. The use of dynamic membrane modules such as rotating and vibrating membrane modules provides a more controllable steady shear and oscillatory shear. However, to the author's knowledge, the influence of these shear patterns on membrane performance

were carried out separately, the effect was therefore not accurately compared. There exists the need for tools which allow direct comparisons between the influence of these shear patterns while capable of operating in various shear configurations.

The study of fouling by algae in microfiltration using DOTM (Chapter 3) and the transmission of EPS and fouling in microfiltration (Chapter 4) fulfill further understanding of foulant behaviour in the mixed feed system under various conditions. The first generation of Direct Shear Stress Test Cell (DSSTC) was fabricated to allow for direct comparisons between influence of shear of various patterns on membrane fouling during microfiltration. The influence of shear patterns on fouling and transmission of macromolecules and the effect of shear patterns and EPS on fouling in microfiltration have been extensively studied with DSSTC and are presented in Chapter 5 and Chapter 6, respectively.

3 Study of Fouling in Microfiltration of Algae using DOTM

This chapter is based on the work carried out during my research visit at Nanyang Technological University (NTU), Singapore in Summer 2009. It will start with an introduction to the nature of the feed and its characteristics as these are essential to understanding the experimental results. This chapter is concerned with critical and threshold flux measurements for diluted algal suspensions and in particular with a comparison of its detection through Direct Observation Through Membrane (DOTM) observations and TMP changes. Some of these results have been published in the *Journal of Membrane Science* under the title "Microfiltration of algae (*Chlorella sorokiniana*): Critical flux, fouling and transmission" and in the *Desalination and Water Treatment* as "Transmission of and fouling by long chain molecules during crossflow microfiltration of algal suspensions: influence of shear"

This chapter will meet the following objectives

- Comparison between threshold flux obtained from transmembrane pressure data and DOTM.
- Comparison between fouling of algal cells and latex particles of similar particle size.

- Exploration of the effect of crossflow velocities on particle deposition and fouling rate in constant flux filtration when flux stepping started from sub-critical and supercritical flux level.
- Exploration of the effect of feed characteristics such as feed concentration and salt addition on particle deposition and fouling rate in constant flux filtration when flux stepping started at sub-critical and supercritical flux level.
- The effect of air bubbling on membrane performance.

Chlorella Sorokiniana was chosen as the the main feed as it represents natural occurring green algae, moreover it is relatively easy to cultivate in the laboratory. Chlorella Sorokiniana broth was harvested after 14 days of cultivation. The experimental filtration methods used were standard, but intensive testing of feed compositions revealed changes in EPS-polysaccharide content of diluted algal suspension with algae age. This resulted in differentiation of observed transmembrane pressure if, results from 1 day old algae were compared with results from 2 week old algae. Presenting the data by taking an average of results and its repeat will be inappropriate in this case. It is more reasonable and accurate that only the results from filtrations performed within days of one another are directly compared, and this is the explanation for the absence of error bars in this chapter. With the large amount of noise in the data, it is reasonable to focus on general trend and large changes in dTMP/dt rather than minor changes. For filtration of diluted live feed, it is important that one should focus on the trend rather than the exact numbers obtained from calculations.

3.1 Introduction

Membrane technology is very attractive in today's world as it often offers not only a potentially more economic but also an environmental friendly solution compared

to more established technologies. Membrane usage is particularly important in the water industries. However, fouling and cleaning of membranes is still an important issue. The presence of algae in natural water is a major obstacle in membrane operations, as it results in an increase in transmembrane pressure (TMP) or a decrease in flux (J)[125]. In desalination processes, fouling of microfiltration and ultrafitration membranes during seawater pretreatment is more pronounced during algae bloom[126]. In some cases, after an algae bloom, it is necessary for the membranes to be taken off-line and cleaned[126]. The deposition of algal cells on the membrane surface results in an increase in operating costs[125]. Many studies of algal filtration have been made, but their fouling mechanism has not been well understood. Understanding the nature and characteristics of the algae is crucial as this is the key to the interpretation of the results.

The algae used throughout the chapter are a fresh water algae called Chlorella Sorokiniana. This has been chosen as it is one of the genus that represents green algae which are commonly found in natural water[127]. Similar to many other macromolecules, they secrete extracellular polysaccharides (EPS). Members of the Chlorella genus usually inhabit a hydrosphere. The hydrosphere around the algal cells is also known as the sheath, it is believed that the substance is produced in order to aid symbiotic association as well as absorption of metal ions[128]. Generally, the sheath produced in microalgae leads to aggregation of cells in aquatic systems[128]. It provides an intermediate role for communication of cells in symbiotic association[129][130] which promotes algal growth by creating a suitable habitat[128]. For *Chlorella Sorokiniana* IAM C212, a polysaccharide gel is produced as a sheath under photoautotrophic conditions. *Chlorella Sorokiniana* was seen to have adherence to its symbionts and were bound together through the sheath produced[131]. The sheath of *Chlorella Sorokiniana* consisted of a metal and algal photosynthate[128]. Although some information regarding the symbiotic association is available, symbionts of Chlorella as well as relationships between microalgal sheath and symbiosis

are not clearly identified[128].

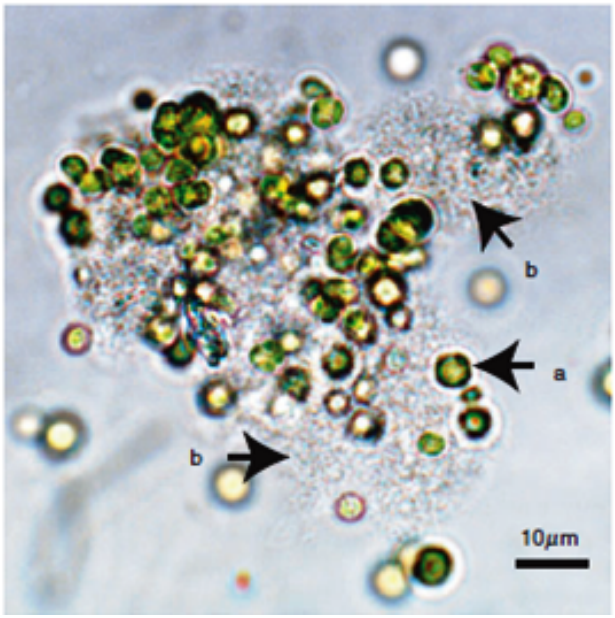

Figure 3.1: Sheath matrix produced by *Chlorella Sorokiniana* IAM-212 (a) *C. Sorokiniana* (b) sheath. (Reproduced with permission [130])

The composition of the mucilage sheath or extracellular polymeric saccharide around the algal cells has been found to consist of a variation of saccharides generated as photosynthetic metabolites, divalent cations contained in the culture medium, as well as proteins, lipids and inorganic ash[128]. An image of the sheath matrix produced by *Chlorella Sorokiniana* is shown in Figure 3.1. The EPS characteristic and productivity are affected by metal cations[128]. *Chlorella Sorokiniana* sheath can be increased by introduction of calcium chloride solution which results in coflocculation of the algae and the associated symbiotic bacteria[128]. The precipitation/sedimentation of gelatinous saccharides was found to increase as the concentration of calcium and strontium chlorides increased. However with addition of NaCl, KCl, or $MgCl_2$, no saccharide precipitation was observed even though Mg^{2+} is the major metal ion component in the sheath[130]. This may be "due to differences in the affinity between the secreted saccharide and the metal ions." [128]. Alginate gelation was influenced differently by different types of metal ions. The amount of sheath produced increased, and the cells were flocculated in the gelatinous sheath.

The saccharide concentration in the broth decreased, but this decrease is equivalent to the quantity of gelled saccharides adhering to the algal cells[128].

It has been hypothesised that amelioration of fouling can be achieved through the use of operations and transient shear; for example, crossflow velocity and air-sparging. Nevertheless for some cases such as MBRs, it has been reported that too large a crossflow velocity and/or too high an aeration rate can lead to higher overall resistances and a greater portion of irreversible fouling[132]. For algae filtration, it is known that the EPS secreted is responsible for severe membrane fouling. The specific cake resistance of membranes in Chlorella algae filtration has been found to relate directly to the amount of extracellular organic matter within the feed[133]. Moreover, Babel et al[134] found that the developed cake resistance did not vary with the membrane materials used. Chiou et al compared filtration of 3 algae species, and the species which has the highest amount of EPS fouled the membranes most severely[135]. There are a few studies on shear and algae filtration. Crossflow filtration was believed to result in better performance than dead end filtration[136]. The effects of shear on the feed stock prior to algae microfiltration and ultrafiltration have also been observed[126]. As expected, pre-shear samples with higher EPS substances led to higher membrane fouling[126]. Several algae fouling mitigation techniques have been used, these include coagulation and preozonation[137]. Nevertheless, the formation of a more compact cake as a result of the coagulants may lead to a higher fouling rate as found in bacterial floc microfiltration[138].

Greater understanding of the foulant behaviour is required for fouling mitigation. Analysis of macroscopic parameters such as transmembrane pressure and flux data as well as real time in-situ observations can reveal information in greater detail leading to better understanding of these phenomena[50]. The use of Direct Observation Through Membrane(DOTM) system allows a non-invasive optical observation of the foulant on the membrane surface. With DOTM, deposit-membrane interactions during flux stepping can be observed. A main advantage of DOTM over other

membrane observation tools, such as multiphoton microscopy[139], is that clear images can be captured without the need to stop the fluid flow. Nevertheless, it is necessary that the membranes must be transparent.

DOTM enables the first deposits to be observed and is more sensitive than an analysis of transmembrane pressure-flux data in establishing the point of the critical flux. This is because the changes in TMP are subject to sensitivity of pressure transducer as well as permeability of the deposit layer. With low sensitivity pressure transducers, the critical flux calculated from analysis of transmembrane pressure flux data will be higher than the real critical flux. Moreover, foulant adhesion and removal mechanisms can be visually observed continuously.

The optical images were used together with TMP to observe membrane fouling of *Chlorella Sorokiniana* and Polystyrene latex of similar size to the algae. Understanding the transmission of polysaccharides by the membranes is of importance in many applications including desalination and MBR operations. A brief review of transport of polymer through pore were included in Chapter 2 as they help explaining the fouling phenomena.

3.2 Materials and methods

Direct Observation Through Membrane, or DOTM, equipment is available at SMTC and was used throughout for Chapters 3 and 4. This section will outline the basic principles of DOTM, and detail membrane modules and experimental procedures used.

3.2.1 Direct Observation Through Membrane

DOTM consists of a transparent crossflow cell that is connected with a microscope so that when used with a transparent membrane particle deposition on the membrane can be observed. Particles of 1μm in size and larger can be clearly seen[140]. Suitable

choices of membrane for this equipment include the Anopore anodised aluminium membrane and the Millipore Teflon membrane[140]. DOTM was first used by Li et al. in 1998 to observe deposition by yeast cells and latex particles[141]. Information from DOTM is usually more sensitive than TMP data; it is therefore a very useful technique especially for determination of the critical flux or the threshold flux for particle deposition.

Although the deposition on the membrane surface can be clearly seen and quantified, the limitation of DOTM include difficulties in observation of concentration profile[140]. Cake layer can be seen, but quantification of thickness may not be possible.

3.2.1.1 Crossflow membrane filtration module

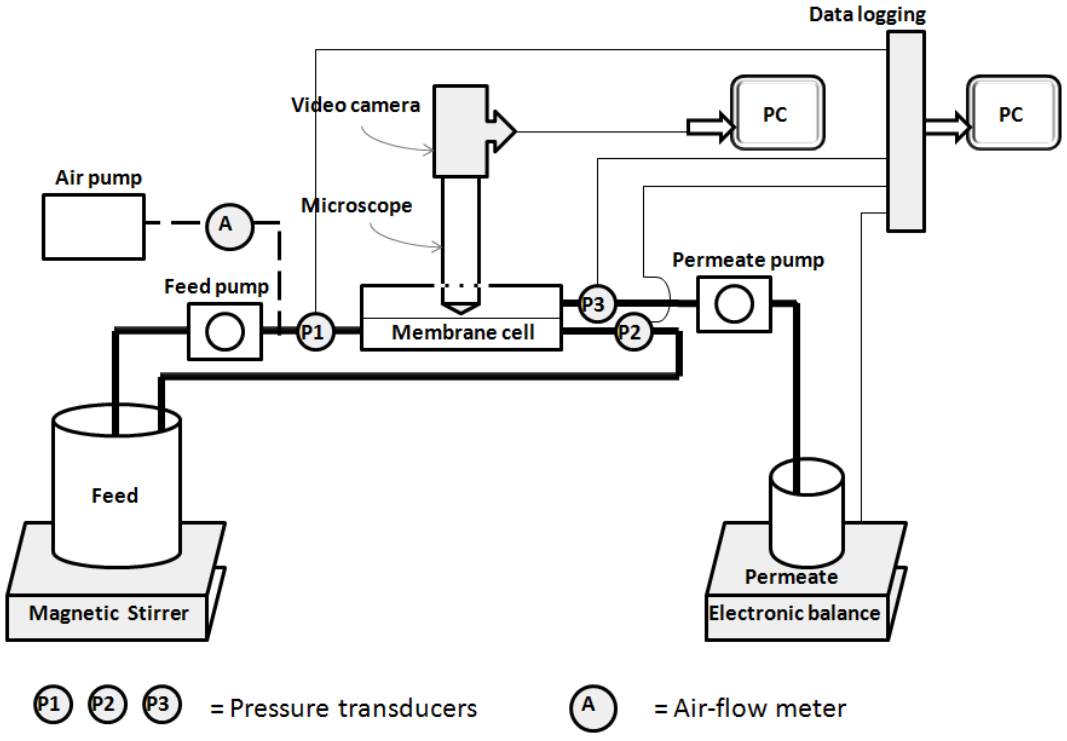

Figure 3.2: Schematic drawing of DOTM

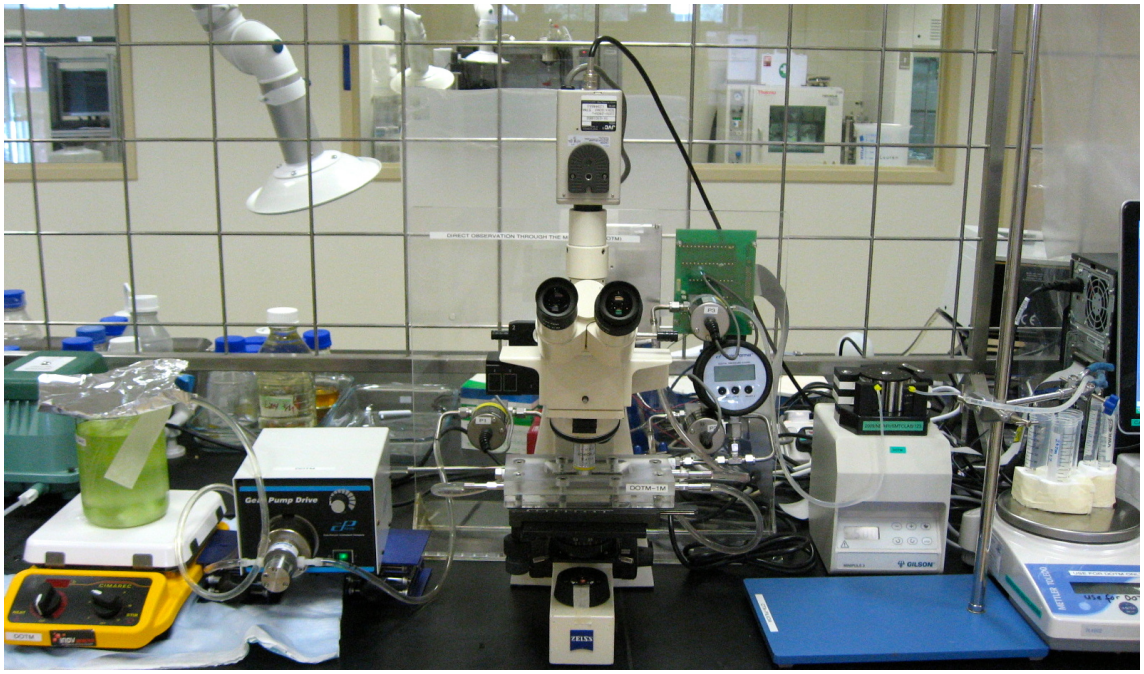

Figure 3.3: Experimental set-up of DOTM

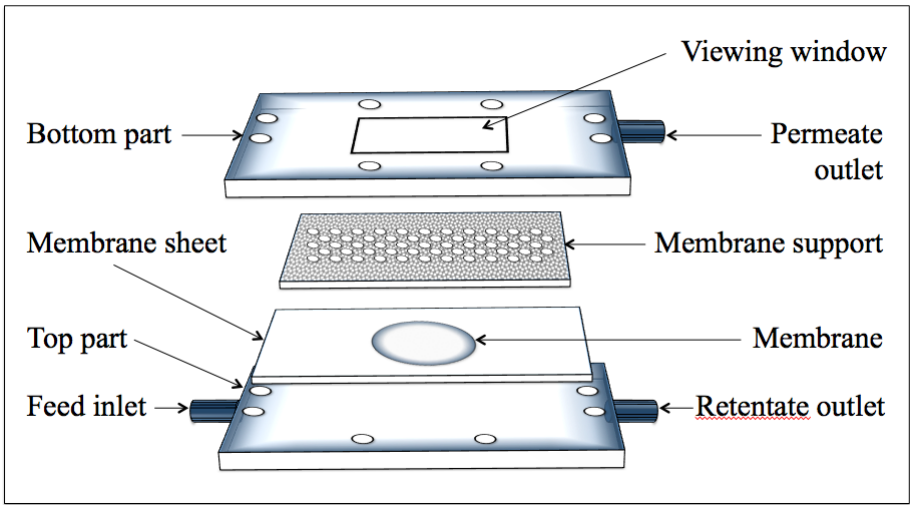

Figure 3.4: Openview of DOTM filtration module

A schematic drawing of DOTM filtration process and the experimental set up is shown in Figure 3.2 and 3.3 respectively. DOTM cross-flow filtration cell consists of a conventional crossflow cell that is made of Perspex with glass viewing window (see Figure 3.4). An optical microscope (Axiolab, Zeiss) was used to focus through the back of the membrane, and images of the membrane skin on feed side were periodically captured by colour video camera, JVC, TK-C921BEG. These images

were captured using Image pro plus software, the same software was used for image analysis. Magnification of 10x was found to produce clear images for image analysis. The transparent membranes used for image analysis experiments were Anopore flat sheet membrane from Whatman.

The orientation of the crossflow filtration cell is down so that settling of the feed material on to the membrane due to gravity is avoided. The inlet, outlet, and the permeate were connected with identical pressure transducers (Model 206, Cole Palmer). Crossflow velocity was generated by a gear pump (Gear pump drive, Cole Palmer). A peristaltic pump (Minipuls3, Gilson) was connected at the permeate side to control flux. An electronic balance (Model PL4002, Mettler Toledo) was used to measure the permeate. These data are fed to PC via datalogging system using Labview software. The feed was continuously stirred at 500rpm by a magnetic stirrer bar with magnetic coupling generated by a Barnstead Cimarec Digital Hot Plate Stirrer(Barnstead/Thermolyne). During air-bubbling experiments, an air pump (Hiblow HP-80, Techno Takatsuki) was used together with an air-flow meter.

Deionised water was used throughout, this was prepared by MilliQ system with 0.22um Millipak express (Millipore). Prior to starting each experiment, the system was flushed thoroughly with deionised water for at least half an hour.

For each experiment, a new membrane sheet was used and its water permeability was measured. All experiments operated using 100% recirculation. For analysis of organic content, a small sample was collected from the feed tank at the beginning and the end of each flux stepping. The permeate was also collected separately for each 17.5 minutes period. Flux-Transmembrane pressure measurements were collected every 10 seconds.

3.2.1.2 Development of membrane module

The original module used by Li et al.[142] had several leakages and therefore the new module was fabricated. The modules were made principally of Perspex with their

viewing windows being made of glass. A rubber gasket was used on each module together with 8 screws to hold the top and bottom part of the module tightly together. The top part of the old and new module is shown in Figure 3.5(left). It is necessary that the module contains a stable porous material to support the membrane. The membrane module therefore consists of the top part, the membrane support, and the bottom part. Figure 3.5(right) shows the two types of membrane support that were tested. The thin transparent plastic support (top right) is easy to fabricate but is too flexible resulting in movements of membrane sheet during a filtration run. This results in inaccuracy of experiments as well as breakage of the fragile Anopore membrane. The metal support (Figure 3.5, bottom right) was therefore used throughout. Unassembled DOTM module is shown in Figure 3.6.

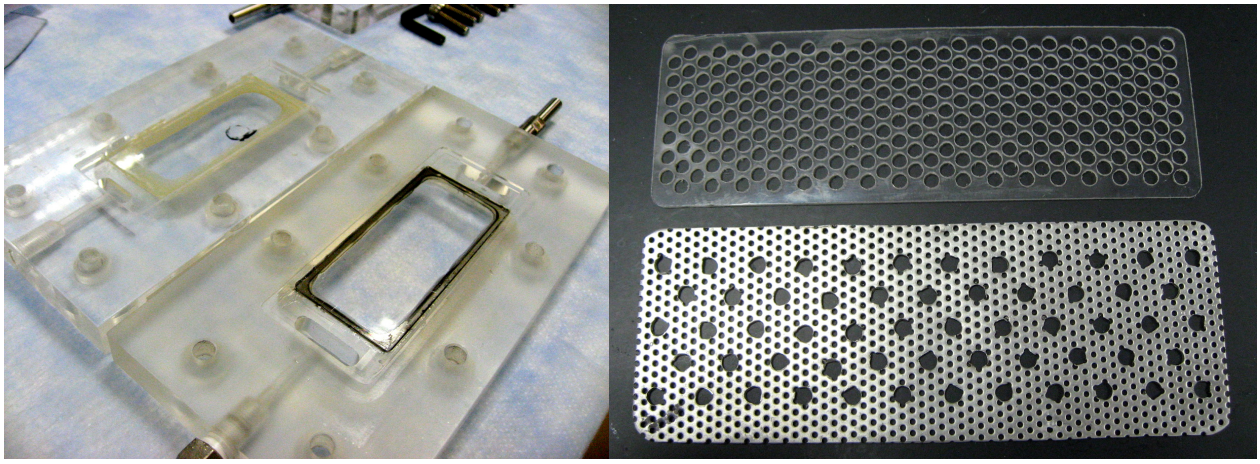

Figure 3.5: Top part of old and new filtration module (left), and membrane supports (right)

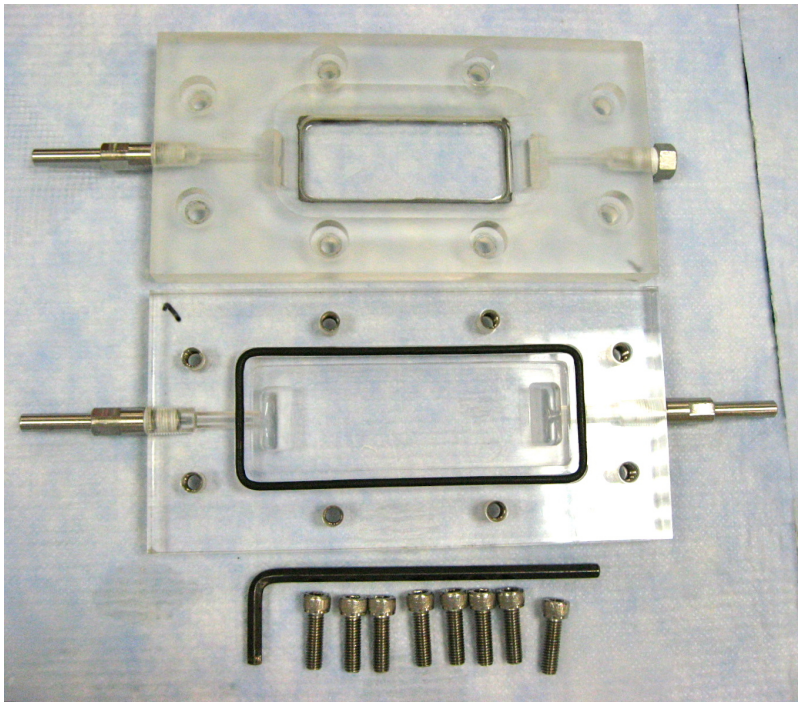

Figure 3.6: Unassembled DOTM module

3.2.1.3 Experimental Procedure for flux stepping mode

The standard experimental procedure for flux stepping experiments is stated below.

1. The membrane sheet (Section 3.2.2.2) is mounted into the module and filled with deionised water.

2. The module is then placed on the set up as shown in Figure 3.2. The filtration loops are connected.

3. The system is filled with deionised water, crossflow velocity is set, and trans-membrane pressure and DOTM of clean membrane are taken at the lowest flux.

4. The feed is diluted to the desired concentration.

5. The water reservoir is replaced with the feed reservoir. The feed pump is started, followed by the permeate pump. Crossflow velocity is carefully varied by adjusting the feed pump (Gear pump drive, Cole Palmer) to a desired level.

Care must be taken as any rapid changes will result in fracture of the delicate Anopore membane.

6. The system is kept running while the images are being taken. In order to obtain high quality images, the microscope focal length is adjusted prior to each image capture. Maximum effort has been made to keep the membrane module at the same position for all experiments. A series of images were taken 5 minutes and 15 minutes after a flux was imposed.

3.2.2 Materials

3.2.2.1 Membranes

Anopore (Anodisc) 0.2μm hydrophilic membranes were mainly used in these experiments unless otherwise stated. Anopore is a hydrophilic aluminium oxide membrane with precise, non-deformable, highly controlled, uniform capillary honeycomb[143].

3.2.2.2 Membrane Sheet preparation

Each membrane is mounted between 150gsm paper in order to accommodate a circular disk in a rectangular cell. This is also a technique used to provide the membrane area with stable flow, and minimize entrance effects which give rise to unstable flow. The arrangement is the common technique used for DOTM.

The mixture of GlobalCast 939 A&B glue was employed, it resulted in the supporting sheets having low flexibility but with the desired non-permeability. The glue has low viscosity; it could penetrate through the paper and form film-like layer on the paper. Blank test membrane sheet (without membrane) was tested to confirm that the surface was not permeable to water or damaged by the flow even at the highest crossflow velocity used for the experiments for the limited time used. The membrane sheet was also tested by soaking in water overnight as well as testing it rigorously in the test cell. An appropriate amount of glue must be applied as

too much would result in glue leakage on to the edge of the membrane, and too little would make the membrane sheet too flexible, resulting in the movement of membrane during the filtration and eventually resulting in breakage of the brittle Anopore membrane.

This system appears to work fine but for long term experiment and at high cross-flow velocity, a dent of the membrane sheet in an area near the feed inlet was visible. However, the distance between the Anopore membrane and this dent is large and so the effect on membrane filtration is considered minimal. This indicates that an improvement of the DOTM test cell design in terms of flow distribution near the inlet could be made.

3.2.2.3 Feed suspension

Feed suspension consists of *Chlorella Sorokiniana* and Polystyrene latex particles (3μm). The main concentration used was 29mg/L of microalgae. Also 14.5mg/L and 58mg/L algal suspension were used to observe the effect of feed concentration. The algae used here were grown in batch mode, and 2 batches were needed to complete all experiments. For maximum accuracy, experimental results using different batch of algae were not compared directly with each other.

Algae (*Chlorella Sorokiniana*)

Chlorella Sorokiniana, fresh water algae was used as feed. The cultures from American Type Culture Collection (ATCC) were cultivated in modified ATCC medium 616 (BG-11 medium) (see table 3.1) under photoautotrophic condition in a custom-made 3L photoreactor at room temperature (25^{o}C) by Thiengi Aung (PhD student, NTU). The medium was prepared using analytical grade chemicals, and its pH was adjusted to 7.1. The medium was autoclaved at 121^{o}C prior to the cultivation. During the cultivation, 8 of 13-watt fluorescent lights were used to provide necessary light source, and the CO_2-air volume ratio of 3:100 was also continuously provided.

Harvesting of the algae was done at around 14 days where algal concentration is at its maximum(approximately 2g/L). Dry weight together with calibration curves relating Algae concentration to UV absorbance (UV1800, Shimaszu) were carried out.

$NaNO_3$		1.5 g
K_2HPO_4		0.04 g
$MgSO_4.7H_2O$		0.075 g
$CaCl_2.2H_2O$		0.036 g
Citric acid		0.006 g
Ferric ammonium citrate		0.006 g
EDTA (disodium salt)		0.001 g
$NaCO_3$		0.02 g
Trace metal mix A5:		1.0 mL
H_3BO_3	2.86 g	
$MnCl_2.4H_2O$	1.81 g	
$ZnSO_4.7H_2O$	0.222 g	
$NaMoO_4.2H_2O$	0.39 g	
$CuSO_4.5H_2O$	0.079 g	
$Co(NO_3)_2.6H_2O$	49.4 mg	
Distilled water	1.0 L	
Distilled water		1.0 L

Table 3.1: Modified ATCC medium 616 (BG-11)

UV spectrophotometer (UV-1800, Shimadzu UV Spectrophotometer) was set to measure the absorbance at various wavelengths. It was found that the sensitivity of these measurements for the whole range of dilution data peaked at both wavelength 440nm and 490nm. However sensitivity for dilution below 50mg/L peaked at wavelength 490nm and 500nm. Measurements at 490nm were therefore used throughout.

3.2.3 Analysis for algae suspension

3.2.3.1 Measurement of Algae concentration

A UV spectrophotometer (UV-1800, Shimadzu UV Spectrophotometer) was used to relate algae concentration to UV absorbance. A linear relationship between these occurred for the dilution range used for the experiments. Measurement at wavelength 490nm was used for data interpretation for the reason stated earlier. Algae concentration of the feed tank was measured every 17.5 minutes via the above method. As

the membrane pore size of 0.2 and 0.1μm is much smaller than the size of the algae (around 3μm), none of the algae cells were present on the permeate side.

3.2.3.2 Measurement of viscosity

Viscosity of algae feed solution was measured. At the dilutions used in the experiments, the viscosity of the algae solution did not deviate noticeably from that of water; the fraction of solutes present in the feed solution was very small in comparison to the water.

3.2.3.3 Measurement of Particle size distribution

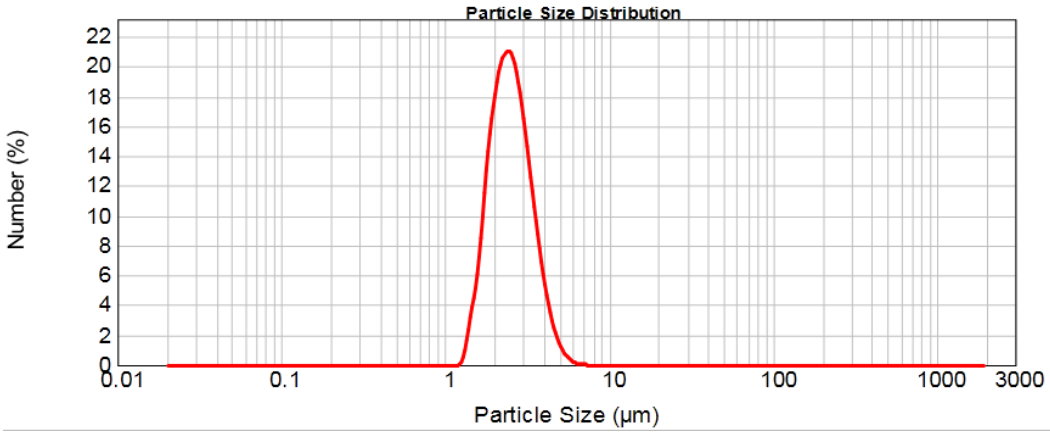

Figure 3.7: Particle size distribution of *Chlorella Sorokiniana* measured using Mastersizer 2000

Particle size distribution was measured using a Particle analyzer (Mastersizer 2000, Malvern, UK). The flow rate was set to 2500 rpm. Figure 3.7 shows particle size distribution of *Chlorella Sorokiniana* diluted with deionised water. The peak of particle size (number %) was approximately 2.52 μm. This was expected as the size of algal cells is approximately 3 μm.

3.2.4 Analysis of transmembrane pressure

Due to a large amount of noise in the data, and for additional accuracy of data analysis, a different approach to the conventional one used in membrane filtration

was employed. A signal processing technique, the Savitzky-Golay filter smoothing method (OriginLab), was used to remove noise from the raw data signal. Savitzky-Golay is a polynomial regression which reveals the data smoothed values while the peak height and width is preserved[144]. The initial transmembrane pressure data were shifted to the same starting point. From the TMP-J data average transmembrane pressure and average flux for each flux step were plotted. Rate of increase of transmembrane pressure was then revealed. In this way, the overview of transmembrane pressure and the rise in transmembrane pressure at each flux step for various systems can be easily compared.

In general for complete pore blocking, the rate of increase of transmembrane pressure during each flux of the flux-stepping experiments is expected to increase as flux increases until a plateau is reached (steady state). This is true especially if the operating flux is above the critical flux. For feed solution of mixed species (where the solutes include those which are deformable and have a smaller or a comparable size to the membrane pore size) deviation of dTMP/dt from the expected model could occur. Fouling mechanisms can be divided into External and Internal. External fouling[145] (known as the Cake filtration model) is assumed when the rate of increase of transmembrane pressure decreases with time. Internal fouling [145](known as the standard blocking or pore blocking model) is assumed to occur when the rate of increase of transmembrane pressure increases with time.

dTMP/dt was calculated to illustrate fouling tendency for flux stepping during the first few minutes after the initial flux step was induced and then throughout the rest of the run. The appropriate length of time was chosen, and this was 5 minutes and 10 minutes respectively for the initial change and the rest of the run. In summary, the averaged increase of transmembrane pressure during the first 5 minutes and the average rate of increase of transmembrane pressure for the next 10 minutes were used in membrane fouling analysis.

3.2.5 Analysis of DOTM images$^{\Delta}$

With the use of DOTM, image analysis revealed the number of algal cells deposition on the membrane surface. As mentioned earlier, the images were taken and analysed using Image Pro plus software. Images were taken at the 5th and 15th minutes of each flux step. This is shown as a trend of the fraction of membrane covered by these cells plotted against time during each flux step (17.5 minutes). The deposition and removal of the algal cells was dynamic and occurred simultaneously throughout the filtration.

Tasks	**PP**	**FW**	**Others**
Cultivation of algae			x
Preparation of DOTM apparatus and membrane sheets		x	
Experiments: effect of crossflow velocity above Jc	x		
Experiments: effect of crossflow velocity below Jc	x		
Experiments: effect of crossflow velocity, set E	x		
Experiments: effect of salt addition 1	x		
Experiments: effect of salt addition 2	x		
Experiments: effect of feed concentration above Jc	x		
Experiments: effect of feed concentration below Jc	x		
Experiments: captures of DOTM images	x		
Adapting DOTM apparatus for air-bubbling effect	x	x	x
Experiments: effect of air-bubbling	x		
Experiments: effect of air-bubbling intermittency	x		
Suspension tests	x	x	
Analysis of data	x		
Analysis of DOTM images (Image pro)		x	

PP: Pharima Pongpairoj, FW: Filicia Wicaksana

Table 3.2: Work distributions

3.2.6 Comparisons between shear rate for DOTM

Crossflow velocity (m/s)	$\dot{\gamma}_{WRec}(s^{-1})$	$\dot{\gamma}_{WSlit}(s^{-1})$
0.1	294	300
0.18	530	540
0.24	706	720

Table 3.3: Wall shear rate calculated using rectangular die ($\dot{\gamma}_{WRec}$) and slit die ($\dot{\gamma}_{WSlit}$) approximation at different crossflow velocities for DOTM module

Permeate flux		**11 LMH**	**200LMH**
Pore wall shear rate (s^{-1})	Porosity 25%	489	8889
($\dot{\gamma}_{wp} = \frac{8J}{\varepsilon d}$) , 0.2$\mu$m Anopore	Porosity 50%	244	4444
Pore wall shear rate (s^{-1})	Porosity 25%	978	17778
($\dot{\gamma}_{wp} = \frac{8J}{\varepsilon d}$), 0.1$\mu$m Anopore	Porosity 50%	489	8889

Table 3.4: Shear rate (s^{-1}) within the pore for Anopore membrane calculated using information provided at [146]

Wall shear rates at different crossflow velocities for DOTM module were calculated using rectangular die and slit die approximation, and are shown in table 3.3. This table demonstrates the difference in wall shear rate when slit die and rectangular die approximation are used. Slit die approximation is less complicated and can be employed instead of the rectangular die approximation when the channel width is infinitely larger than the channel height height (W >> H)[107]. DOTM module has channel height to width ratio of 0.0571. Son et al[107] relates height to width ratio to wall shear rate using the following equations.

$$\dot{\gamma}_w = \dot{\gamma}_a \left(\frac{2}{3}\right)\left(\frac{b^*}{f^*} + \frac{a^*}{f^*}\frac{1}{n}\right) \tag{3.1}$$

where

$$\dot{\gamma_a} = \frac{6Q}{WH^2}\left(1 + \frac{H}{W}\right) f\left(\frac{H}{W}\right) \tag{3.2}$$

where γ_w and γ_a are the wall shear rate and the apparent shear rate for rectangular die. H and W refer to the channel height and width respectively. a^*, b^*, and f are the geometric constants which depend on H/W. Geometric constants a^*, b^*, and f for DOTM module were obtained by 2nd order polynomial regression using the values given in a table from Son's paper[107].

while the apparent shear rate for slit die approximation can be written as

$$\dot{\gamma}_a = \frac{6Q_{CFV}}{WH^2} \tag{3.3}$$

The relation between shear rate by slit die approximation and regtangular die

approximation for the current geometry is therefore

$$\dot{\gamma}_{aRec} = 0.981\dot{\gamma}_{aSlit} \tag{3.4}$$

Table 3.4 shows pore wall shear rate at different fluxes and membrane porosity for Anopore membrane 0.1 and 0.2μm. The pore wall shear rate can be written as

$$\dot{\gamma}_{wp} = \frac{4Q_j}{\pi r_p^3} \tag{3.5}$$

where Q_j is the average flow rate through membrane and r_p is the membrane pore radius. This is equivalent to

$$\dot{\gamma}_{wp} = \frac{4u}{r_p} \tag{3.6}$$

where u is the fluid velocity through membrane pore. Table 3.4 reveals significantly larger values for pore wall shear rate at 200LMH than wall shear rate values for any crossflow velocities illustrated in table 3.3. Increases in permeate flux resulted in greater pore wall shear rate due to increased flow rate. A reduction in porosity or an increase in membrane pore blocking affects pore wall shear rate directly by increasing the average permeate flow rate in other pores.

3.3 Results and discussion

Crossflow filtration of *Chlorella Sorokiniana* was carried out in different conditions in order to determine the effect of crossflow velocity, feed concentration, salt addition, turbulence by air-bubbling, membrane pore size, and membrane type. Crossflow velocities were set at three levels: CFV2, CFV3 and CFV4 correspond to 0.107, 0.175, and 0.237 m/s respectively. The step size and the starting flux were varied in order to observe behaviour of the *Chlorella Sorokiniana* at different conditions, and the duration of each flux step remained constant. All possible efforts were made

to maintain fluxes level. Nevertheless, it was not possible to replicate exactly the same flux values, and there existed a small distribution of flux for these experiments. A summary of the experiments is shown in table 3.5. Fouling behaviour of Latex particles of a comparable size to the algae cells was also studied in order to observe fouling mechanism of particles in the absense of EPS.

	SET-A	SET-B	SET-C	SET-D	SET-E
Stepping	Y	Y	Y	N	Y
Average starting flux (LMH)	105	17	70		17
Average final flux (LMH)	200	120	330		180
Effect of crossflow velocity	Y	Y		Y	Y
Effect of feed concentration	Y	Y			
Effect of salt addition			Y		Y
Effect of bubbling		Y	Y	Y	
Effect of membrane pore size					Y
Effect of membrane type					Y

Table 3.5: Summary of experiments

SET-A A set of flux stepping was carried out at three crossflow velocities to determine the effect of shear on critical flux, six steps each of 17.5 minutes. Fluxes were between 105 and 200LMH. Effect of concentration was also determined at both 0.107 and 0.237m/s.

SET-B A set of flux stepping experiment set to observe the effect of crossflow velocity in subcritical flux range, the range of the fluxes here were between 17 and 120LMH. Both the effects of concentration and crossflow velocity was carried out.

SET-C The effect of bubbling was assessed at 0.107m/s using flux stepping in the high flux range and with larger flux steps. The flux range was between 70 to 330LMH. The aim was to observe if the former cake that has been built slowly by SET-A has any effect on the growth of fouling of the *Chlorella Sorokiniana* cake layer. Effect of addition of salt KCl and $CaCl_2$ were observed.

The effect of bubbling (1L/min) was also studied in order to investigate the effect of bubbling on fouling mitigation above critical flux.

SET-D Crossflow filtration using clean membrane was carried out at various fluxes at 0.107 and 0.237m/s. This was to observe whether the cake structure formed under different starting flux had any effect on the rate of membrane fouling.

Effect of bubbling was further studied at constant fluxes. Intermittent bubbling with 17.5 minute interval was then carried out to see the effect of bubbling when it is used periodically. Results from this set are not included in this thesis.

SET-E A set of flux stepping experiment carried out between 17 to 180LMH to observe the behaviour of smaller particles during the filtration process, as well as to determine the effect of crossflow velocity. The composition of the feed and the permeate was closely monitored periodically for the content of carbohydrate and protein, as well as for organic carbon content (TOC and IC). The results from this set are shown in Chapter 4.

3.3.1 Effect of crossflow velocities

Effect of crossflow velocities during crossflow filtration of microalgae (*Chlorella Sorokiniana*) at 29mg/L was observed via the flux-stepping method. Three sets of experiment were carried out to examine this by starting flux stepping at supercritical flux (SET A) and at subcritical flux (SET B). Polystyrene latex particles (3μm) was also used as feed to observe fouling behaviour of a model particle in absence of EPS in comparison with the microalgae (with EPS).

3.3.1.1 Fouling behaviour of model feed

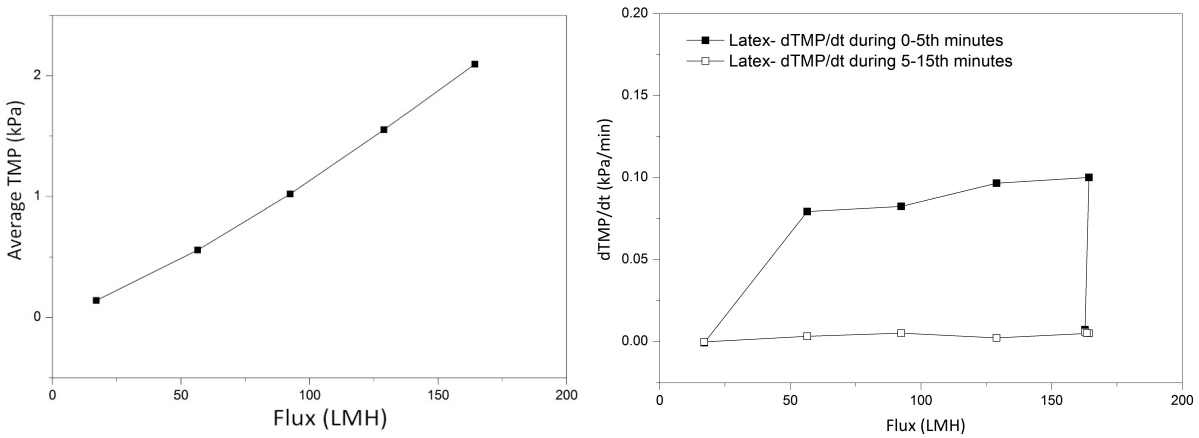

(a) TMP against flux during microfiltration of 3µm latex particles suspension

(b) dTMP/dt against flux during microfiltration of 3µm latex particles suspension

Figure 3.8: TMP against flux (a) and dTMP/dt against flux during microfiltration of 3µm latex particles suspension (b)

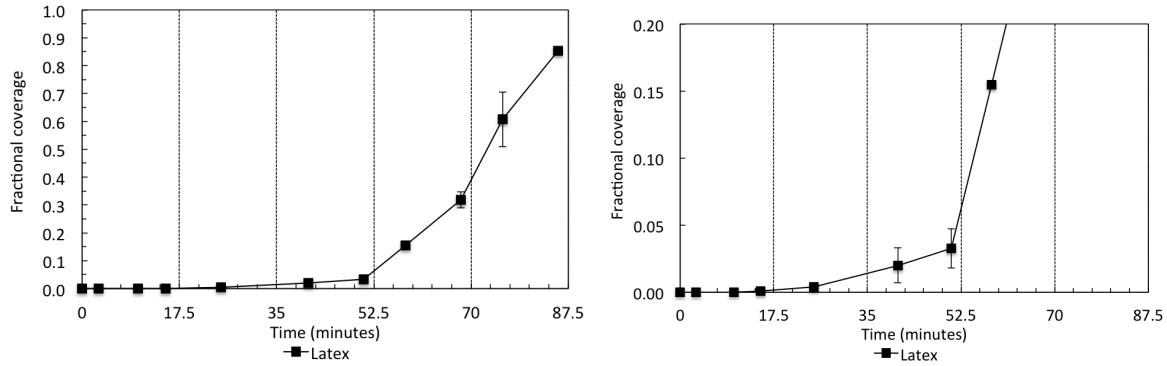

(a) Fractional coverage of latex particles on membrane surface against operating time

(b) Close-up of fraction coverage against operating time

Figure 3.9: Fractional coverage of latex particles on membrane surface

Flux stepping crossflow microfiltration experiments of latex particles were carried out at crossflow velocity of 0.107m/s. Figure 3.8 indicates 4 steps of approximately 38LMH. Figure 3.8a shows average TMP during each flux step, while dTMP/dt during 0-5th minutes and during 5-15th minutes were shown on 3.8b. Figure 3.9a and Figure 3.9b present fractional coverage of membrane against time and a close-up image of the same diagram respectively.

The starting flux was selected as 17LMH as this is below the critical flux of latex particles previously determined experimentally (results not shown). As soon as flux increased to 55LMH, latex deposition rate increased from negligible to 0.02%coverage per minute. Critical flux obtained by DOTM images was therefore between 17 and 55LMH. Similarly, critical flux obtained from transmembrane pressure data was also between 17 and 55LMH as initial rate of increase of TMP increased to nearly 0.08kPa per minute after the flux was increased to 55LMH. Threshold flux obtained from TMP happened as dTMP/dt during 0-5th minutes increased further to nearly 0.1kPa/min, nevertheless it is also the same value as that obtained from image analysis. Critcal flux and threshold flux obtained by different methods are summarised in table 3.6.

Type	**By TMP**	**By DOTM fractional coverage**
Critical flux	17-55LMH(0.08kPa/min)	17-55LMH (0.0002 per minute)
Threshold flux	93-131 LMH(nearly 0.1kPa/min)	93-131 LMH(0.002 per minute)

Table 3.6: Critical flux and threshold flux for latex suspension at crossflow velocity 0.1m/s

For all fluxes carried out, the rate of increase of transmembrane pressure was high only for the first 5 minutes (initial) after the flux was increased. After which, the rate of increase of transmembrane pressure remains relatively low (less than 0.006kPa per minute). The rate of increase of transmembrane during 5-15th minutes remained low even after 70 minutes at 166LMH. It is likely that the rate of increase of transmembrane pressure with the increasing flux steps here is due to external pore blocking.

3.3.1.2 Fouling behaviour of algae at different crossflow velocities during flux stepping starting at supercritical flux

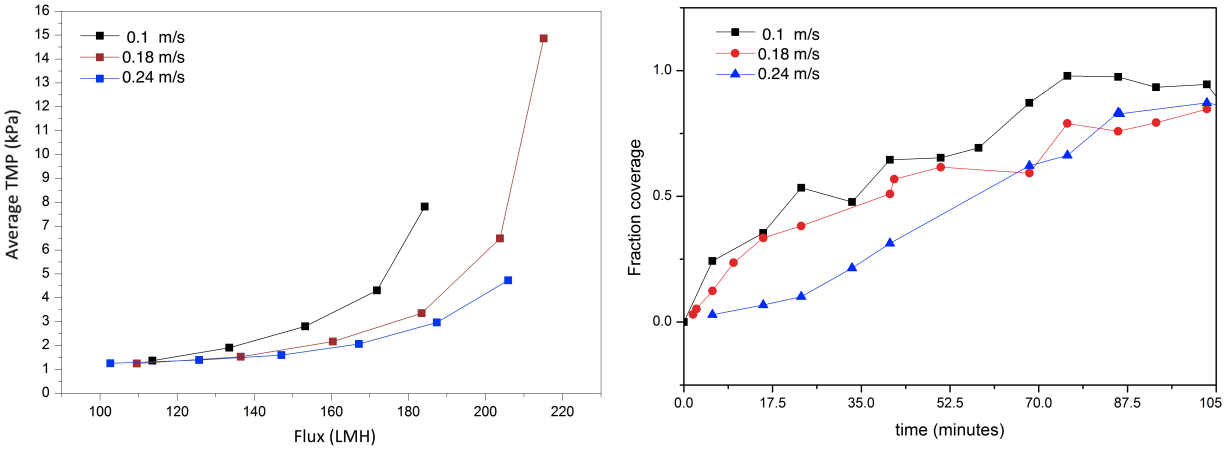

(a) TMP against flux at different crossflow velocities during microfiltration of algal suspension

(b) Fraction of membrane coverage by the algae cells at different crossflow velocities during microfiltration of algal suspension

Figure 3.10: TMP against flux and fraction of membrane coverage by the algae cells at different crossflow velocities during microfiltration of algal suspension: SET-A.

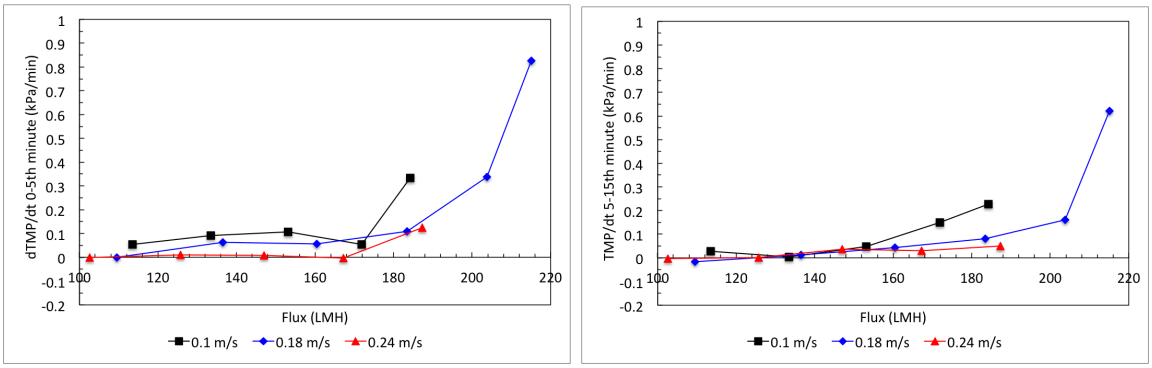

(a) Initial rate of increase of transmembrane pressure against flux for 29mg/L algae solution at different crossflow velocities when flux stepping started from above critical flux for the algal cells

(b) 5-15th minute rate of increase of transmembrane pressure against flux for 29mg/L algae solution at different crossflow velocities when flux stepping started from above critical flux for the algal cells

Figure 3.11: Initial and 5-15th minute rate of increase of transmembrane pressure against flux for 29mg/L algae solution at different crossflow velocities when flux stepping started from above critical flux for the algae cells: SET-A

Experiments were carried out to observe behaviour of algae at supercritical flux, the flux that is well above the critical flux of algae cells. The deviation of average transmembrane pressure against flux from the clean water values was less significant at high crossflow velocity (shown in Figure 3.10a. This result is supported by DOTM images, that at higher crossflow velocity resulted in slower or lower deposition of the algae cells on the membrane surface than at lower crossflow velocity (shown in Figure 3.10b).

Crossflow velocities	**Threshold flux 0-5th minute**	**Threshold flux 5-15th minute**
0.1 m/s	175 LMH	162 LMH
0.18 m/s	180 LMH	188 LMH
0.24 m/s	184 LMH	Above 205 LMH

Table 3.7: A table displaying threshold flux identified as the flux resulting in dTMP/dt reaching 0.1kPa per minute: SET-A

Figure 3.11 illustrates rate of membrane fouling against flux. The initial rate of dTMP/dt and the 5-15th minute dTMP/dt are shown in Figure 3.11a and 3.11b respectively. At crossflow velocity of 0.1m/s, transmembrane pressure increased as soon as the first flux started with initial dTMP/dt of 0.054kPa/min, while the dTMP/dt for the first flux at crossflow velocity of 0.18m/s and 0.24m/s still remained negligible for both 0-5th and 5-15th minute. It is therefore reasonable to assume that at crossflow velocity of 0.18m/s and 0.24m/s these starting fluxes are below critical flux for algal cells by TMP. The rate of increase of transmembrane pressure during the 5-15th minutes shows a trend that is exerted to rise above 0.1kPa per minute at a flux of around 162, 188, and above 205LMH at crossflow velocity of 0.1, 0.18 and 0.24m/s respectively. Nevertheless, at crossflow velocities of 0.1m/s the flux below 130LMH was low enough to maintain a negligible rate of increase of transmembrane pressure during 5-15 minutes. After this flux, the shear was no longer efficient, and the increase in transmembrane pressure occurred throughout, not just at the beginning. As the flux was raised from 130 to 170LMH, a drop in the rate of increase of transmembrane pressure at 170LMH occurred during the

first 5 minutes, this showed that a portion of the cake resistance has been removed. Since this phenomena was followed by a higher rate of increase of transmembrane pressure during the rest of the run (dTMP/dt jump), it could be concluded that, some of the deposition was removed from the membrane surface by being pushed through the pores, resulting in an initial reduction in resistance but (due to some retention) some pore narrowing. The latter effect caused a much steeper rate of increase of transmembrane pressure thereafter. Threshold flux 0-5th and 5-15th minute at different crossflow velocities are summarised in table 3.7. A comparison of critical fluxes by analysis of TMP and by DOTM are summarised in table 3.8. It is clear that the critical flux observation using the DOTM method was generally more sensitive than that using the TMP method. Note that in order to find the exact value of the critical flux using the flux stepping method, further experiments with fine-tuned flux steps are necessary.

CFV	**Critical flux by TMP**	**Critical flux by DOTM**	**Sensitivity of methods**
0.1 m/s	below 114LMH	below 114LMH	Equal
0.18 m/s	between 109 and 136LMH	below 109 LMH	DOTM is more sensitive
0.24 m/s	between 102 and 125LMH	below 102 LMH	DOTM is more sensitive

Table 3.8: Comparison of critical flux for 29mg/L *Chlorella Sorokiniana* by transmembrane pressure and by DOTM

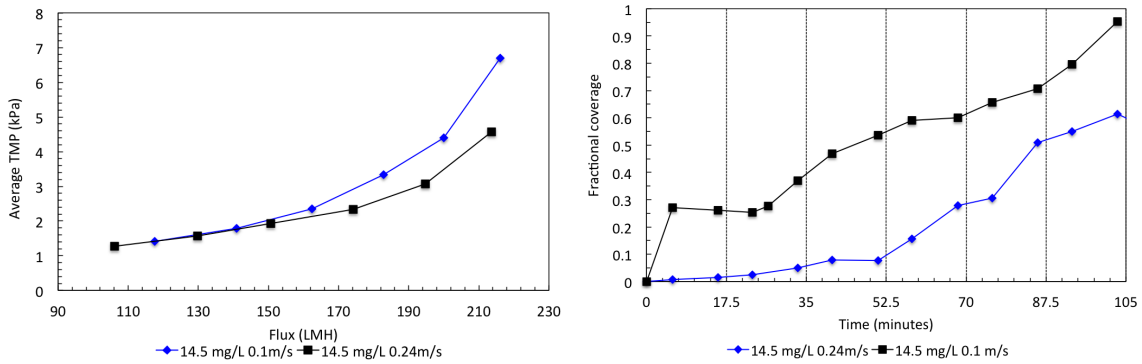

(a) TMP against flux at different crossflow velocities during microfiltration of 14.5mg/L algal suspension

(b) Fraction of membrane coverage by the algae cells at different crossflow velocities during microfiltration of 14.5mg/L algal suspension

Figure 3.12: TMP against flux and fraction of membrane coverage by the algae cells at different crossflow velocities during microfiltration of 14.5mg/L algal suspension

Figure 3.12a illustrates that the higher crossflow velocity of 0.24m/s did also result in lower average transmembrane pressure for 14.5mg/L algal suspension. Again, DOTM image analysis revealed that higher crossflow velocity of 0.24m/s led to lower deposition of algal cells on the membrane surface (Figure 3.12b). The rate of increase of fractional coverage started to increase severely as flux increased to 141 LMH and 174LMH for CFV 0.1m/s and 0.24m/s respectively. The greater membrane coverage by algal cells at all fluxes for CFV 0.1m/s could contribute to the elevated transmembrane pressure seen in Figure 3.12a.

Figure 3.12b reveals algal depositions on the membrane during the run. It can be clearly seen that even at the lowest fluxes in Figure 3.12a used for all crossflow velocities, algal deposition occurred within 5 minutes of starting. This means that these fluxes are well above critical flux for algal cells. With DOTM image analysis, critical flux for algal cells can be clearly and easily determined. Details on lower fluxes are given later in section 3.3.1.3.

3.3.1.3 Fouling behaviour of algae at different crossflow velocities during flux stepping starting at subcritical flux

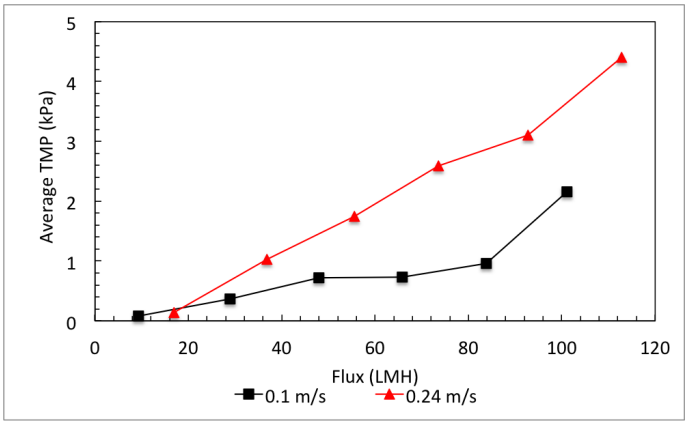

Figure 3.13: TMP against flux for 29mg/L algal solution at different crossflow velocities when flux stepping started from below critical flux for the algae cells: SET-B.

Behaviour of algae at subcritical flux was studied, and a small-step flux stepping was used. The starting flux of the flux stepping was below the critical flux for algal cells. The algae have already started to age, and could result in higher extracellular polysaccharide content. Figure 3.13 shows average transmembrane against average flux, while membrane fractional coverage is shown on Figure 3.15.

The adverse effect of crossflow velocities was found here. Figure 3.13 clearly shows that the high crossflow velocities of 0.24m/s no longer resulted in lower average transmembrane pressure than the low crossflow velocities (0.1m/s). In fact, the average transmembrane pressure during each flux were higher for higher crossflow velocity. For crossflow, it is generally believed that the effect of shear induced diffusion normally reduces deposition of the solutes as shear increases. Thus higher crossflow velocity would normally results in less deposition of particles on the membrane surface and hence a lower rate of increase of transmembrane pressure is normally expected. Reasons for an adverse effect are discussed in section 4.3.3.

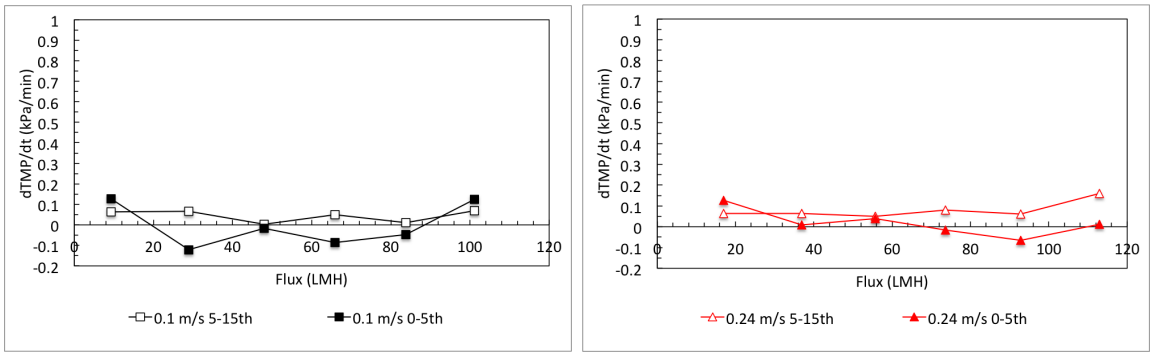

(a) Initial rate of increase of transmembrane pressure against flux for 29mg/L algae solution at different crossflow velocities when flux stepping started from below critical flux for the algal cells

(b) 5-15th rate of increase of transmembrane pressure against flux for 29mg/L algae solution at different crossflow velocities when flux stepping started from below critical flux for the algal cells

Figure 3.14: Initial (0-5th) and 5-15th minute rate of increase of transmembrane pressure against flux for 29mg/L algae solution at different crossflow velocities when flux stepping started from below critical flux for the algae cells: SET-B.

The dTMP/dt (Figure 3.14) 0-5th minute were higher than dTMP/dt 5-15th minute for the first flux for both crossflow velocities. This implies that initially external fouling was the dominant mechanism. As flux was raised, the trend showed that dTMP/dt 5-15th generally were higher than dTMP/dt 0-5th, this implied that internal fouling dominated during those fluxes. Moreover, as flux increased, negative values of dTMP/dt 0-5th minute were found. It could be possible that the cake or fouling layer was susceptable to flux as well as shear. Further information such as critical flux and threshold flux can not be clearly deduced from analysis of transmembrane pressure alone, although one could conclude that the threshold flux (resulting in dTMP/dt 5-15th reaching 0.1kPa/min) was around 100LMH for both crossflow velocities.

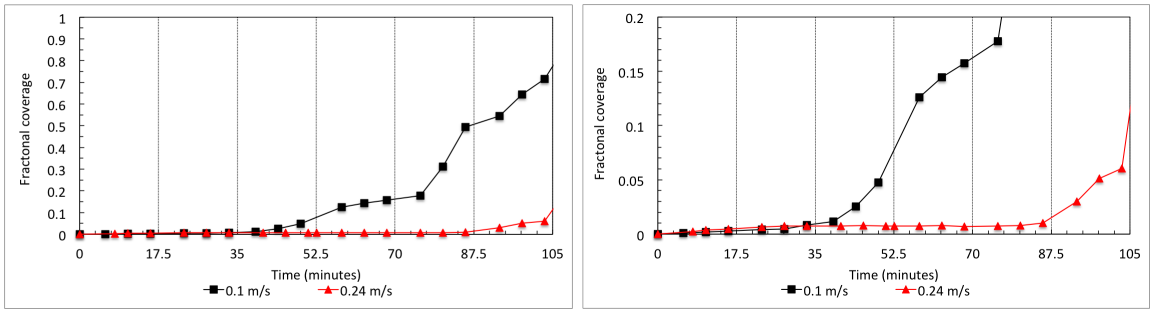

(a) Normal view (b) Close-up view

Figure 3.15: Fractional membrane coverage by the algae cells against time for 29mg/L algae solution at different crossflow velocities when flux stepping started from below crtical flux for the algae cells: SET-B.

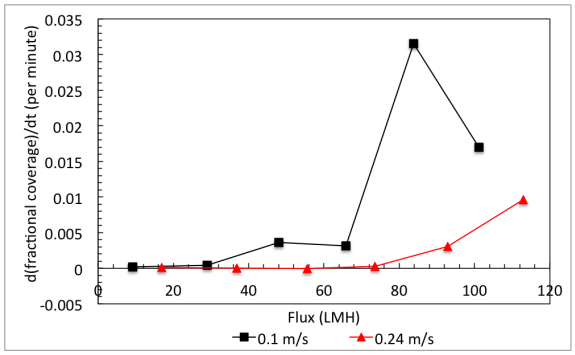

Figure 3.16: Rate of increase of membrane fractional coverage (per minute)

With the use of DOTM, the deposition of the solutes on the membrane surface was investigated. As expected, higher crossflow velocity led to higher removal of algae cells and resulted in less deposition of algae cells on the membrane. This is shown in Figure 3.15. Measurement of critical flux for the algae by image analysis is rather tricky because the algal cells do attach to the membrane surface even at zero flux. The attachment is due to extracellular polysaccharide around the cells, ie. sheath. In this case, critical flux by DOTM was identified as the flux at which deposition of algal cell deviated from the general minimal values and rate of increase of membrane coverage can be used. This critical flux can be taken to be a critical flux of the weak form rather than the strong form[41]. The critical flux

for algal cells at CFV 0.1m/s and 0.24m/s were between 29 and 48LMH and 93 and 113LMH respectively (summarised in table 3.9). For CFV 0.24m/s, increases in transmembrane pressure occurred with minimal deposition of algal cells up until 93LMH. With image analysis of membrane surface, it could be concluded that the deviation of transmembrane pressure from clean water values was due to other substances within the feed solution, not just the algae. Further experiments were carried out and this will be reported in section 4.2.1.

CFV	**Critical flux by TMP**	**Critical flux by DOTM**	**Sensitivity of methods**
0.1 m/s	N/A	between 29 and 48 LMH	DOTM is more sensitive
0.24 m/s	N/A	between 93 and 113 LMH	DOTM is more sensitive

Table 3.9: Comparison of critical flux for 29mg/L *Chlorella Sorokiniana* by transmembrane pressure and by DOTM

3.3.2 Effect of feed concentration

Effect of feed concentration was carried out in flux stepping experiments starting at supercritical flux level as well as starting at subcritical flux level. The lowest CFV (0.1m/s) and the highest CFV (0.24m/s) will be used here to compare the effect of feed concentration on membrane performance under low and high shear.

3.3.2.1 Effect of feed concentration during flux stepping experiments starting at supercritical flux and starting at subcritical flux under low crossflow velocities (0.1m/s)

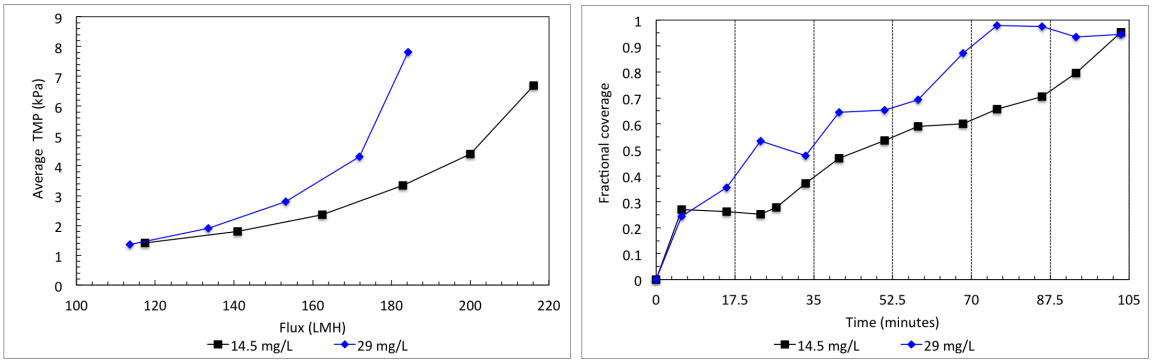

(a) TMP against flux (b) Fraction of membrane coverage agaist time

Figure 3.17: TMP against flux, and fraction of membrane coverage by the algae cells against time for algae solution at different dilutions at CFV 0.1m/s when flux stepping started from above critical flux for the algae cells: SET-A.

Figure 3.17a illustrates transmembrane pressure against average flux, and Figure 3.17b shows fractional membrane coverage during flux stepping at crossflow velocity of 0.1m/s. The trend here was as expected, higher algal concentration led to higher transmembrane pressure. DOTM fractional coverage revealed that algal deposition on membrane surface was higher for 29mg/L of algae suspension than 14.5mg/L algal suspension but not doubled. The fluxes used here were at supercritical level, algal depositions occurred as soon as the fluxes started.

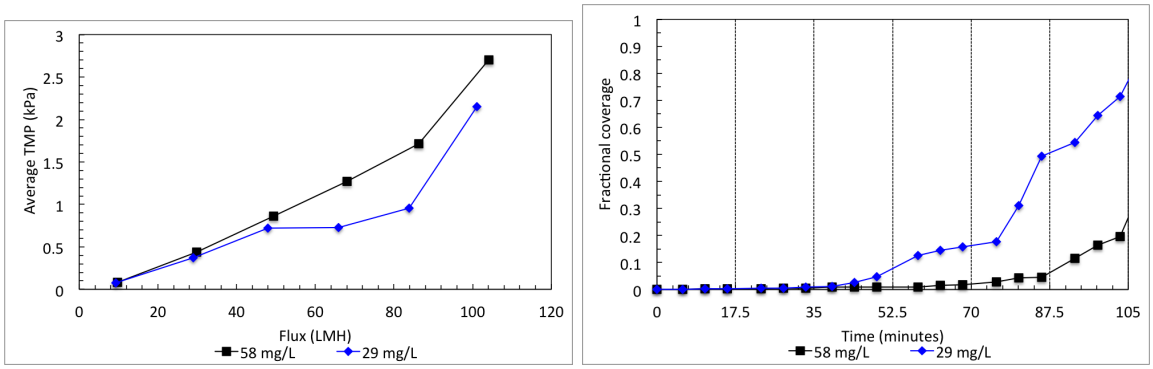

(a) TMP against flux

(b) Fraction of membrane coverage by the algae cells against time

Figure 3.18: TMP against flux and fraction of membrane coverage by the algae cells against time flux for algal solution at different dilutions at CFV of 0.1m/s when flux stepping started from below critical flux for the algae cells: SET-B.

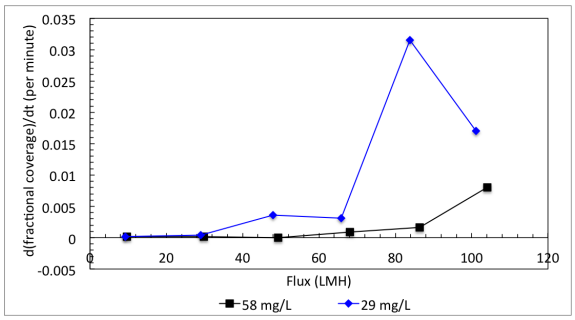

Figure 3.19: Rate of increase of fractional membrane coverage against flux for different algal concentration: SET-B

For experiments starting at subcritical fluxes, effect of algal concentration on average transmembrane pressure, fractional membrane coverage, and rate of increase of fractional coverage at low crossflow velocity of 0.1 m/s are present in Figure 3.18a, 3.18b and 3.19 respectively. Interestingly, even though higher concentration did result in greater average transmembrane pressure, the membrane fractional coverage was lower for 58mg/L algal suspension than 29mg/L algal suspension. One can speculate that the nature of the high concentration feed was different; may be the effective particle size was greater. It is well known that larger particles have a higher critical flux[43].

3.3.2.2 Effect of feed concentration during flux stepping experiments starting at supercritical flux and starting at subcritical flux under high crossflow velocities

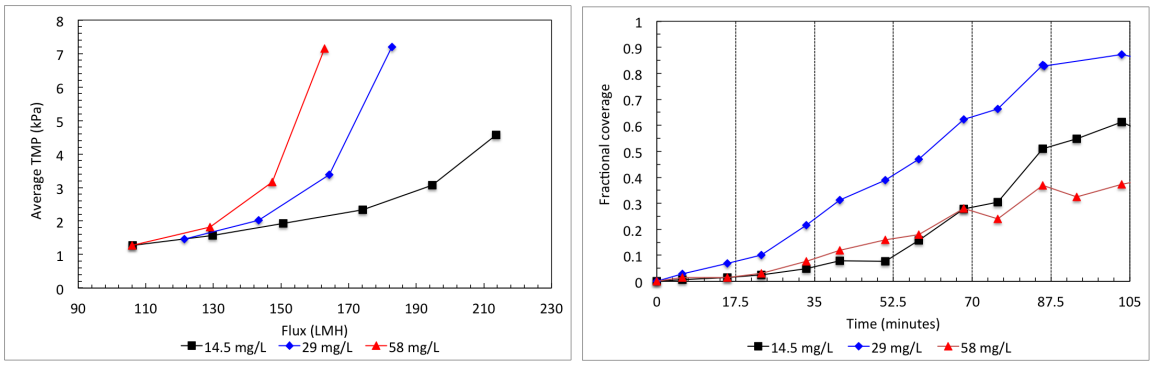

(a) TMP against flux

(b) Fraction of membrane coverage by the algae cells against time

Figure 3.20: Transmembrane Pressure against flux and fraction of membrane coverage by the algae cells against time for algae solution at different dilutions at CFV 0.24m/s when flux stepping started from above critical flux for the algae cells: SET-A.

Figure 3.20a illustrates effect of concentration on transmembrane pressure during flux stepping experiment starting at supercritical fluxes at high crossflow velocity of 0.24m/s. Higher algal concentration resulted in higher average transmembrane pressure. At the same flux, the rate of increase of transmembrane pressure were indeed greater for 58mg/L, than 29mg/L and 14.5mg/L algal suspension. Nevertheless, the membrane fractional coverage (Figure 3.20b) shows that this increase was not purely due to deposition of algal cells on the membrane surface, since 29mg/L algal suspension led to higher algal deposition than 14.5mg/L algal suspension, while the 58mg/L suspension resulted in similar deposition to 14.5mg/L at early fluxes.

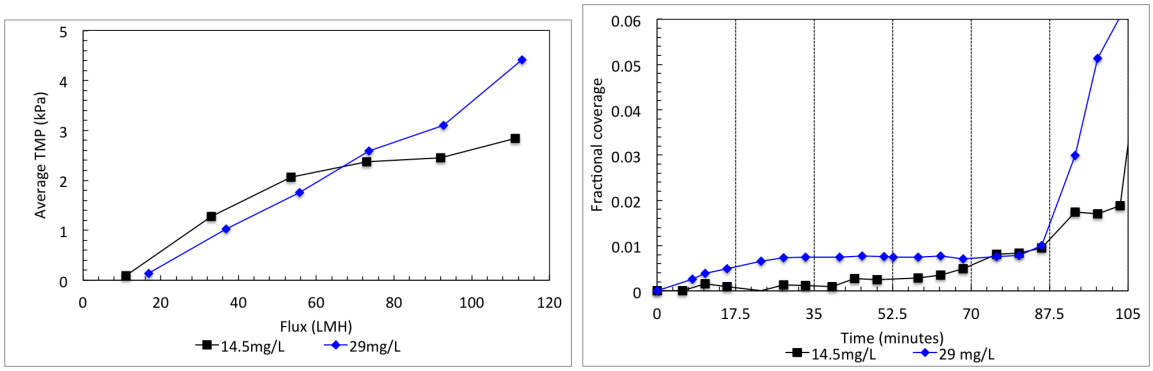

(a) TMP against flux

(b) Fraction of membrane coverage by the algae cells against time

Figure 3.21: TMP against flux and fraction of membrane coverage by the algae cells against time for algae solution at different dilutions at CFV 0.24m/s when flux stepping started from below critical flux for the algae cells: SET-B.

Figure 3.21a shows effect of concentration on transmembrane pressure during flux stepping experiment starting at subcritical fluxes at high crossflow velocity of 0.24m/s. At low fluxes, the average TMP for filtration for 14.5mg/L algal suspension was unexpectedly higher than for 29mg/L algal suspension. Nevertheless, Figure 3.21b reveals that the algal deposition on the membrane surface was indeed lower for lower algal concencentration at all fluxes. This implied that the increase in average transmembrane pressure was influenced by other substances, not the algal cells alone, which is further evidence of the influence of EPS.

3.3.3 Effect of air bubbling

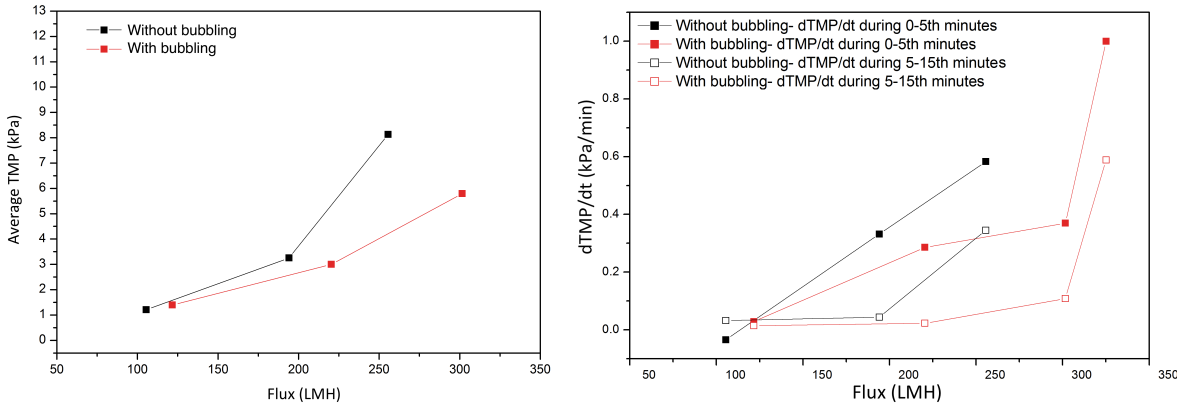

(a) TMP against flux

(b) dTMP/dt against flux

Figure 3.22: TMP against flux and dTMP/dt against flux for algae solution at 29 mg/L with and without bubbling at CFV 0.1m/s when flux stepping started from above critical flux for the algae cells.

Figure 3.22 illustrates average transmembrane pressure against flux for 29mg/L algal suspension with and without air bubbling at crossflow velocity of 0.1m/s. Each flux stepping step height was increased so that the effect of air-bubbling can be seen more clearly. Feed crossflow velocity were set at 0.1m/s, and the air-flow rate was approximately 1L/min. This is equivalent to Liquid:air ratio of 0.4. As seen in Figure 3.22, with air-bubbling the average transmembrane pressure were much lower than without bubbling. Without air-bubbling, breakage of membrane occurred as flux increased to approximately 250LMH (transmembrane pressure reached 11kPa), while with air-bubbling, it was possible to operate at 320LMH.

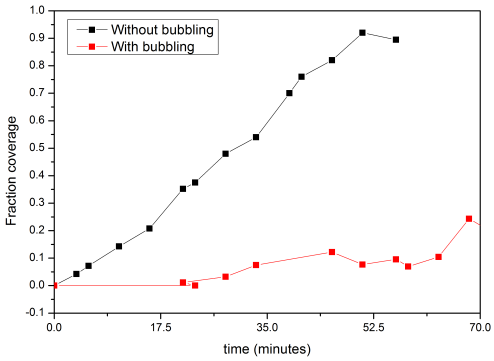

Figure 3.23: Fractional coverage by the algae cells against time for algae solution at 29 mg/L with and without bubbling at CFV 0.1m/s when flux stepping started from above critical flux for the algae cells.

Bubbling	**Threshold flux by TMP**	**Threshold flux by DOTM**	**Sensitivity of methods**
Without	220 LMH	below 100 LMH	DOTM is more sensitive
With	310 LMH	below 220LMH	DOTM is more sensitive

Table 3.10: Threshold flux by TMP (for dTMP/dt reaching 0.1kPa/min) versus by DOTM

Figure 3.23 reveals fractional coverage of the membrane by algal cells with time. It can be seen that without air-bubbling the membrane was rapidly fouled by the algal cells as soon as the flux started as this flux is well above the critical flux. For the same flux with air-bubbling, the membrane surface remained relatively free of algal cell deposition, and the rate of increase of membrane coverage was negligible. As flux increased further, the algal deposition continued to increase for the non-bubbling case, whilst for bubbling, the fractional coverage remained relatively low despite the high flux imposed. The critical flux for bubbling was between 120 and 220LMH. Threshold flux obtained by TMP and by DOTM image analysis are summarised in table 3.10.

The rate of increase in TMP for with-bubbling increased significantly at high fluxes, even though DOTM images revealed a low algal deposition on the membrane surface. It is therefore reasonable to conclude that again the membrane fouling in

this case was the result of other substances within the feed, not the algal cells alone.

Type	**Apparent shear rate (s^{-1}) Slit die**	**% increase from CFV0.1m/s**
CFV 0.1m/s	300	0
CFV 0.18m/s	540	80%
CFV 0.24m/s	720	140%
Air-bubbling	1014	238%

Table 3.11: Apparent shear rate during crossflow microfiltration without and with air bubbling.

Table 3.11 illustrates the apparent shear rate (s^{-1}) at different crossflow velocities and with air-bubbling. With air-bubbling, the shear rate increased by 238% without addition of algal cells passing the membrane surface, ie. shear rate per mg of algal cells per second increased from approximately $8 * 10^3$ to $28 * 10^3$.

3.3.4 Effect of salt addition

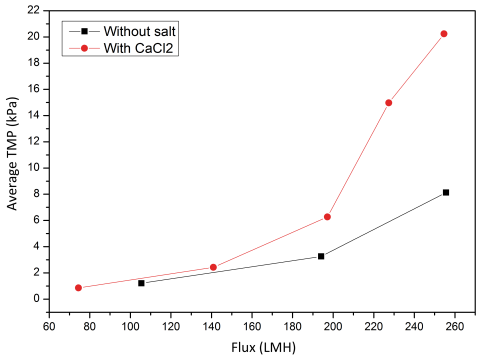

(a) TMP against flux

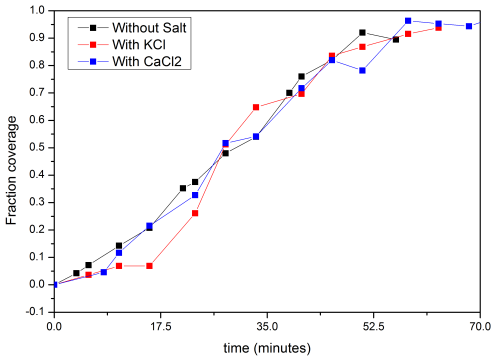

(b) Fractional membrane coverage by the algae cells against time

Figure 3.24: TMP against flux, and fractional membrane coverage by the algae cells against time at CFV 0.1m/s when flux stepping started from above critical flux for the algae cells.

Experiments were carried out to investigate the effect of salt type on fouling and deposition of microalgae. 5mM of $CaCl_2$ and KCl were added to the feed suspension prior to filtration. Figure 3.24a illustrates the effect of salt addition on average

transmembrane pressure. For algal concentration of 29mg/L, the addition of 5mM $CaCl_2$ resulted in higher average transmembrane pressure than without salt at all fluxes. Aqueous 5mM KCl did not result in any noticeable variation in transmembrane pressure (graph not shown). Figure 3.24b reveals the deposition of algal cells on the membrane surface. With KCl, the fractional coverage was slightly lower at the initial flux, however, there was no significant change in overall fouling behaviour observed. These results were expected as literature suggested that noticable changes in algal mucilage sheath are mainly due to $CaCl_2$ (see section 3.1). The increase in transmembrane pressure resulted from either external pore blocking by the the algal cells and their sheath or internal pore blocking by the EPS. As the supplies of both the membranes and the algal broth were limited, further experiments were carried out to observe the effect of $CaCl_2$, rather than other salts.

3.4 Summary

Crossflow velocities largely affect both fouling and transmission. At algal concentration of 29mg/L, the effect of crossflow velocities was observed at 0.1, 0.18 and 0.24m/s. At higher crossflow velocities, the fractional coverage of membrane surface was lower. Shear from crossflow velocities was efficient for algal cell removal from the membrane surface, this trend was illustrated by Figure 3.10 and Figure 3.13. Lower algal deposition on the membrane surface indicates lower external fouling, and therefore lower average transmembrane pressure should be observed. This was the case for section 3.3.1.2 when flux stepping started at a supercritical flux. When the starting flux was below critical flux, it was found (Figure 3.13) that the average transmembrane pressure was greater at high crossflow velocity (Case A). This is an unusual case and will be further discussed in Section 4.3.1. Analysis of dTMP/dt (see Figure 3.14) revealed that for low crossflow velocity, the initial rate of dTMP/dt was negative at many fluxes, this was then followed by positive 5-15th

minute dTMP/dt, while for high CFV, negative dTMP/dt started to occur at the 4th flux (75LMH). In both situations, the fractional coverage for both was still at a minimal level. This implies that fouling was dominated by substances other than algal cells, and the fouling tendency of this substance was also influenced by cross-flow velocity. It was confirmed that DOTM can offer a more sensitive method for detecting membrane fouling than traditional TMP but Section 3.3.1.3 revealed that analysis of DOTM images alone could lead to misleading conclusions, due to fouling by other substance (EPS). Further observation relating to transmission of EPS and fouling in algae microfiltration will be reported in Chapter 4.

4 Transmission of EPS and Fouling in Microfiltration

This chapter is based on the work carried out during my research visit at Nanyang Technological University (NTU), Singapore in Early 2010. This chapter relates to some interesting observations on fouling and transmissions. This was published in part in *Desalination and Water Treatment* as "Transmission of and fouling by long chain molecules during crossflow microfiltration of algal suspensions: influence of shear" and in the *Journal of Membrane Science* under the title "Microfiltration of algae (*Chlorella sorokiniana*): Critical flux, fouling and transmission".

This chapter has the following objectives

- Exploration of the influence of crossflow velocities on transmission of EPS
- Exploration of the effect of salt addition on transmission of EPS
- Exploration of the effect of membrane type on transmission of EPS
- Exploration of the effect of membrane pore size on transmission of EPS

4.1 Materials and methods

The set up of microscope, filtration module, and filtration circuit were as described in chapter 3. Experiments were carried out using mainly 0.2μm Anopore membranes. Additionally, 0.1μm Anopore membranes and 0.2μm PVDF membranes

were also used to observe the effect of membrane pore size and membrane type. Each membrane was prepared into a membrane sheet before mounting onto the DOTM filtration module (see Chaper 3 for details). A fresh membrane was used for each experiment.

To observe the influence of various effects on EPS transmission, the permeate was periodically analysed for protein content, polysaccharide content, and total organic carbon content every 17.5 minutes throughout all experiments. Membrane performance was assessed by the following factors: average transmembrane pressure; rate of increase of TMP; in-situ observation on membrane surface; and transmission of EPS through the membranes.

4.1.1 Measurement of Extracellular Polysaccharide and Organic content

A feed sample was collected at the start of the filtration run. Both feed sample and the permeate sample were then collected at 17.5 minute time intervals for up to 105 minutes. Then the final samples of both the feed and permeate were collected at the end of the experiment.

The feed samples were centrifuged in a refrigerated centrifuge (Sorvall Legend Mach 1.6R, Thermo scientific) at 4000rpm at 4^{o}C for 10 minutes. The fluid was removed and labelled as supernatant. The remaining was labelled pellets and was extracted via the chemical method. 0.6ml of 8.5 wt% NaCl and 0.22 wt% formaldehyde solution and 4.4ml of deionised water were added to 10ml samples and this mixture was incubated at 4^{o}C for one hour. After that, 0.4ml of 1.0M NaOH and 4.6ml of deionised water were added. A further incubation period of 3 hours was required. After the extraction procedure had been completed, the solution was transferred to 2ml centrifuge tubes and centrifuged at 13200 rpm at 4^{o}C for 20 minutes (CT15E Series, Hitashi Koki Co. Ltd). The extracted liquid was labelled as pellet extraction.

Supernatant, extraction of pellets, as well as the permeate sample of each flux step were then analysed using the following methods to be examined for its protein, polysaccharide, Total Organic Carbon, and Inorganic Carbon contents.

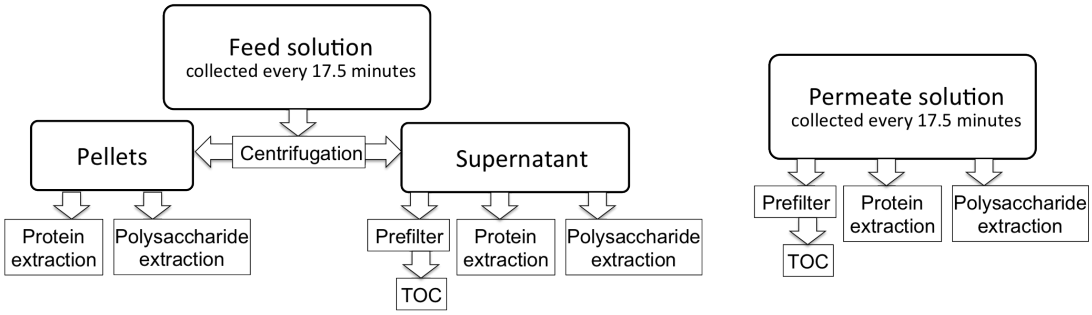

Figure 4.1: Diagram showing processes of suspension analysis of EPS and organic content

Colorimetric determination of polysaccharide concentration (EPS-Polysaccharide)

Measurements of Polysaccharides of the collected samples were analysed using the Sulphuric-Phenol method proposed by Dubois et al. (1956). This was done by addition of 1ml 5wt% phenol solution and 5ml of concentrated sulphuric acid (H_2SO_4) to 2ml of analyte and mixed well. After 10 minutes of reaction time, UV absorbance of the analyte was carried out at 492nm. The UV absorbance was found to be proportional to the total carbohydrate concentration within the solution (Glucose equivalent).

Colorimetric determination of protein concentration (EPS-Protein) BCA Protein assay kit for protein assay using Bicinchoninic acid (Product number 23225, Thermo Scientific) was used. BCA Protein assay Reagent A was used together with BCA Protein assay Reagent B, at an A:B ratio of 50:1. The solution was added into the supernatant, the extraction of pellets as well as the permeate sample at a ratio of 20 to 1 (2ml of BCA working solution per 0.1ml of analyte). These solutions were incubated at room temperature for exactly 120 minutes, then UV absorbance was measured at 562nm by UV spectrophotometer (UV-1800, Shimadzu

UV Spectrophotometer). The UV absorbance relates to the concentration of proteins within the solution.

4.1.2 Measurement of Total Organic Carbon

Measurement of Total Organic Carbon (TOC) of supernatant solution and the permeate samples from each flux stepping were carried out using a Total organic carbon analyser (TOC-V CSH, Shimadzhu). Prior to the measurement, each sample was filtered through a 0.45μm syringe filter (Acrodisc syringe filter, Pall) to assure that the size of any particles within the solution was below the machine's highest threshold limit.

4.1.3 Extracellular polysaccharide classification and definition

Since the microalgae suspension used in these experiments contains a substantial amount of extracellular polysaccharide (EPS), classification and definition of EPS are clarified here in order to avoid confusion, since there is no standard for classification of EPS[147]. EPS can roughly be classified into 3 types: soluble EPS (supernatant EPS or SMP); loosely bound EPS; and tightly bound EPS. Membrane Bioreactor (or MBR) researchers refer to soluble EPS as SMP or EPS within the supernatant. Loosely bound EPS is that for EPS of the pellets extractable via chemical or physical (eg. sonication) methods. Tightly bound EPS requires further extraction of the pellets where heating is involved. It can be concluded that in MBRs, classification of EPS is due to the strength of polymer linkages.

In this report, soluble EPS refers to small molecules that remain in supernatant after 10 minutes of centrifugation at 4000rpm. They can enter the pores more easily; however, a fraction can be retained on the membrane due to its stickiness. Bound EPS refers to EPS that is chemically extracted from the pellets collected from centrifugation at 4000rpm for 10 minutes. Loosely bound EPS (LB-EPS) surrounds the algal cells helping the EPS molecules to attach to one another, but the algae are

mostly free within the network. LB-EPS is deformable and its linkage can be broken more easily by the shear range used in the experiments. LB-EPS is also affected by the presence of $CaCl_2$. Definition of deformable in this report is a reference to deformation when subject to shear within the system.

4.2 Results and discussion

In this section, transmembrane pressure information and DOTM image analysis will be reported, together with analysis of feed and permeate. Both the feed and permeate were collected every 17.5 minutes throughout the run, and analysed for extracellular polysaccharide content (EPS), concentration, protein content, and total organic carbon content (TOC). EPS-polysaccharide within the feed supernatant, and of the pellet extracts had values between 1-2ppm and 6-8ppm respectively. TOC of the feed supernatant remained around 0.2 mg per mg of algae. Analysis of the protein content for the feed supernatant, the feed pellets, and the permeate every 17.5 minutes were all negligible. This indicated that under the condition used, no damage of the algal cells were detected.

4.2.1 Effect of crossflow velocities

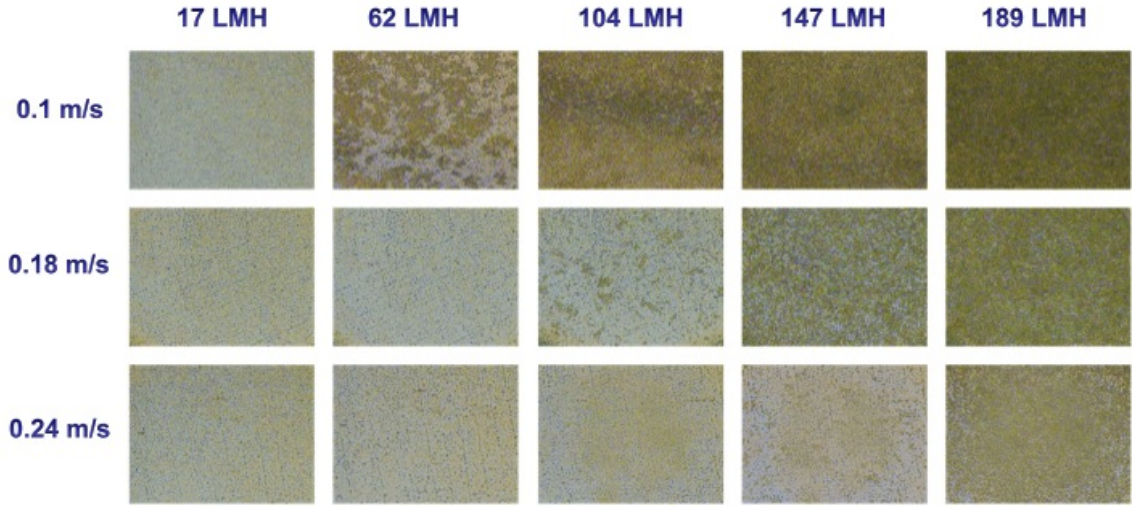

Figure 4.2: Comparison of microalgae deposition at various fluxes and crossflow velocities

Figure 4.2 shows a comparison of microalgae deposition at various fluxes and crossflow velocities. The algae used for experiments in section 4.2.1 was from a different batch from those in section 3.3.1, but was grown at the same conditions. The pattern of behaviour of average transmembrane pressure iterated by flux stepping was very similar for each crossflow velocity. Similar trends were shown throughout for all the crossflow velocity values. At higher fluxes, the rate of increase of transmembrane pressure increased. The analysis of organic content of both the permeate and the feed revealed a more intriguing observation which is the main focus of this chapter.

4.2.1.1 Analysis of Organic Content

Extracellular polysaccharide (Carbohydrate content) Extracellular polysaccharide (EPS) content of the feed remained relatively constant. The supernatants had values of around 2ppm whilst the pellets had values in the range 6-8ppm. EPS-protein was also measured throughout; however, its concentration was negligible or was below the detection limit.

Figure 4.3 shows permeate EPS vs flux at different crossflows. As crossflow veloc-

ity increased, the peak of polysaccharide content in the permeate shifts towards the left, from a flux of around 180 lmh to 116 lmh at a crossflow velocity of 0.175m/s and 0.237m/s respectively. The peak value has also become more noticeable at a crossflow velocity of 0.175m/s and 0.237m/s than at 0.107m/s. This indicates that during the flux stepping, as flux increases, greater amounts of EPS-polysaccharide were caused to penetrate through the membrane. There exists a flux at which the penetration of EPS is a maximum. After this flux, the concentration of EPS-polysaccharide in the permeate reduces. This could be due to fouling within the membrane pores by EPS.

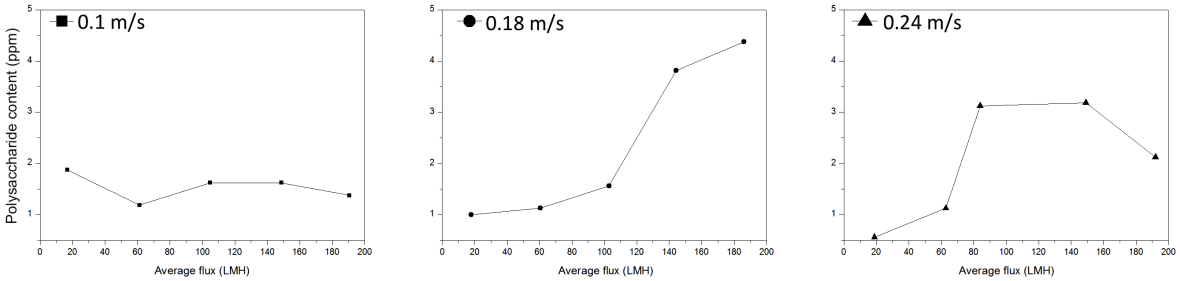

Figure 4.3: EPS-polysaccharide of the permeate at different crossflow velocities.

EPS-polysaccharide concentration of the collected permeate eventually became higher than the concentration of EPS-Polysaccharide in the feed supernatant, but it is still lower than EPS-Polysaccharide concentration extracted from the pellets. The concentration polarisation equation yields $C_w = (C_b - C_p) * exp(\frac{J}{k}) + C_p$, which implies lower concentration at the membrane surface as mass transfer coefficient increases as a result of higher crossflow velocity. In principle, the sources of this extra amount of EPS-Polysaccharide in the permeate are: (i) the EPS of the supernatant of the feed solution accumulating on the membrane surface, or (ii) the EPS from the sheath surrounding the algal cells, or (iii) extra EPS released by the algal cells due to stress experienced at the membrane surface or some combination of these.

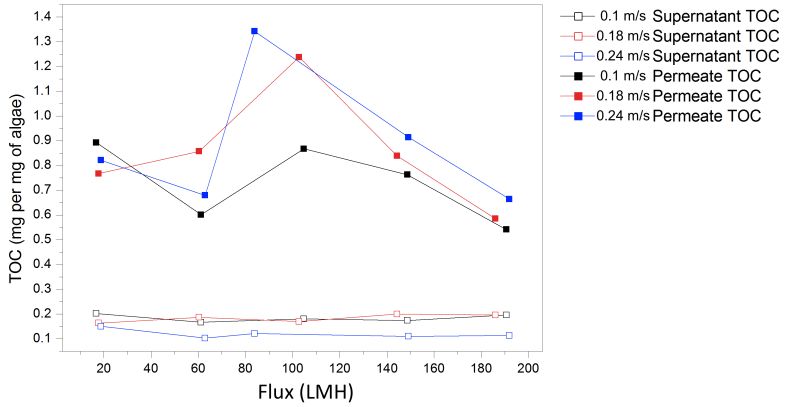

Figure 4.4: TOC (per mg of algae) of the permeate and the feed supernatant at different crossflow velocities

TOC and IC Figure 4.4 shows total organic carbon (TOC) content (mg per mg of algae) within the feed supernatant (open symbols), and in the permeate(closed symbols) at a crossflow velocity of 0.1m/s. 0.18m/s, and 0.24m/s at different fluxes. Most feed concentrations had an inorganic carbon concentration of 0.15+/-0.05 mg per mg of algae. For all conditions, the TOC content of the permeate was much higher than that of the feed solution. Higher crossflow velocities generally resulted in greater TOC in the permeate especially at high fluxes. Information from TOC content indicates that there is a possibility of retained carbon content on the membrane surface during the second flux stepping at all crossflow velocities. This retained carbon content could be EPS molecules resulting from accumulation of the cake on the membrane surface or within the membrane pore. It is hypothesized that, as flux increases, local fluxes became high enough to disturb the retained solutes, resulting in more small solutes passing through the membrane pores; hence increased values would be detected in the permeate. As flux increased further, the resulting EPS-Polysaccharide and TOC content reduced which might be explained by intend fouling of membrane leading to pore narrowing. It is also possible that, at this point, the flux is above the critical flux of the algal cells, and the fouling mechanism due to external pore blocking by the algal cells has started to dominate.

4.2.2 Effect of salt addition

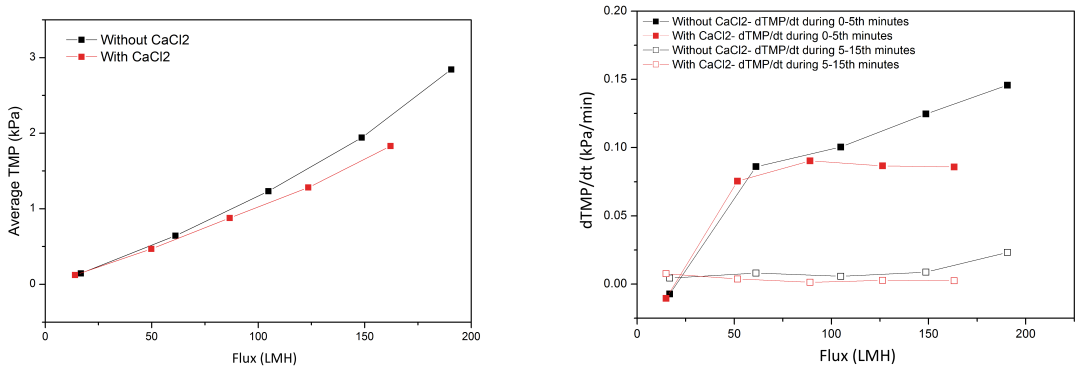

(a) TMP against flux

(b) dTMP/dt against flux

Figure 4.5: TMP against flux and initial and 5-15th minute rate of increase of transmembrane pressure against flux for algal solution at 29 mg/L with and without addition of $CaCl_2$ at CFV 0.1m/s when flux stepping started from below critical flux for the algae cells.

Figure 4.5 illustrates the effect of a higher concentration of $CaCl_2$ on fouling behaviour of microalgae. 0.5M $CaCl_2$ was used. The addition of a large amount of $CaCl_2$ resulted in lower average transmembrane pressure during flux stepping experiments than without salt addition. The flocculation of algae could be visually observed. The algal sheath seemed to be stickier, and attach more to surfaces. Nevertheless, the 0-5th minute dTMP/dt for algae with $CaCl_2$ was less severe at high fluxes than for the algae without $CaCl_2$ addition. 0-5th minute dTMP/dt increased from approximately 0.09 kPa/min at the lowest flux to 0.15kPa/min at the highest flux. The 5-15th dTMP/dt for algae with and without were both very small at most fluxes (see Figure 4.5b).

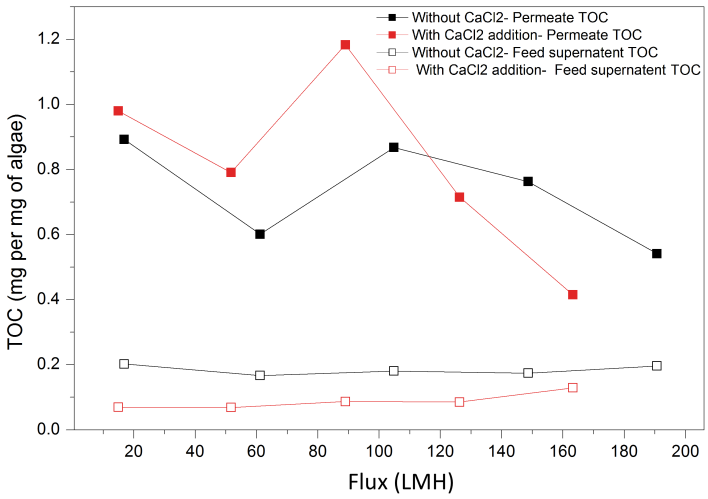

Figure 4.6: Total Organic Carbon (mg per mg of algae) of the permeate and the feed supernatant for algae solution at 29 mg/L with and without addition of $CaCl_2$ at CFV 0.1m/s when flux stepping started from below critical flux for the algae cells.

Figure 4.6 revealed total organic carbon content (TOC) of the feed supernatant and the permeate during the run. With the addition of $CaCl_2$, the feed supernatant's TOC reduced by approximately a half. TOC of the permeate was significantly higher than TOC of the feed supernatant at all conditions. Possible reasons include consideration of C_g and loosely bound EPS. It is possible that the accumulated EPS on the membrane surface led to C_g that was much higher than C_b and a large portion of this was transmitted through the membranes, or that the increase in TOC in the permeate was due to bound EPS around algal cells.

4.2.3 Effect of membrane type

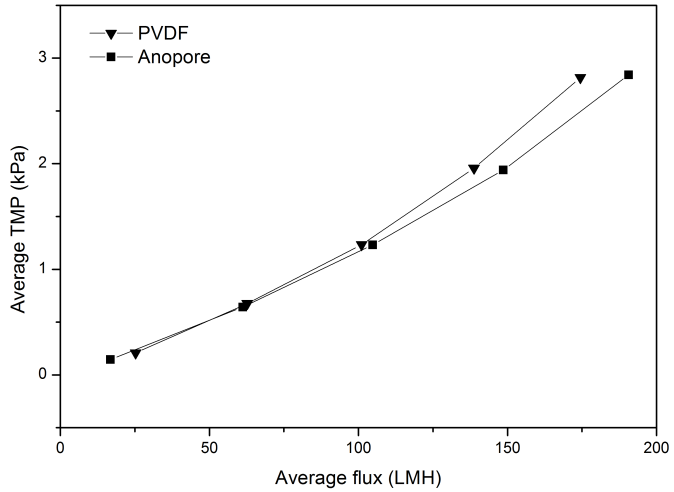

Figure 4.7: Transmembrane Pressure against flux for 29mg/L algal suspensiom for Anopore and PVDF membranes at CFV 0.1m/s.

PVDF membranes of the same pore size as Anopore membrane (0.2μm) were use to compare fouling bahaviour of algal suspension. Figure 4.7 shows average transmembrane pressure against flux for flux stepping of algal suspension using different kinds of membranes. Based on transmembrane pressure data, PVDF resulted in very similar behaviour to that of the Anopore membrane at early fluxes. At approximately 150LMH and above, fouling of PVDF membranes was slightly higher.

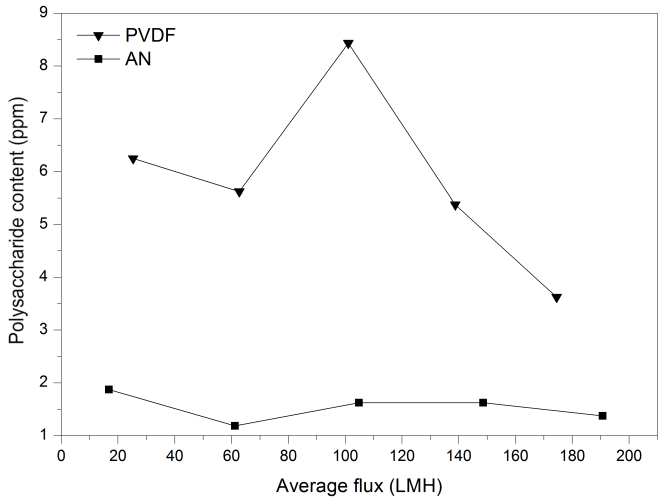

(a) Extracellular polysaccharide in the permeate

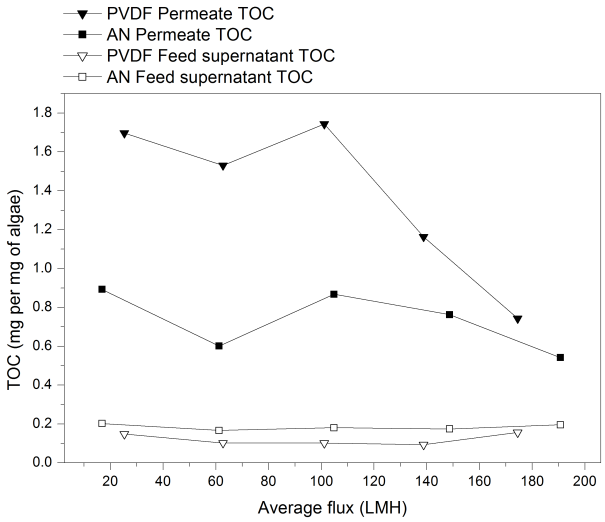

(b) Total Organic Carbon (mg per mg of algae) in the permeate and the feed supernatant

Figure 4.8: Extracellular Polysaccharide in the permeate and Total Organic Carbon (mg per mg of algae) in the permeate (closed symbols) and in the feed supernatant (open symbols) for Anopore and PVDF 0.2µm membranes at CFV of 0.1m/s with algal concentration of 29 mg/L.

Analysis of permeate and feed content revealed that PVDF membranes, with its broader pore size distribution and interconnected pores, resulted in considerably more EPS and TOC transmission than Anopore membranes. EPS in the feed super-

natant and the feed pellets were between 1-2ppm and 6-8ppm respectively. Figure 4.8a shows that EPS in the permeate for PVDF membranes was about 3 times greater than the permeate for Anopore membranes. The EPS in the permeate for PVDF membranes was high even at low fluxes, and these values were much higher than the EPS content of the feed. The trend of the EPS concentration was similar to the TOC content trend (see Figure 4.8b). TOC of the permeate for PVDF membranes was approximately twice as much as TOC of the permeate for Anopore membranes, and TOC of the permeate were always much higher than the TOC of feed supernatant. Decreasing values of EPS and TOC concentration of the permeate at later fluxes could result from the dynamic cake layer. The membrane pores were obstructed, therefore less of the organic molecules could pass through.

4.2.4 Effect of Membrane pore size

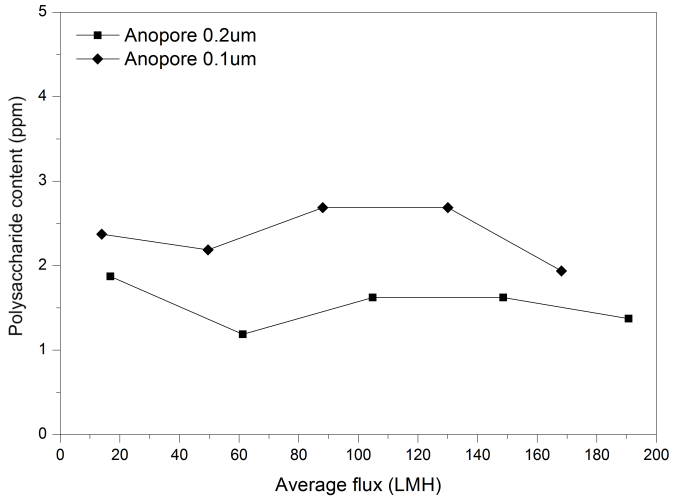

(a) Extracellular polysaccharide (ppm) in the permeate from Anopore membranes with pore size 0.1µm and 0.2 µm for 29mg/L algal suspension at CFV of 0.1 m/s.

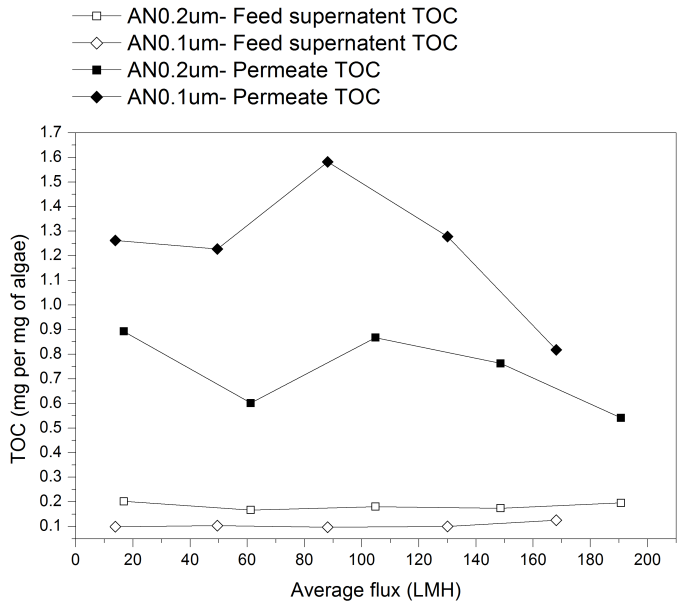

(b) TOC (mg per mg of algae) in the permeate and in the feed supernatant with Anopore membranes of pore size 0.1µm and 0.2 µm. Operation at CFV of 0.1m/s with 29mg/L algal suspension.

Figure 4.9: Extracellular polysaccharide in the permeate and TOC (mg per mg of algae) in the permeate (closed symbols) and in the feed supernatant (open symbols) for Anopore 0.1 and 0.2µm membranes at CFV of 0.1m/s with algal concentration of 29 mg/L.

The trend of average transmembrane pressure against flux of filtration of algae at CFV of 0.1m/s using 0.1µm and 0.2µm Anopore membranes were very similar. However analysis of organic content revealed interesting differences as shown in Figures 4.9a and 4.9b. With 0.1µm, EPS concentration of the permeate at different fluxes was found to remain low compared with pellet EPS, however it was slightly higher than the EPS concentration of the feed supernatant. The peak values of TOC remained at a flux of 100LMH for both 0.1µm and 0.2µm. It can be seen clearly in Figures 4.9a and 4.9b that both the EPS and TOC content in the permeate were much higher than that in the feed. Also this effect was much more pronounced at all fluxes for the 0.1µm membrane, the smaller pore size membrane, than for the 0.2µm membrane. It is possible that higher shear rate in the 0.1µm membrane was responsible for higher transmission of EPS.

4.3 Discussion and conclusion

The main aim of this section is to propose a fouling mechanism of algal cells under the influence of shear. It will start with a summary of findings, followed by a rationalisation of the observations, after which, a brief discussion and a final conclusion will be made.

4.3.1 Summary of findings

Information on the amount of EPS in the feed, and the permeate would greatly help explaining fouling behaviour reported in Chapter 3. Effect of crossflow velocity was again repeated with feed and the permeate being monitored for EPS, protein content, concentration, and TOC every 17.5 minutes throughout the run. The result for EPS is summarized in table 4.1. Feed concentration of 29mg/L and similar flux stepping range as Chapter 3 were used. While at low CFV, the permeate contained

similar EPS-polysacchride as the feed supernatant, at medium and high CFV, the amount of EPS was significantly higher in the permeate than in the feed supernatant but lower than in EPS extracted from the pellets. Figure 4.3 shows that flux did not result in much variation in EPS in the permeate at low crossflow velocities, while at medium and high CFV the EPS-transmission was induced by higher fluxes. Similarly, Figure 4.4 illustrates that higher CFV generally led to higher TOC content in the permeate at higher fluxes. Again, permeate TOC was significantly higher than feed supernatant TOC at all fluxes. Subsequent decreases in EPS and TOC in the permeate at higher fluxes was thought to be due to fouling.

It is of interest to seek an explanation for these observations 1) The greater amount of EPS-polysaccharide and TOC detected in the permeate than in the feed supernatant 2) Greater amount of EPS-polysaccharide detected in the permeate at high crossflow velocity and 3) Greater amount of EPS in the permeate when smaller pore size membrane is used. For 1), it is possible that the source of extra EPS-polysaccharide/ TOC came from (i) the EPS of the supernatant of the feed solution accumulating on the membrane surface, or (ii) the EPS from the sheath surrounding the algal cells, or (iii) extra EPS released by the algal cells due to stress experienced at the membrane surface or some combination of these. One could assume that the lack of algal cells at high crossflow velocity that could otherwise act as filter-aid[18], preventing EPS from approaching the membrane surface, was responsible for 2). Nevertheless, this assumption can not explain the earlier result mentioned as Case A (where average transmembrane pressure was higher for higher crossflow velocity while fractional coverage of membrane of both were still at minimal level). It is therefore reasonable to conclude that 2) was due to a relation between EPS and crossflow velocity, whether (i) higher crossflow velocity induces higher EPS content in feed supernatant, or (ii) higher crossflow velocity induces higher deposited EPS

Condition	Feed solution				Permeate solution	
	Pellets		Supernatant			
	EPS-Protein	EPS-Polysaccharide	EPS-Protein	EPS-Polysaccharide	EPS-Protein	EPS-Polysaccharide
Crossflow velocities 0.1m/s, 0.18 m/s, 0.24m/s	Negligible	Remain unchanged, value is between 6 and 8ppm	Negligible	Remain unchanged, value is between 1 and 2ppm	Negligible	At 0.1m/s: Between 1 and 2 ppm At 0.18m/s: Increasing, from1ppm to approximately 4.5 ppm as flux increased At 0.24m/s: Increased then decreased, from 0.1ppm to approximately 3.2 ppm as flux increased, then decreased to about 2ppm as flux increased further
Membrane type Anopore and PVDF 0.2um	Negligible	Remain unchanged, value is between 6 and 8ppm	Negligible	Remain unchanged, value is between 1 and 2ppm	Negligible	For PVDF membranes, transmission was between 3.5-8.5ppm. This was much higher than for Anopore (1-2ppm). Transmission initially increased as flux increased, then decreased as flux increased further.
Membrane pore size Anopore 0.1 and 0.2um	Negligible	Remain unchanged, value is between 6 and 8ppm	Negligible	Remain unchanged, value is between 1 and 2ppm	Negligible	At all fluxes, transmission through 0.1um membranes (1.8-2.5ppm) was higher than transmission through 0.2um membrane. Nevertheless, the transmission profile (conc. Vs flux) was similar.
0.5mM KCl and $CaCl_2$ addition	Not tested					
Air-bubbling	Not tested					

Table 4.1: A table summarized EPS results

on the membrane surface (loosely bound deposition and/or released EPS by deposited cells), or (iii) higher crossflow velocity directly led to higher EPS transmission need to be further observed. There is a low possibility that (i) was the case, as significant changes in EPS/TOC in feed supernatant was not detected. With DOTM observation, (ii) can be concluded as one of the reasons. To further explore if (iii) (influence of crossflow velocity on transmission of feed supernatant EPS in absence of cells) made a contribution, microfiltration of algal supernatant alone (without cells) was planned. Unfortunately, this could not be carried out due to lack of Anopore membrane availability at the time.

In conclusion, it is noticable that shear due to crossflow velocity, although several magnitudes smaller than the shear due to permeate flux, plays an important part in membrane performance in particular dislodging the algal cells from its sheath during their contact with the membrane surface. Whether the shear on the feed side has a direct effect on fouling and transmission of EPS should be explored. The effect of shear on fouling and transmission of a model EPS is covered in the next Chapter.

Filtration performance did not seem altered with addition of KCl, while addition of a small amount of $CaCl_2$ worsens membrane performance (see Chapter 3). Addition of a large amount of $CaCl_2$ on the other hand led to improved membrane performance. TOC content in the permeate with $CaCl_2$ addition was higher than without $CaCl_2$ even though the feed supernatant for algal suspension with $CaCl_2$ contained less amount of TOC than algal suspension without $CaCl_2$. This indicates that the bound EPS may be responsible for the increased TOC in the permeate rather than the supernatant EPS. Lower TOC content in the permeate at higher fluxes was assumed to be due to the better filter-aid performance by the algal cells and its $CaCl_2$ -sticky sheath. The layer of algal cells with sticky but high water permeability sheath prevents further feed supernatant EPS entering the membrane pore directly.

Observation of membrane surface under microscope revealed that high $CaCl_2$ addition led to the algal cells behaving very similar to algal cells from aged broth. Both resulted in thicker or larger EPS. These EPS formed a web-like structure that trapped the algal cells, and seem more difficult to be removed by crossflow velocity. The water permeability of the web-like cake was high, and resulted in a very low rate of increase of transmembrane pressure. Under these conditions it was possible to run experiments at high flux for a long period of time without breakage of the membrane.

PVDF membranes of the same pore size as Anopore membrane (0.2μm) were use to compare fouling bahaviour of algal suspension. PVDF membranes allow higher transmission of EPS through the membrane than Anopore membranes. It is reasonable to assume that the significantly greater transmission of EPS through PVDF membranes at all fluxes was due to interconnectivity of PVDF membrane structure.

The influence of membrane pore size of 0.1μm and 0.2μm Anopore membrane was observed. It is interesting to find that smaller membrane pores allowed greater transmission of EPS through membranes. For a membrane with straight through pore with the same membrane porosity, smaller pore size will result in higher shear rate within the membrane pore at the same flux. Even though when flux for 0.2μm membrane was 4 times higher than the initial flux for 0.1μm membrane, hence greater in-pore shear rate, EPS content in the permeate of 0.2μm membrane was significant lower than that of 0.1μm membrane. Three possible explanations arised; 1) The membrane porosity was lower for 0.1μm membranes, 2) Transport of EPS through membranes at higher fluxes was inhibited by deposited algal cells and EPS during earlier flux steps, and 3) Transport of EPS through membrane is due to other mechanisms, eg. transport of polymer.

4.3.2 Rationalisation of visual observation of algae deposition and removal on membrane surface.

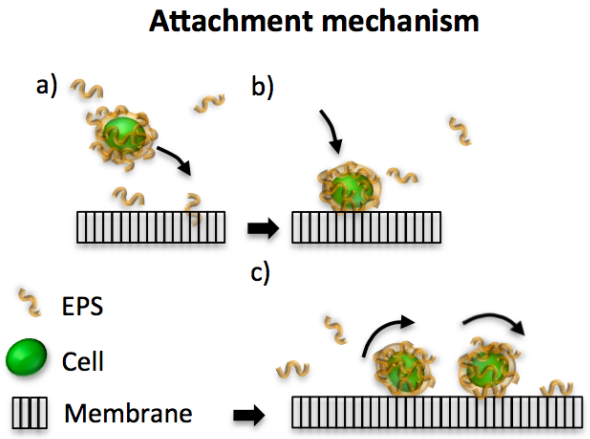

Figure 4.10: Algal interactions with membrane surface: Attachment mechanism

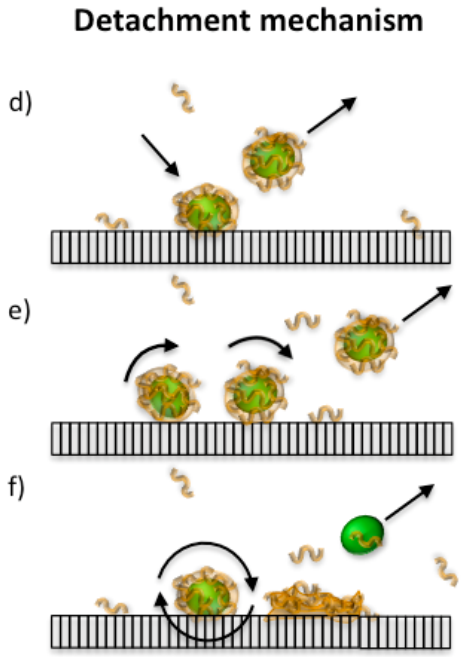

Figure 4.11: Algal interactions with membrane surface: Detachment mechanism

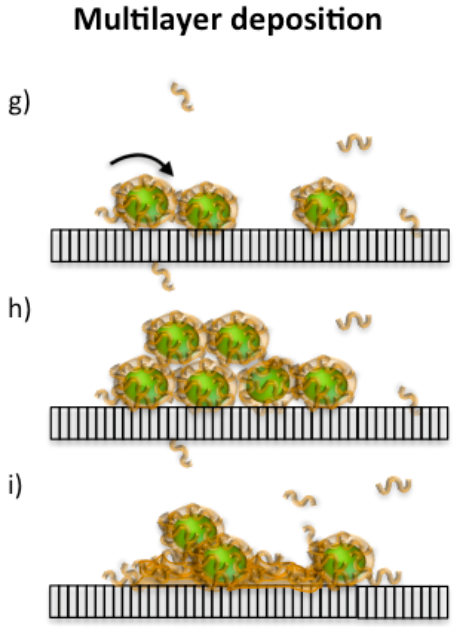

Figure 4.12: Algal interactions with membrane surface: Multilayer deposition

With the use of DOTM, deposition and removal mechanism of algal cells can be visually observed. A schematic picture describing this is shown in Figure 4.10 to 4.12. When the algal cells, surrounded by its EPS sheath, come into contact with the membrane surface (a), the algae may attach to the membrane surface (b), or be seen to roll along the membrane surface (c). If the tangential shear exceeds the adhesion force (EPS-membrane adhesion force), then the algae will be lifted away from the membrane surface (d) or roll to the surrounding area prior to taking off (e). If the tangential shear is less than the adhesion force, the algae will stick to and rotate about itself at that specific point on the membrane until the tearing of the sheath occurs. When the shear force experienced is greater than the EPS molecule-molecule linkage force, the algae will be released from the sheath and rolled out leaving the sheath behind (f). The attachment of the sheath and the membrane is very strong, and removal of this sheath from the membrane surface was rarely observed. The tearing of the sheath also occurred at higher fluxes. If the local flux, especially the local flux near to the deposited algae is higher than critical shear of

the EPS, then the EPS may be deformed and pass through the pores leaving the algae with a reduced adhesion force to the membrane. After this, whether the algal cell will get stuck to a neighbouring part of the membrane surface depends on the remaining amount of EPS in the surrounding algal cells. If the algal cell is still surrounded by an sufficient amount of remaining sheath, the algae removal process will repeat until the tangential shear exceeds the adhesion force or lead to the release of the cell from its sheath.

In the case where the algae have aged, and when salt concentration of the feed was altered, especially with $CaCl_2$ addition, agglomeration of the EPS around the algae occurred. It was visible through a microscope that the EPS deposition on the membranes became thicker and larger. The EPS were visually observed to be more abundant and tear less easily, leading to lower algal removal from the membrane surface as well as thicker formation of the algal cell layer on the membrane surface.

Multilayer deposition of algal cells occurred especially above the critical flux. The newly arrived algal cells tend to attach to the area adjacent to the previously attached cells (g); the surrounding sheath provides extra force for adhesion. The formation of cake layer can occur in patches and it is not necessary that the first layer must be formed all over the membrane before second layer deposition occurs (h). Detachment of algal cell from its sheath (f) which resulted in a sheath remaining on the membrane attracts further algal deposits.

4.3.3 Discussion

There are three significant findings from this experimental study. Firstly, the influence of crossflow velocity and flux on fouling and transmission. Secondly, the effect of microalgae environment and aging on deposition and fouling of membrane. Thirdly, the attachment, detachment and multilayer deposition of the algal suspension during filtration.

While DOTM image analysis always revealed the lower amount of algal deposition

on the membrane surface at higher crossflow velocity, the adverse effect of crossflow velocity on transmembrane pressure was also observed under certain filtration condition. The changes in EPS transmission at the same flux with increases in crossflow velocity suggests that transport of EPS through the membrane varied with shear on the feed side and the permeate flux used. The adverse effect of shear on membrane performance has been previously observed; examples include the increase in cake resistance when the systems operated at increasing crossflow velocities and at an aeration rate [132, 148, 149, 150, 151] that are above a certain level.

Attachment of the particles on the membrane surface under the influence of flux has previously been visuallised. Mackley et al. observed that when flux dominates, particles are found to direct towards the filter surface[152]. At the initial stage, particles took a parabolic motion to deposit and remain at the membrane surface under the circumstance where crossflow velocity and filtrate velocity were similar[152]. Later on, crossflow velocity dominated, and the particle flow direction was almost parallel to the surface. Attachment of particles occurred after particles arrived to the surface; they rolled until they met an edge[152]. This resulted in a "highly selective" packing, which led to greater cake specific resistance[152, 153]. The back diffusion of particles were not found[152].

The introduction of air-sparging or bubbling increases shear on the feed side, even though this results in removal of larger particles from the membrane surface and selective packing of smaller particles, it may also lead to elongation of the polymeric molecules which may enter the pores' mouth. Polymeric molecule transport through membranes is known to be sensitive to changes in operating conditions, such as the permeate flux and pressure[122, 123, 124]. The importance of biopolymer molecular flexibility on membrane performance has been observed[154]. It does not seem surprising if the polymeric molecule transport through narrow channels or membranes is also shear dependent, since these molecules often have shear thinning properties. At low flux, where the local flux within the pore is subcritical of the critical shear

for polymer elongation, the effect of bubbling will only increase the internal fouling within the membrane pores. Moreover, the extra shear on the feed side can disturb microorganisms, and lead to the production of foulant, e.g. when algae are subject to stress, more EPS are released.

Adhesion between the EPS and membrane surface has been found to be dependent on ionic strength (NaCl) of the solution[155]. High ionic strength compresses Debye length, i.e., nullified the charge between EPS and membrane surface. This allows van der Waals attraction force to dominate which causes higher fouling tendency. The ionic strength also affects conformation of polymers[155]. Increases in the ionic strength led to the collapse of the adsorbed EPS layer[155]. The influence of salt addition on EPS modification varied, depending on the type of salt. Divalent salts, in particular, are known to form ionic bridging between two Carboxyl groups, or between Carboxyl and Hydroxyl groups which resulted in crosslinking between polymers[156]. For example, the algal EPS has been found to be more susceptible to change by $CaCl_2$ addition than NaCl, KCl, or $MgCl_2$ addition[130, 128]. From DOTM observation, the influence of $CaCl_2$ resulted in thicker and sticker sheaths which were easier to deposit and were rarely removed by crossflow velocity. From the experiments, it was concluded that addition of sufficient amount of $CaCl_2$ resulted in not only agglomeration of the EPS arounding the algae but also that the deformability of overall EPS was reduced.

Many MBRs have been studied, one of the interesting findings is that fouling resistance is caused by mostly loosely bound EPS rather than tightly bound EPS[132]. Ramesh et al. observed that even though TB-EPS is responsible for high filtration resistance, in mixed suspension the filtration resistance was controlled by LB-EPS fraction[147]. This fits well with DOTM observation.

After the initial deposition, further deposition of algal cells is similar to that observed by Bustness et al[51]. The trapped biomass grows in size by capturing further biomass that passes. Bustness reported that this behaves in a similar way

to the "ripening" effect in deep-bed filtration studies[51]. Ripening effect in sand filtration is achieved by allowing a slow flow through the sand filtration to provide Schmutzdecke (a gelatinious layer of microbial)[157]. The Schmutzdecke layer can be liable for more than 50% of pollutant removal for wastewater treatment using sand filtration[158]. This helps explain lower TOC transmission at the higher fluxes for filtration of microalgae with $CaCl_2$ addition than for that without $CaCl_2$. However, at lower fluxes, the TOC transmission was greater for filtration of microalgae with $CaCl_2$ addition.

The rationalisation of DOTM observation on microalgae filtration can contribute towards a future model for microbial fouling. For example, Maniero et al. has considered several mechanisms for particle detachment in his model[159]. These are the commonly considered three detachment mechanisms, lifting, sliding and rolling[159, 160]. It has also been suggested that the rolling mechanism was accountable for glass particle detachment from a glass surface, and this was the only mechanism used that Maniero chose to include in his model[159, 161]. In this model it is assumed that rolling occurred when the torque of adhesion is equal to or greater than the sum of the hydrodynamic torque induced by surface stresses which consists of the drag force parallel to the wall times distance between particle and the wall, and lift force times the radius of contact. The lift force contribution was found to be negligible. Overall the critical wall shear stress is related to the work of adhesion force, particle size, and the reduced elastic modulus[159].

In my work it was observed that with regard to microalgae detachment, sliding occurred only at low flux, and only when the algae was relatively fresh, i.e., less sticky. At higher fluxes and when the algal broth used was slightly aged, the sliding was rarely observed because the sheath became much stickier. Moreover, it was also observed that a certain amount of shear could result in tearing of the sheath of deposited algae and hence the release of algal cells from the membrane surface; however, this substantial reduction in the number of deposited algal cells does not

necessarily always lead to improved overall membrane performance. A future model for microbial fouling especially when fouling by supernatant is negligible may classify the detachment mechanisms, depending on the level of shear stress experienced by the cell. In other words, re-entrainment of the cell together with its attached sheath and removal of the cell from its torn-apart sheath. As mentioned earlier, the latter will lead to changes in surface adhesion property because the remaining sheath attracts further cell adhesion.

4.3.4 Conclusion

Microfiltration of microalgae was carried out at various condition using DOTM. The algal deposition on the membrane was compared with transmembrane pressure data, and in most cases, DOTM was shown to be a more sensitive method for fouling monitoring and obtaining the threshold flux. The algal environment had a strong effect on algal deposition and transmembrane pressure. It is important that further studies should seek an understanding of the nature of microbes prior to using them in membrane processes. Microalgae contains both the cells and soluble component, and the optical observation alone can result in misleading information. The analysis of permeate results also showed that the transport of EPS through microfiltration membranes was affected by both the permeate flux and the crossflow velocity. The increased crossflow velocity resulted in higher transmission of EPS at the same flux, as well as a higher rate of increase of transmembrane pressure. Several mechanisms have been considered and a rationalisation of observations has been made.

5 Effect of Shear Patterns on Transmission and Fouling of Dextran Blue through Microfiltration Membranes

In this chapter, the work focuses on transmission, membrane fouling rate, and membrane irreversible fouling during microfiltration of Dextran Blue under the influence of shear in various shear patterns. The readily available filtration modules are incapable of generating a wide-range of precisely controlled shear patterns. A novel filtration module, Direct Shear Stress Test Cell (DSSTC), was therefore fabricated and used throughout for experiments in this chapter. The purpose of this chapter is to investigate the effect of steady shear, oscillatory shear, and intermittent shear on fouling and transmission of a model EPS in the absence of large particles or cells. The performance of steady shear and oscillatory shear on filtration of the same feed, at the same initial feed concentration and total permeate volume, were directly compared using the same filtration module. The influence of shear of various patterns on membrane irreversible fouling is also reported.

5.1 Introduction

The introduction of shear stress has been widely and commonly used in filtration processes to reduce concentration polarisation and membrane fouling. The conventional systems such as dead-end test cells are commonly equipped with a magnetic stirrer bar to create shear stress on the feed side of the membrane. In a cross flow filtration system, shear stress is directly controlled by fluid velocity which is generated by a pumping system. Introduction of unsteady shear stress can be easily done by adding an air pump to a crossflow system, this creates a flow of air bubbles on the feed side of the membrane. This method is known as air-bubbling or air-sparging. It reduces fluid pumping costs as well as creating unsteady secondary flow which consequently lowers concentration polarisation[162].

More innovative systems for fouling mitigation include the use of unsteady movement of feed fluid or the membrane. This is known as Dynamic filtration. Dynamic filtration refers to a system where high shear rate was produced near to the membrane by the movement or rotation of the membrane itself or the movement or rotation of a disk near to the membrane[84]. Dynamic filtration affects the permeate flux or transmembrane pressure and has an impact on membrane selectivity[84]. A well established dynamic filtration includes the Vibratory Shear Enhanced Processing or VSEP[163]. VSEP is composed of a stack of membranes that is designed to vibrate at its resonant frequency of 60.75Hz.

Other interesting dynamic filtration modules include Cone-Plate Test Cell (CPTC) and Microfiltration Cone and Plate Test Cell (MFCP) [10, 18]. These cells were designed and fabricated previously in Oxford in an attempt to overcome non-uniformity of shear in a typical filtration module. Uniform surface shear on the feed side was achieved by equipping a shallow cylinder-shape feed-side channel with a rotating inverted wide angle cone. The cone was positioned so that its apex was very close to the membrane surface, and theoretically as the cone rotates, the shear stress across the membrane radius is constant. The motion of both CPTC and MFCP cone was

driven by an electric motor and the combination resulted in a very limited ability to achieve oscillatory movement, due to inertia[18]. Despite their capability in creating uniform shear throughout, the limited shear configurations in CPTC and MFCP are the main obstacle in assessing the benefit of shear on filtration performance, in particular, the benefit of intermittent shear stress.

Investigation on effectiveness of fouling mitigation between different shear regimes is generally limited. In a crossflow module, in order to increase shear rate near to the membrane surface, alteration of module dimension and/or increasing the feed velocity is necessary. These not only require high pumping energy but the large velocity and pressure gradient results in decreasing TMP along the feed channel[84]. Moreover, the effectiveness of shear can not be accurately compared with non-shear systems such as dead-end. Stirred-cell module allows for the use of shear, however it is not capable of providing stable and easily characterised shear distribution. The stress pattern is non-uniform and significantly affected by the agitator geometry[106]. Dynamic membrane modules which are capable of generating vibratory shear are usually not able to operate in rotating mode and vice versa. Alterations between shear patterns during filtration are difficult to perform, and the generation of abrupt changes in shear profile is generally impossible.

The understanding of the effect of various shear configurations on membrane performance during microfiltration of macromolecules is essential, but it can be challenging. One of the reasons is because there is a lack of accuracy and equipment availability for comparisons to be made between various shear regimes. Moreover, general filtration modules are not capable of generating sharp changes in the direction of shear. DSSTC was therefore fabricated and was used for these purposes. Information obtained from this module will aid understanding of the influence of various shear regimes and its intermittency on membrane filtration performance. This is beneficial for the design of future filtration modules, as well as determination of the shear regimes used especially for mixed feed suspension and expensive

valuable feeds such as those in the pharmaceutical industry.

5.2 Direct Shear Stress Test Cell (DSSTC)

To address the above challenge, the DSSTC was designed and fabricated to be compatible with an Anton-Paar rheometer plate. Using a rheometer as a driving force generator eliminates the need of an electric motor, moreover this also means that DSSTC is possible to operate at precisely controlled shear configurations. Steady shear, or rotation of the rheometer plate at a constant speed, oscillatory shear both in smooth motion (sinusoidal wave) and in abrupt changes of motion (square wave) can all be carried out in the DSSTC. As the movement of rheometer plate can be programmed to start and finish precisely, membrane operations under intermittent shear are very accurate and highly reproduceable.

In this part, the basic principles of DSSTC are reported with the details of the design and development of the DSSTC apparatus. DSSTC is a tool to provide highly customisable patterns of shear stress on the feed side of the membrane. It is capable of providing a wide range of shear configurations, with an extremely fast response time compared with traditional methods. The shear rate produced is not only very reliable but can also be precisely reproduced. The effect of shear configurations on membrane filtration performance can be compared in the same filtration module.

5.2.1 Direct Shear Stress Test cells

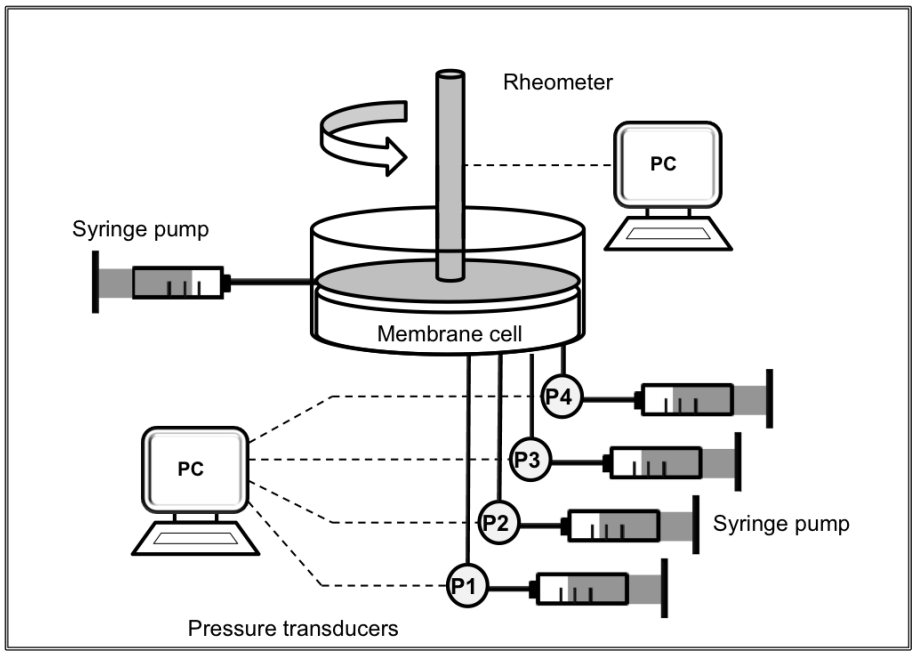

Figure 5.1: Schematic of filtration system

DSSTC is a semi-dead end, constant flux filtration device. The filtration circuit for DSSTC is illustrated by Figure 5.1. DSSTC consists of a new membrane filtration cell that was designed to fit an Anton Paar rheometer (Anton Paar, MCR 301). The rheometer was used to create shear on the feed side while the flux was generated by a syringe pump (PHD2000 Infusion/Withdraw, Harvard apparatus). Another identical syringe pump is connected to the filtration cell to replenish the fluid loss on the feed side. Since pressure transducers were connected to each permeate channel, TMP information for each channel can be seperately observed. The shear on the feed side is precisely controlled by the rheometer. It has been programmed to give a very wide variety of shear regimes and the effect of shear and transient shear on filtration of a model feed were investigated. The rheometer flat disc of 50mm diameter was used for all experiments.

5.2.1.1 Apparatus development

As mentioned earlier, Vasan et al.[10] as well as Hughes[18] have investigated the effect of uniform shear on filtration using a novel Uniform Shear Test Cell (USTC). USTC consists of a flat membrane surface with an inverted wide angle cone that is controlled by an electric motor. The module was designed so that theoretically the shear generated is uniform throughout; nevertheless, velocity and Reynolds number are not[164]. The original USTC had so much inertia that rapid changes in the shear were not possible. A new special membrane filtration cell was therefore fabricated to fit a rheometer whose movement can be precisely controlled using the rheometer software. As it is possible to create a very wide variety of shear regimes that is also highly reproducible, both the effect of shear and transient shear can be thoroughly investigated. As with the Hughes cell[18], transmembrane pressure is limited to less than 1 bar.

DSSTC can be equipped with either a flat or cone rheometer plate. A flat disc was chosen mainly because there is a distribution of shear along the radius. The permeate channels of the cell are designed to have 4 regions of equal effective membrane areas. An Isopore membrane (Millipore) was used throughout. This membrane has straight through pores. The surface shear in DSSTC is proportional to radius, angular velocity, and channel height. Each of the permeate channels are connected separately to a syringe pump which provides a very stable flow rate. This will be beneficial for investigating the effect of shear on filration, especially for filtration of live feed where the feed properties alter with time. As feed properties are one of the crucial factors affecting membrane fouling, having the same feed going simultaneously to three channels will eliminate some errors. Moreover, the cone-and-plate system should create uniform shear throughout; however when the size of the solute is comparable to that of the gap between the cone's tip and the membrane, it could lead to inaccurate results.

5.2.1.2 Geometry

The open view of the filtration module is illustrated by Figure 5.2. The inner diameter of the feed channel is 51mm. The membrane is tightly sealed between a rubber seal and an O-ring. The feed channel is held to the base of the rig using 6 screws. The permeate side is divided into 4 channels of equal effective membrane area of 4.91 cm^2 (see Figure 5.3). Four pressure transducers (PXM219-VAC000G10V, Omegadyne, Inc) are connected to a computer via a USB data acquisition system (Omega-DAQ-54, Omega). Personal Daqview Plus software was used for datalogging. The data was collected every 5 seconds.

The gap between the membrane and the rheometer plate was set to 3.6 mm, which gives a working volume of 7.35ml with a 50mm diameter plate in a 51mm feed channel. The channel height was chosen so that it is comparable to that of VSEP (3.5mm)[86] as well as having channel height-radius ratio that is within the validity of several correlation equations. Estimation of membrane surface position was measured by varying gap height using a 50mm rheometer plate. This process was repeated several times for each type of membrane to obtain an average value that was then used in subsequent experiments. Afterwards, these membranes were discarded and not used for experiments as it is likely that they had been damaged by contact with the rheometer plate.

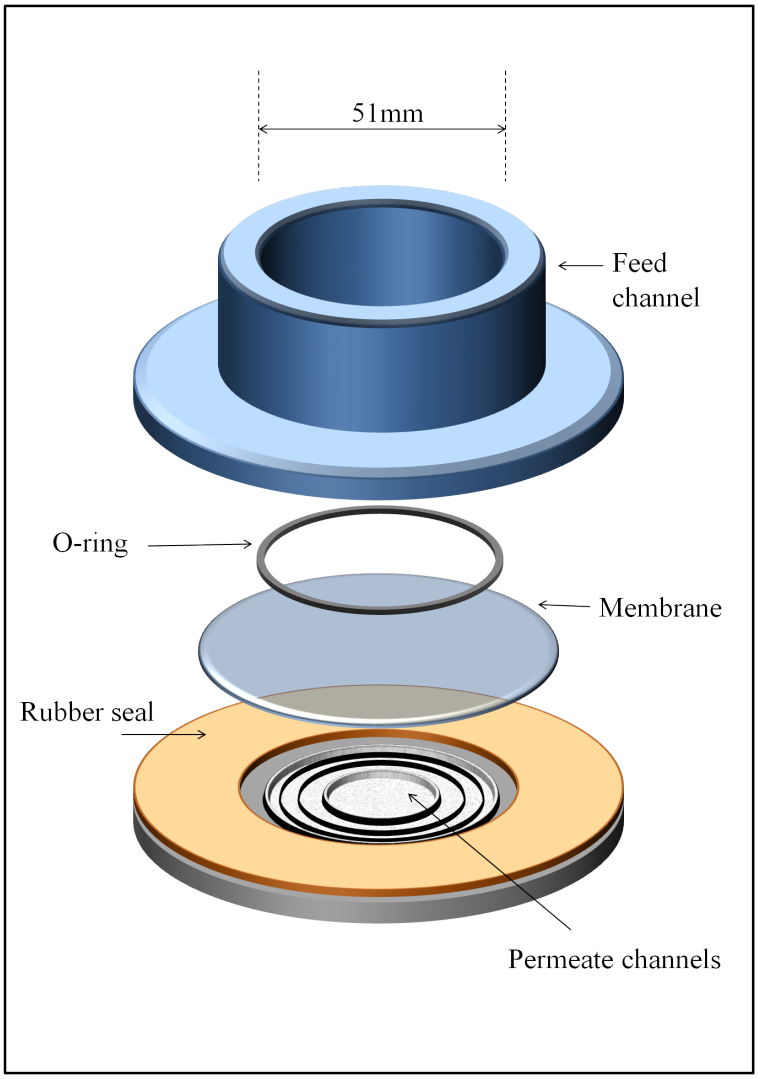

Figure 5.2: Open view of the DSSTC filtration module.

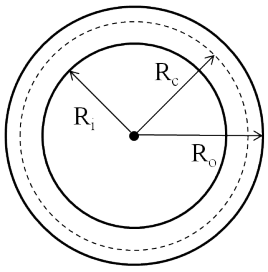

Zone	R_i (cm)	R_o (cm)	R_c (cm)
1	0	1.25	0.88
2	1.25	1.77	1.53
3	1.77	2.17	1.98
4	2.17	2.50	2.34

R_i = Inner radius of the channel
R_o = Outer radius of the channel
R_c = Centre of the channel

Figure 5.3: Radial dimensions of permeate channels of the DSSTC filtration module.

5.2.2 Theoretical design

The feed flow through the model was between 60 to 193ml/hr, which corresponds to fluid radial velocity at the rim of 2.97 to 9.48 $*10^{-5}$m/s. This value is negligible (ie. less than 1%) when compared with the plate velocity in either steady shear (range from 0.013 to 2.199 m/s), or oscillatory mode. Therefore, the effect due to radial velocity will be neglected here.

5.2.3 Characterisation of mass transfer and shear in DSSTC

Empirical and theoretical correlations for mass transfer at the enclosed fixed disc and rotating disc under steady shear are illustrated in Figure 5.1 and 5.2 respectively. The Reynolds number reported by Cavalcanti et al.[165] are substituted with DSSTC equivalent plate rotational speed (PRS).

5.2.3.1 Mass transfer co-efficient during steady shear operation

The theoretical estimation for mass transfer co-efficient (k_d) can be calculated using the equation developed by Cavalcanti[165].

$$k_d(r) = 0.761 * D^{\frac{2}{3}} * \nu^{-\frac{1}{6}} * \omega^{\frac{1}{2}} * \left(\frac{r}{(R_T^3 - r^3)^{\frac{1}{3}}} \right) \tag{5.1}$$

where $k_d(r)$ is the local mass transfer coefficient at the fixed surface, D is the molecular diffusion coefficient (m^2/s), ν is the fluid kinematic viscosity (m^2/s), ω is the angular velocity (s^{-1}), r is the radial position (m), and R_T is the radius of the rheometer plate (m).

Diffusion coefficient of Dextran in the liquid (D_{aq}) was used. According to Kommedal et al.[173] The diffusion coefficient of Dextran in the liquid can be estimated using:

$$D_{aq} = 2.8 * 10^{-9} M_w^{-0.401} \tag{5.2}$$

where M_w is the molecular weight in Da. However, one may also use a diffusion

Correlation	Validity	PRS equivalent for valid Re_{RT}	Method	Author
$\overline{Sh}_{R_F} = 0.761 Re_{R_T}^{\frac{1}{2}} Sc^{\frac{1}{3}}$	-	-	T, (A)	[166]
$\overline{Sh}_{R_F} = 0.28 Re_{R_T}^{0.567} Sc^{\frac{1}{3}}$	$H/R_T = 0.112$; $R_T/R_F = 0.9$	122.7 PRS $\leqslant$ 490.9	D, (B)	[167]
$\overline{Sh}_{R_F} = 0.0443 Re_{R_T}^{0.746} Sc^{\frac{1}{3}}$		490.9 $\leqslant$ PRS $<$ 1257.9	D, (B)	
$\overline{Sh}_{R_F} = 0.5376 Re_{R_T}^{\frac{1}{5}} Sc^{\frac{1}{3}}$		PRS $<$ 460 (Laminar)	D, T, (B)	
$\overline{Sh}_{R_F} = 0.0262 Re_{R_T}^{0.8} Sc^{\frac{1}{3}}$		PRS $>$ 460 (Turbulent)	D, T, (B)	
$\overline{Sh}_{R_F} = 0.134 Re_{R_T}^{0.68} Sc^{\frac{1}{3}}$	387 $<$ Sc $<$ 1622	89 $<$ PRS $<$ 1687.4	D, (B)	[168]
$\overline{Sh}_{R_F} = 0.2 \left(H/R_T\right)^{-0.28} Re_{R_T}^{\frac{1}{2}} Sc^{\frac{1}{3}}$	0.1 $\leqslant H/R_T \leqslant$ 1.7	1.3 $\leqslant$ PRS $<$ 138	E, (B)	[165]

Note: For DSSTC: $H/R_T = 0.144$; $R_T/R_F = 0.98$.
PRS = plate rotational speed (rpm), T = theoretical, D = dialysis, E =electrochemical; (A) and (B) = system used as instructed below, R_T = radius of the rotating plate, R_F = radius of the stationary plate.

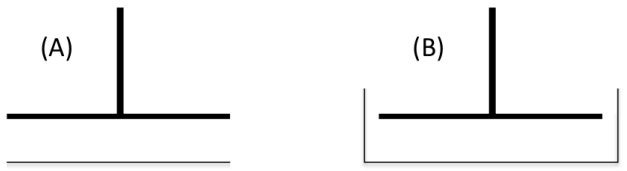

Table 5.1: Empirical and theoretical correlations for mass transfer at the enclosed fixed disc under steady shear (modified from [165])

Correlation	**Validity**	**PRS equivalent for valid Re_{RT}**	**Method**	**Author**	**Validity for DSSTC**
$\overline{Sh}_{R_F} = 0.196\,(H/R_T)^{0.26}\,Re_{R_T}^{0.63}Sc^{\frac{1}{3}}$	$0.314 < R_T/R_F < 0.575$; $3.74{*}10^{-3} < \mathrm{H}/R_T < 0.33$	$44.5 < \mathrm{PRS} < 1963.5$	DS	[169]	Not valid due to R_T/R_F
$\overline{Sh}_{R_F} = 0.04\,(H/R_T)^{-0.16}\,Re_{R_T}^{0.75}Sc^{\frac{1}{3}}$	$R_T/R_F \approx 1$; $0.0127 < H/R_T < 0.217$	$920.4 < \mathrm{PRS} < 61360$	TM	[170]	Valid
$\overline{Sh}_{R_F} = 0.05\,(H/R_T)^{0.1}\,Re_{R_T}^{0.8}Sc^{\frac{1}{3}}$		$\mathrm{PRS} > 1288.6$			Valid
$\overline{Sh}_{R_F} = 0.05\,(H/R_T)^{0.075}\,Re_{R_T}^{0.8}Sc^{\frac{1}{3}}$		$\mathrm{PRS} > 1288.6$			Valid
$\overline{Sh}_{R_F} = 0.0122\,(H/R_T)^{-0.25}\,Re_{R_T}^{0.75}Sc^{\frac{1}{3}}$	$5\ {*}10^{-3} \leqslant H/R_T \leqslant 0.125$	$481.7 < \mathrm{PRS} < 644279.6$	T	[171]	Not valid due to H/R_T
$\overline{Sh}_{R_F} = 0.0155 Re_{R_T}^{0.8} Sc^{\frac{1}{3}}$	$H/R_T = 0.0199$	$\mathrm{PRS} > 4602$	T	[172]	Not valid due to H/R_T
$\overline{Sh}_{R_F} = 0.85 Re_{R_T}^{0.5} Sc^{\frac{1}{3}}$	$R_T/R_F \approx 1$; $0.1 < H/R_T < 2.26$	$1.3 < \mathrm{PRS} < 148.8$	E	[165]	Valid

Note: For DSSTC: $H/R_T = 0.144$; $R_T/R_F = 0.98$. PRS = plate rotational speed (rpm), T = theoretical, TM = torque measurement, D = dialysis, DS = dissolution, E =electrochemical, , R_T = radius of the rotating plate, R_F = radius of the stationary plate.

Table 5.2: Empirical and theoretical correlations for mass transfer at the enclosed rotating disc under steady shear (modified from [165])

coefficient for Dextran in biofilm which is equivalent to[173]:

$$D_f = 0.3 * D_{aq} \tag{5.3}$$

From Equation 5.2 and 5.3, together with M_w of 2000kDa yields a D_f value of approximately 0.25*10^{-11} m^2/s; this is similar to the diffusion coefficient of 0.5*10^{-11} m^2/s used by Mc Donogh et al.[174]. Example results are shown in Figure 5.4 for a dilute aqueous system with water kinematic viscosity at 20ºC (ν= 1.004*10^{-6} m^2/s), and diffusion coefficient for Dextran in liquid (D = 8.33*$10^{-12}$$m^2/s$).

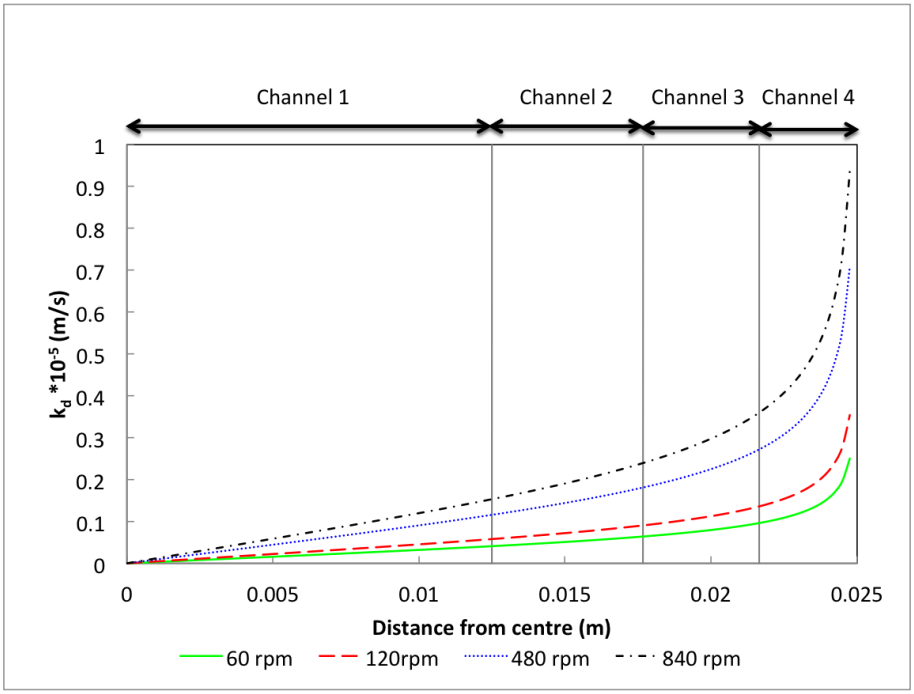

Figure 5.4: Mass transfer co-efficient (k_d) at different plate rotational speed (rpm) for different DSSTC channels.

5.2.3.2 Pressure increase due to plate rotational speed during steady shear operation

Pressure (Pa) increases due to the rotating plate at the centre of each channel was calculated for plate rotational speed between 0 to 1000rpm using Bernoulli's equation. This method has also been used by Jaffrin in 2004[175]. Pressure is proportional to the square of plate rotational speed and can be written as[175]

$$P_\omega = 0.5 * \rho * (k_{vc} * \omega * r)^2 \tag{5.4}$$

where ρ is the fluid density, k_{vc} is the velocity coefficient, ω is the angular velocity (rad/s) and r is the radius. Example results are shown in Figure 5.5 for a dilute aqueous system with velocity coefficient for a smooth disk of 0.42. This value was used in a similar system[84].

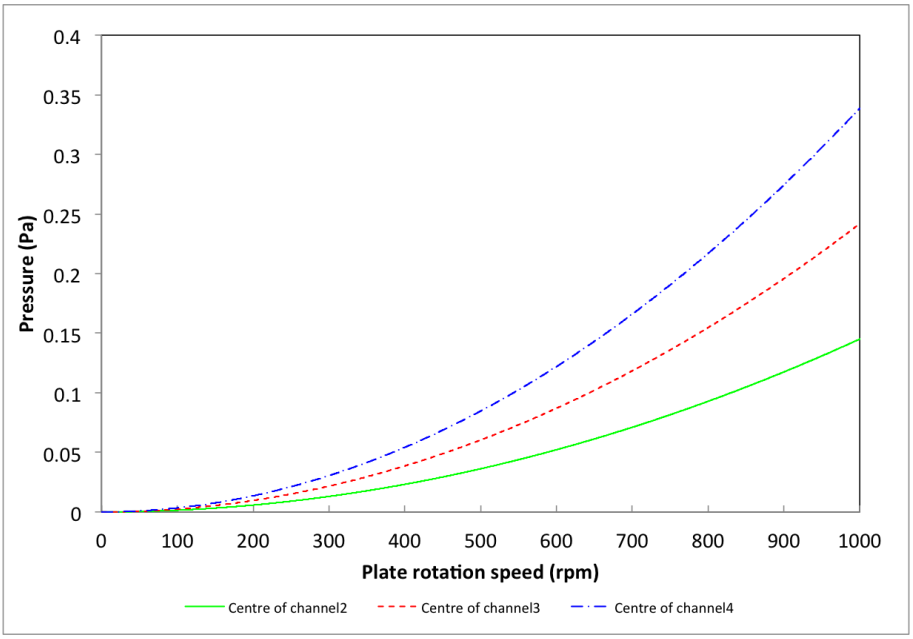

Figure 5.5: Pressure (Pa) due to plate rotational speed (rpm) at the centre of each channel

Under the range of plate rotational speed used, the pressure was below 0.4Pa. This is considered to be negligible when compared with the increases in transmembrane pressure due to fouling of the membrane, which were typically several kPa in magnitude.

5.2.3.3 Local shear rate during steady shear operation

Fluid mechanics of a plate spinning near a stationary membrane with speed below 2000rpm has been investigated by Bouzerar[109]. For laminar flow, local shear rate for this system varies with plate rotational speed as well as kinematic viscosity of

the fluid, where r in the original equation[84] was substituted with R_c (radius at centre of channel). The equation for the local shear rate becomes

$$\dot{\gamma}_{wl} = 0.77 * \nu^{-\frac{1}{2}} * (k_{vc}\omega)^{\frac{3}{2}} * R_c \tag{5.5}$$

where ν is the fluid kinematic viscosity, k_{vc} is the velocity coefficient, ω is the angular velocity and R_c is the radius at the centre of the membrane channel.

For turbulent flow (Reynolds number $> 2.5{*}10^5$), the local shear rate becomes

$$\dot{\gamma}_{wt} = 0.0296 * \nu^{-\frac{8}{10}} * (k_{vc}\omega)^{\frac{9}{5}} * R_c^{\frac{8}{5}} \tag{5.6}$$

The velocity coefficient (k_{vc}) does not change with flow regime or radial position[109].

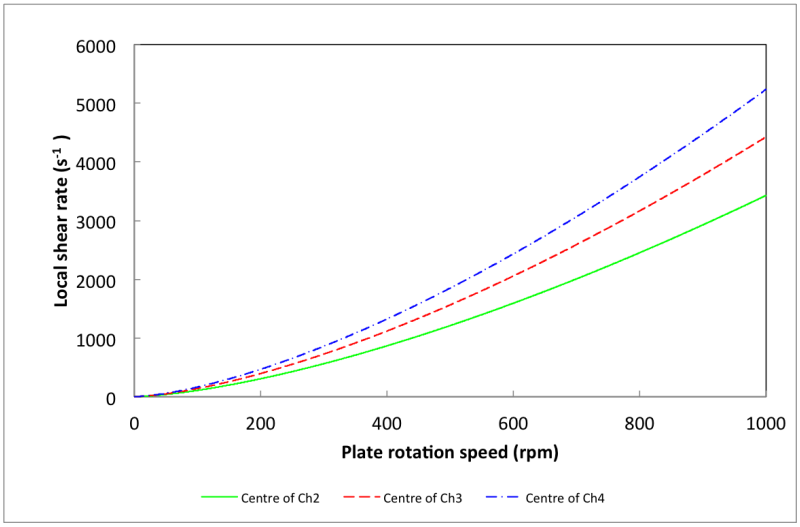

Figure 5.6: Local shear rate for laminar flow range calculated at the centre of each channel

5.3 Experimental set-up and operational issues.

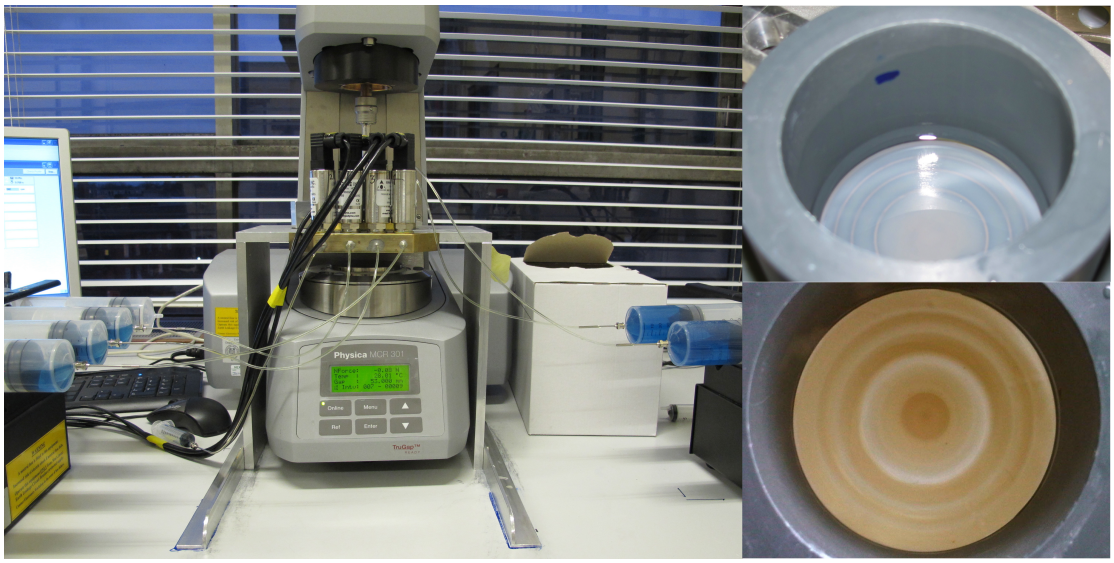

Figure 5.7: Experimental set-up (left). Mounted membrane after a Dextran experiment (Top right). Non-mounted membrane after a yeast experiment (Bottom right).

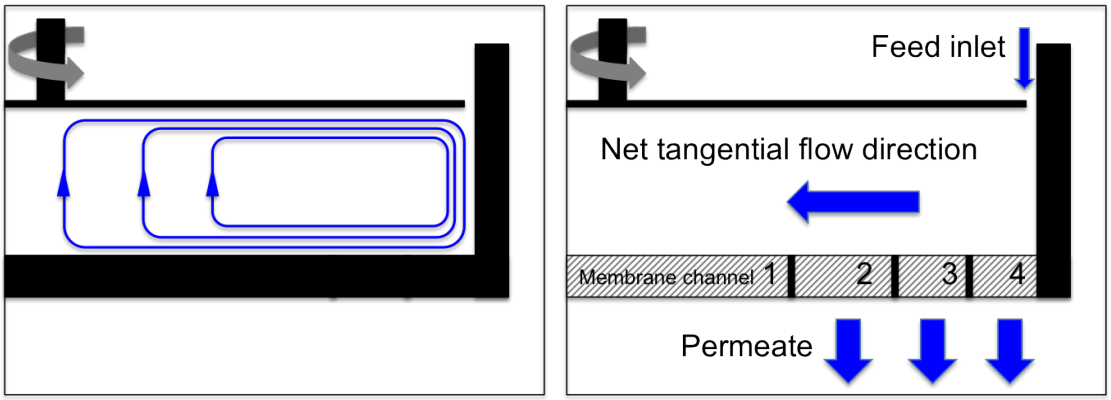

(a) Proposed flow patterns near base of a stirred tank (modified after [167])

(b) Expected net tangential flow direction during filtration using DSSTC

Figure 5.8: Proposed flow patterns near base of a stirred tank and expected net tangential flow direction during filtration using DSSTC

Figure 5.7 shows the experimental set-up (left), a mounted membrane after a Dextran Blue experiment (top right) and a non-mounted membrane after a yeast

experiment (bottom right). The proposed flow patterns within the rig when steady shear is applied is shown in Figure 5.8a. The net tangential flow direction of the feed during filtration is towards the centre of the membrane (Figure 5.8b). Both the net tangential flow during filtration and the effect of shear are therefore greater in the channel closer to the rim than that near the centre.

Two operational issues for the DSSTC were discovered. Firstly, there was some leakage from the membrane cell. This necessitated a placement of an additional piece of rubber seal between the membrane and the permeate side. This created a better seal, and for the operating conditions used, no further leakage was then found.

Secondly there was suction loss as the membrane becomes more fouled or when the feed concentration was too high. This limits the range of feed concentration that can be used for experiments. For current usage, the experiments are carried out using low concentration of solutes or for relatively short periods of time to avoid this problem. Design improvements are mentioned in Chapter 7.

5.4 Materials and methods

5.4.1 Experimental procedure

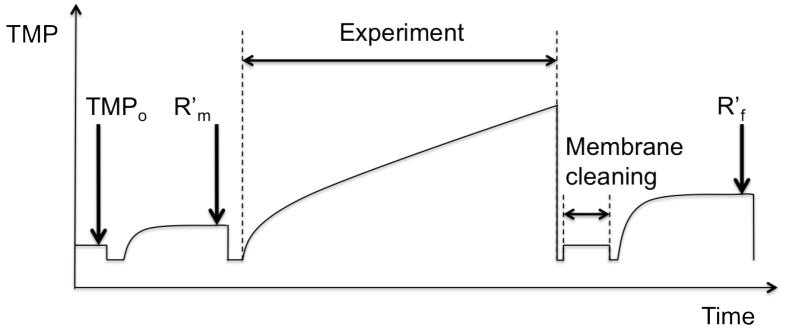

Figure 5.9: Schematic of transmembrane pressure measurement

The experimental procedure is illustrated by Figure 5.9. The procedure consists of 3 stages, pretreatment, experiment, and membrane cleaning.

For pretreatment, the permeate channels were first filled with deionised water. A membrane and feed channel were then inserted into place. The feed channel was filled with deionised water to a marked level, and a syringe pump was operated at a required flux for 10 minutes to allow membrane compaction to take place. The pump was then switched off for approximately 2 minute, and a reference transmembrane pressure (TMP_0) was measured. Afterwards, the pump was switched back on for a further 5 minutes before transmembrane pressure for a clean membrane (R'_m) is taken while the deionised water level is at the marked level. In the case where buffer was used, this step was repeated again using buffer solution. Permeate channel syringes were then emptied prior to starting an experiment.

For the experiment, a 10ml of feed suspension (Dextran Blue) was used to rinse the feed channel prior to refilling with fresh feed solution. This was to minimise the amount of deionised water left in the feed channel. For the case of yeast suspension, this step was omitted to avoid accumulation of excess cells. Immediately afterwards the rheometer plate was lowered into position and the syringe pumps were turned on to start an experiment.

For membrane cleaning, membrane cleaning was carried out using deionised water without removing the membrane from the rig to minimise error. Cleaning agents such as NaOH were not used, as it is preferable to preserve the characteristic of foulants. After each experiment, the retentate was drawn using a syringe. The feed channel was rinsed once using 50ml of deionised water, before being filled with another 50ml of deionised water and left to soak for 10 minutes. After 10 minutes, the solute was drawn out, and the feed channel was rinsed again using 50ml deionised water. The feed channel was then filled to the marked level, and the fouled membrane resistance was measured once a stable transmembrane pressure had been reached.

5.4.2 Membranes

Experiments were carried out using commercial microfiltration membranes: Isopore (Millipore) membranes with pore size of 0.2μm. Unless stated otherwise, a fresh membrane was used. Isopore is a track-etch polycarbonate membrane with a straight honeycomb-like pore structure.

5.4.3 Feed suspensions

Dextran Blue

Dextran Blue 2000, GE Healthcare, with a mean molecular weight of 2000 kDa was used as model feed. Dextran blue was diluted in deionised water, generated using Elix3, Millipore, to the concentration of $0.5 kg/m^3$. A magnetic stirrer (Jenway1000) and a magnetic stirrer bar were used to prepare the solution. The Dextran Blue solution was stirred until all powder completely dissolved prior to use. Concentration of Dextran Blue was measured by a UV spectrophotometer (UV4, Unicam) at 623nm.

5.4.4 Analysis of fouling

Determination of membrane fouling was carried out by TMP observation obtained from three pressure transducers. Retentate and permeate were measured for concentration at the end of each experiment. After the filtration, the membrane was cleaned as described in Chapter 3, and the irreversible portion of membrane fouling was determined.

Type	**Normalised with**
Normalised dTMP/dt	No shear (0rpm)
Normalised permeate concentration	No shear (0rpm)
Normalised observed transmission	No shear (0rpm)
Normalised irreversible fouling resistance, R_{irN}	Clean membrane
Irreversible fouling resistance ratio, IFRR	No shear (0rpm)

Table 5.3: Summary of terms used in determination of fouling resistance and transmission

The determination of membrane fouling and transmission are reported in terms of normalised dTMP/dt, normalised permeate concentration, normalised observed transmission, normalised irreversible fouling resistance, and Irreversible fouling resistance ratio. These terms are summaried in table 5.3. Measurements were made for each channel.

Normalised dTMP/dt is the ratio between rate of increase of TMP under the influence of shear in that particular channel to the rate of increase of TMP that would occur in the absence of shear in the same channel. Normalised $dTMP/dt = \frac{dTMP/dt_{\gamma}}{dTMP/dt_{\gamma 0}}$

Normalised permeate concentration refers to the ratio between permeate concentration under the influence of shear in a particular channel to the permeate concentration in the absence of shear in the same channel. Normalised permeate concentration$= \frac{C_{p\gamma}}{C_{p\gamma 0}}$.

Normalised observed transmission refers to the ratio between observed transmission under the influence of shear in a particular channel to the observed transmission in the absence of shear in the same channel. Observed transmission refers to the ratio between the permeate concentration and the feed concentration.

Normalised irreversible fouling resistance, R_{irN}, refers to the ratio between used membrane irreversible fouling resistance in a particular channel to the clean mem-

brane resistance for the same channel, $R_{irN} = \frac{R_{ir}}{R_m}$

Irreversible Fouling Resistance Ratio (IFRR) relates normalised irreversible fouling resistance under the influence of shear to that under zero rotational shear (0rpm) for the same channel. An IFRR value between zero and 1 indicates that the shear introduced led to less irreversible fouling, while an IFRR of higher than 1 demonstrates that the presence of shear resulted in greater irreversible fouling of the membrane. Irreversible Fouling Resistance Ratio can be written as IFRR$= \frac{R_{irN\gamma}}{R_{irN\gamma 0}}$

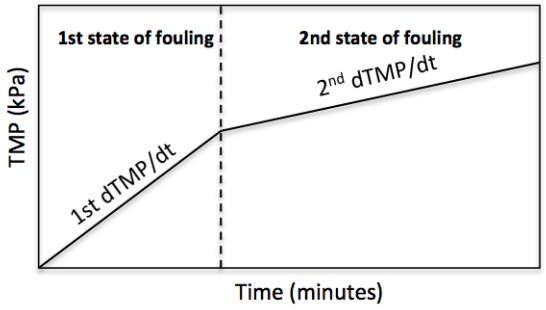

Figure 5.10: Diagram showing the first and second state of fouling during microfiltration

As shown by Figure 5.10, membrane fouling was generally observed to have an initially more rapid rate of fouling preceding the main state of a more gentle rise in transmembrane pressure. Segmented or piecewise linear regression for two segments was performed on transmembrane pressure data to obtain the breakpoint, initial gradient, and latter gradient. 1st dTMP/dt, and 2nd dTMP/dt will be reported in terms of normalised dTMP/dt values. The correlation coefficient for obtaining the gradients was maximised, and with the exception of filtration in shear intermittency mode the values were above 0.98.

5.5 Results

Firstly, the preliminary observations on Dextran Blue transmission at medium to high flux during zero rotational shear (0rpm) are made. The analysis of the permeate enables a better understanding of the transmission profile of Dextran Blue. Then the influence of various shear patterns on membrane fouling and transmission will be reported. A wide range of steady shear in both laminar and turbulent flow regimes was carried out at two permeate fluxes.

For the influence of time-varying shear on membrane filtration performance, the effect of amplitude and frequency of sinusoidal operation were examined. Comparisons between fouling mitigation efficiency by "sharp change in direction" and "general change in direction" were explored using Square wave and Sinusoidal wave motion of the plate at various displacement amplitudes. Several aspects of shear intermittency were investigated. Also the influence of ionic strength on Dextran Blue fouling and transmission at two extreme levels was tested. These experiments were at zero rotational shear and at a high steady shear of 840rpm. The chapter outline is shown in Figure 5.11.

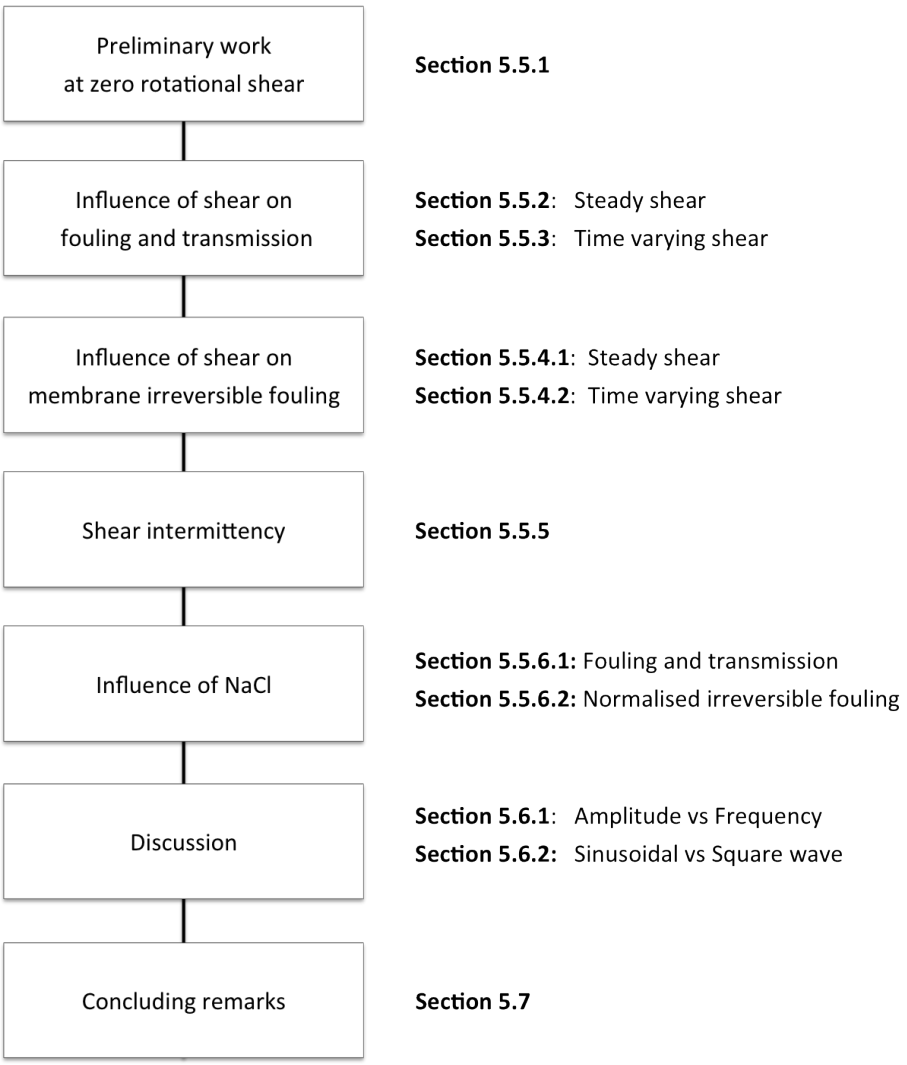

Figure 5.11: Chapter outline

5.5.1 Effect of permeate flux and accumulated permeate volume on Dextran Blue fouling and permeation

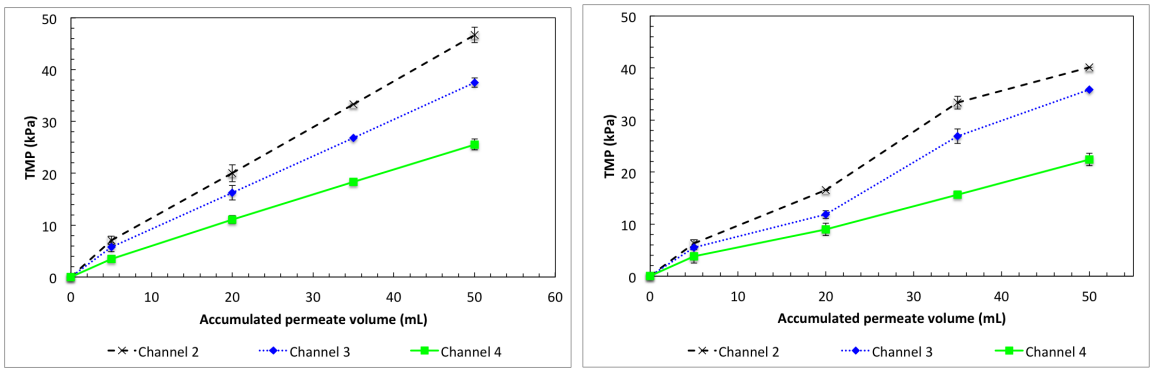

(a) At 71 LMH (b) At 101 LMH

Figure 5.12: Effect of accumulated permeate volume on transmembrane pressure (TMP) at different permeate channels for microfiltration of Dextran Blue solution using 0.2 µm Isopore membrane at constant permeate flux of 71 and 101 LMH. Channel 4 is the outermost channel.

Figure 5.12 shows some preliminary work on the variation of transmembrane pressure (TMP) with accumulated permeate volume with zero rotational shear (0rpm) for permeate fluxes of 71 LMH and 101 LMH respectively. For both permeate fluxes, the lowest TMP was found at channel 4 (the outermost channel) and the highest TMP was found at channel 2. Variation in TMP along these channels was due to increased feed concentration as well as decreased fluid velocity. At 71 LMH, dTMP/dt for all channels was found to be quite stable with respect to accumulated permeate volume. However, for 101 LMH, dTMP/dt increased more rapidly after an accumulated permeate volume of 20mL for channels 2 and 3.

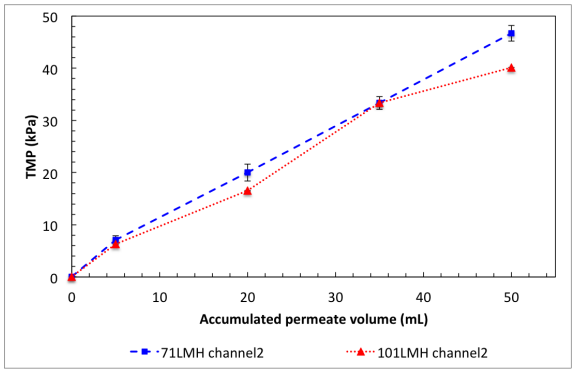

(a) Channel 2

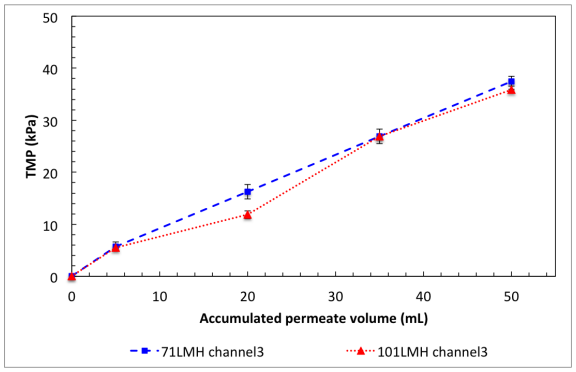

(b) Channel 3

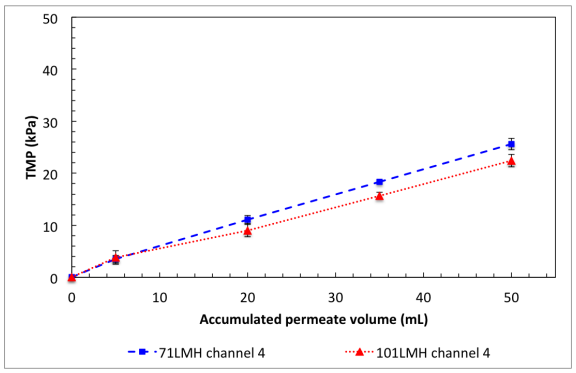

(c) Channel 4

Figure 5.13: Channel by channel comparisons of influence of permeate flux of 71 LMH and 101 LMH on TMP at various accumulated permeate volumes

A channel by channel comparison of the influence of permeate flux on TMP is given in Figure 5.13. For all channels, TMP was lower for the higher flux (101 LMH) than for the lower flux (71 LMH). This was clear especially at channel 4, for which the reduction in TMP was around 15% for accumulated permeate volume over 25mL. The reason for a lower TMP at higher flux was probably due to greater fluid tangential velocity which results in lower concentration polarisation. Increasing

permeate flux from 71 LMH to 101 LMH results in a 42% increase in fluid velocity and under laminar conditions the mass transfer coefficient is proportional to fluid velocity raised to the power 1/3[48].

5.5.1.1 Effect of permeate flux on permeate concentration

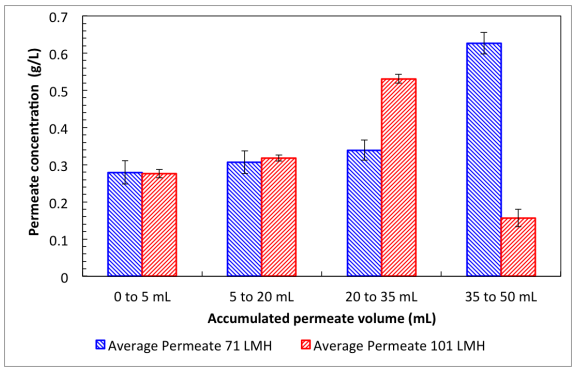

(a) Membrane average permeate concentration of Dextran Blue during 0-5mL, 5-20mL, 20-25mL, and 35-50mL accumulated permeate volume

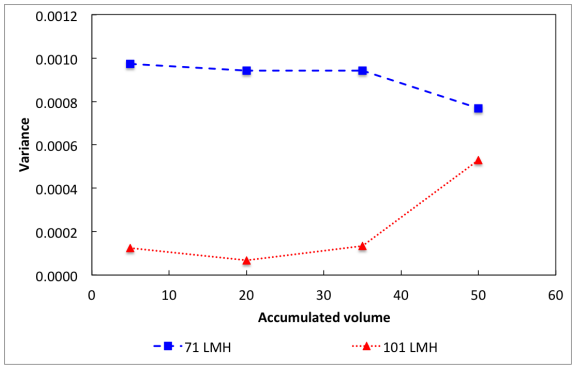

(b) Variance indicating channel variation in permeate concentration

Figure 5.14: Average permeate concentration and variance of permeate concentration during Dextran Blue filtration at constant permeate flux of 71 and 101 LMH

The influence of permeate flux on permeate concentration of 0.5g/L Dextran Blue is illustrated in Figure 5.14. Figure 5.14a shows a variation in permeate concentration at 71 and 101 LMH as accumulated volume increased. Permeate concentration was not dependent on flux at low accumulated volume. But as the filtration

progressed, accumulation of rejected solute resulted in an enhanced Dextran Blue permeation through the membranes. This occurred during an accumulated volume of 20-35mL and 35-50mL for 101 LMH and 71 LMH respectively. Higher solute concentration at the membrane surface and/or changes in membrane properties due to a deposited layer could be responsible for this change in permeate concentration. Figure 5.14b demonstrates the spread of data; it reveals how permeate concentration varies between channels. For zero rotational shear, the variation in permeation was very low (below 0.001), being greater at 71 LMH than 101 LMH.

5.5.2 Effect of plate rotational speed on membrane fouling and transmission

5.5.2.1 Effect of radial position on dTMP/dt under zero rotational shear

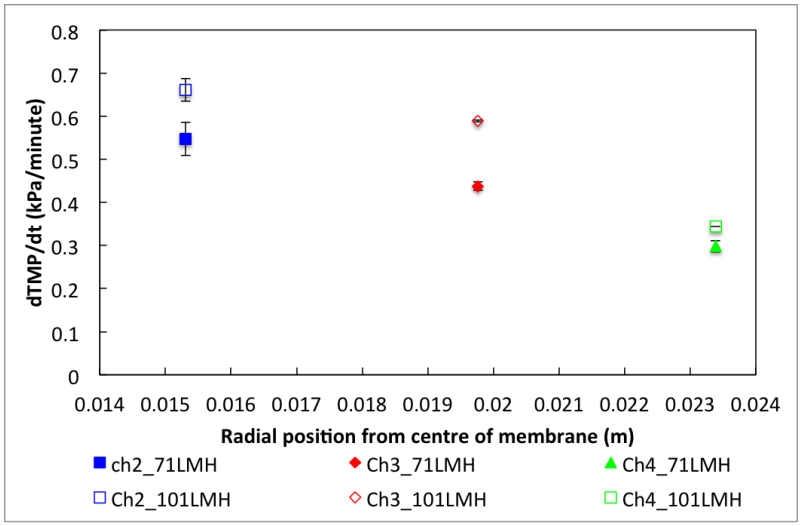

Figure 5.15: Effect of radial position on overall dTMP/dt for one hour microfiltration of Dextran Blue solution at zero rotational shear at 71 LMH (solid symbols) and 101 LMH (open symbols).

At 71 LMH the outermost channel (Ch4) had the least dTMP/dt of 0.3 kPa/min, while the innermost channel (Ch2) had an average dTMP/dt of 0.55 kPa/min (See Figure 5.15). This can be explained by 2 mechanisms, firstly it is due to increases in feed concentration along the membrane radius as the feed becomes more concen-

trated towards the middle of the membrane. Secondly, it is because tangential flow velocity is higher nearer to the membrane edge. For a filtration flux of 101 LMH, dTMP/dt were higher than that of 71 LMH at all channels. Similarly, the rate of increase of transmembrane pressure was lower further away from the centre of the membrane; the rate of transmembrane pressure at channel 4 and channel 2 was 0.34 and 0.66 kPa/min respectively.

5.5.2.2 Effect of plate rotational speed on membrane fouling rate at 71 LMH

71 LMH, 0.5g/L Dextran Blue 2000	**5 rpm**	**60 rpm**	**120 rpm**	**183.3 rpm**
% Decrease in transmission per rpm	0.93	0.91	0.45	0.37
% Decrease in membrane average dTMP/dt per rpm	5.13	0.52	0.26	0.20

Table 5.4: % Decrease in membrane average dTMP/dt and transmission as plate velocity increases from stationary during flux of 71 LMH

The introduction of steady shear led to a lowered rate of dTMP/dt for both 1st and 2nd state of fouling. As expected, the introduction of plate rotation resulted in lower rate of transmembrane pressure increase at all channels, hence lower rate of overall transmembrane pressure. At 71 LMH, a sharp decrease in membrane average dTMP/dt of 25% occurred as the plate went from stationary to 5 rpm, this is equivalent to 5% decrease in dTMP/dt per rpm, while further increase in plate rotational speed from 5 to 60rpm and from 60 to 120 rpm resulted in less dramatic changes.

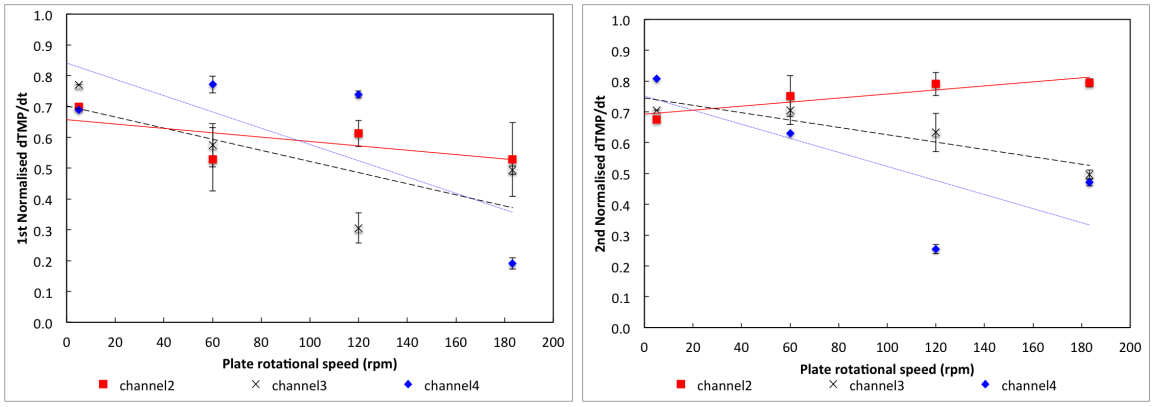

(a) Normalised dTMP/dt against plate rotational speed during first state of fouling

(b) Normalised dTMP/dt against plate rotational speed during second state of fouling

Figure 5.16: Effect of plate rotational speed on normalised dTMP/dt during first and second state of fouling at constant flux of 71 LMH

Figure 5.16 clearly illustrates influence of plate rotational speeed on rate of fouling. Normalised dTMP/dt for the 1st and 2nd state are shown in Figure 5.16a and 5.16b respectively.

Increases in plate rotational speed led to lower dTMP/dt (ie. NdTMP/dt < 1) for both 1st and 2nd state of fouling. Greater reduction of NdTMP/dt was generally found for the channel closer to the rim. As expected for the 2nd state, increases in plate rotational speed led to lower normalised dTMP/dt both for channel 3 and 4, while for channel 2, normalised dTMP/dt slightly increased as plate rotational speed increased from 5rpm to 183.3rpm, however these values were less than 1. This is probably a result of higher feed concentration for channel 2 since the membrane rejection for channel 3 and 4 was greater at higher plate rotational speed.

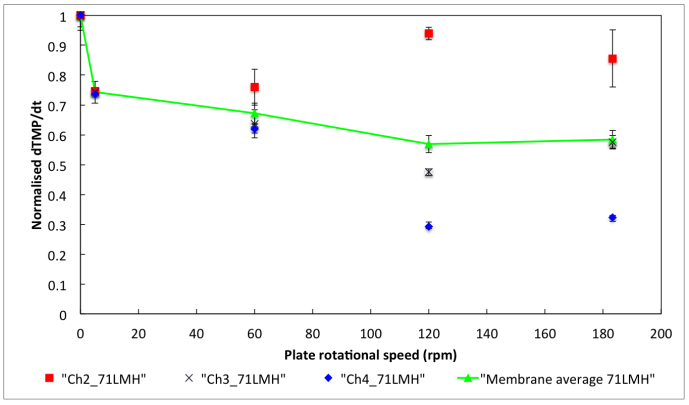

Figure 5.17: Effect of plate rotational speed on normalised dTMP/dt during 60 minute filtration period of microfiltration of Dextran Blue at constant flux of 71 LMH

Figure 5.17 shows the overall effect of plate rotational speed on the rate of membrane fouling. A sharp decrease in overall reduction in dTMP/dt occurred as plate rotational speed increased from stationary to 5 rpm. At this speed, the efficiency was similar at all channels. This implies that the plate rotational speed of 5 rpm managed to reduce dTMP/dt at all channels by a similar proportion. Further increase in plate rotational speed led to variation in efficiency at different membrane channels. The increase in plate rotational speed resulted in better overall membrane performance.

5.5.2.3 Effect of plate rotational speed on membrane fouling rate at 101 LMH

% Decrease (per rpm)	5 rpm	120 rpm	242.5 rpm	422.5 rpm	480 rpm	840 rpm
Transmission	0.10	0.54	0.27	0.42	0.15	0.09
dTMP/dt	4.94	0.81	0.41	0.24	0.09	0.07

Table 5.5: % Decrease in transmission and dTMP/dt for microfiltration of 0.5 g/L Dextran Blue 2000 at 101 LMH as plate rotational speed increases from stationary

The average rate of increase of transmembrane pressure (dTMP/dt) decreased as rheometer plate rotational speed increased for 101 LMH. The plate rotational speed

also affects the distribution of dTMP/dt along the channels; generally, it lowered the rate of increase of transmembrane pressure at channel 4 more than at channel 2. dTMP/dt at both channel 3 and 4 decreased as plate rotational speed increased. This resulted in lower rate of overall transmembrane pressure increase as plate rotational speed increased. Introduction of plate rotation of 5 rpm led to approximately 5% decrease in dTMP/dt per rpm. Further increase in plate rotational speed resulted in small changes in dTMP/dt per rpm. % decrease in dTMP/dt per rpm decreased as plate velocity increased, this can be seen in table 5.5.

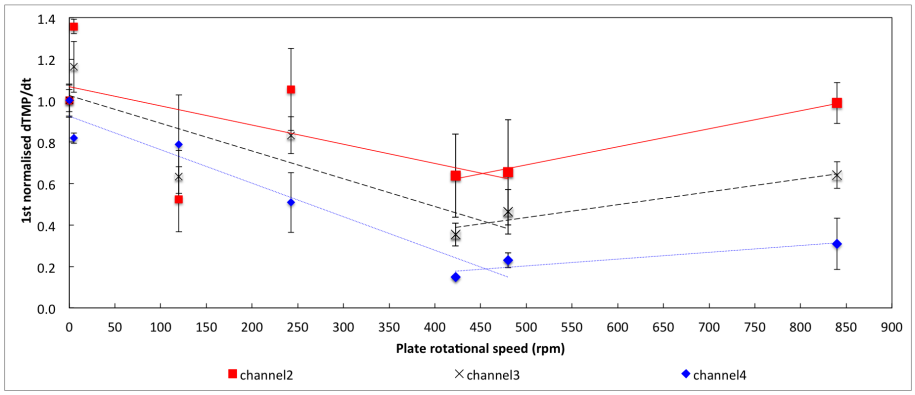

(a) Normalised dTMP/dt during the first state of fouling

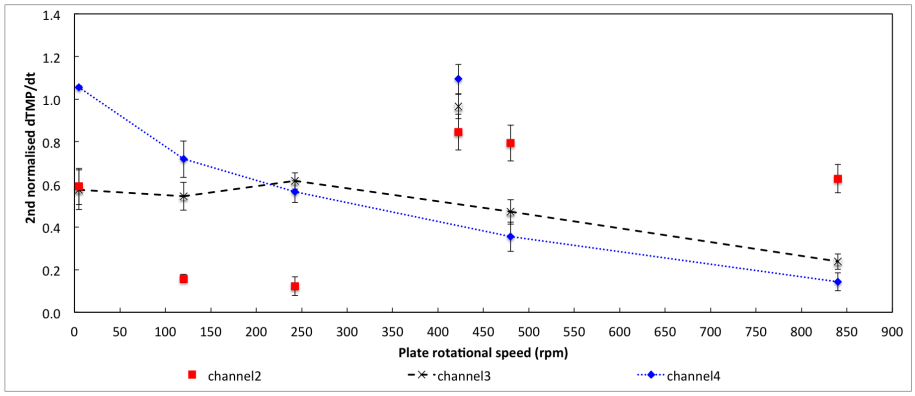

(b) Normalised dTMP/dt during the second state of fouling

Figure 5.18: Effect of plate rotational speed on normalised dTMP/dt during the first and second state of fouling at constant flux of 101 LMH

Normalised dTMP/dt for the 1st and 2nd state are shown in Figure 5.18a and 5.18b respectively. These are the ratio of dTMP/dt under influence of shear to

dTMP/dt under zero rotational shear (0rpm). At most plate rotational speeds, 1st normalised dTMP/dt was generally lower at channel 4 than at channel 3 and 2. 1st normalised dTMP/dt of value higher than 1 occurred at channel 2 and 3 at plate rotational speed of 5 rpm. This implies that the increase in feed concentration at channel 2 and 3 due to rejected solutes by channel 4, offset the benefit of plate rotational speed at 5 rpm at that particulate channel. During the 1st state of fouling, the maximum dTMP/dt reduction was found at plate rotational speed of 422.5rpm, further increase in plate rotational speed led to higher 1st normalised dTMP/dt at all channels.

Figure 5.18b demonstrates 2nd normalised dTMP/dt as plate rotational speed increased from 0 to 840 rpm. Higher plate rotational speed generally resulted in lower 2nd normalised dTMP/dt for channel 3 and 4. However, for channel 2, increases in the plate rotational speed up to 242.5rpm led to reduction in 2nd normalised dTMP/dt, further increase in plate rotational speed did not result in any further reduction. The reason for this is probably because the benefit from greater plate rotational speed for channel 2 was offset by the increased feed concentration due to rejected species from channel 3 and 4. A sudden change in the trend of normalised 2nd dTMP/dt occurred at 422.5rpm for all three channels. It is likely that the transition from laminar to turbulent flow took place around this plate rotational speed. An equation by Colton and Smith[167] suggests that for H/R_T of 0.112 and R_T/R_F of 0.9, the expected equivalent plate rotational speed for laminar-turbulent transition would be 460rpm (Re_{R_T} =3 *10^4)[165].

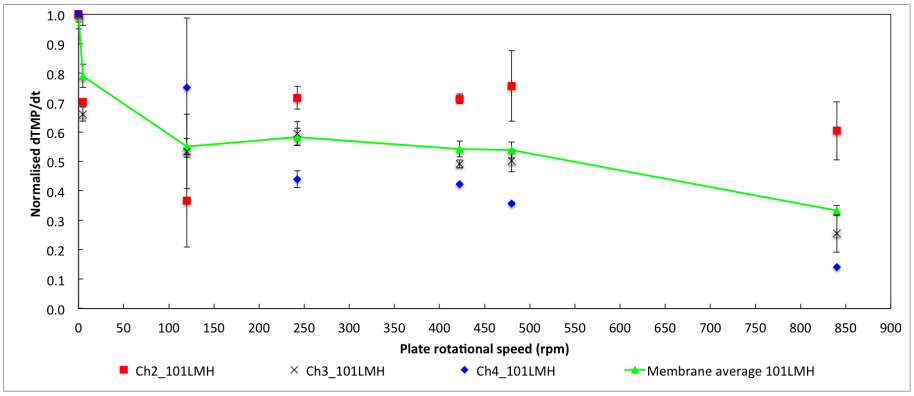

Figure 5.19: Normalised rate of increase of transmembrane pressure at various plate rotational speeds for 0.5g/L Dextran Blue 2000 at 101 LMH for during 60 minute filtration period

Figure 5.19 shows the effect of plate rotational speed on overall normalised dTMP/dt. An apparent decrease in membrane average normalised dTMP/dt to 0.79 and 0.55 occurred when plate rotational speed increased to 5 and 120 rpm from stationary. Further increase in plate rotational speed did not result in further dramatic decrease in membrane average dTMP/dt.

5.5.2.4 Effect of plate rotational speed on normalised observed transmission at 71 and 101 LMH

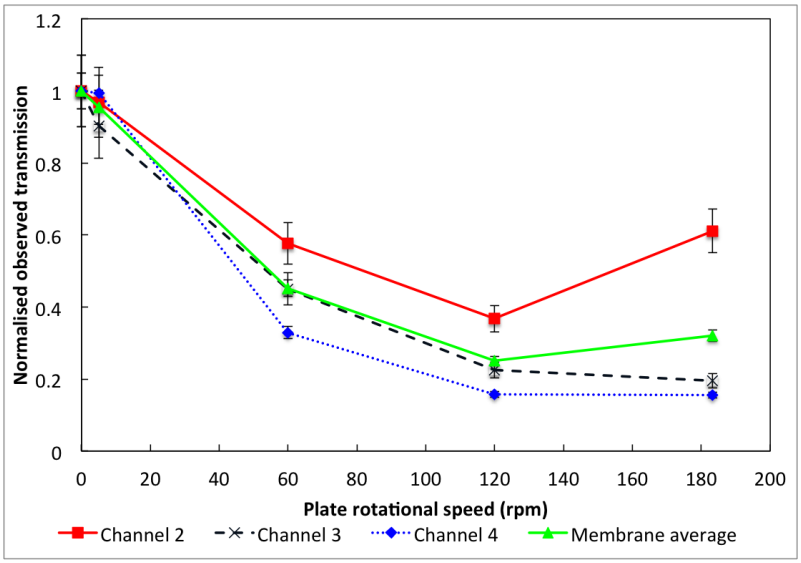

Figure 5.20: Effect of plate rotational speed on normalised observed transmission of Dextran Blue microfiltration at constant flux of 71 LMH

Figure 5.20 demonstrates the influence of plate rotational speed upon normalised observed transmission during sixty minute microfiltration of Dextran Blue solution at constant flux of 71 LMH. Introduction of steady shear of all magnitudes during microfiltration resulted in lower observed transmission than microfiltration under zero plate rotational speed. In most cases, normalised observed transmission was greater at channel 2 than channel 3 and 4. Normalised observed transmission for steady shear of 5rpm was comparable to that at zero rotational shear at channel 4, while slight decrease in NTr was observed at channel 2 and 3. Further increases in plate rotational speed led to a sharp reduction in NTr, especially for channel 4 where the maximum decrease in observed transmission of 84% was observed at 120rpm and at 183.3rpm. Similar trend was found at channel 3, the maximum decrease in observed transmission was 81% at 183.3rpm. For channel 2, the lowest observed transmission was found at 120rpm, this was equivalent to 63% reduction compared with that under zero rotational shear.

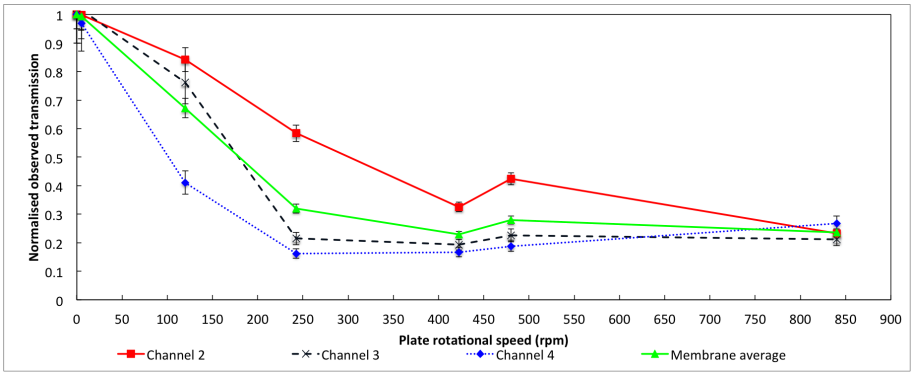

Figure 5.21: Effect of plate rotational speed on normalised observed transmission of Dextran Blue microfiltration at constant flux of 101 LMH

At 101 LMH, as the plate rotational speed increased from stationary to 120rpm, membrane average transmission was lowered to 0.58 compared with that of 0.21 at 71 LMH. Increases in plate rotational speed led to lower membrane average transmission. However it can be seen from Figure 5.21 that as plate rotational speed increased to 422.5rpm, the permeate concentration of channel 3 and 4 slightly increased as plate rotational speed increased.

To compare the effect of rotational speed on transmission at two fluxes, as expected the increase in plate rotational speed led to lower transmission at the lower flux (71 LMH) than at higher flux (101 LMH). In order to reduce transmission to approximately 0.2, the plate rotational speed must be as high as 242.5 rpm, while at 71 LMH only 120rpm was necessary.

5.5.3 Effect of time varying shear on fouling and transmission

For a sinusoidal wave motion experiments were carried out to explore the effect of amplitude and frequency. For effect of frequency, the amplitude was kept constant at 0.209rad while rotational frequency was increased from 2 to 14.32Hz. For effect of amplitude, frequency remained at 2 Hz, while the amplitude was varied.

5.5.3.1 Effect of frequency on membrane fouling and transmission

The membrane average dTMP/dt for sinusoidal motion at 0.209 rad, 2Hz was essentially the same as for a stationary plate; the values being 0.42 and 0.43 kPa/min. The rate of increase of transmembrane pressure decreases to 0.33 kPa/min as frequency increases to 14.32Hz. The trend for the first and second normalised dTMP/dt is shown in Figure 5.22.

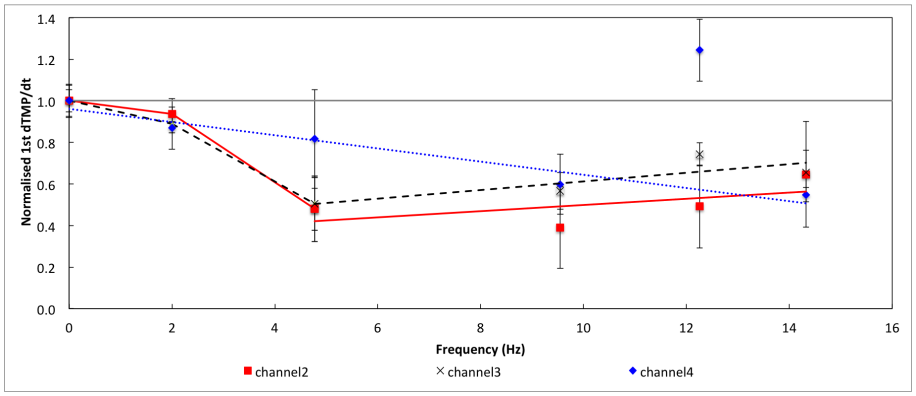

(a) Normalised dTMP/dt during the first state of fouling

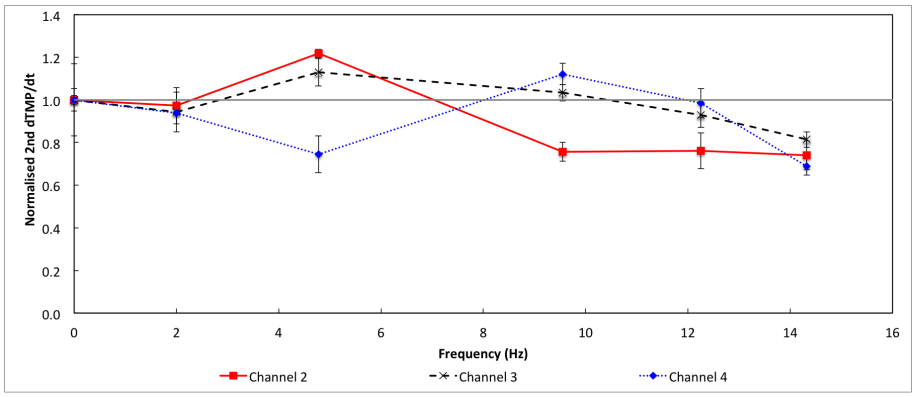

(b) Normalised dTMP/dt during the second state of fouling

Figure 5.22: Effect of frequency of shear in Sinusoidal wave motion on normalised dTMP/dt during the first and second state of fouling

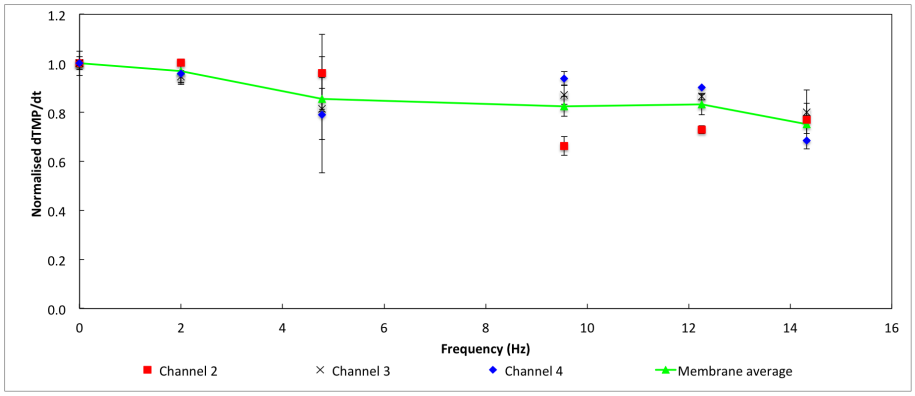

Figure 5.23: Effect of frequency of shear in Sinusoidal wave motion on normalised dTMP/dt of Dextran Blue microfiltration at constant flux of 71 LMH

With introduction of sinusoidal wave motion, initial or 1st state of normalised dTMP/dt was generally lower than 1, indicating better membrane performance soon

after filtration has started. Figure 5.22b shows normalised dTMP/dt for 2nd state of fouling against frequency. Higher frequency did not always result in better membrane performance during 2nd state of fouling, this is illustrated by normalised 2nd dTMP/dt of value greater than 1. The values for membrane average show a small benefit overall. Figure 5.23 reveals combined effect of 1st and 2nd state of fouling as normalised dTMP/dt over a sixty minute filtration period.

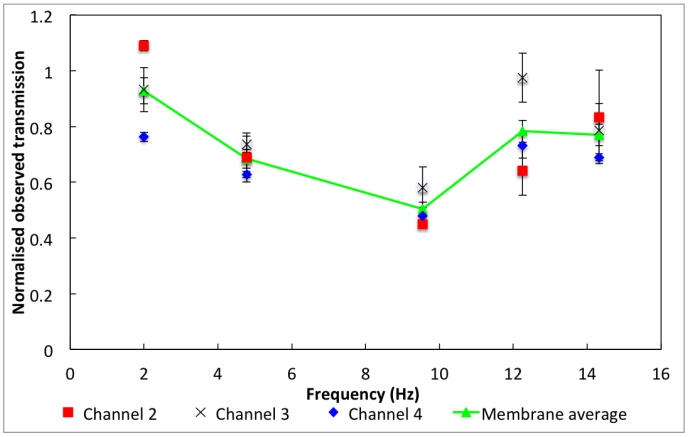

Figure 5.24: Effect of frequency of shear in Sinusoidal wave motion on normalised observed transmission of Dextran Blue microfiltration at constant flux of 71 LMH

Figure 5.24 shows variation in normalised observed transmission at different sinusoidal frequency. Membrane average observed transmission reduced from 0.8 to 0.4 as frequency increased from 2 to 9.55Hz. Further increases in frequency however led to greater transmission. An analysis based upon a fixed intrinsic transmission constant (i.e., $\frac{C_p}{C_m}$ = constant) cannot explain the minimum in the curve. It is therefore concluded that the transmission of the Dextran Blue depends upon the shear stress at the surface; this varies with frequency.

5.5.3.2 Effect of displacement amplitude on membrane fouling and transmission

Effect of amplitude on dTMP/dt and transmission was explored with sixty minute filtration experiments of 0.5g/L Dextran Blue at 71 LMH. The frequency was kept

constant at 2Hz while amplitude was increased from 0.209 rad to 1rad, which is equivalent to a minimum amplitude at the centre of channel 2 of 0.32cm, and a maximum amplitude at the centre of channel 4 of 2.34cm.

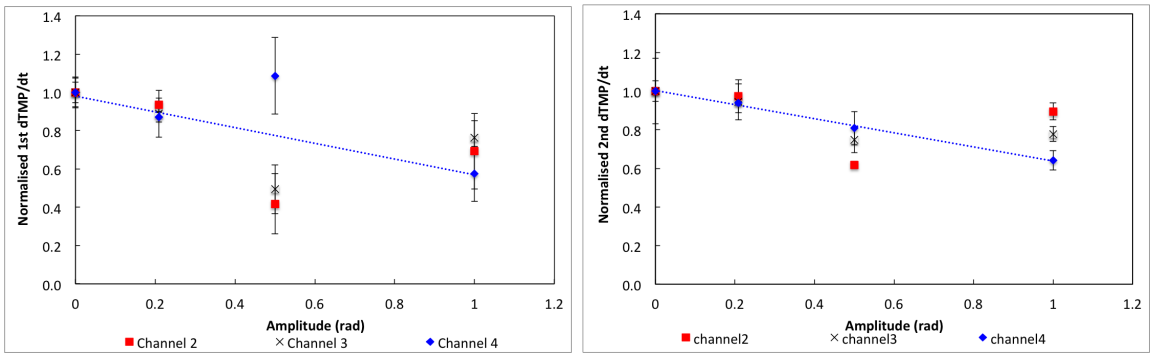

(a) 1st normalised dTMP/dt (b) 2nd normalised dTMP/dt

Figure 5.25: Effect of displacement amplitude of shear in Sinusoidal wave motion on normalised dTMP/dt during the first and second state of fouling of Dextran Blue microfiltration at constant flux of 71 LMH

Figure 5.25 illustrates the effect of sinusoidal amplitude on first and second state of fouling when compared with filtration under zero rotational shear. Increases in displacement amplitude generally led to lower normalised dTMP/dt both for the first and second state of fouling.

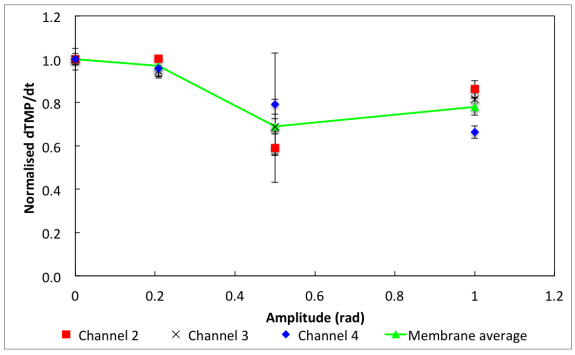

Figure 5.26: Effect of displacement amplitude of shear in Sinusoidal wave motion on normalised dTMP/dt during Dextran Blue microfiltration at constant flux of 71 LMH

The effect of displacement amplitude on membrane average normalised dTMP/dt is shown in Figure 5.26. Increases in displacement amplitude from 0.209 to 0.5 rad

led to approximately 30% reduction in dTMP/dt. The benefit of further increase in displacement amplitude from 0.5 rad to 1 rad was not found.

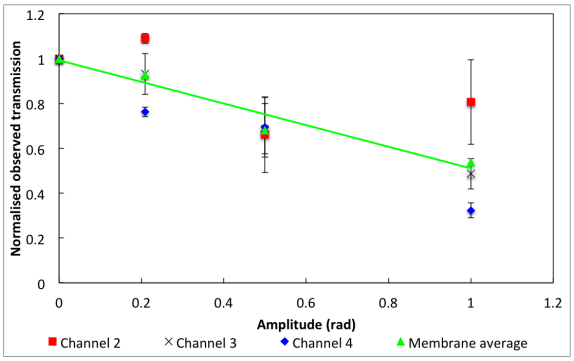

Figure 5.27: Effect of displacement amplitude of shear in Sinusoidal wave motion on normalised observed transmission during Dextran Blue microfiltration at constant flux of 71 LMH

Figure 5.27 shows the effect of Sinusoidal amplitude on normalised observed transmission when frequency was kept constant at 2Hz. For channel 3 and 4, increases in amplitude always have a positive effect on reduction of observed transmission. Membrane average normalised observed transmission reduced by approximately 40% as sinusoidal amplitude increased from 0.209 to 1 rad. Increase in sinusoidal amplitude resulted in consistent reduction of membrane average observed transmission.

5.5.3.3 Effect of displacement amplitude of square wave on fouling and transmission

The effect of displacement amplitude of shear in square wave motion on transmembrane pressure during Dextran Blue microfiltration was carried out at a constant flux of 71 LMH. The frequency of square wave was kept constant at 2Hz, while the amplitude was varied. Membrane average dTMP/dt was 0.1, 0.15, and 0.09 kPa/min at 0.209, 0.5, and 1 rad respectively.

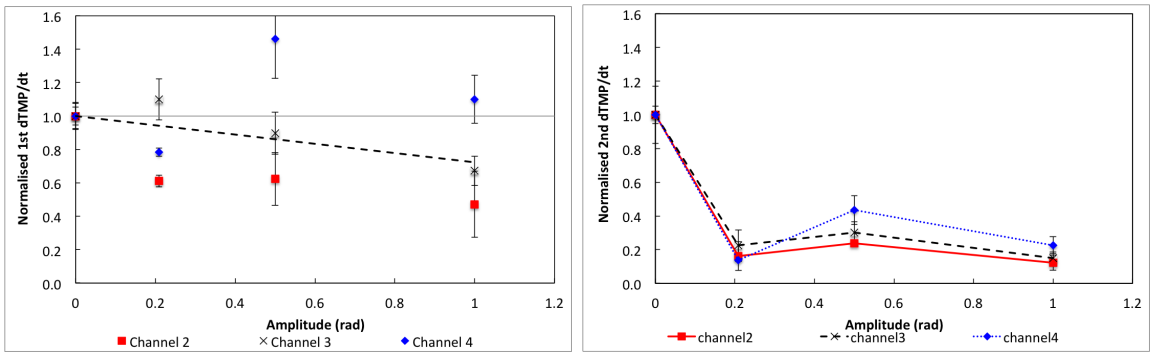

(a) Normalised 1st dTMP/dt (b) Normalised 2nd dTMP/dt

Figure 5.28: Effect of displacement amplitude of shear in square wave motion on normalised dTMP/dt during the first and second state of fouling of Dextran Blue microfiltration at constant flux of 71 LMH

The rate of increase of membrane fouling under influence of square wave during 1st and 2nd state of fouling is illustrated in terms of normalised dTMP/dt in Figure 5.28. Figure 5.28b shows that the normalised 2nd dTMP/dt was roughly constant at 0.2. The influence of the square wave on the first stage was complex and in overall terms (as shown by the trend for the average) modest.

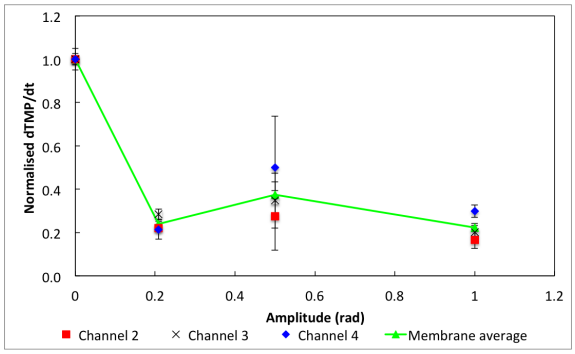

Figure 5.29: Effect of displacement amplitude of shear in square wave motion on normalised dTMP/dt during Dextran Blue microfiltration at constant flux of 71 LMH

The influence of square wave top-plate motion on membrane filtration performance is summarised in Figure 5.29. On average, membrane fouling rate under influence of square wave decreased to approximately a third of membrane fouling rate under zero rotational shear.

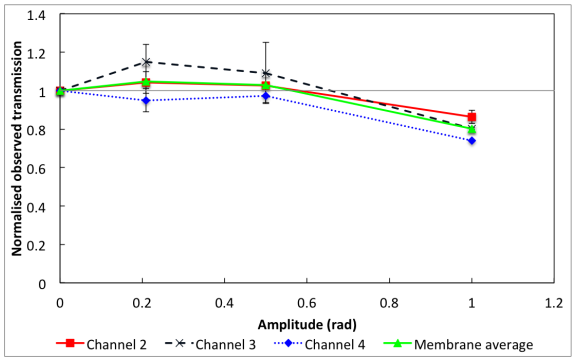

Figure 5.30: Effect of displacement amplitude of shear in square wave motion on normalised observed transmission during Dextran Blue microfiltration at constant flux of 71 LMH

Figure 5.30 reveals the influence of displacement amplitude of shear in square wave motion on normalised observed transmission. The benefit of SQ wave on overall reduction of transmission was observed only at 1 rad. But for the amplitude below this, the benefit is unclear since the slight increase in transmission occurred at both 0.209 and 0.5 rad.

5.5.4 Effect of shear on membrane irreversible fouling

With the current DSSTC module, membrane cleaning by backwashing is inappropriate because it would involve removal of membranes from the module. Removal of membrane and re-depositing the membrane back on to the module may result in inaccuracy due to misalignment of membrane and membrane channels. Irreversible fouling in this case is therefore defined as fouling resistance of the membrane after the membrane cleaning procedure.

5.5.4.1 Effect of steady shear on irreversible fouling resistance of membrane

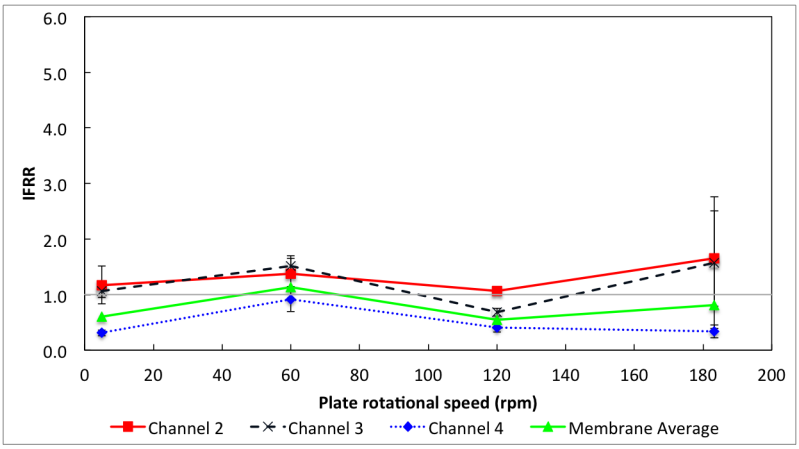

(a) IFRR for steady shear at 71 LMH

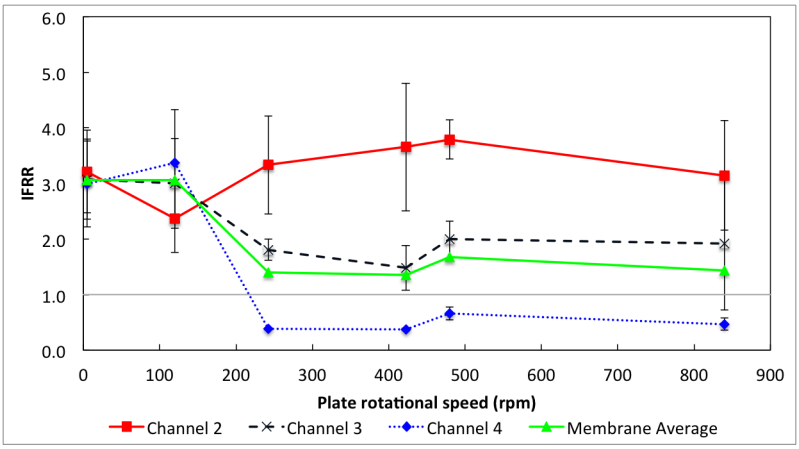

(b) IFRR for steady shear at 101 LMH

Figure 5.31: Effect of plate rotational speed during microfiltration on membrane irreversible fouling ratio (IFRR) at 71 LMH and 101 LMH for different membrane channels

Membrane irreversible fouling resistances are represented using Irreversible Fouling Resistance Ratio(IFRR). This is the ratio between normalised irreversible fouling resistance under influence of shear and that under zero rotational shear. For steady shear at permeate flux of 71 LMH and 101 LMH, this is shown by Figure 5.31.

The influence of plate rotational speed on irreversible fouling was different for 71LMH and 101LMH. For 71LMH there was no benefit for channel 2 but on average there was minor benefit. However the adverse effect of steady shear on irreversible membrane fouling under flux of 101LMH is clearly illustrated by Figure 5.31b. There

was some benefit for channel 4 at 242.5rpm and above but overall there was no benefit.

5.5.4.2 Effect of time-varying shear on irreversible fouling resistance of membrane

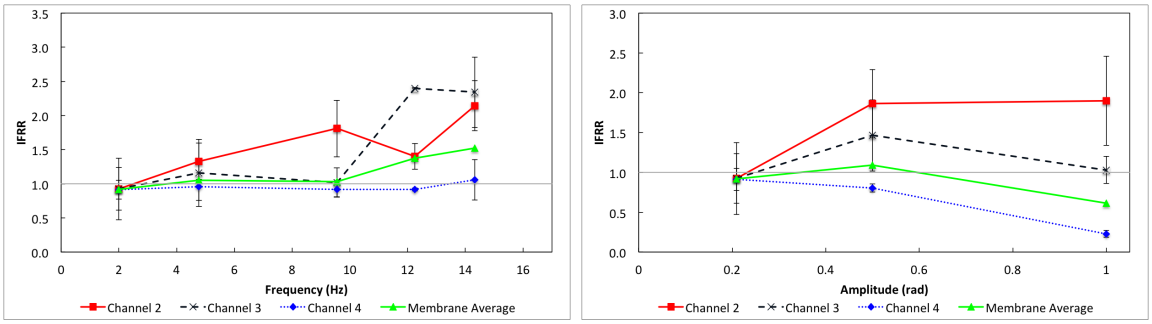

(a) Effect of frequency on IFRR

(b) Effect of amplitude on IFRR

Figure 5.32: Effect of displacement amplitude and frequency of plate rotation in Sinusoidal operation on IFRR during microfiltration on membrane irreversible fouling resistance ratio (IFRR) at constant flux of 71 LMH

Figure 5.32a reveals the effect of frequency of the Sinusoidal wave on irreversible membrane fouling for different membrane channels when displacement amplitude was kept constant at 0.209rad. For channel 4, the benefit of the increase in frequency was not found since the IFRR was approximately 1 at all frequencies, while the adverse effect of the increase in frequency occurred for other channels, especially at a frequency above 9.55Hz.

Figure 5.32b shows the effect of increases in Sinusoidal wave amplitude on irreversible membrane fouling for different membrane channels when the frequency was kept constant at 2Hz. While the benefit of the increase in sinusoidal wave amplitude is clear for channel 4, the adverse effect was found in other channels. The significant overall benefit of displacement amplitude on IFRR occurred only for displacement amplitude of 1rad.

In general increased surface shear (and it would increase with either increased

frequency or increased amplitude) leads to lower fouling. This is especially true of fouling on the surface. However increased shear can encourage material to enter the pores causing plugging and it is this material which is the main component of irreversible fouling. It thus concluded that increased frequency and increased amplitude led to more pore plugging.

It is important to note that the IFRR compares the irreversible fouling for each channel under shear to that under zero rotational shear. The membrane average value of IFRR compares the average membrane irreversible fouling under shear to that under zero rotational shear. The membrane average IFRR (the green) is therefore not the average of all other IFRRs.

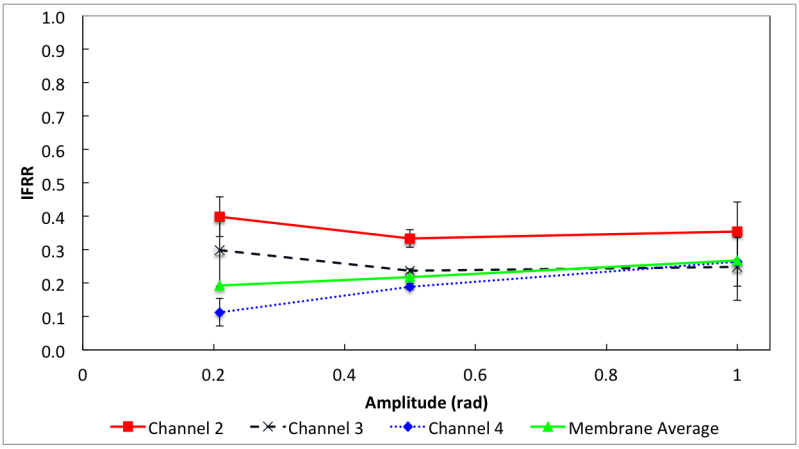

Figure 5.33: Effect of displacement amplitude of plate rotation in Square wave operation on IFRR during microfiltration on membrane irreversible fouling ratio (IFRR) at constant flux of 71 LMH

The effect of displacement amplitude of Square wave operation on IFRR during microfiltration on membrane irreversible fouling ratio (IFRR) at constant flux of 71 LMH is illustrated by Figure 5.33. For channel 4, it is interesting to observe that the greatest reduction in IFRR occurred at square wave amplitude of 0.209rad rather than at higher amplitude. For channel 4 approximately 90% reduction in membrane irreversible fouling was found at 0.209rad. Increases in square wave amplitude to 0.5 and 1rad led to lower reduction in IFRR. Overall the benefit of square wave on IFRR was significant at all conditions for all membrane channels.

5.5.5 Effect of intermittency of shear on fouling and transmission of membrane.

Introduction of shear into a microfiltration system is known to reduce concentration polarisation and fouling, which effectively result in lower frequency of membrane cleaning and/or the need of new membranes[14]. Continuous use of high shear can be expensive. To reduce operating cost, intermittency of high shear is sometimes utilized to remove deposits or reduce concentration polarisation accumulated during low shear/no shear period[162, 176]. Generation of reproducable intermittent steady shear can be challenging in typical crossflow modules. This is because the level of shear relates directly to fluid flow rate or feed flow rate.

Several aspects of the effect of intermittent shear on membrane fouling rate and transmission have been carried out using the DSSTC. First objective was to observe the influence of the level of shear during the high-shear period on fouling and transmission. Second objective involved comparisons between the effect of a sharp change of direction of steady shear at a medium level, with the effect of continuous steady shear at the same average shear. The third objective was observation of the influence of time interval. The conditions used are summarised in table 5.6.

Section	**Shear$_1$**	**Shear$_2$**	**Intermittent interval (s)**
Section 5.5.5.1	Steady: 5rpm	Steady: 480 and 840rpm	300s
Section 5.5.5.2	Steady: 422.5 rpm clockwise	Steady: 422.5 rpm anti-clockwise	300s
Section 5.5.5.3	Steady: 5rpm	Steady: 840rpm	120s, 300s, 600s

Table 5.6: Summary of experiments: effect of shear intermittency

5.5.5.1 Effect of high plate rotational speed on fouling and transmission during intermittency

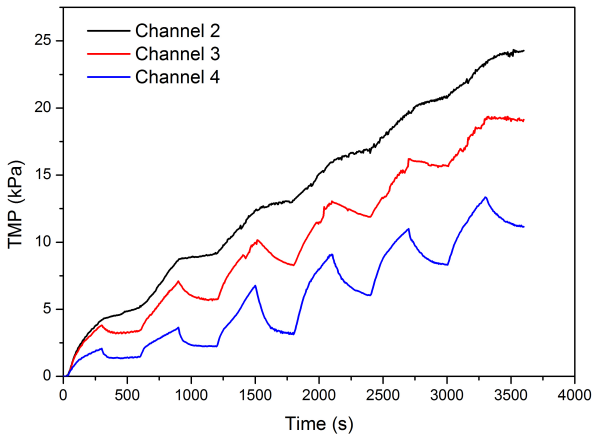

Figure 5.34: TMP profile during filtration with intermittent steady shear of 5 and 840 rpm with intermittent interval of 300s

Microfiltration of 0.5g/L Dextran Blue at a constant flux of 101 LMH was observed. Experiments were started with low-shear period at 5rpm to allow development of depositions and fouling layers. Afterwards, alternations between high plate rotational speed and low plate rotational speed at 5rpm were then carried out at time intervals of 300s. Two levels of high plate rotational speed were selected to observe its efficiency on fouling removal and transmission of Dextran Blue. These were 480 and 840rpm. The average normalised dTMP/dt were 0.54 and 0.33 respectively over 60 minute filtration. Figure 5.34 illustrates the variation between channels. The decrease in TMP during high steady shear was more significant at channels closer to the rim, this was due to higher shear rate as well as lower concentration.

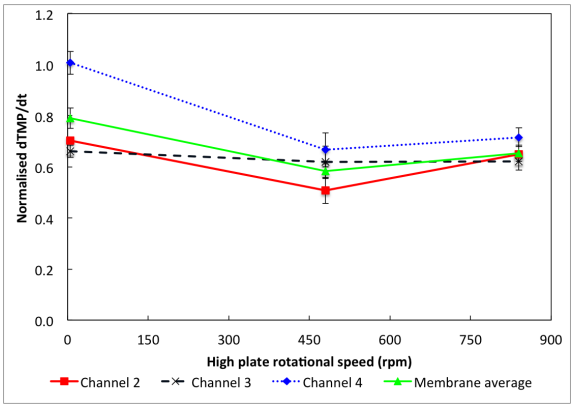

Figure 5.35: Effect of high plate rotational speed during intermittent low-high steady shear on normalised average dTMP/dt at different membrane channels

Normalised dTMP/dt is represented in Figure 5.35. Membrane average normalised dTMP/dt were 0.58 and 0.65 respectively for 5-480rpm and 5-840rpm ie. when medium plate rotational speed of 480rpm was used during high shear period, improvement in dTMP/dt was greater than when high plate rotational speed of 840rpm was used. Table 5.7 summarises the normalised observed transmission at different membrane channels and membrane average value for both normalised observed transmission and normalised dTMP/dt. It is interesting to observe that 5-480rpm resulted in normalised dTMP/dt (0.58) that is similar in values to normalised dTMP/dt for steady shear at 242.5rpm (0.58) but is lower than an average of normalised dTMP/dt for steady shear at 5rpm and 480rpm(0.67). For intermittent steady shear 5-840rpm the improvement in normalised dTMP/dt was not observed.

System	**Normalised observed transmission (NTr)**				**Normalised dTMP/dt**
	Ch 2	**Ch 3**	**Ch 4**	**Membrane average**	**Membrane average**
Steady: 5rpm	1	1	0.97	0.99	0.79
Steady: 242.5rpm	0.58	0.21	0.16	**0.32**	**0.58**
Steady 422.5rpm	0.33	0.19	0.17	**0.23**	**0.54**
Steady: 480 rpm	0.43	0.23	0.19	0.28	0.54
Steady: 840 rpm	0.23	0.21	0.27	0.24	0.33
Intermittency: 5-480 rpm	0.68	0.35	0.28	**0.44**	**0.58**
Intermittency: 5-840 rpm	0.44	0.32	0.30	**0.35**	**0.65**
Average of steady: 5 & 480rpm	0.72	0.62	0.58	0.64	0.67
Average of steady: 5 & 840rpm	0.62	0.61	0.62	0.62	0.56

Table 5.7: Summary of normalised observed transmission and normalised dTMP/dt

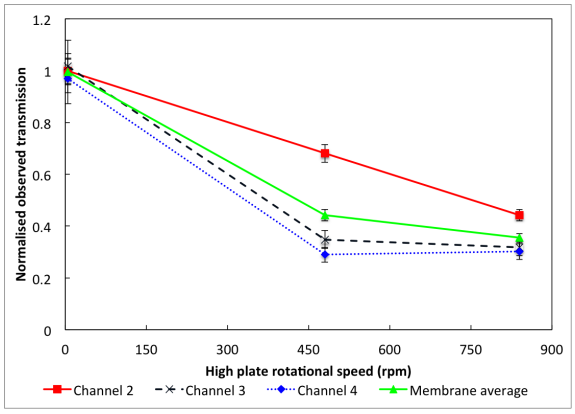

Figure 5.36: Effect of high plate rotational speed during intermittent low-high steady shear on normalised observed transmission at different membrane channels

Effect of intermittent steady shear on normalised observed transmission is illustrated in Figure 5.36. Intermittent steady shear of 5-480rpm and 5-840rpm resulted in membrane average normalised observed transmission of 0.44 and 0.35 respectively. The normalised observed transmission was lower at channel closer to the rim, ie. $\mathrm{NTr}_{ch2} > \mathrm{NTr}_{ch3} > \mathrm{NTr}_{ch4}$. This was expected because the feed concentration at the channel closer to the rim (i.e., channel 4) was lower than that at the channel closer to the centre (i.e., channel 2). Membrane average NTr for intermittent steady shear of 5-840rpm was greater than NTr for continuous steady shear at 422.5rpm, but lower than average NTr for continuous steady shear of 5 & 840rpm by almost a half. Other results are given in Table 5.7. In general the use of intermittent shear did not lower normalised dTMP/dt. However the transmissions were improved.

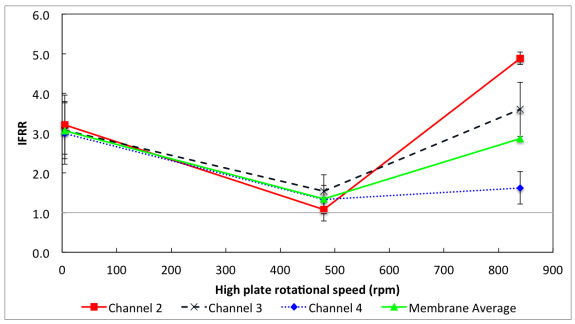

Figure 5.37: Effect of high plate rotational speed during intermittent low-high steady shear on irreversible fouling resistance ratio (IFRR) at different membrane channels

Figure 5.37 shows influence of high plate rotational speed during intermittent low-high steady shear on irreversible fouling resistance ratio (IFRR) at different membrane channels. It is clear that while the introduction of high plate rotational speed of 480rpm reduced membrane irreversible fouling drastically, further increase in high plate rotational speed resulted in a great variation in IFRR at different membrane channels.

5.5.5.2 Effect of periodic sharp change in rotational direction of steady shear on fouling and transmission

Observation of filtration performance under the effect of sharp change of direction of steady shear at a medium level, the effect of continuous steady shear, and intermittency of shear at the same average shear were compared under constant flux of 101 LMH. The effect of sharp change in direction of a medium steady shear was carried out by alternations between clockwise and anti-clockwise steady shear at 422.5rpm at time interval of 300s. The additional effect of sharp change in direction can be compared with steady shear of 422.5rpm as well as intermittent steady shear of 5-840rpm at the same intermittent interval.

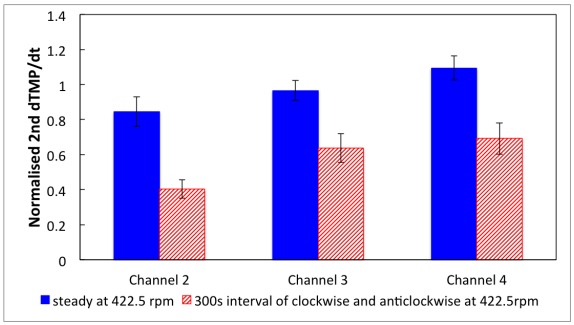

Figure 5.38: Normalised second dTMP/dt at different membrane channels.

The first dTMP/dt were within experimental error unaffected by the flow reversals. With periodic sharp change of direction, normalised second dTMP/dt at

channels 3 and 4 were reduced to 0.64 and 0.69 respectively. For channel 2, reduced from 0.85 to approximately half. Results are shown in Figure 5.38.

The normalised observed transmission under steady shear without and with periodic sharp change of direction at different channels were very similar. It can therefore be concluded that the introduction of periodic sharp change of direction to filtration under medium steady shear did not result in significant variation in transmission.

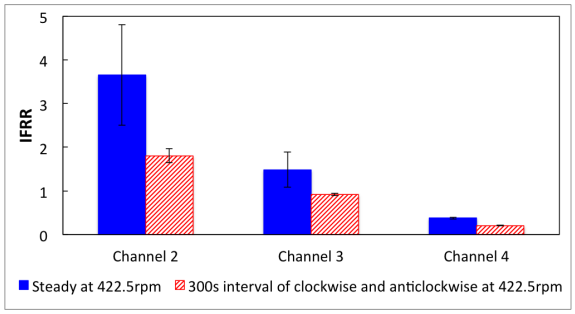

Figure 5.39: Effect of steady shear without and with periodic sharp change in direction on irreversible fouling resistance ratio (IFRR) at different membrane channels

Figure 5.39 shows the influence of steady shear without and with periodic sharp change in direction on irreversible fouling resistance ratio (IFRR) at different membrane channels. For both shear patterns, membrane irreversible fouling ratio was lower at channels closer to the rim. Introduction of periodic sharp change in direction reduced membrane average IFRR by nearly a half from IFRR of 1.35 without sharp change in direction to IFRR of 0.73 with sharp change in direction.

5.5.5.3 Effect of intermittent time interval length on fouling and transmission

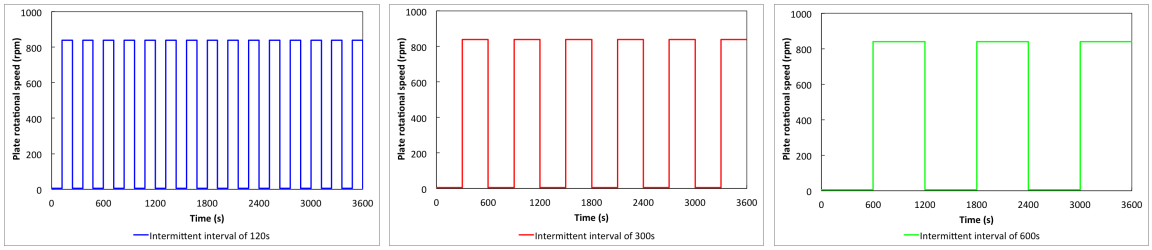

(a) Intermittent interval of 120s (b) Intermittent interval of 300s (c) Intermittent interval of 600s

Figure 5.40: Plate rotational speed against operating time at different intermittent interval (s)

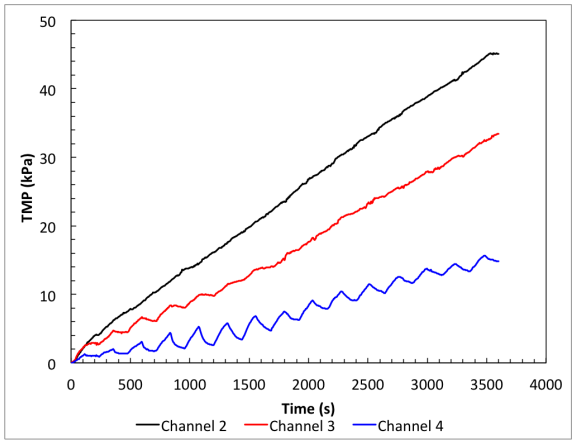

Figure 5.41: Effect of intermittent low-and-high steady shear at intermittent interval of 120s on transmembrane pressure at different membrane channels

Steady shear of 5rpm and 840rpm which resulted in 33% and 79% reduction in fouling rate compared with the system under zero rotational shear were chosen for low shear and high shear periods. The plate rotational speed profiles against operating time are illustrated by Figure 5.40. Figure 5.41 shows change of TMP with time.

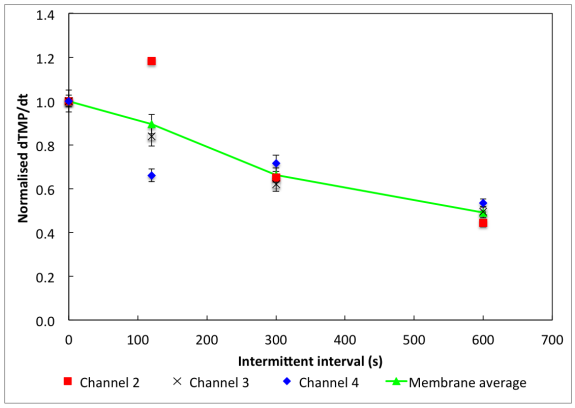

Figure 5.42: Effect of intermittent interval (s) during intermittent low-and-high steady shear on normalised dTMP/dt at different membrane channels.

The effect of intermittent interval is illustrated by Figure 5.42. An increase in the intermittent time interval from 120s to 600s resulted in a drop in membrane average NdTMP/dt from 0.89 to 0.49 respectively. Greater variation in NdTMP/dt between channels occurred at shorter time intervals. The variance for 120s, 300s, and 600s was 0.047, 0.002, and 0.001 respectively. This indicates that longer intermittent time intervals not only resulted in lower membrane average NdTMP/dt but also consistently led to lower NdTMP/dt at all three channels.

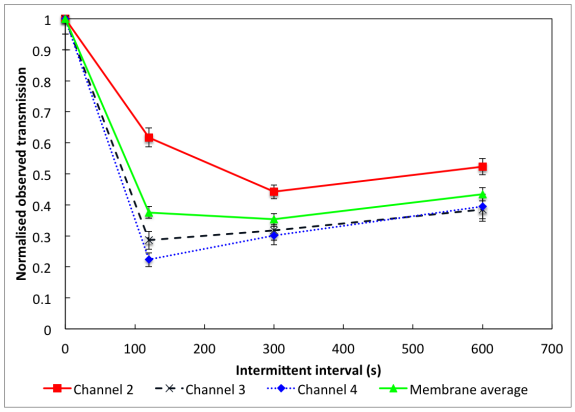

Figure 5.43: Effect of intermittent interval (s) during intermittent low-and-high steady shear on normalised observed transmission at different membrane channels.

The trend for normalised observed transmission is shown by Figure 5.43. Again there is greater variation between channels at the shortest time interval.

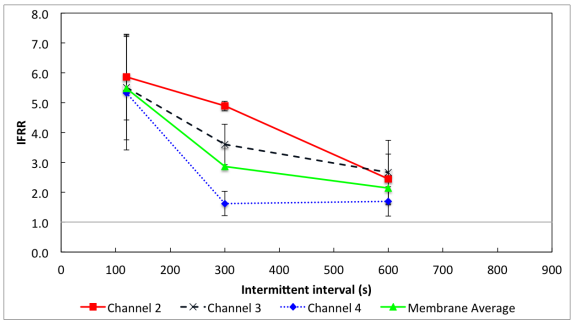

Figure 5.44: Effect of intermittent interval (s) during intermittent low-and-high steady shear on irreversible fouling resistance ratio (IFRR) at different membrane channels

Figure 5.44 shows the effect of intermittent interval(s) during intermittent low-and-high steady shear on irreversible fouling resistance ratio (IFRR) at different membrane channels. It is important to notice that IFRR for all intermittent intervals was greater than 1. This demonstrates that the use of intermittency of low-and-high steady shear resulted in greater membrane irreversible fouling than filtration under zero rotational shear. Membrane average IFRR for continuous steady shear at 5rpm and 840rpm was approximately 3 and 1.43 respectively. This is equivalent to a calculated average IFRR of 2.25, which was slightly greater than IFRR for intermittent interval at 600s, but was lower than IFRR for shorter intermittent intervals. Membrane average IFRR for continuous steady shear at 422.5rpm was 1.35, this was lower than IFRR for intermittent steady shear at all intervals. Intermittency of low-and-high steady shear resulted in greater membrane irreversible fouling than if a medium steady shear were used continously. % increase was approximately 300%, 100% and 60% for intermittent interval of 120, 300s and 600s respectively.

5.5.6 Effect of NaCl on Dextran Blue microfiltration

The primary aim of this section was to observe the effect of NaCl on transmission and fouling of membrane during Dextran Blue microfiltration at zero rotational shear and under the influence of high steady shear. The second objective focuses on the effect of high steady shear on the normalised irreversible fouling resistance

when the feed contains NaCl.

Firstly, filtration of Dextran Blue solution with NaCl addition (S1) was performed using the identical procedure as for filtration of Dextran Blue solution without NaCl addition at no rotational shear and at high steady shear of 840rpm. Secondly, a modified procedure was used for filtration, this includes filtration of 0.2M NaCl for 10 minutes prior and after filtration of Dextran Blue in NaCl solution (S2). Afterwards used membrane water resistance was measured. The fouling resistance during filtration of 0.2M NaCl after the filtration is refered to as "S3(S)", and the used membrane water resistance is refered to as "S3(W)". Table 5.8 is included for easy interpretation.

Test	**Pre-filtration**		**Filtration**	**Cleaning**	**Post-filtration**	
S1	W		W+D	W	W	
S2	W		S+D	W	W	
S3	W	S	S+D	S	S	W

Table 5.8: Comparisons of filtration procedures in different test conditions (W = deionised water, D = Dextran Blue, S = NaCl solution)

5.5.6.1 The effect of NaCl on fouling and transmission of Dextran Blue microfiltration

With NaCl addition, the observed transmission increased to nearly 1 for all channels and procedures tested, this is much greater than the observed transmission of Dextran Blue filtration without NaCl. Under zero rotational shear the rate of increase of transmembrane pressure during filtration of Dextran Blue with NaCl addition was less than 6% of that during filtration without NaCl addition.

The reason for substantial decrease in dTMP/dt for Dextran Blue filtration with NaCl addition is due to the presence of NaCl, which increases the ionic strength. Now according to the classic Derjaguin-Landau-Verwey-Overbeek (DLVO) theory of colloidal stability, high electrolyte concentration can compress the Debye layer of a double layer of counter-ions so reducing the energy barrier between the foulants.

Originally they repulsed each other due to the electrostatic repulsion forces but this is now nullified so allowing van der Waals attraction forces to dominate. It destabilises the colloids and they tend to aggregate together to form large flocs in the solution that may deposit more easily onto the surface of a membrane[177].

At 840rpm the filtration was affected by steady shear. The rate of increase of transmembrane pressure was significantly lower at channel 3 and 4 than at channel 2. The values were between 0.03-0.05kPa/min and 0.15-0.16kPa/min for channel 3 and 4 and for channel 2 respectively. Membrane average transmembrane pressure during filtration of Dextran solution with 0.2M NaCl was 0.08kPa/min. Unlike the filtration of Dextran Blue without NaCl addition where NdTMP/dt at 840rpm was approximately 0.33, the NdTMP/dt during filtration of Dextran Blue with NaCl addition at 840rpm was 2.7. While steady shear helped mitigate fouling during filtration of Dextran Blue-deionised water solution, it resulted in increases in the rate of transmembrane pressure to nearly three fold during the filtration of Dextran Blue-0.2M NaCl solution. This result occurred when there had been no prefiltering of 0.2M NaCl through the membrane. However in the case where the membrane has been pre-filtered using 0.2M NaCl for 10 minutes prior to use, the influence of steady shear on fouling rate was no longer held. Fouling was invariant with membrane radial position, and the average rate of increase of transmembrane pressure of 0.04kPa/min under both zero rotational shear and 840rpm.

5.5.6.2 The effect of NaCl on normalised irreversible fouling resistance

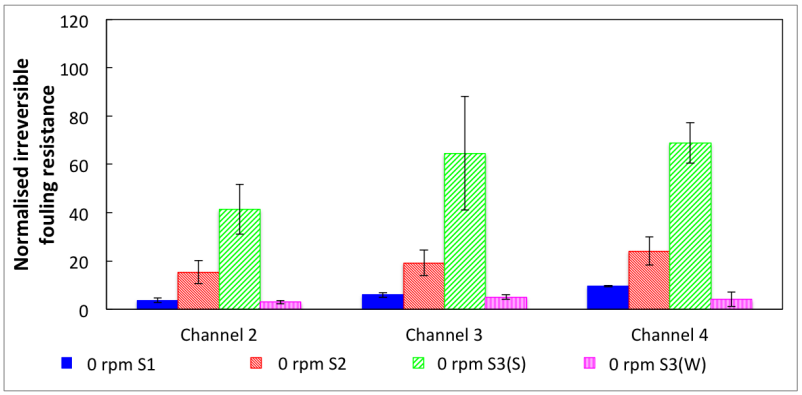

Figure 5.45: Comparison between normalised irreversible fouling of membrane for filtration under zero rotational shear when different feed and procedure were used

Figure 5.45 compares the normalised irreversible fouling resistance of the membrane at the different permeate channels for filtration under zero rotational shear for operation with and without salt . These consist of (1) normalised irreversible fouling resistance measured using deionised water for Dextran Blue in deionised water using the original procedure (S1), (2) normalised irreversible fouling resistance measured using deionised water for Dextran Blue with 0.2M NaCl addition using the original procedure (S2), (3) normalised irreversible fouling resistance measured using 0.2M NaCl for Dextran Blue with 0.2M NaCl addition using the modified procedure (S3(S)), and (4) normalised irreversible fouling resistance measured using deionised water for Dextran Blue with 0.2M NaCl addition at the final stage of the modified procedure (S3(W)).

Although the filtration of Dextran Blue with NaCl (0rpm S2) led to a lower membrane fouling rate, it resulted in a greater normalised irreversible fouling resistance compared with that obtained for filtration of Dextran Blue without NaCl. This was so for all channels. The normalised irreversible fouling resistance (0rpm S3(S)) was more than two fold greater than that for "0rpm S2". And "0rpm S3(W)" resulted in a dramatically lower normalised irreversible fouling resistance than that for other

cases with/without NaCl at all channels.

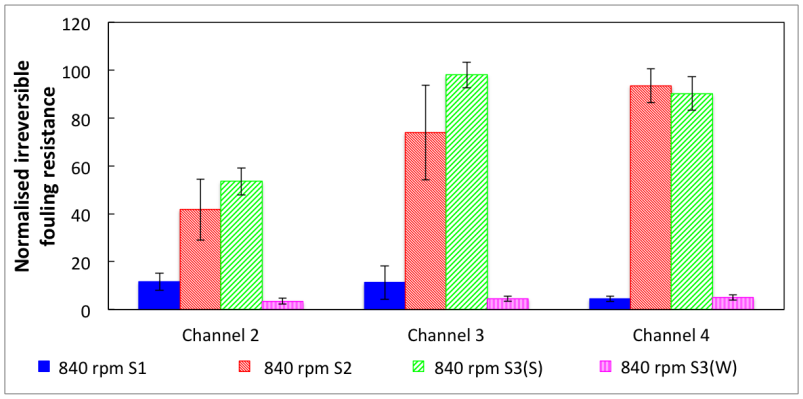

Figure 5.46: Comparison between normalised irreversible fouling of membrane for filtration under steady shear of 840rpm when different feed and procedure were used

Figure 5.46 shows normalised irreversible fouling resistance for various conditions under steady shear of 840rpm. The trend for the normalised irreversible fouling resistance under high steady shear was very similar to that under zero rotational shear (Figure 5.45). Both "840rpm S2" and "840rpm with S3(S)" resulted in much higher normalised irreversible fouling resistance than "840rpm S1" for all channels. Similar to the case for "0rpm S3(W)", the normalised irreversible fouling for "840rpm S3(W)" was dramatically lower than "840rpm S3(S)" where 0.2M NaCl was used to measure the used membrane resistance.

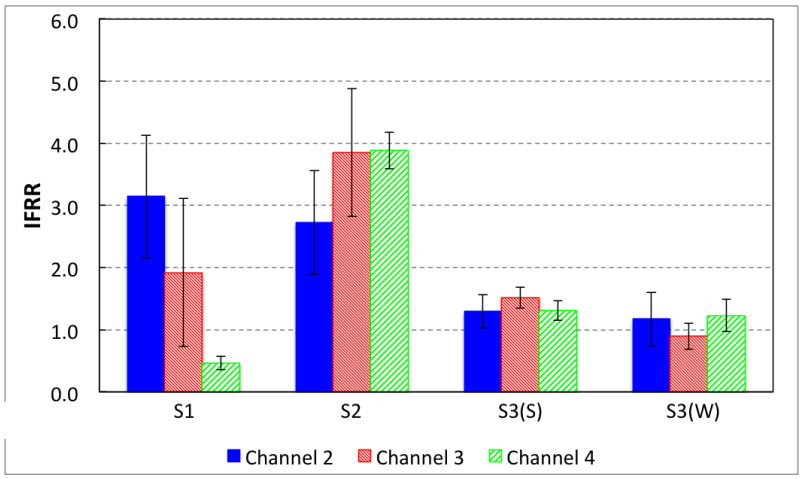

Figure 5.47: Comparison between irreversible fouling resistance ratio (IFRR) at 840rpm when different feed and procedure were used.

Emphasis summary of this section is reported in Figure 5.47 which shows the irreversible fouling resistance ratio (IFRR) obtained at 840rpm for various conditions. The benefit of high steady shear for Dextran Blue microfiltration at 101LMH was observed only at channel 4. The effect of high steady shear on microfiltration of Dextran Blue with NaCl varied significantly with the procedures used. High steady shear resulted in an adverse effect especially when the pretreatment of membrane with NaCl solution was not used.

5.6 Discussion

5.6.1 Comparison between the influence of displacement amplitude and frequency during Sinusoidal operation

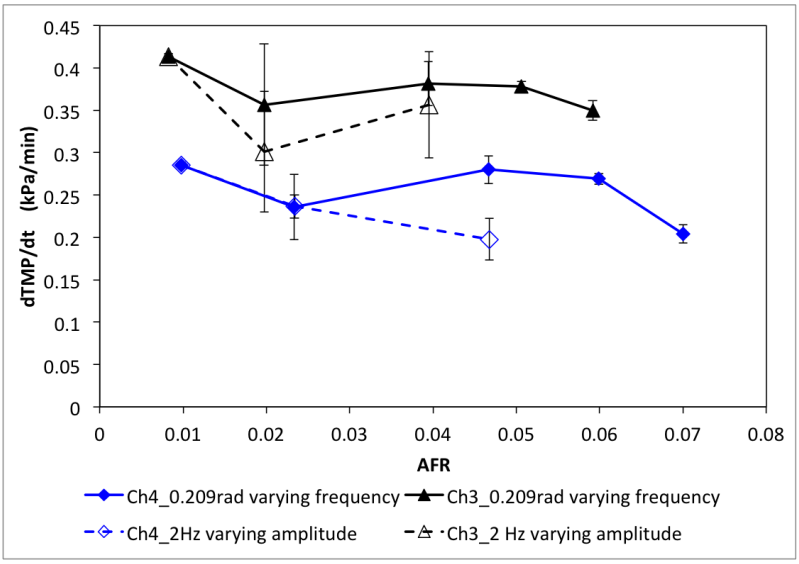

Figure 5.48: Effect of AFR on rate of increase of transmembrane pressure at channel 3 and 4

The effect of displacement amplitude and frequency on dTMP/dt is illustrated by Figure 5.48. The rate of increase of transmembrane pressure was plotted against AFR which is the product of displacement amplitude in radians, oscillation frequency in Hz, and the distance from the centre of the permeate channel to the centre of

membrane (the radius). The product of the oscillation amplitude and the radius gives the arc length (in metres). The AFR is a measure of the maximum velocity of the oscillation.

The comparison between dTMP/dt at channel 3 and 4 for the same AFR values is shown in Figure 5.48. At the same AFR, the increase in AFR due to increases in displacement amplitude was more effective at lowering dTMP/dt than that due to frequency. This is clear especially for channel 4 at AFR of 0.47.

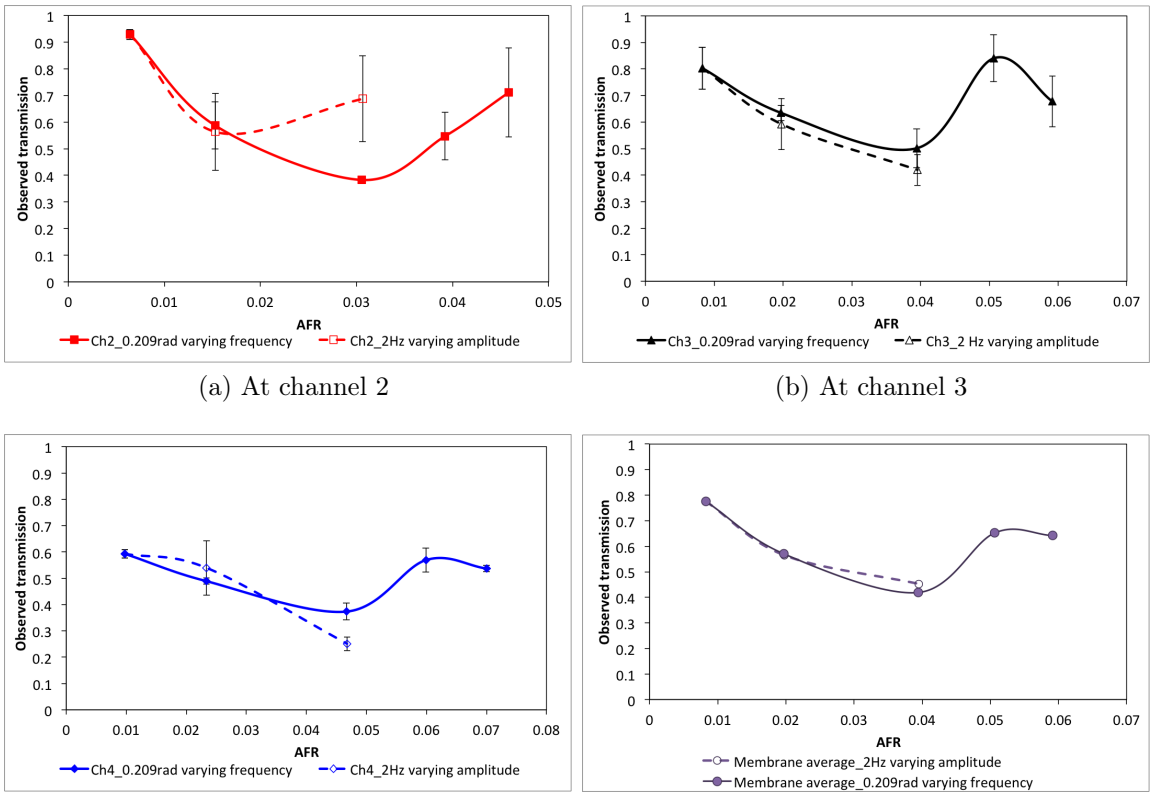

(a) At channel 2

(b) At channel 3

(c) At channel 4

(d) Membrane average

Figure 5.49: The influence of AFR on observed transmission at different radial position. Lines shown are trendlines.

Figure 5.49 shows the observed transmission for various AFR at different membrane channels and the membrane average values. Figure 5.49a to 5.49c show that the observed transmission varied between the membrane channels, but it is interesting to observe that the membrane average observed transmission values were similar at the same AFR values as shown in Figure 5.49d. It can be concluded that the

membrane average observed transmission reduced as AFR increased up to about 0.04, and that the increase in AFR due to displacement amplitude was as effective for lowering membrane average observed transmission as the increase in AFR due to oscillation frequency.

It is important to notice the variation in transmembrane pressure and observed transmission at different membrane channels (radial positions) at the same AFR values, because this can be useful for future designs of membrane filtration modules.

5.6.2 Comparisons between the influence of square wave and sinusoidal wave.

5.6.2.1 Effect of sharp-change and sinusoidal variation on membrane fouling

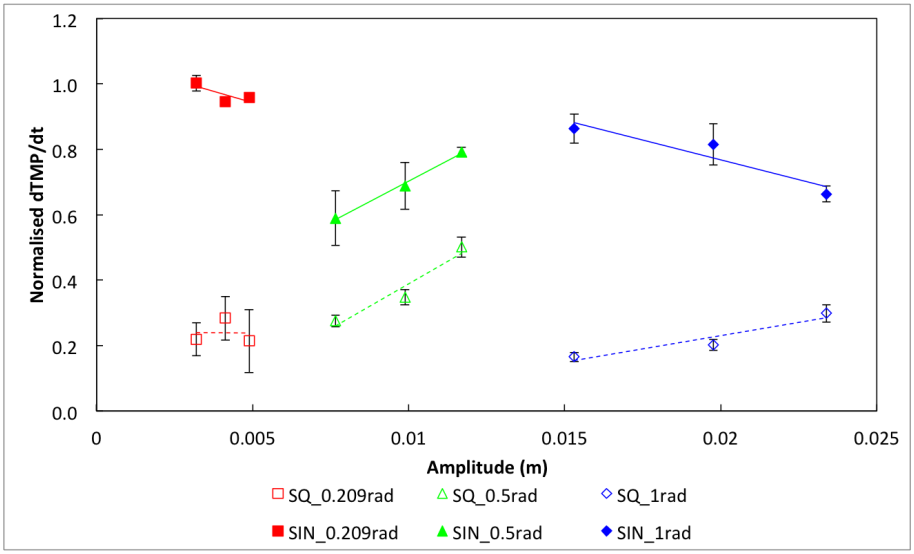

Figure 5.50: Effect of sinusoidal and square wave mode of operation on membrane normalised dTMP/dt at various amplitudes. Lines added for illustrative purposes only.

This section compares fouling mitigation efficiency achieved by "sharp change in direction" with that of a sinusoidal variation, which are represented by SQ and SIN respectively. Figure 5.50 allows comparisons between the influence of SQ and SIN operation at different amplitude (m) on membrane fouling. Amplitude (m) is calculated in metres, taking into account angular amptitude and the radius at the centre

of each membrane channel. Figure 5.50 shows that normalised dTMP/dt for SQ operation was much lower than that for SIN operation at all amplitudes. I.e., the sharp change in oscillation in SQ, even at comparatively low displacement amplitude, was much more effective at maintaining low rate of increase of transmembrane pressure in Dextran Blue microfiltration than the smooth change in SIN. It can be concluded that the sharp change in oscillation in SQ operation was more effective at fouling control than the smooth change in SIN operation for Dextran Blue microfiltration. This is because SQ was able to maintain uniform superior filtration performance across all membrane channels.

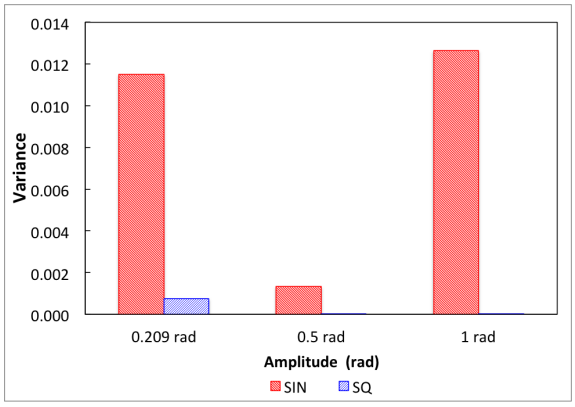

Figure 5.51: Variance of dTMP/dt across channels for Sinusoidal and square wave operation. (Variance for SQ at 0.209 and 1 rad were negligible.)

The variation in dTMP/dt or variance for dTMP/dt for both sinusoidal and square wave operation are shown in figure 5.51. The variance of dTMP/dt was small for SIN operation, especially at amplitude of 0.5rad. For SQ operation, the variance was nearly negligible. This indicates that fouling of membranes was very well distributed between all channels under SQ operation.

5.6.2.2 Effect of sharp-change and sinusoidal variation on normalised irreversible fouling resistance

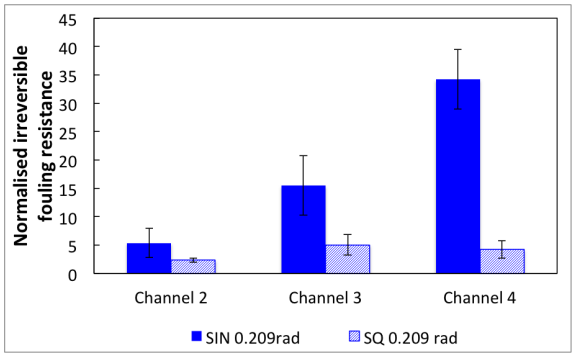

(a) At amplitude of 0.209rad

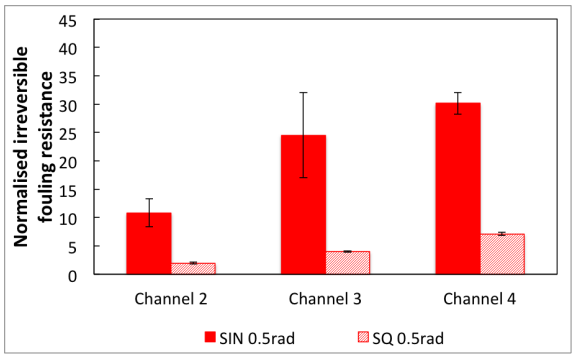

(b) At amplitude of 0.5rad

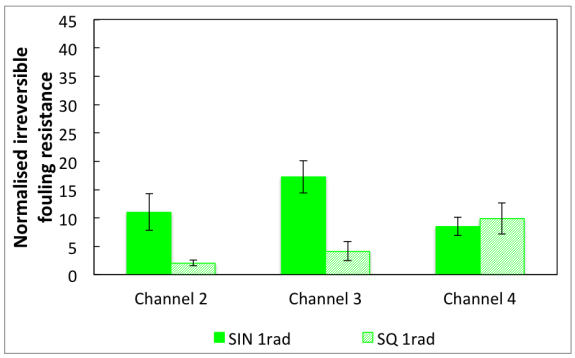

(c) At amplitude of 1rad

Figure 5.52: Effect of displacement amplitude of shear in Sinusoidal and square wave mode of operation on irreversible portion of membrane fouling

Figure 5.52 compares influence of sharp-change and sinusoidal-change in direction for the different channels. Normalised irreversible fouling resistance refers to

the ratio between used membrane irreversible resistance in a particular channel to the clean membrane resistance for the same channel. Figure 5.52a to c show the normalised irreversible fouling resistance for different membrane channels for the membranes used for Dextran Blue microfiltration under SIN and SQ operation at 0.209, 0.5 and 1rad 2Hz respectively. SQ operation generally resulted in lower normalised irreversible fouling resistance than SIN operation at the same displacement amplitude (rad) used. It can be concluded that Dextran Blue microfiltration under SQ operation led to lower membrane irreversible fouling than that under SIN operation.

5.7 Concluding remarks

5.7.1 Summary

DSSTC was fabricated to enable observation of the effect of various shear patterns on fouling and transmission for microfiltration under constant flux mode. DSSTC is capable of generating a wide range of shear patterns which are precisely reproducable, and the effect of sharp change in shear can also be investigated. A model polysaccharide, Dextran Blue 2000 was used as test fluid and straight through-pore membranes (Isopore) were used throughout.

5.7.2 Numerical summary of optimal conditions for each shear pattern

	Shear patterns	Average NdTMP/dt		Normalised observed transmission	
		Minimum value	Condition	Minimum value	Condition
1	Steady shear 101 LMH	0.33	840rpm	0.23	422.5rpm
2	Steady shear 71 LMH	0.57	120rpm	0.25	120rpm
3	Sinusoidal shear (amplitude effect at 2Hz)	0.69	0.5rad	0.54	1rad
4	Sinusoidal shear (frequency effect at 0.209rad)	0.75	14.32Hz	0.50	9.55Hz
5	Square wave shear (amplitude effect at 2Hz)	0.22	1rad	0.80	1rad
6	Intermittency (time interval)	0.49	600s	0.35	300s
7	Intermittency (high plate rotational speed)	0.58	480rpm	0.35	840rpm
8	Intermittency (with/without sharp change)	0.51	With sharp change	0.23	Both

Table 5.9: Comparisons of optimum values of NdTMP/dt and normalised observed transmission obtained with various shear patterns

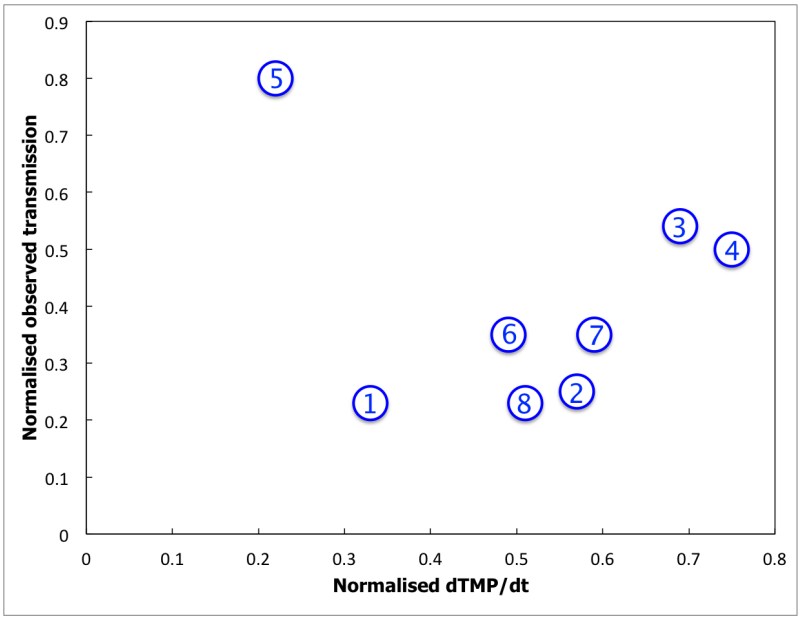

Figure 5.53: Normalised observed transmission against NdTMP/dt of optimum values obtained with various shear patterns as shown in Table 5.9.

1. As shown in Figure 5.53, under the range of conditions tested, the three most effective shear patterns for minimising normalised observed transmission of Dextran Blue are 1, 8, and 2 which correspond to the steady shear at 101, shear intermittency with sharp change of direction, and steady shear at 71LMH respectively. The three most effective shear patterns for minimising normalised dTMP/dt are 5, 1, and 6, which correspond to Square wave shear, steady shear at 101LMH, and shear intermittency with long time intervals respectively.

2. The introduction of steady shear generally led to lower dTMP/dt.

3. The influence of square wave oscillatory shear on fouling control was significantly more effective than that of sinusoidal wave. Increases in square wave of displacement amplitude up until 0.5rad did not significantly alter membrane average observed transmission from that in zero rotational shear, but further increases in amplitude did. Unlike that for sinusoidal oscillatory shear, the IFRR for square wave oscillatory shear was extremely low at all displacement amplitudes.

4. For intermittent steady shear, the level of shear during the high shear period had no direct effect on membrane performance. High plate rotational speed for high shear period of 840rpm resulted in membrane performance similar to when low steady shear of 5rpm was used continously. It can be concluded that for the range of value tested, intermittent steady shear with 300s time interval was not capable of improving membrane performance during microfiltration of Dextran Blue in the same way as when continuous steady shear was used.

5. In the presence of NaCl, the influence of steady shear on the fouling and transmission of Dextran Blue solution was different from that of Dextran Blue in deionised water. Under zero rotational shear, the rate of increase of transmembrane pressure during filtration of Dextran Blue with NaCl addition was less than 6% of that during filtration without NaCl addition. For all conditions tested, the observed transmission for Dextran Blue with NaCl had the values of approximately 0.95. It is clear that there exists a high possibility that a greater colloid trapping or higher irreversible membrane fouling can be induced when the high steady shear was used during filtration. This was significant for both Dextran Blue filtration without and with NaCl addition (i.e., the case S1 (with exception of channel 4) and S2). However, the effect of shear induced colloid trapping during the filtration ceased when the membrane has been pretreated with ionic (NaCl solution) prior to use.

6 Effect of Shear Patterns and EPS on Yeast Microfiltration

It is of interest to explore the effect of shear on a feed suspension containing both cells and EPS. Although it would be ideal if the feed were an algal suspension, the availability of fresh culture, the short life-cycle of the algae, as well as the complications involved during EPS monitoring made this impracticable. The use of freshly made yeast suspension was considered to be more appropriate. The main focus of this chapter is therefore on the influence of different shear patterns for the EPS alone, and the cells alone, and for a mixture of cells and EPS.

6.1 Introduction

Membrane filtration is used widely for separation between solid and liquid. During filtration, the accumulation of solutes occurs on the membrane surface or within the membrane pores causing increases in resistance, hence higher operating cost. The common solution to this problem is to apply a form of shear to the filtration system in order to reduce concentration polarisation and deposition of solutes. These can be a tangential velocity in crossflow modules or sinusoidal shear (or other cyclic) in dynamic membrane modules. Crossflow velocity is known to lower hydraulic resistance, due to decreased amounts of deposits on the membrane[67, 68]. When the feed contains solutes of various size, crossflow velocity is more effective at removal of

larger particles while leaving the smaller particles behind. This can cause increased membrane resistance due to a less porous cake[67, 68, 69].

Many literature studies reported the enhancement of flux and transmission when oscillation was introduced[178, 84]. Schluep et al. concluded that alternating the fluid flow direction during crossflow cannot enhance yeast filtration performance[179]. The influence of different shear patterns on fouling of multicomponent feed has not been well understood.

Unwashed yeast suspension is a multi-component feed; it contains yeast cells and high molecular weight substances. These substances are commonly found in microbial suspension or its supernatant, and are known as extracellular polymeric substances or extracellular polysaccharides (EPS)[180]. EPS has been identified as the most crucial factor accountable for fouling during microbial filtration[180]. Nevertheless, the positive influence of EPS on filtration characteristic has also been observed[181, 180]. The presence of EPS may assist filtration under a shear pattern but cause severe fouling in another.

The primary aim of this chapter is to observe and compare the influence of various shear patterns on membrane fouling resistance during microfiltration of microbial suspensions containing different amount of cells and soluble components. Unwashed yeast, washed yeast and yeast EPS will be used as representives for the mixed suspension, the suspension containing mainly cells, and the suspension consisting of soluble components. The flux stepping method used here aimed to cause further increase in membrane resistance so that the effectiveness of each shear pattern can be observed. The drawback of DSSTC using the current configuration includes increases in bulk feed concentration during filtration which is the common disadvantage of typical modules in dead-end operation. The observations on critical flux using the flux stepping method in DSSTC are therefore not ideal, due to the change in feed concentration. The term threshold flux used in this chapter refers to the threshold flux for that particular shear pattern and feed concentration which as

mentioned earlier increased with operating time. The four shear patterns that will be studied in this chapter are zero rotational shear, steady shear, sinusoidal oscillatory shear, and square wave oscillatory shear. The latter three patterns have high absolute shear rate so that the effect of tangential velocity due to the feed flow rate is negligible. The results yield the influence of each shear pattern on membrane performance, rather than the influence of superposition between two types of shear.

6.2 Materials and methods

The set up of of DSSTC was as described in chapter 5 using mainly 3g/L yeast suspension. Experiments were carried out using 0.1μm Isopore membranes because these provided the best variation in membrane fouling between different feed channels and significant effects of shear could be observed. New membranes were used for each experiment. Clean membrane resistance was measured for both deionised water, and phosphate buffer prior to use. Unwashed yeast suspension, washed yeast suspension, and yeast EPS suspension were used in these experiments. 3g/L yeast suspension was freshly prepared with Phosphate buffer prior to filtration. The supernatant of initial yeast suspension was labelled as yeast EPS, and this was used for filtration within two and a half hours of obtaining it. For washed yeast, the filtration started as soon as the washed yeast cells were resuspended back into a fresh phosphate buffer.

The experimental procedure is as detailed in chapter 5. Flux stepping microfiltration of 4 flux steps (41, 71, 101, and 131 LMH) was carried out using DSSTC. DSSTC was operated under various shear patterns to compare the performance of each shear configuration for the different feeds used. DSSTC's upper plate movement was either kept stationary or set to rotate at (i) 50rpm, (ii) a square wave at 1rad 2Hz, or (iii) a sinusoidal wave at 1 rad 2Hz. Rotational speed of 50rpm was chosen, as it was the maximum rotational speed possible that did not result in

accumulation of yeast cells at the centre of the membrane channel as checked by visual observation. The interpolated membrane average normalised transmission for Dextran Blue experiments at this rotational speed had similar values to that under sinusoidal shear of 1rad 2Hz. Moreover, both square wave and sinusoidal wave operated at this amplitude-frequency gave the best performance for Dextran Blue experiments.

The determination of membrane fouling by unwashed yeast suspension, washed yeast suspension, and yeast EPS suspension is reported in terms of normalised membrane resistance, fouling resistance ratio (FRR), and variance. Methods for obtaining these are reported in section 6.2.2.

6.2.1 Feed suspension

Yeast

Yeast suspension was prepared by mixing dried yeast (YSC2, Sigma-Aldrich) with 0.01M Phosphate buffer at pH 7.5. The suspension of 3g of dried yeast per litre of phosphate buffer was made fresh prior to each experiment. For washed yeast cell suspension, the yeast cells were washed 3 times using the same phosphate buffer solution. The yeast suspension was concentrated by refrigerated centrifuge (ALC PK 130R) at 4000rpm at 4^{o}C for 10 minutes. The 43mL of fluid from each 50mL centrifuge tube was removed and labelled as supernatant or yeast EPS suspension. The pellet remaining was resuspended with 43mL fresh phosphate buffer, shaken for 1 minute at 2500Hz (MS1 Minishaker, IKA), then the centrifugation was repeated. This process was repeated once more, and another 43mL of fluid was removed prior to adding 43mL of fresh phosphate buffer. This was labelled as washed yeast suspension. The reason for withdrawing the exact same amount of fluid after each centrifugation is to minimised experimental errors.

As the yeast cells were washed three times, the expected concentration of EPS within the feed was calculated to be 0.27% of initial feed EPS suspension. However,

the result yield EPS concentration in washed yeast suspension to be 15-20% of initial EPS in unwashed yeast suspension. This indicates that there exists additional EPS generated by the cells in the washed yeast suspension. Nevertheless, concentration of EPS in washed yeast suspension was much lower than that in unwashed yeast suspension, and washed yeast suspension may be claimed as containing mainly cells.

6.2.2 Analysis of fouling

Normalised membrane fouling resistance was used as, unlike transmembrane pressure, this takes into account permeate flux. This enables comparison of fouling resistance at different fluxes. As a variation in clean membrane resistance was found for $0.1\mu m$ Isopore membranes, it is of interest to report fouling of membranes in terms of normalised resistance rather than just membrane resistance to minimise errors due to intrinsic membrane properties.

Normalised membrane fouling resistance (R_N) is the ratio of increased membrane resistance due to fouling to clean membrane buffer resistance. It can be written as:

$$R_N = \frac{(R_T - R'_m)}{R'_m} \tag{6.1}$$

or

$$R_N = \frac{R_f}{R'_m} \tag{6.2}$$

where R_f is the increased membrane resistance due to fouling, and R'_m is the membrane buffer resistance. The membrane resistance was calculated by Darcy's law:

$$R = \frac{TMP}{\mu J} \tag{6.3}$$

where TMP is the transmembrane pressure, μ is the viscosity, and J is the per-

meate flux.

The influence of shear is of importance. Fouling resistance ratio (FRR) relates normalised membrane resistance under influence of shear to that under zero rotational shear (0rpm). An FRR value between zero and 1 indicates that the shear introduced led to a positive effect on fouling mitigation, while an FRR of value higher than 1 demonstrates that an adverse effect was found. When shear did not result in a significant change in membrane fouling resistance, FRR value will be approximately 1.

Fouling resistance ratio, FRR, was defined as

$$FRR = \frac{R_{N\gamma}}{R_{N0}} \tag{6.4}$$

where $R_{N\gamma}$ is the normalised membrane resistance with influence of shear, and R_{N0} is the normalised membrane resistance with stationary plates.

Another measure presented here is variance of R_N along the membrane radius. Variance is a measure of spread. A high value of variance illustrates that changes in amount of shear and/or feed concentration along membrane channels led to a high variation in fouling resistance. Variance was calculated based on standard deviation which assumes the entire population was presented.

6.3 Results

Results obtained under influence of zero rotational shear (0rpm), steady shear (50rpm), sharp change in shear (square wave shear, or SQ), and sinusoidal shear (SIN) against flux will be presented for yeast EPS, washed yeast, and unwashed yeast suspension. Then a comparison will be made before ending with a set of conclusions.

6.3.1 The influence of different shear patterns on microfiltration of yeast EPS

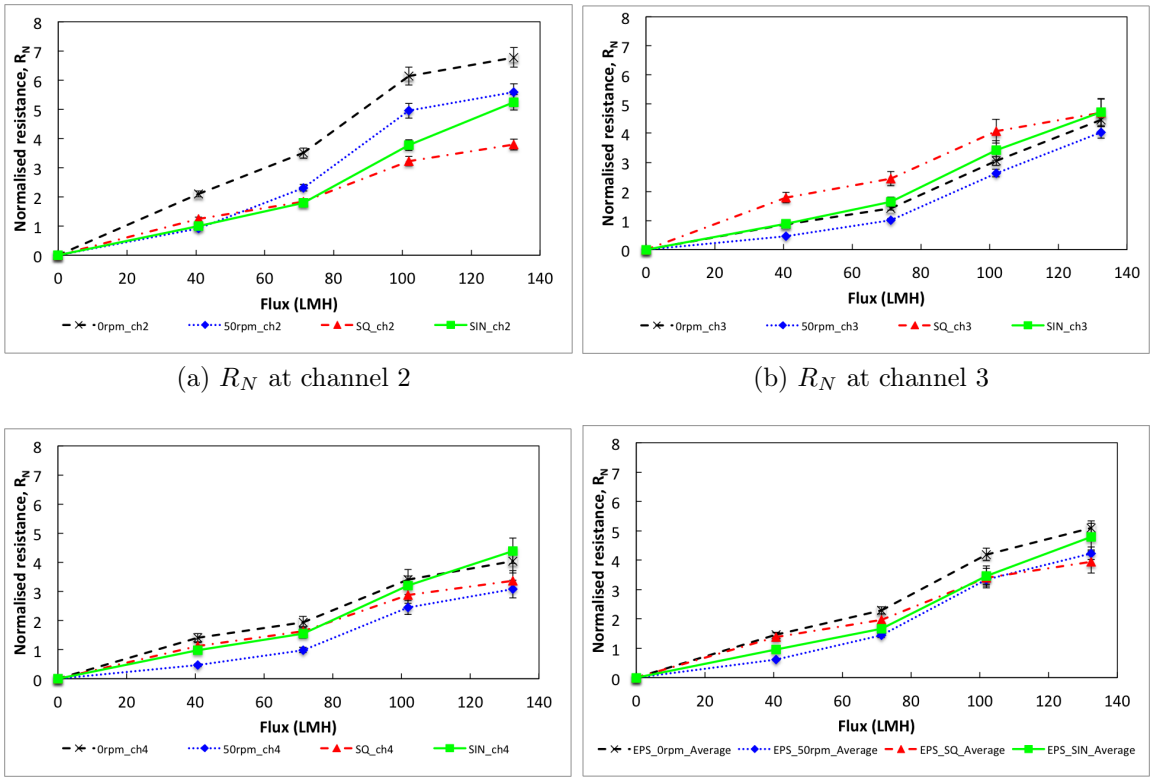

(a) R_N at channel 2

(b) R_N at channel 3

(c) R_N at channel 4

(d) Membrane average R_N

Figure 6.1: Effect of different shear patterns on normalised fouling resistance of membranes with flux during microfiltration of yeast EPS.

Figure 6.1 shows the variation of normalised membrane fouling resistance of microfiltration of yeast EPS with flux for various shear patterns. Figure 6.1a to 6.1c are for R_N at channel 2 which is the innermost channel, channel 3, and channel 4 respectively, while membrane average R_N is illustrated in Figure 6.1d. Here it is seen that the averaged value of R_N increased approximately linearly with flux for 0rpm but increased in a roughly exponential manner for 50rpm and SIN operation.

At 0rpm, R_N increased as flux increased for all channels. Figure 6.1c shows that it is noticable that fouling at low fluxes was slightly greater at channel 4 than at channel 3. This was unexpected as feed concentration is higher at channel 3 than at channel 4. The increase in fouling resistance was more pronounce at channel 2

as seen in Figure 6.1a. Even at the lowest flux of 41 LMH, R_N was already twice the intrinsic membrane resistance. It can be concluded that at 0rpm, the variation in R_N at different channels at the same flux was mainly due to the increase in feed concentration.

At channel 4, where the entering feed concentration was similar for all shear patterns, normalised resistance for filtration with imposed shear of any patterns was lower than that without or at zero rotational shear for all fluxes apart from the highest flux. For zero rotational shear, a much greater normalised resistance was observed when permeate flux increased from 71 LMH to 101 LMH; permeate flux of 101 LMH can therefore be regarded as being above the threshold flux for yeast EPS fouling. Steady shear of 50rpm resulted in the best filtration performance, however the threshold flux still remained at 101 LMH. Further increase in flux did not result in further sharp change in normalised resistance. Sinusoidal and Square wave oscillation resulted in similar normalised resistance at low fluxes of 41 LMH and 71 LMH; this indicates that the influence of a general change in direction and sharp change in direction was not significantly different for yeast EPS filtration at relatively low feed concentration and at permeate flux below the threshold level. When the flux increased to 101 LMH and above, normalised fouling resistance for both sinusoidal and square wave wave oscillation continued to increase. However, square wave oscillation outperformed sinusoidal oscillation. In other words, at above the threshold flux for yeast EPS a sharp change in direction was more effective than smooth change of direction. The slope of normalised resistance against flux between flux of 101 and 131 LMH was similar for zero rotational shear, steady shear, square wave oscillatory shear. This slope for sinusodal oscillatory shear was greater than the rest. This indicates that sinusoidal oscillation at well above threshold flux resulted in worse membrane performance especially if the flux was increased further.

At channel 3, normalised resistance at all fluxes was lowest under steady shear. While the performance for sinusoidal shear and zero rotational shear was identical

at 41 LMH, at higher fluxes similar trend between these two shear patterns was found with normalised resistance for sinusoidal mode being greater. The unexpected results were found for square wave oscillation at channel 3; with exception of 131 LMH normalised resistance was much greater than other shear patterns at all other fluxes. The slope of normalised resistance against flux divided into two parts, a more gentle slope prior to threshold flux and a steeper one after the threshold flux has been reached.

At channel 2, normalised resistance under zero rotational shear was greatest at all fluxes indicating highest fouling of membrane. At the lowest flux of 41 LMH, all shear patterns resulted in very similar normalised resistance. At 71 LMH, the performance of sinusoidal and square wave oscillation was identical and was lower that that of steady shear. This implies that a steady shear of 50rpm is less effective than oscillation in this case. It is likely that this is due to greater feed concentration in this channel and that the low steady shear along this channel is inefficient for reducing concentration polarisation. Feed concentration in this channel is expected to be higher than that at other channels due to rejected solutes by the membrane. It is reasonable to assume that the feed concentration especially for this channel is higher for steady shear than for square wave oscillation.

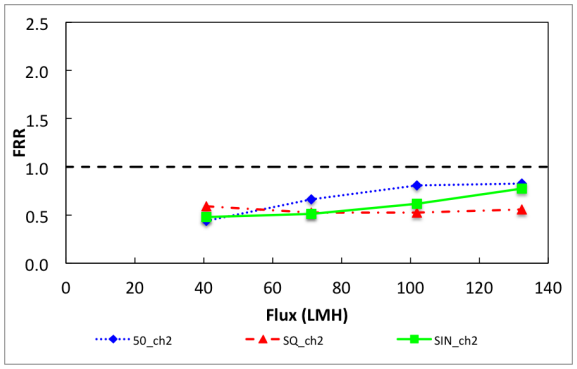

(a) FRR of yeast EPS at channel 2

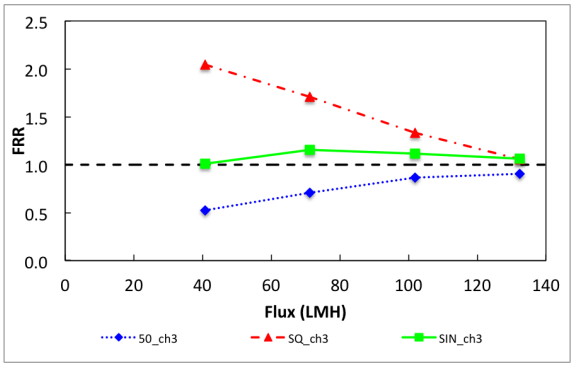

(b) FRR of yeast EPS at channel 3

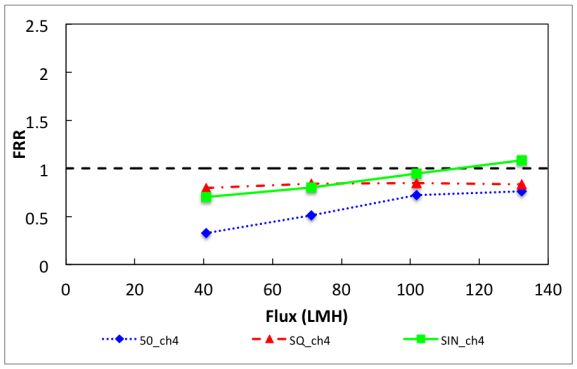

(c) FRR of yeast EPS at channel 4

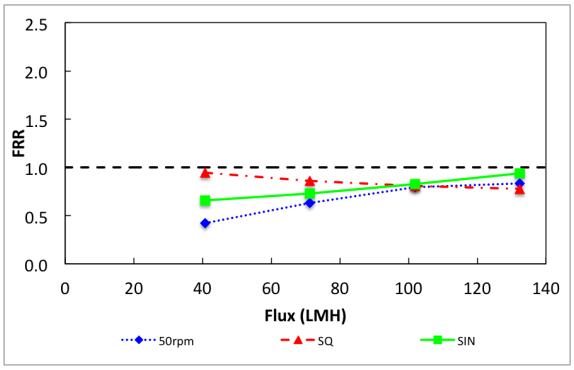

(d) Membrane average FRR of yeast EPS

Figure 6.2: Fouling resistance ratio (FRR) of yeast EPS suspension during flux stepping experiment under various shear conditions (◇ 50rpm, △ Square wave, □ Sinusoidal wave).

The influence of 3 shear patterns on membrane fouling were compared with zero rotational shear (0rpm). Figure 6.2 compares the effectiveness of each shear configuration. Starting with channel 4 where the feed suspension enters at the membrane rim, Figure 6.2c reveals that the introduction of any shear during filtration generally resulted in lower normalised membrane fouling resistance, with steady shear (50rpm) being the most effective method, it reduced membrane average R_N by 57% at 41 LMH. Effciency of this steady shear on membrane average R_N dropped as flux increased further to only approximately 20% improvement at 101 and 131 LMH. Similarly, the introduction of both sinusoidal and square wave oscillation led to reduced FRR at channel 4 (Figure 6.2c), these effects were more pronounced at lower fluxes than at higher fluxes. For square wave, the FRR for channel 2 and 4 were both

invariant with flux, with average FRRs of 0.55 at channel 2 and 0.83 at channel 4. For sinusoidal wave, improvement of FRR decreased as flux increased in all channels as seen in Figure 6.2a to 6.2c. The reason for FRR being higher than 1 at channel 3 for sinusoidal and square wave cannot be clearly explained. It is possible that this is due to more accumulation of solutes on this area with these flow patterns. Figure 6.2d reveals membrane average performance; steady shear and sinusoidal oscillation are superior to the square wave oscillation owing to the worse performance of square wave oscillation at channel 3.

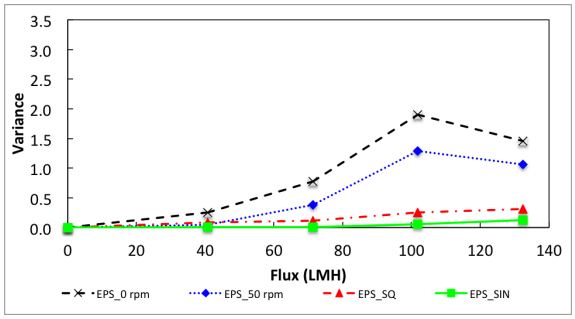

Figure 6.3: Variance R_N for microfiltration of yeast EPS suspension

Figure 6.3 demonstrates the spread of data, it reveals how the membrane fouling resistance varies between channels. For yeast EPS suspension, fouling in each channel differs most at zero rotational shear (0rpm) due to increase in feed concentration from channel 4 to channel 2. The variation in membrane fouling resistance at different channels was minimal under sinusoidal shear and very low for SQ operation. Low value of variance indicates consistency in fouling mitigation in the case of sinusoidal and square wave oscillation to effective radial mixing.

6.3.2 The influence of different shear patterns on microfiltration of washed yeast

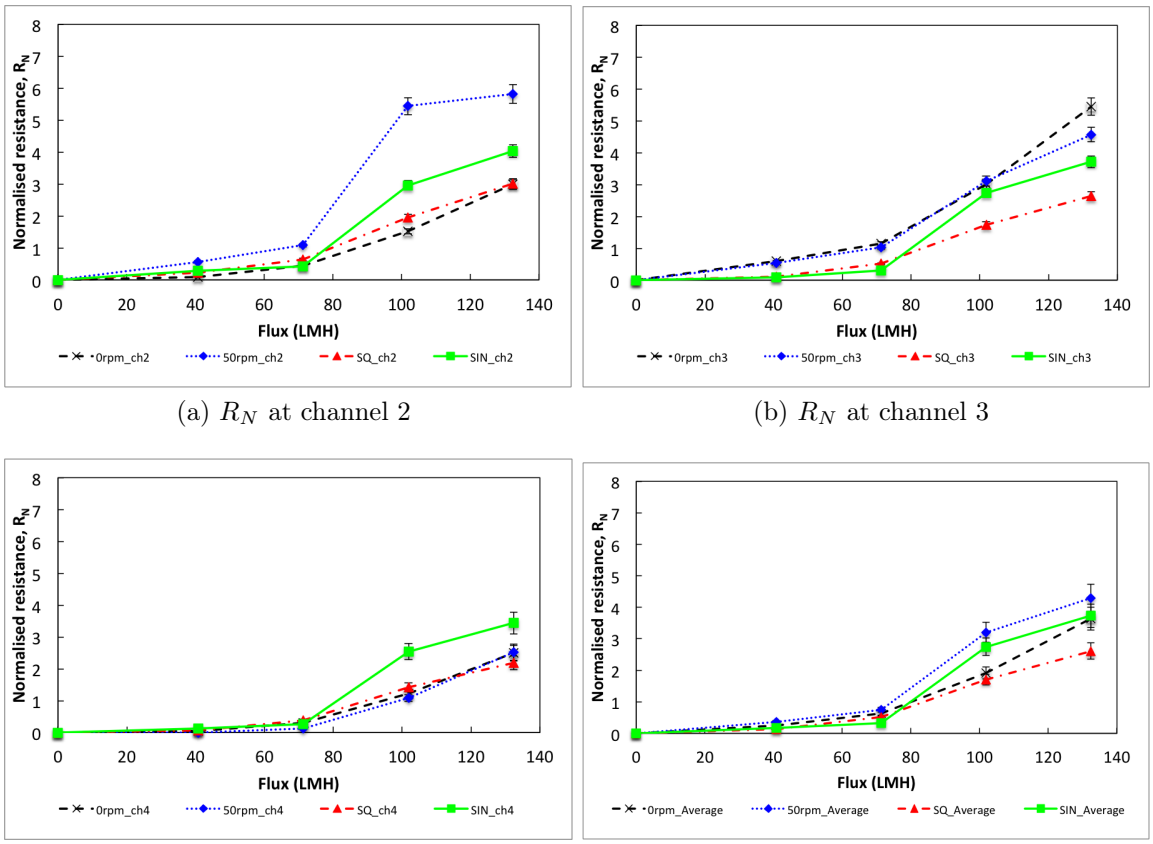

(a) R_N at channel 2

(b) R_N at channel 3

(c) R_N at channel 4

(d) Membrane average R_N

Figure 6.4: Normalised resistance (R_N) during flux stepping microfiltration of washed yeast cells as feed.

Figure 6.4 shows the variation of normalised membrane fouling resistance of microfiltration of washed yeast suspension with flux for various shear patterns. Figure 6.4a to 6.4c shows R_N for channel 2 to channel 4 respectively, while membrane average R_N is illustrated by Figure 6.4d. There exists a flux above which significant increase in R_N occurs, this will be refered to as threshold flux. Threshold flux for washed yeast suspension resulted in much more difference in normalised resistance than the threshold flux for yeast EPS, this was between 71 and 101 LMH regardless of level of shear introduced and probably closer to the lower value.

At channel 4, it is obvious that increases in flux from 71 LMH to 101 LMH

resulted in elevated normalised resistance. The influence of zero rotational shear, steady shear, and square wave oscillatory shear on normalised fouling resistance were similar. Sinusoidal oscillatory shear resulted in worse membrane performance. Washed yeast suspension contains mainly cells which are completely rejected by the 0.1 μm membrane. In the case where suspension consists of particles much larger than the membrane pore size, fouling mechanisms are usually assumed as intermediate pore-blocking and/or cake filtration. Assuming 100% cell rejection and well mixed suspension, the average feed concentration at this flux step is expected to be 21.3g/L, when unwashed yeast contains 75% cells by weight[18]. At this concentration, the increase in R_N is likely to be dominated by the cake. Cake compressibility and resistance are dependent on the structure. Sinusoidal oscillatory shear caused rearrangement of this yeast cake structure leading to a more compact cake hence greater membrane resistance that is similar in values for all channels. Similar membrane performance for zero rotational shear, steady shear, and square wave shear at channel 4 indicates that both steady shear and square wave oscillatory shear at 50rpm and 1rad 2Hz respectively were either not capable of removing the cells from the membrane surface and did not alter the cake structure or the positive effect due to removal of depositions balanced negative effect due to a more compact cake by cell rearrangement.

Normalised resistance for zero rotational shear at channel 3 was greater than that at both channel 4 and channel 2. Steady shear resulted in similar R_N to zero rotational shear especially at lower fluxes. Both sinusoidal and square wave oscillatory shear performed similarly well especially at low fluxes. At 71 LMH and 101 LMH, the sharp change in shear in square wave led to better membrane performance than smooth change in oscillatory shear in sinusodal operation.

At channel 2, both sinusoidal and square wave oscillatory shear had similar trend and values as those in other channels. Steady shear at this channel resulted in the highest R_N at all fluxes. The absence of shear resulted in the lowest R_N. This is

due to a more porous cake which led to lower cake resistance. A similar result was obtained by Mackley and Sherman[153].

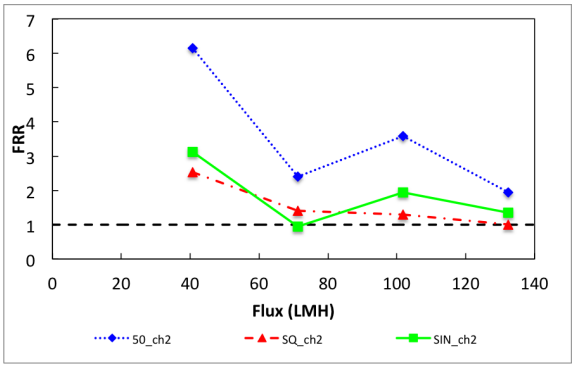

(a) FRR of washed yeast suspension at channel 2

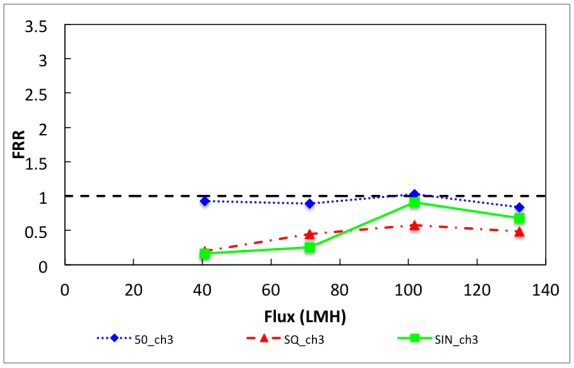

(b) FRR of washed yeast suspension at channel 3

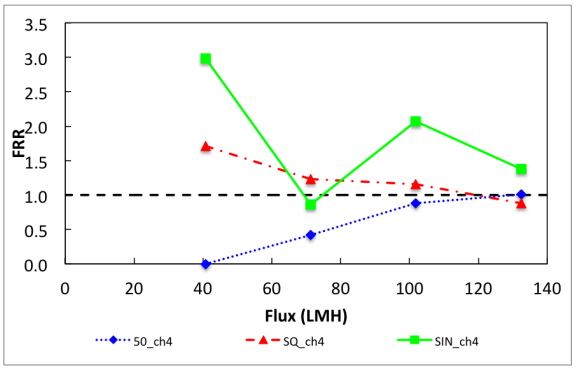

(c) FRR of washed yeast suspension at channel 4

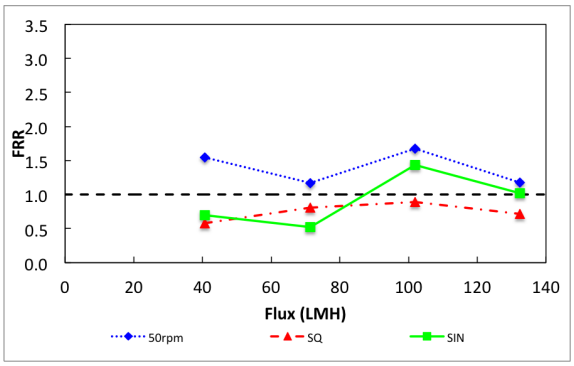

(d) Membrane average FRR of washed yeast suspension

Figure 6.5: Fouling resistance ratio (FRR) of washed yeast suspension during flux stepping experiment under various shear conditions (◇ 50rpm, △ Square wave, □ Sinusoidal wave).

Figure 6.5 relates membrane fouling under the influence of different shear to that at 0rpm. For steady shear of 50rpm, the benefit of shear at channel 4 (Figure 6.5c) was off-set by higher membrane fouling at channel 2, which resulted in a decreased performance on average as seen in Figure 6.5d, while for sinusoidal wave and square wave, the FRR was much greater than 1 in channel 2 and 4, indicating that the introduction of these shear patterns led to greater fouling of the membranes. Sinusoidal wave was only effective for fluxes below the threshold flux. The feed was washed yeast suspension which contains mainly cells, and FRR being greater than 1 is the result of changes in cake structure due to shear.

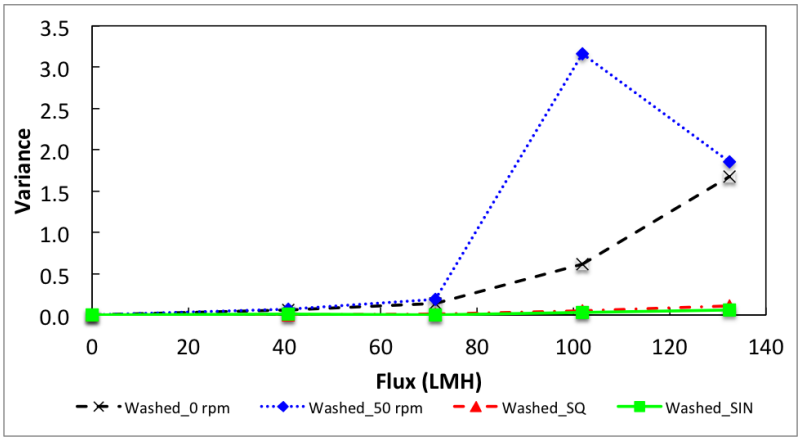

Figure 6.6: Variance of R_N for microfiltration of washed yeast suspension

Figure 6.6 revealed that membrane fouling resistance in each channel was very consistent under sinusoidal wave and square wave configuration for all fluxes. For the other two conditions there was little variation below the threshold flux but significant variation above. Similar R_N values at all fluxes in different channels indicated that similar fouling propensity at each channel occurred during the filtration.

6.3.3 The influence of different shear patterns on microfiltration of unwashed yeast

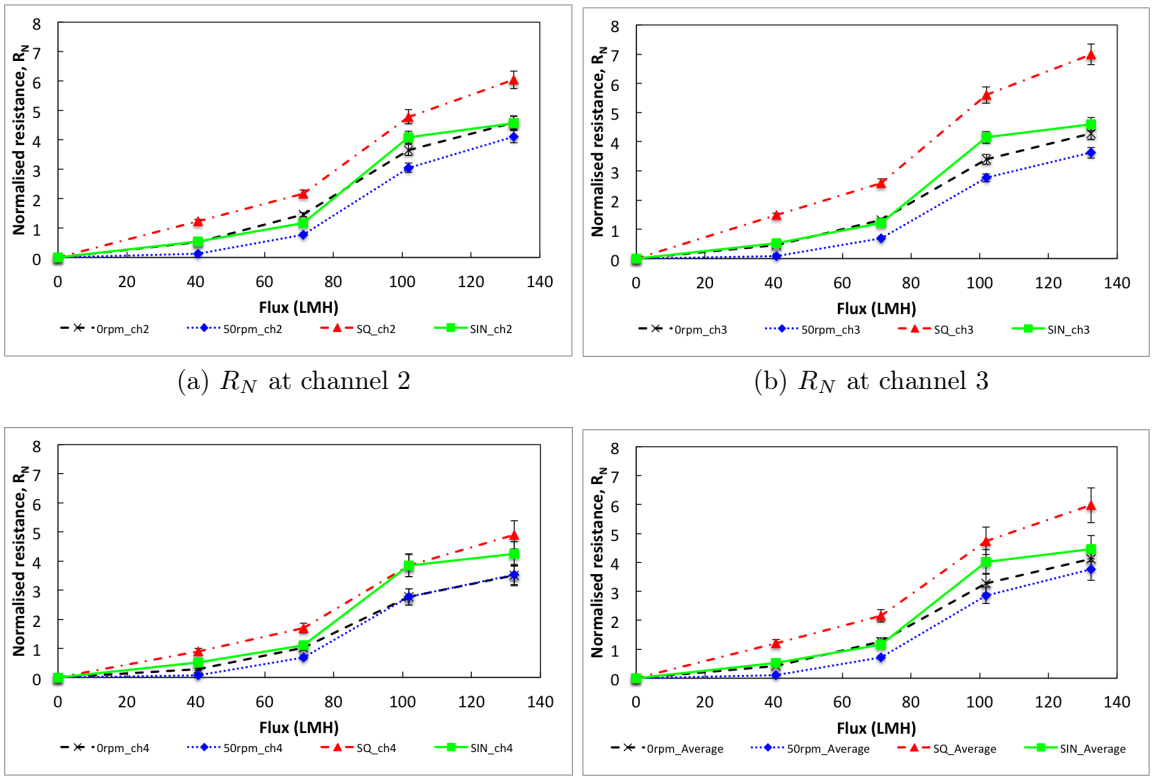

(a) R_N at channel 2

(b) R_N at channel 3

(c) R_N at channel 4

(d) Membrane average R_N

Figure 6.7: Normalised resistance (R_N) during flux stepping microfiltration of unwashed yeast cells as feed.

Unwashed yeast suspension consists of yeast cells as well as a high amount of extracellular polysaccharide. Figure 6.7a to c gives normalised membrane fouling resistance of microfiltration of unwashed yeast suspension with flux for various shear patterns for the various channels. Figure 6.7d gives the overall result, there was a threshold flux at around 70LMH for all shear patterns. Only the steady shear of 50rpm resulted in an improvement of overall membrane average R_N for unwashed yeast cells. At 0rpm, R_N increased as flux increased at all channels (see Figure 6.7c). There exists a flux above which significant increase in R_N occurs, this will be refered to as threshold flux. Threshold flux for unwashed yeast suspension was between 71 and 101 LMH regardless of level of shear introduced. At steady shear

of 50rpm, R_N was generally lower than R_N at 0rpm, even at channel 2 where the bulk feed concentration was high. Square wave resulted in greater membrane fouling at all channels, while the adverse effect of sinusoidal oscillatory shear was only significant at higher fluxes of 101 LMH and 131 LMH. Only the steady shear led to improvement of overall membrane average R_N for unwashed yeast cell filtration.

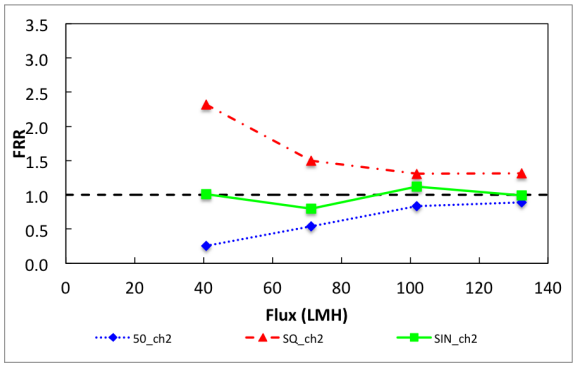

(a) FRR of unwashed yeast suspension at channel 2

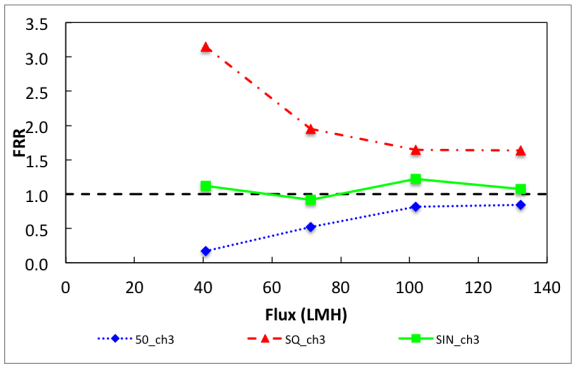

(b) FRR of unwashed yeast suspension at channel 3

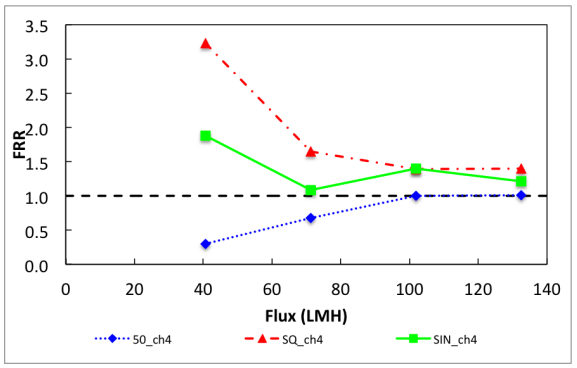

(c) FRR of unwashed yeast suspension at channel 4

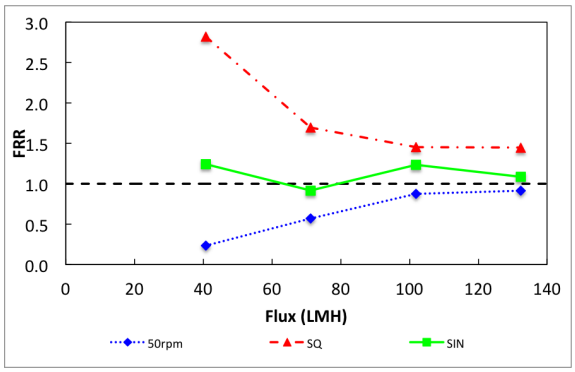

(d) Membrane average FRR of unwashed yeast suspension

Figure 6.8: Fouling resistance ratio (FRR) of unwashed yeast suspension during flux stepping experiment under various shear conditions (◇ 50rpm, △ Square wave, □ Sinusoidal wave).

Figure 6.8 compares membrane fouling resistance when filtration operated with shear and without (0rpm). It can be seen that the trend in Figure 6.8a, 6.8b, and 6.8c is very similar with steady shear (50rpm) being beneficial but the square wave gave FRRs much higher than 1. As flux increased, FRR tended to 1. Figure 6.8d shows that the effect of a sinusoidal wave led to membrane average FRR being nearly

1, i.e., similar to filtration at 0rpm. At channel 4, during fluxes of 41 LMH and 71 LMH, both square wave and sinusoidal wave generally led to FRR greater than 1 even at low fluxes.

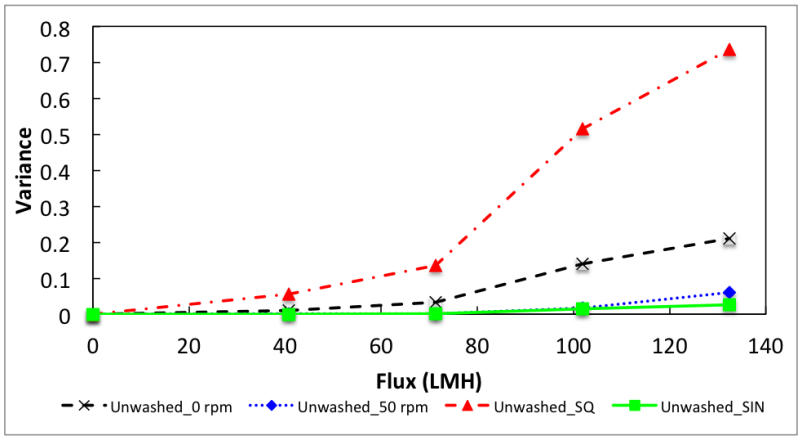

Figure 6.9: Variance of R_N for microfiltration of unwashed yeast suspension
Note: Range shown on y-axis is different from that in Figure 6.3 and 6.6.

Figure 6.9 indicates that the variation of membrane performance between the channels during filtration of mixed feed was much lower than in the case of either cells (washed yeast suspension) or EPS (yeast EPS suspension) alone. Sinusoidal wave and steady shear of 50rpm resulted in minimal variance. While the square wave led to greater variation in R_N between channels (0.7 at 131 LMH), this was rather unexpected as the variance for filtration of both cells alone and EPS alone suspension was much smaller (0.1 and 0.3 respectively at 131 LMH). The reason why the fouling propensity of filtration of mixed feed suspension under influence of square wave shear varied significantly from that of either single feed (cells alone, or EPS suspension alone) is unclear but the absolute value of the variances in Figure 6.9 are much smaller than those in Figure 6.3 and 6.6.

6.3.4 Comparison of fouling by yeast EPS, washed yeast suspension and unwashed yeast suspension

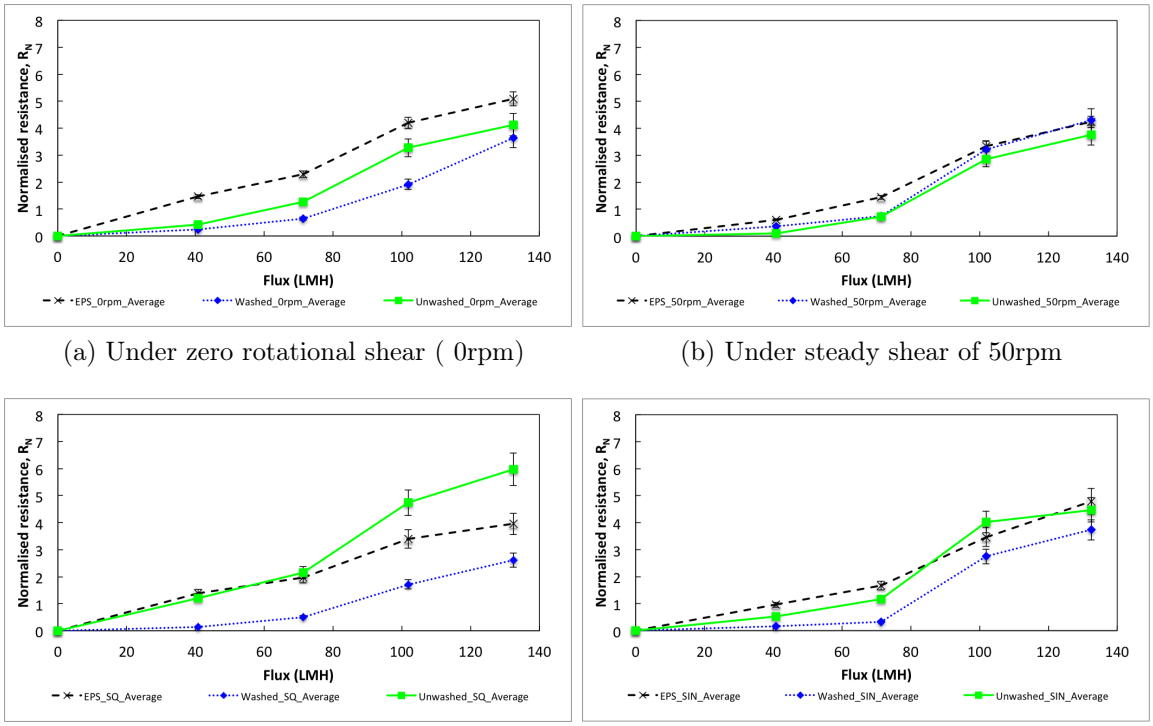

(a) Under zero rotational shear (0rpm)

(b) Under steady shear of 50rpm

(c) Under square wave

(d) Under sinusoidal wave

Figure 6.10: Comparison of normalised fouling resistance by yeast EPS, washed yeast suspension and unwashed yeast suspension under different shear patterns

Figure 6.10 shows the variation in membrane average normalised fouling resistance against flux for different feeds. Figure 6.10a compares membrane average R_N of microfiltration of washed yeast, unwashed yeast, and yeast EPS suspension under zero rotational shear (0rpm). Microfiltration of washed yeast suspension resulted in the least membrane fouling at all fluxes, while the microfiltration of yeast EPS suspension led to high fouling even at a low flux. Average fouling resistance for microfiltration of unwashed yeast suspension (i.e., mixed feed) was similar to microfiltration of washed yeast at 41 LMH. However, as flux increased, R_N became much higher than R_N for washed yeast filtration. At all fluxes, R_N of unwashed yeast microfiltration was always lower than R_N of yeast EPS microfiltration. This

suggests that under zero rotational shear (0rpm), the presence of yeast cells helped prevent fouling by yeast EPS especially at low fluxes.

Figure 6.10b compares fouling by single feed and mixed feed under steady shear of 50rpm. Again, the microfiltration of yeast EPS resulted in highest R_N values at all fluxes. Fouling by the feed containing yeast cells remained low at low fluxes, but as flux increased membrane fouling of both washed and unwashed yeast suspension approached that of yeast EPS. Under steady shear, the unwashed yeast cake may have a different structure to that of washed yeast. The presence of EPS in unwashed yeast supported the yeast cell cake structure making them less susceptible to cell rearrangement due to the high flux and steady shear. Fouling by unwashed yeast suspension (i.e., with cells) was always lower than fouling by yeast EPS alone (without cells).

Figure 6.10c shows normalised membrane resistance against flux for unwashed yeast, washed yeast and yeast EPS microfiltration under square wave oscillatory shear. Square waves were more effective for washed yeast than for unwashed yeast and yeast EPS. A sharp change in normalised resistance for washed yeast filtration under square wave shear occurred when the flux was above 71 LMH, indicating that threshold flux for the yeast cells are between 71 LMH and 101 LMH. Square wave oscillatory shear was however not as effective for filtration with feed containing the EPS. Both yeast EPS and unwashed yeast filtration under square wave shear had much greater normalised resistance even at low fluxes. At above threshold flux even greater resistance was found for unwashed yeast, while for yeast EPS the increase in R_N was not significant. At below threshold flux, fouling during unwashed yeast under square wave shear was dominated by the yeast EPS. At above threshold flux, normalised resistance for unwashed yeast was roughly the combination of fouling by the cells and by the yeast EPS.

Figure 6.10d shows membrane average R_N of microfiltration of washed yeast, unwashed yeast, and yeast EPS suspension under sinusoidal oscillatory shear. Similar

to all other cases, R_N for yeast EPS was much greater than that for unwashed yeast at all fluxes. At below threshold flux, fouling by washed yeast was extremely low, however above that a sudden increase in R_N occurred. Normalised resistance for yeast EPS filtration under sinusoidal operation increased as flux increased. Fouling by unwashed yeast suspension was generally less than that by yeast EPS but greater than that by washed yeast. The presence of yeast cells within unwashed yeast suspension resulted in improvement in R_N below threshold flux. At above threshold flux, filtration of unwashed yeast under sinusoidal shear behaved similar to that of yeast EPS.

6.4 Discussion

The influence of shear of various patterns affects filtration performance of feed with different composition differently. Researches have been carried out in dynamic membrane modules to observe the effect of oscillatory shear on membrane performance; however, these studies cannot be directly compared with the influence of steady shear using the same modules. DSSTC is capable of operating at both modes of shear. Effect of zero rotational shear, steady shear, smooth change in oscillatory shear, and sharp change in oscillatory shear were directly compared for microfiltration of unwashed yeast, washed yeast, and yeast EPS. In the case of DSSTC, the effectiveness of the shear pattern was dependent upon the level of flux as well as the feed composition. The normalised resistance changes with radial position of the membrane.

For microfiltration of yeast EPS suspension, all shear patterns led to improved membrane average performance. The efficiency of shear was more significant at low fluxes. Steady shear of 50rpm provided the highest amelioration on yeast EPS fouling at all channels, while sinusoidal wave resulted in least variation in R_N between channels. The FRR or the improvement in membrane fouling resistance compared

with microfiltration at zero rotational shear (0rpm) was most stable for square wave pattern, this was clear in channel 2 and 4. Foley et al. suggested internal membrane fouling as the underlining fouling mechanism for yeast supernatant filtration[65].

For microfiltration of washed yeast cell suspension, the threshold flux can be clearly seen, and it was between 71 LMH and 101 LMH. In general, the introduction of shear of all patterns resulted in greater membrane average resistance than that at no rotational shear. Steady shear was effective at keeping normalised resistance low below threshold flux for channel 4, while it resulted in higher resistance at channel 2. Similar to the yeast EPS case, efficiency of steady shear decreased as flux increased. The shear caused rearrangement of the cake layer hence greater fouling resistance due to lower cake permeability. This fouling mechanism has been observed by Mackley et al. for the cake of polyethylene particles. The cake specific resistance grown under influence of crossflow was approximately three times that grown under static condition[152]. In their studies, imposing sinusoidal oscillation on crossflow was found to improve membrane performance especially at high crossflow velocity[153]. The re-entrainment of particles during the sinusoidal oscillation occurred due to eddy circulation formed both upstream and downstream of the baffle[153]. For DSSTC, the positive effect of sinusoidal shear occurred only below the threshold flux. It is important to note that very low tangential flow occurred in DSSTC during filtration and the baffle was not used in DSSTC, hence a lack of eddy circulation; this explains inefficiency of sinusoidal operation for filtration application containing particles at higher fluxes. It has been reported that introduction of the vanes in a rotating disk system can largely improve filtration performance[109], if the DSSTC were equipted with the vanes it may give different trend.

To compare the influence of the two oscillatory shear patterns in DSSTC for washed yeast, the smooth change in oscillatory shear resulted in greater resistance than the sharp change in shear especially above the threshold flux. Below the threshold flux, square wave oscillatory shear led to similar membrane average resist-

ance to that of zero rotational shear. At above threshold flux, the benefit of square wave started to reveal, this was clear at 132LMH. This suggests that during filtration of larger particles the sharp change led to improvement in membrane performance at above threshold flux but the smooth change led to opposite result. Both oscillatory shear gave consistent performance regardless of the radial position.

The effect of shear on microfiltration of unwashed yeast cell suspension was different from the effect on microfiltration of washed yeast and EPS suspension. Steady shear of 50rpm led to improvement in membrane performance at all channels, nevertheless the enhancement reduced as flux increased. As this was similar to microfiltration of EPS alone, it may suggest that fouling by EPS dominates in this case, while FRR at early fluxes of channel 4 for sinusoidal wave and square wave suggests similar fouling behaviour as microfiltration of washed yeast suspension. Sinusoidal wave did not result in much change in membrane average filtration performance, while square wave led to a higher fouling resistance than filtration at 0rpm for all flux. Square wave oscillatory shear was the only shear pattern for which fouling of unwashed yeast was dominated by the EPS, even at low flux, while SQ was effective in keeping FRR for the yeast EPS below 1. It is clearly less effective for the mixed feed, since the normalised resistance for unwashed yeast at above the threshold flux was roughly the combination of fouling by washed yeast and yeast EPS.

The combined fouling mechanism under influence of various shear patterns has been analysed. This aimed to compare the resistance during filtration of washed yeast and yeast EPS with that of unwashed yeast. In most cases, the combined fouling mechanism was better explained as "filter-aid" rather than "over-clogging". Over clogging situation during unwashed yeast filtration was not observed for DSSTC. However Hughes et al. have found that the combined dTMP/dt for EPS and washed yeast was lower than dTMP/dt for unwashed yeast indicating that combined fouling mechanism which resulted in over-clogging situation has taken place during unwashed yeast filtration at low permeate flux of 12LMH through 0.1μm polysulfone

membrane[18]. Unlike polysulfone membrane, Isopore membrane used for DSSTC has straight through pore structure. Accumulation of yeast EPS within the pore structure was therefore expected to be lower for Isopore membrane membranes. Lower permeate flux of 12LMH used by Hughes was likely to cause looser-packed cake which allows higher initial EPS penetration, hence an over clogging situation. It has also been reported that the cause of increased resistance during mixed fouling was due to EPS accumulated on the top few layers of the cake[182]. For DSSTC operating under zero rotational shear, EPS was the main cause of increased resistance at all fluxes. Fouling by washed yeast remained low until the threshold flux has been reached. Unwashed yeast fouling was similar to that of washed yeast at low fluxes and although it became greater as flux increased, the total resistance was lower than that of EPS filtration alone. This indicates that the presence of cells protected the membrane from fouling by EPS during zero rotational shear.

Under steady shear, the normalised resistance for unwashed yeast was generally lower than that for washed yeast. It is possible that the adhesion properties of the EPS in the unwashed yeast suspension obstructed the movement of yeast cells in the cake that would otherwise have moved to form a denser cake due to steady shear. Foley et al. refers to the change in extracellular properties of microbial cells as the change in cell surface properties[183, 30]. The filtration performance was found to be dependent on the extracellular matrix in the case of the bacteria[183]. The cell wall structure for the same specie can be varied by the cell environment, and this directly affects specific cake resistance[34]. And in the case of DSSTC, the presence of EPS in unwashed yeast slightly improved membrane performance, especially above the threshold flux. Sharp change in direction and smooth change in direction resulted in very different fouling behaviour, especially for the unwashed yeast. Fouling during sinusoidal oscillatory shear by different feed was quite similar to fouling during zero rotational shear. However in sinusoidal operation, yeast cells in unwashed yeast generally acted as “filter aid”.

7 Conclusions and Future Work

The objective of this research was to gain a better understanding of the fouling phenomena and to observe the influence of shear on fouling and transmission during constant flux microfiltration. Two novel tools have been used for the analysis. Firstly, the DOTM module (SMTC, NTU, Singapore) serves as optical tool for in-situ visual observation of the deposition of particles onto the membrane surface as well as their removal. And secondly, DSSTC was fabricated and developed to provide an integrated module capable of generating different shear patterns necessary for thorough studies. Microalgal suspension was used as feed for DOTM analysis. A model polysaccharide, Dextran Blue, and yeast suspensions were used as feed for DSSTC study.

7.1 Concluding remarks

7.1.1 Microfiltration of microalgae using DOTM

DOTM allows in-situ visual observation of the membrane surface during microfiltration. The main advantage of DOTM is that the fluid flow does not need to be stopped in order to obtain good image clarity. DOTM is essentially a transparent crossflow module equipped with a transparent membrane. DOTM module was placed on a microscope and images were obtained by a video camera connected to the microscope viewing channel.

The main focus of DOTM work was to study microfiltration of microalgae un-

der various conditions. Deposition and removal mechanisms of microalgae were observed. Algal suspension contains both the algae and their EPS. DOTM images were periodically captured at specific times, and these were used to compare critical flux for algal cells observed via image analysis and TMP - filtration time data.

The principal conclusion from DOTM observation of microalgae MF are listed below:

- Generally DOTM has proven to be a more sensitive method for obtaining the threshold flux than analysis of transmembrane pressure. However when EPS exists, DOTM image analysis can be misleading and the analysis of transmembrane pressure - filtration time data is a more appropriate method for fouling monitoring. So whilst DOTM is a useful tool that provides information unobtainable by TMP-flux-time data alone, the use of DOTM should still be accompanied by analysis of these measurements.

- Fouling by microalgae is more severe than fouling by latex particles because of the presence of EPS in the microalgal suspension.

- Crossflow velocities can aid removal of deposited microalgae from the membrane surface but the algal cells may be tore off from their sheath. The remaining sheath on the membrane surface causes increase in the membrane resistance and attracts further deposition due to sheath-sheath adhesion.

- Solution environment has significant effect on fouling behaviour. Increases in ionic strength can result in positive or negative effect on membrane performance. Lower feed concentration does not necessarily lead to lower algal cell deposition.

- Air bubbling reduced the fraction of membrane coverage by the algal cells and reduced the rate of TMP increase.

DOTM is, however, a type of crossflow module where shear cannot be precisely

controlled. The lack of adjustability of level and patterns of shear in DOTM makes it difficult for thorough study of the influence of shear on fouling and transmission. Dynamic membrane modules have been popular recently and oscillatory vibration has been used to enhance membrane performance. In order to understand and compare the influence of the oscillatory shear to that of steady shear, it is essential to obtain a filtration equipment which can provide a wide range of shear patterns. Shear patterns of interest include oscillatory shear and intermittency of shear.

7.1.2 Effect of shear on fouling in Microfiltration using DSSTC

Whilst shear is known to reduce concentration polarisation and fouling, the influence of various shear patterns on dTMP/dt, transmission, and irreversible fouling are so not well understood. DSSTC was designed and fabricated in house to provide a wide range of precisely controlled shear patterns for microfiltration and provide much better control on the level of shear than a typical crossflow cell. Advantages of DSSTC include its capability to create steady shear, oscillatory shear, sharp change in shear, and intermittency of shear using one single module which allow better comparisons between filtration performance. DSSTC also has 4 permeate channels which enable permeate composition through different membrane radial positions, hence different shear rate, to be detected. Moreover, providing that feed concentration is the same at all membrane radial positions, having 4 permeate channels will allow a more accurate observation of the effect of shear on filtration of a complex live feed. This is because composition of many microbial suspensions may change within a matter of hours or days, and replicating exactly the same filtration condition will not necessarily lead to exactly the same result due to changes in feed composition.

The current set-up of DSSTC is in semi-deadend mode and three of the four channels are operable. The main focus of the first part of this work using DSSTC was to study the effect of shear on fouling and transmission of Dextran Blue.

The principle conclusions are:

- Steady shear generally led to lower dTMP/dt. For steady shear, normalised observed transmission exponentially increased as normalised dTMP/dt increased.

- The effect of sinusoidal wave amplitude and frequency on membrane average transmission was similar at the same maximum shear rate (AFR). But the effect of increases in displacement amplitude on dTMP/dt reduction was more significant at the same AFR value.

- Square wave oscillatory shear was more effective than sinusoidal shear at reducing dTMP/dt. Observed transmission for sinusoidal waves was much lower than that for square wave for all conditions. And irreversible fouling for sinusoidal wave was generally greater than that for square wave.

Intermittency of shear has been used, aiming to achieve good filtration performance while reducing the system energy cost. The influence of intermittency of shear at different conditions was studied and the principle results are:

- The level of high plate rotational speed can influence overall membrane performance. The effect of high plate rotational speed was greater in reducing observed transmission than in decreasing the rate of increase of transmembrane pressure. For the range tested, use of a medium steady shear continuously was more beneficial than using alternating low-high steady shear.

- The introduction of periodic sharp change in the direction of rotation to a medium shear rate can not dramatically alter overall membrane performance but it can significantly reduce membrane irreversible fouling.

- The effect of time interval between the periodic low-high alternating shear forces was significant. Increases in the time interval led to lower dTMP/dt.

But observed transmission was greater for longer time interval due to greater build-up of concentration polarisation.

The increase in ionic strength is known to alter membrane performance. The presence of NaCl in Dextran Blue solution alters the molecules conformation. Experiments carried out in this part were to observe the influence of steady shear on dTMP/dt, solute transmission and irreversible fouling when the feed component and filtration procedure was altered. The principal conclusions are:

- The presence of NaCl in Dextran Blue solution led to much lower dTMP/dt. Under zero rotational shear the rate of fouling for Dextran Blue with NaCl present was less than 6% of that without.
- Microfiltration of Dextran Blue with NaCl under high steady shear led to increased dTMP/dt and greater irreversible membrane fouling than that under zero rotational shear. But the observed transmission was not affected.
- The use of high steady shear is not always beneficial. Since it may result in greater irreversible fouling of membrane. The effectiveness of shear depends upon the level of shear used, the feed characteristic, and the filtration procedure employed. It is therefore essential to control shear stress to an appropriate level, as greater amount does not always lead to better membrane performance.

The main focus of the second part of this work using DSSTC was to observe the effect of shear patterns and EPS on fouling by yeast suspension. The principal conclusions are:

- The efficiency of shear of all patterns was more significant at low flux. Above threshold flux, the influence of shear was greatly reduced.
- Only for the microfiltration of EPS did all shear patterns lead to improved membrane performance.

- Sharp change of direction of rotation was effective at fouling control of washed yeast, especially at or above the threshold flux, while the smooth change of the direction resulted in greater membrane resistance possibly due to rearrangement giving a more compact cake layer.

- Fouling of microfiltration of unwashed yeast can be more effectively controlled using steady shear. Sinusoidal oscillatory shear resulted in similar fouling resistance to that under zero rotational shear whilst the application of square wave increased membrane fouling for unwashed yeast.

7.2 Future work

There are many possibilities for future research in this area. DOTM is a convenient visual observation technique, and DSSTC is capable of applying numerous patterns of shear. A few suggestions for both modules in terms of module design and filtration experiments are listed below.

- Improvement of module design for DOTM module especially for the inlet flow and the membrane support will greatly enhance filtration performance and repeatability.

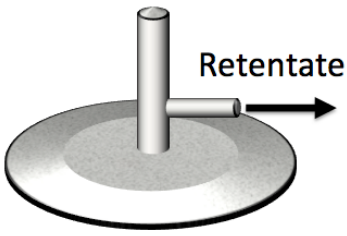

Figure 7.1: Alteration of rheometer plate to allow retentate channel

- Improvement of module design for DSSTC. DSSTC is the first generation test cell that includes a rheometer. The design of DSSTC is not perfect and its performance can be improved by alteration to the module. It is worth considering modification of DSSTC into that of crossflow type. A simple modification includes allowing retentate channel through the rheometer plate (see Figure 7.1). A more complex modification involves the alteration of the module base to fit the annular membrane, similar to that of VSEP to allow the retentate to exit at the centre, however, this requires precise manufacture to avoid leakage of the module. The syringe pumps currently in-use for DSSTC permeate channels provide extremely stable flow, but in order to monitor changes in the permeate concentration with time without disturbing the flux, it involves redoing the experiments several times and back calculating the permeate concentration. Addition of valves that can guide the flow, with another identical syringe pump, should solve this complication. With adequate financial resources, it is possible to modify the rig so that it combines the advantages of DOTM and DSSTC together. The feed channel could be equipped with measurement probes or sample collecting channels, these will enable in-situ observation of changes in feed concentration. A cone-plate rheometer could be used instead of the current plate-plate rheometer for fouling studies at uniform shear stress.

- Computational modelling of flow profile in the DSSTC is also of interest, this will allow more accurate local shear calculation.

- Researches based on critical shear for microbial fouling mitigation are interesting. Microbial cells such as algae and bacteria are known to secrete extracellular polysaccharide. In many cases, these polysaccharide are classified as soluble, loosely bound, and tightly bound. Understanding microbial adhesion force and factors affecting it is extremely beneficial for fouling studies. The

application of shear mechanically alters the composition of both the bulk and deposited EPS. It is possible that the right level of shear is able to control fouling better than others. Studies of critical shear for fouling control for feed containing gelatinous-coated particles whose adhesion force is easy to characterise are interesting. It is likely that the critical shear value can be obtained from rheometric properties of the feed.

Bibliography

[1] N.F. Gray. *Water technology: An introduction for environmental scientists and engineers*. Butterworth-Heinemann, 2010.

[2] S.S. Madaeni, T. Mohamamdi, and M.K. Moghadam. Chemical cleaning of reverse osmosis membranes. *Desalination*, 134(1-3):77–82, 2001.

[3] Melissa Christensen, editor. *Microfiltration And Ultrafiltratiion Membranes In Drinking Water*. American Water Works Association, 2005.

[4] A.I. Schafer, U. Schwicker, M.M. Fischer, A.G. Fane, and T.D. Waite. Microfiltration of colloids and natural organic matter. *Journal of Membrane Science*, 171(2):151 – 172, 2000.

[5] J.D. Seader and E. J. Henley. *Separation process principles*. Wiley, 2006.

[6] Munir. Cheryan. *Ultrafiltration handbook*. Technomic Pub. Co., Lancaster, Pa., 1986.

[7] http://membranes.edu.au.

[8] M. Schouppe. *Membrane technologies for water applications*. European Commission, 2010.

[9] Benjamin M.M. Shi, W. Membrane interactions with nom and an adsorbent in a vibratory shear enhanced filtration process (vsep) system. *Journal of Membrane Science*, 312(1-2):23–33, 2008.

[10] S. S. Vasan, Raja Ghosh, and Zhanfeng Cui. Design of cone-and-plate test cell for ultrafiltration. *Desalination*, 146(1-3):219 – 224, 2002.

[11] Raja. Ghosh. *Protein bioseparation using ultrafiltration : theory, applications, and new developments*. Imperial College Press ; Distributed by World Scientific Pub., London; River Edge, NJ, 2003.

[12] Leos J. Zeman and Andrew L. Zydney. *Microfiltration and ultrafiltration : principles and applications*. M. Dekker, New York, 1996.

[13] Robert Field. *Membranes for Water Treatment: Volume 4*, chapter Fundamental of fouling, pages 1–23. Wiley-VCH, 2010.

[14] M. Mulder. *Basic principles of membrane technology*. Kluwer, Dordrecht, 2003.

[15] J.G. Wijmans, S. Nakao, and C.A. Smolders. Flux limitation in ultrafiltration: Osmotic pressure model and gel layer model, 1984.

[16] R. B. Bird, W.E. Stewart, and E.N. Lightfoot. *Transport phenomena*. Wiley, 2007.

[17] Richard Baker. *Membrane Technology and Applications*. Wiley, 2012.

[18] Hughes D. and Field R.W. Crossflow filtration of washed and unwashed yeast suspensions at constant shear under nominally sub-critical conditions. *Journal of Membrane Science*, 280(1-2):89 – 98, 2006.

[19] Chris J. Wright Nidal Hilal, Mohamed Khayet, editor. *Membrane Modification: Technology and Applications*. CRC Press, 2012.

[20] C.H. Koo, A.W. Mohammad, F. Suja', and M.Z. Meor Talib. Review of the effect of selected physicochemical factors on membrane fouling propensity based on fouling indices. *Desalination*, 287:167–177, 2012.

[21] X. Shi, R. Field, and N. Hankins. Review of fouling by mixed feeds in membrane filtration applied to water purification. *Desalination and Water Treatment*, 35:68–81, 2011.

[22] K. Hwang, Y. T. Wang, E Iritani, and N Katagiri. Effect of gel particle softness on the performance of cross-flow microfiltration. *Journal of Membrane Science*, 365(1-2):130 – 137, 2010.

[23] Wenshan Guo, Huu-Hao Ngo, and Jianxin Li. A mini-review on membrane fouling. *Bioresource Technology*, 122(0):27 – 34, 2012.

[24] K. Hwang and C Hsueh. Dynamic analysis of cake properties in microfiltration of soft colloids. *Journal of Membrane Science*, 214(2):259 – 273, 2003.

[25] M.L. Christensen, C. Johansson, M. Sedin, and K. Keiding. Nonlinear filtration behavior of soft particles: Effect of dynamic cake compression. *Powder Technology*, 207:428 – 436, 2011.

[26] Frederic Pincet, Eric Perez, and Georges Belfort. Molecular interactions between proteins and synthetic membrane polymer films. *Langmuir*, 11(4):1229–1235, April 1995.

[27] Pierre Le-Clech, Vicki Chen, and Tony A.G. Fane. Fouling in membrane bioreactors used in wastewater treatment. *Journal of Membrane Science*, 284(1-2):17 – 53, 2006.

[28] Y Ye, P. Le-Clech, V Chen, A.G. Fane, and B Jefferson. Fouling mechanisms of alginate solutions as model extracellular polymeric substances. *Desalination*, 175(1):7 – 20, 2005.

[29] R.W. Field and G.K. Pearce. Critical, sustainable and threshold fluxes for membrane filtration with water industry applications. *Advances in Colloid and Interface Science*, 164(1-2):38–44, 2011.

[30] Greg Foley. A review of factors affecting filter cake properties in dead-end microfiltration of microbial suspensions. *Journal of Membrane Science*, 274:38 – 46, 2006.

[31] Takaaki Tanaka, Ken-Ichi Abe, Hiroyuki Asakawa, Hidetoshi Yoshida, and Kazuhiro Nakanishi. Filtration characteristics and structure of cake in cross-flow filtration of bacterial suspension. *Journal of Fermentation and Bioengineering*, 78(6):455 – 461, 1994.

[32] M. Meireles, C. Molle, M.J. Clifton, and P. Aimar. The origin of high hydraulic resistance for filter cakes of deformable particles: cell-bed deformation or surface-layer effect? *Chemical Engineering Science*, 59(24):5819 – 5829, 2004.

[33] T. Tanaka, S.I. Tsuneyoshi, W. Kitazawa, and K. Nakanishi. Characteristics in crossflow filtration using different yeast suspensions. *Separation Science and Technology*, 32(11):1885–1898, 1997.

[34] K. Ohmori and C.E. Glatz. Effects of ph and ionic strength on microfiltration of c. glutamicum. *Journal of Membrane Science*, 153(1):23–32, 1999.

[35] K.L. Tung, C.C. Hu, C.J. Chuang, K.J. Hwang, and T.-Y. Wu. Effects of soft particle deformability and particle/pore size ratio on the blocking mechanism in dead-end microfiltration. *Chemical Engineering and Technology*, 33(8):1341–1348, 2010.

[36] Z. Gagnon, J. Mazur, and H.C. Chang. Glutaraldehyde enhanced dielectrophoretic yeast cell separation. *Biomicrofluidics*, 3(4), 2009.

[37] R.W. Field and J.J. Wu. Modelling of permeability loss in membrane filtration: Re-examination of fundamental fouling equations and their link to critical flux. *Desalination*, 2011.

[38] S. Chellam and N.G. Cogan. Colloidal and bacterial fouling during constant flux microfiltration: Comparison of classical blocking laws with a unified model combining pore blocking and eps secretion. *Journal of Membrane Science*, 382(1-2):148–157, 2011.

[39] S. Chellam and W. Xu. Blocking laws analysis of dead-end constant flux microfiltration of compressible cakes. *Journal of Colloid and Interface Science*, 301(1):248–257, 2006.

[40] P. Kovalsky, G. Bushell, and T.D. Waite. Prediction of transmembrane pressure build-up in constant flux microfiltration of compressible materials in the absence and presence of shear. *Journal of Membrane Science*, 344(1-2):204–210, 2009.

[41] R. W. Field, D. Wu, J. A. Howell, and B. B. Gupta. Critical flux concept for microfiltration fouling. *Journal of Membrane Science*, 100(3):259 – 272, 1995.

[42] www.scopus.com.

[43] P. Bacchin, P. Aimar, and R.W. Field. Critical and sustainable fluxes: Theory, experiments and applications. *Journal of Membrane Science*, 281(1-2):42–69, 2006.

[44] A.S. Kim and Y. Liu. Critical flux of hard sphere suspensions in crossflow filtration: Hydrodynamic force bias monte carlo simulations. *Journal of Membrane Science*, 323(1):67–76, 2008.

[45] Pierre Cote. From critical flux workshop, oxford. september 2003. see advances in colloid and interface science 164(2011)38-44 for details, 2003.

[46] D. Wu, J.A. Howell, and R.W. Field. Critical flux measurement for model colloids. *Journal of Membrane Science*, 152(1):89–98, 1999.

[47] G. Gesan-Guiziou, R.J. Wakeman, and G. Daufin. Stability of latex crossflow filtration: Cake properties and critical conditions of deposition. *Chemical Engineering Journal*, 85(1):27–34, 2002.

[48] Georges Belfort, Robert H. Davis, and Andrew L. Zydney. The behavior of suspensions and macromolecular solutions in crossflow microfiltration. *Journal of Membrane Science*, 96(1-2):1–58, November 1994.

[49] Francisco López Carme Güell, Montserrat Ferrando, editor. *Monitoring and Visualizing Membrane-Based Processes*. Wiley-VCH, 2009.

[50] V. Chen, H. Li, and A. G. Fane. Non-invasive observation of synthetic membrane processes - a review of methods. *Journal of Membrane Science*, 241(1):23 – 44, 2004.

[51] T.E. Bustnes, C.F. Kaminski, and M.R. Mackley. Direct visualization of flowing biomass capture and release within a fibrous matrix. *Biochemical Engineering Journal*, 18(3):231–234, 2004.

[52] Mihir K. Purkait Kaustubha Mohanty, editor. *Membrane Technologies and Applications*. CRC Press, 2011.

[53] L.E.S. Brink, S.J.G. Elbers, T Robbertsen, and P Both. The anti-fouling action of polymers preadsorbed on ultrafiltration and microfiltration membranes. *Journal of Membrane Science*, 76(2-3):281 – 291, 1993.

[54] T. Meyn, T.O. Leiknes, and A. Konig. Ms2 removal from high nom content surface water by coagulation - ceramic microfiltration, for potable water production. *AIChE Journal*, 58(7):2270–2281, 2012.

[55] S. Babel and S. Takizawa. Chemical pretreatment for reduction of membrane fouling caused by algae. *Desalination*, 274(1-3):171–176, 2011.

[56] W. Gao, H. Liang, J. Ma, M. Han, Z.L. Chen, Z.S. Han, and G.B. Li. Membrane fouling control in ultrafiltration technology for drinking water production: A review. *Desalination*, 272(1-3):1 – 8, 2011.

[57] L Fiksdal and T. Leiknes. The effect of coagulation with mf/uf membrane filtration for the removal of virus in drinking water. *Journal of Membrane Science*, 279(1-2):364 – 371, 2006.

[58] T. Weigert, J. Altmann, and S. Ripperger. Crossflow electrofiltration in pilot scale. *Journal of Membrane Science*, 159(1-2):253–262, 1999.

[59] W Richard Bowen and A Latif Ahmad. Pulsed electrophoretic filter-cake release in dead-end membrane processes. *AIChE journal.*, 43(4):959–, 1997.

[60] Zhaoxiang Zhong, Dongyan Li, Bingbing Zhang, and Weihong Xing. Membrane surface roughness characterization and its influence on ultrafine particle adhesion. *Separation and Purification Technology*, 90(0):140 – 146, 2012.

[61] V. Kochkodan, S. Tsarenko, N. Potapchenko, V. Kosinova, and V. Goncharuk. Adhesion of microorganisms to polymer membranes: a photobactericidal effect of surface treatment with tio2. *Desalination*, 220(1-3):380–385, 2008.

[62] M.L. Carman, T.G. Estes, A.W. Feinberg, J.F. Schumacher, W. Wilkerson, L.H. Wilson, M.E. Callow, J.A. Callow, and A.B. Brennan. Engineered antifouling microtopographies - correlating wettability with cell attachment. *Biofouling*, 22(1):11–21, 2006.

[63] S.H. Maruf, L. Wang, A.R. Greenberg, J. Pellegrino, and Y. Ding. Use of nanoimprinted surface patterns to mitigate colloidal deposition on ultrafiltration membranes. *Journal of Membrane Science*, 428:598–607, 2013.

[64] Y. Liu, G He, B Li, Z Hu, and J Ju. A comparison of cake properties in traditional and turbulence promoter assisted microfiltration of particulate suspensions. *Water Research*, 46(8):2535 – 2544, 2012.

[65] G. Foley, P.F. MacLoughlin, and D.M. Malone. Membrane fouling during constant flux crossflow microfiltration of dilute suspensions of active dry yeast. *Separation Science and Technology*, 30(3):383–398, 1995.

[66] G. Foley, A.A. McCarthy, and P.K. Walsh. Evidence for shape-dependent deposition in crossflow microfiltration of microbial cells. *Journal of Membrane Science*, 250(1-2):311–313, 2005.

[67] O. Le Berre and G. Daufin. Skimmilk crossflow microfiltration performance versus permeation flux to wall shear stress ratio. *Journal of Membrane Science*, 117:261 – 270, 1996.

[68] R.J. Baker, A.G. Fane, C.J.D. Fell, and B.H. Yoo. Factors affecting flux in crossflow filtration. *Desalination*, 53(1-3):81–93, 1985.

[69] B. Riesmeier, K.H. Kroner, and M.-R. Kula. Studies on secondary layer formation and its characterization during cross-flow filtration of microbial cells. *Journal of Membrane Science*, 34(3):245–266, 1987.

[70] B. Riesmeier, K.H. Kroner, and M.-R. Kula. Tangential filtration of microbial suspensions: Filtration resistances and model development. *Journal of Biotechnology*, 12(2):153–172, 1989.

[71] Y. Wang, J. A. Howell, R. W. Field, and D. Wu. Simulation of cross-flow filtration for baffled tubular channels and pulsatile flow. *Journal of membrane science.*, 95(3):243–, 1994.

[72] M. R. Mackley and N. E. Sherman. Cross-flow filtration with and without cake formation. *Chemical Engineering Science*, 49(2):171–, 1994.

[73] S.M. Finnigan and J.A. Howell. The effect of pulsed flow on ultrafiltration fluxes in a baffled tubular membrane system. *Desalination*, 79(2-3):181–202, December 1990.

[74] V. Mavrov, N. D. Nikolov, M. A. Islam, and J. D. Nikolova. An investigation on the configuration of inserts in tubular ultrafiltration module to control concentration polarization. *Journal of Membrane Science*, 75(1/2):197–, 1992.

[75] S Elmaleh and N Ghaffor. Cross-flow ultrafiltration of hydrocarbon and biological solid mixed suspensions. *Journal of membrane science.*, 118(1):111–, 1996.

[76] S. Elmaleh and N. Ghaffor. Upgrading oil refinery effluents by cross-flow ultrafiltration. *Water science and technology : a journal of the International Association on Water Pollution Research.*, 34(9):231–, 1996.

[77] B. J. Bellhouse, G. Costigan, K. Abhinava, and A. Merry. The performance of helical screw-thread inserts in tubular membranes. *Separation and Purification Technology*, 22-23:89–113, 2001.

[78] H.-Y. Li, C. D. Bertram, and D. E. Wiley. Mechanisms by which pulsatile flow affects cross-flow microfiltration. *AIChE J.*, 44(9):1950–1961, 1998.

[79] L Ding, C Charcosset, and MY Jaffrin. Albumin recovery enhancement in membrane plasma fractionation using pulsatile flow. *The International journal of artificial organs*, 14(1):61–5, 1991.

[80] J. A. Levesley and B. J. Bellhouse. Particulate separation using inertial lift forces. *Chemical Engineering Science*, 48(21):3657–, 1993.

[81] Levesley and Bellhouse. The retention and suspension of particles in a fluid using oscillatory flow. *Chemical Engineering Research and Design*, 75(3):288–297, 1997.

[82] K Abel. Influence of oscillatory flows on protein ultrafiltration. *Journal of membrane science.*, 133(1):39–, 1997.

[83] P Blanpain-Avet, N Doubrovine, C Lafforgue, and M Lalande. The effect of oscillatory flow on crossflow microfiltration of beer in a tubular mineral membrane system - membrane fouling resistance decrease and energetic considerations. *Journal of membrane science.*, 152(2):151–, 1999.

[84] M.Y. Jaffrin. Dynamic shear-enhanced membrane filtration: A review of rotating disks, rotating membranes and vibrating systems. *Journal of Membrane Science*, 324(1-2):7–25, 2008.

[85] S.S. Lee, A. Burt, G. Russotti, and B. Buckland. Microfiltration of recombinant yeast cells using a rotating disk dynamic filtration system. *Biotechnology and Bioengineering*, 48(4):386–400, 1995.

[86] O.A. Akoum, M.Y. Jaffrin, L. Ding, P. Paullier, and C. Vanhoutte. An hydrodynamic investigation of microfiltration and ultrafiltration in a vibrating membrane module. *Journal of Membrane Science*, 197(1-2):37–52, 2002.

[87] Kazutaka Takata, Kazuyoshi Yamamoto, Rulin Bian, and Yoshimasa Watanabe. Removal of humic substances with vibratory shear enhanced processing membrane filtration. *Water Supply*, 17(1):93–102, 1999.

[88] S. Prip Beier and G. Jonsson. A vibrating membrane bioreactor (vmbr): Macromolecular transmission-influence of extracellular polymeric substances. *Chemical Engineering Science*, 64(7):1436–1444, 2009.

[89] J. Nuortila-Jokinen, A. Kuparinen, and M. Nystram. Tailoring an economical membrane process for internal purification in the paper industry. *Desalination*, 119(1-3):11–19, 1998.

[90] S.P. Beier, M. Guerra, A. Garde, and G. Jonsson. Dynamic microfiltration with a vibrating hollow fiber membrane module: Filtration of yeast suspensions. *Journal of Membrane Science*, 281(1-2):281–287, 2006.

[91] P Beier and G Jonsson. A vibrating membrane bioreactor (vmbr): Macromolecular transmission-influence of extracellular polymeric substances. *Chemical Engineering Science*, 64(7):1436 – 1444, 2009.

[92] Z. F. Cui and K. I. T. Wright. Gas-liquid two-phase cross-flow ultrafiltration of bsa and dextran solutions. *Journal of Membrane Science*, 90(1/2):183–, 1994.

[93] Z F Cui and K I T Wright. Flux enhancements with gas sparging in downwards crossflow ultrafiltration: Performance and mechanism. *Journal of membrane science.*, 117(1-2):109–, 1996.

[94] S. R. Bellara, Z. F. Cui, and D. S. Pepper. Gas sparging to enhance permeate flux in ultrafiltration using hollow fibre membranes. *Journal of Membrane Science*, 121(2):175–184, 1996.

[95] Z F Cui, S R Bellara, and P Homewood. Airlift crossflow membrane filtration - a feasibility study with dextran ultrafiltration. *Journal of membrane science.*, 128(1):83–, 1997.

[96] Q Y Li, Z F Cui, and D S Pepper. Effect of bubble size and frequency on the permeate flux of gas sparged ultrafiltration with tubular membranes.

The Chemical engineering journal and the biochemical engineering journal., 67(1):71–, 1997.

[97] R Ghosh and Z F Cui. Mass transfer in gas-sparged ultrafiltration: upward slug flow in tubular membranes. *Journal of membrane science.*, 162(1):91–, 1999.

[98] H. W. Sur and Z. Cui. Experimental study on the enhancement of yeast microfiltration with gas sparging. *Journal of chemical technology and biotechnology.*, 76:477–484, 2001.

[99] Mark Valentine Edward. *Fundamental flux enhancement modelling of membrane microfiltration.* Thesis, University of Oxford, 2011.

[100] V. G. J. Rodgers and R. E. Sparks. Reduction of membrane fouling in the ultrafiltration of binary protein mixtures. *AIChE Journal*, 37(10):1517–1528, 1991.

[101] V.G.J. Rodgers and R.E. Sparks. Effect of transmembrane pressure pulsing on concentration polarization. *Journal of Membrane Science*, 68(1-2):149–168, April 1992.

[102] V. G. J. Rodgers and R. E. Sparks. Effects of solution properties on polarization redevelopment and flux in pressure pulsed ultrafiltration. *Journal of Membrane Science*, 78(1/2):163–, 1993.

[103] C. Wilharm and V. G. J. Rodgers. Significance of duration and amplitude in transmembrane pressure pulsed ultrafiltration of binary protein mixtures. *Journal of Membrane Science*, 121(2):217–228, 1996.

[104] J A Levesley and M Hoare. The effect of high frequency backflushing on the microfiltration of yeast homogenate suspensions for the recovery of soluble proteins. *Journal of membrane science.*, 158(1):29–, 1999.

[105] T.M. Qaisrani and W.M. Samhaber. Impact of gas bubbling and backflushing on fouling control and membrane cleaning. *Desalination*, 266(1-3):154–161, 2011.

[106] C.P. Koutsou and A.J. Karabelas. Shear stresses and mass transfer at the base of a stirred filtration cell and corresponding conditions in narrow channels with spacers. *Journal of Membrane Science*, 399-400:60–72, 2012.

[107] Younggon. Son. Determination of shear viscosity and shear rate from pressure drop and flow rate relationship in a rectangular channel. *Polymer*, 48(2):632–637, 2007.

[108] M.Y. Jaffrin. Dynamic filtration with rotating disks, and rotating and vibrating membranes: An update. *Current Opinion in Chemical Engineering*, 1(2):171–177, 2012.

[109] R Bouzerar, M Y Jaffrin, L Ding, and P Paullier. Influence of geometry and angular velocity on performance of a rotating disk filter. *AIChE Journal*, 46(2):257–265, 2000.

[110] W. M. Deen. Hindered transport of large molecules in liquid-filled pores. *AIChE Journal*, 33(9):1409–1425, 1987.

[111] I. Teraoka and Y. Wang. Computer simulation studies on overlapping polymer chains confined in narrow channels. *Polymer*, 45(11):3835–3843, 2004.

[112] G.F. Hermsen, B.A. De Geeter, N.F.A. Van der Vegt, and M. Wessling. Monte carlo simulation of partially confined flexible polymers. *Macromolecules*, 35(13):5267–5272, 2002.

[113] L.I. Klushin, A.M. Skvortsov, H.-P. Hsu, and K. Binder. Dragging a polymer chain into a nanotube and subsequent release. *Macromolecules*, 41(15):5890–5898, 2008.

[114] L.E. Rodd, T.P. Scott, D.V. Boger, J.J. Cooper-White, and G.H.c McKinley. The inertio-elastic planar entry flow of low-viscosity elastic fluids in microfabricated geometries. *Journal of Non-Newtonian Fluid Mechanics*, 129(1):1–22, 2005.

[115] G.H. McKinley, L.E. Rodd, M.S.N. Oliverira, and J. Cooper-White. Extensional flows of polymer solutions in microfluidic converging/diverging geometries. *Journal of Central South University of Technology (English Edition)*, 14(1 SUPPL.):6–9, 2007.

[116] V.W. Krevelen and K Nijenhuis. *Properties of Polymers: Their Correlation with Chemical Structure; their Numerical Estimation and Prediction from Additive Group Contributions*. Elsevier, 2009.

[117] E.J. Hinch. Uncoiling a polymer molecule in a strong extensional flow. *Journal of Non-Newtonian Fluid Mechanics*, 54:209–230, 1994.

[118] C.M. Schroeder, H.P. Babcock, E.S. Shaqfeh, and Chu S. Observation of polymer conformation hysteresis in extensional flow. *Science*, 301:1515–9, 2003.

[119] P. G. de Gennes. Coil-stretch transition of dilute flexible polymers under ultrahigh velocity gradients. *The Journal of Chemical Physics*, 60(12):5030–5042, 1974.

[120] Fan Jin and Chi Wu. Observation of first-order transition in ultrafiltration of flexible linear polymer chains. *Physical review letters*, 2006.

[121] U.S. Agarwal. Effect of initial conformation, flow strength, and hydrodynamic interaction on polymer molecules in extensional flows. *Journal of Chemical Physics*, 113, 2000.

[122] T. Hirasaki, T. Sato, T. Tsuboi, H. Nakano, T. Noda, A. Kono, K. Yamaguchi, K. Imada, N. Yamamoto, H. Murakami, and S. Manabe i. Permeation mechanism of dna molecules in solution through cuprammonium regenerated cellulose hollow fiber (bmm(tm)). *Journal of Membrane Science*, 106(1-2):123–129, 1995.

[123] D.W. Kahn, M.D. Butler, D.L. Cohen, M. Gordon, J.W. Kahn, and M.E. Winkler. Purification of plasmid dna by tangential flow filtration. *Biotechnology and Bioengineering*, 69(1):101–106, 2000.

[124] D.R. Latulippe, K. Ager, and A.L. Zydney. Flux-dependent transmission of supercoiled plasmid dna through ultrafiltration membranes. *Journal of Membrane Science*, 294(1-2):169–177, 2007.

[125] Boksoon Kwon, Noeon Park, and Jaeweon Cho. Effect of algae on fouling and efficiency of uf membranes. *Desalination*, 179(1-3):203 – 214, 2005.

[126] Vardon D.R. Clark M.M. Ladner, D.A. Effects of shear on microfiltration and ultrafiltration fouling by marine bloom-forming algae. *Journal of Membrane Science*, 356(1-2):33–43, 2010.

[127] B. Petrusevski, G. Bolier, A. N. Van Breemen, and G. J. Alaerts. Tangential flow filtration: A method to concentrate freshwater algae. *Water Research*, 29(5):1419 – 1424, 1995.

[128] Masato Imase, Keiji Watanabe, Hideki Aoyagi, and Hideo Tanaka. Construction of an artificial symbiotic community using a chlorella-symbiont association as a model. *FEMS Microbiology Ecology*, 63(3):273–282, 2008.

[129] Gary G. Leppard. The characterization of algal and microbial mucilages and their aggregates in aquatic ecosystems. *Science of The Total Environment*, 165(1-3):103 – 131, 1995.

[130] K. Watanabe, M. Imase, K. Sasaki, N. Ohmura, H. Saiki, and H. Tanaka. Composition of the sheath produced by the green algae chlorella sorokiniana. *Letters in Applied Microbiology*, 42(5):538–543, 2006.

[131] Keiji Watanabe, Noritaka Takihana, Hideki Aoyagi, Satoshi Hanada, Yoshitomo Watanabe, Naoya Ohmura, Hiroshi Saiki, and Hideo Tanaka. Symbiotic association in chlorella culture. *FEMS Microbiology Ecology*, 51(2):187 – 196, 2005.

[132] F. Meng, S.-R. Chae, A. Drews, M. Kraume, H.-S. Shin, and F. Yang. Recent advances in membrane bioreactors (mbrs): Membrane fouling and membrane material. *Water Research*, 43(6):1489–1512, 2009.

[133] Sandhya Babel, Satoshi Takizawa, and Hiroaki Ozaki. Factors affecting seasonal variation of membrane filtration resistance caused by chlorella algae. *Water Research*, 36(5):1193 – 1202, 2002.

[134] S. Babel and S. Takizawa. Microfiltration membrane fouling and cake behavior during algal filtration. *Desalination*, 261(1-2):46 – 51, 2010.

[135] Y.-T. Chiou, M.-L. Hsieh, and H.-H. Yeh. Effect of algal extracellular polymer substances on uf membrane fouling. *Desalination*, 250(2):648–652, 2010.

[136] M.T. Hung and J.C. Liu. Microfiltration for separation of green algae from water. *Colloids and Surfaces B: Biointerfaces*, 51(2):157–164, 2006.

[137] Antoine Montiel and Bénédicte Welté. Preozonation coupled with flotation filtration: Successful removal of algae. *Water Science and Technology*, 37(2):65 – 73, 1998.

[138] J. Wang, J. Guan, S.R. Santiwong, and T. David Waite. Characterization of floc size and structure under different monomer and polymer coagulants on microfiltration membrane fouling. *Journal of Membrane Science*, 321(2):132 – 138, 2008.

[139] D. Hughes, U.K. Tirlapur, R. Field, and Z. Cui. In situ 3d characterization of membrane fouling by yeast suspensions using two-photon femtosecond near infrared non-linear optical imaging. *Journal of Membrane Science*, 280(1-2):124–133, 2006.

[140] A.G. Fane. Non-invasive observation of membrane processes. In *SMTC Special Workshop-13 August 2009*, 2009.

[141] H. Li, A.G. Fane, H.G.L. Coster, and S. Vigneswaran. Direct observation of particle deposition on the membrane surface during crossflow microfiltration. *Journal of Membrane Science*, 149(1):83–97, 1998.

[142] Fane A.G. Li, H. New insights into membrane operation revealed by direct observation through the membrane. *Membrane Technology*, (123):10–14, 2000.

[143] www.2spi.com.

[144] http://www.originlab.com/.

[145] Eve M. Tracey and Robert H. Davis. Protein fouling of track-etched polycarbonate microfiltration membranes. *Journal of Colloid and Interface Science*, 167(1):104 – 116, 1994.

[146] Whatman. http://www.whatman.com/, Retrieved 2009.

[147] A. Ramesh, D.J. Lee, and J.Y. Lai. Membrane biofouling by extracellular polymeric substances or soluble microbial products from membrane bioreactor sludge. *Applied Microbiology and Biotechnology*, 74(3):699–707, 2007.

[148] Fukushi K. Yamamoto K. Jinhua, P. Bacterial community structure on membrane surface and characteristics of strains isolated from membrane surface in submerged membrane bioreactor. *Separation Science and Technology*, 41(7):1527–1549, 2006.

[149] Kuo-Jen Hwang and Ya-Ju Wu. Flux enhancement and cake formation in air-sparged cross-flow microfiltration. *Chemical Engineering Journal*, 139(2):296 – 303, 2008.

[150] Kuo-Jen Hwang and Chin-En Hsu. Effect of gas-liquid flow pattern on air-sparged cross-flow microfiltration of yeast suspension. *Chemical Engineering Journal*, 151(1-3):160 – 167, 2009.

[151] Li Z. Laorko A. Youravong, W. Influence of gas sparging on clarification of pineapple wine by microfiltration. *Journal of Food Engineering*, 96(3):427–432, 2010.

[152] M.R. Mackley and N.E. Sherman. Cross-flow cake filtration mechanisms and kinetics. *Chemical Engineering Science*, 47(12):3067–3084, 1992.

[153] M.R. Mackley and N.E. Sherman. Cake filtration mechanisms in steady and unsteady flows. *Journal of Membrane Science*, 77(1):113 – 121, 1993.

[154] Molek J.R. Zydney A.L. Latulippe, D.R. Importance of biopolymer molecular flexibility in ultrafiltration processes. *Industrial and Engineering Chemistry Research*, 48(5):2395–2403, 2009.

[155] B.P. Frank and G. Belfort. Polysaccharides and sticky membrane surfaces: Critical ionic effects. *Journal of Membrane Science*, 212(1-2):205–212, 2003.

[156] A.J. Domb and N Kumar, editors. *Biodegradable Polymers in Clinical Use and Clinical Developmen*. John Wiley & Sons, 2011.

[157] F. Jettner. Elimination of terpenoid odorous compounds by slow sand and river bank filtration of the ruhr river, germany. *Water Science and Technology*, 31(11):211 – 217, 1995.

[158] X. Cao, J. Liu, and X. Meng. Evaluation of a slow sand filter in advanced wastewater treatment. pages 4942–4944, 2010.

[159] R. Maniero, E. Climent, and P. Bacchin. Adhesion and detachment fluxes of micro-particles from a permeable wall under turbulent flow conditions. *Chemical Engineering Science*, 71:409–421, 2012.

[160] G.M. Burdick, N.S. Berman, and S.P. Beaudoin. Describing hydrodynamic particle removal from surfaces using the particle reynolds number. *Journal of Nanoparticle Research*, 3(5-6):455–467, 2001.

[161] S. Yiantsios and A. Karabelas. Detachment of spherical microparticles adhering on flat surfaces by hydrodynamic forces. *Journal of Colloid And Interface Science*, 176(1):74–85, 1995.

[162] Z.F. Cui, S. Chang, and A.G. Fane. The use of gas bubbling to enhance membrane processes. *Journal of Membrane Science*, 221(1-2):1–35, 2003.

[163] W. Shi and M.M. Benjamin. Effect of shear rate on fouling in a vibratory shear enhanced processing (vsep) ro system. *Journal of Membrane Science*, 366(1-2):148–157, 2011.

[164] S. S. Vasan. *Analysis of mass transfer in Ultrafiltration.* Thesis, University of Oxford.

[165] E.B. Cavalcanti and F. Coeuret. Mass transfer between a liquid and a binary rotating/fixed disc system in a closed cylinder. *Journal of Applied Electrochemistry*, 26(6):655–663, 1996.

[166] H. Matsuda. Theory of stationary current-voltage curves of redox-electrode reactions in hydrodynamic voltammetry. vi. ring electrodes. *Journal of Electroanalytical Chemistry*, 35(C):77–84, 1972.

[167] C.K. Colton and K.A. Smith. Mass transfer to a rotating fluid, part ii. transport from the base of an agitated cylindrical tank. *AIChE J.*, 18(5):958–967, 1972.

[168] T.G. Kaufmann and E.F. Leonard. Mechanism of interfacial mass transfer in membrane transport. *AIChE J.*, 14(3):421–425, 1968.

[169] G.D. Lehmkuhl and J.L. Hudson. Flow and mass transfer near an enclosed rotating disk: Experiment. *Chemical Engineering Science*, 26(10):1601–1613, 1971.

[170] J.W. Daily and R.E. Nece. Chamber dimension effects on induced flow and frictional resistance of enclosed rotating disks. *ASME J. Basic Eng.*, 82(1):217–232, 1960.

[171] S.L. Soo. Laminar flow over an enclosed rotating disk. *Trans. ASME*, 80(2):287–296, 1958.

[172] F. Schultz-Grunow. Der reibungswiderstand rotierender scheiben in gehusen. *ZAMM*, 15(4):191–204, 1935.

[173] R. Kommedal, K. Milferstedt, R. Bakke, and E. Morgenroth. Effects of initial molecular weight on removal rate of dextran in biofilms. *Water Research*, 40(9):1795–1804, 2006.

[174] Bauser H. Stroh N. Grauschopf U. Mc Donogh, R.M. Experimental in situ measurement of concentration polarisation during ultra- and micro-filtration of bovine serum albumin and dextran blue solutions. *Journal of Membrane Science*, 104(1-2):51–63, 1995.

[175] M.Y. Jaffrin, L.-H. Ding, O. Akoum, and A. Brou. A hydrodynamic comparison between rotating disk and vibratory dynamic filtration systems. *Journal of Membrane Science*, 242(1-2):155–167, 2004.

[176] F. Wicaksana, P. Pongpairoj, Field R.W., Z.F. Cui, and A.G. Fane. Critical flux determination of microalgae (chlorella sorokiniana) filtration using direct observation through the membrane (dotm) technique. *Journal of Membrane Science.*, 387-388:83–92, 2012.

[177] M Elimelech, X Jia, J Gregory, and R. Williams. *Particle Deposition & Aggregation: Measurement, Modelling and Simulation*. Butterworth-Heinemann, 1998.

[178] S.P. Beier and G. Jonsson. Separation of enzymes and yeast cells with a vibrating hollow fiber membrane module. *Separation and Purification Technology*, 53(1):111–118, 2007.

[179] T. Schluep and F. Widmer. Initial transient effects during cross flow microfiltration of yeast suspensions. *Journal of Membrane Science*, 115(2):133–145, 1996.

[180] S. Nataraj, R. Schomäcker, M. Kraume, I.M. Mishra, and A. Drews. Analyses of polysaccharide fouling mechanisms during crossflow membrane filtration. *Journal of Membrane Science*, 308(1-2):152 – 161, 2008.

[181] S. Rosenberger and M. Kraume. Filterability of activated sludge in membrane bioreactors. *Desalination*, 151(2):195–200, 2003.

[182] T. Tanaka, R. Kamimura, R. Fujiwara, and K. Nakanishi. Crossflow filtration of yeast broth cultivated in molasses. *Biotechnology and Bioengineering*, 43(11):1094–1101, 1994.

[183] P.H. Hodgson, G.L. Leslie, R.P. Schneider, A.G. Fane, C.J.D. Fell, and K.C. Marshall. Cake resistance and solute rejection in bacterial microfiltration: The role of the extracellular matrix. *Journal of Membrane Science*, 79(1):35–53, 1993.